UNIVERSITY OF CALIFORNIA

Los Angeles

ON THE MASSES OF WHITE DWARFS IN CATACLYSMIC BINARIES

A dissertation submitted in partial satisfaction of the

requirements for the degree Doctor of Philosophy
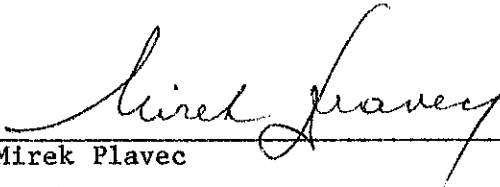
in Astronomy
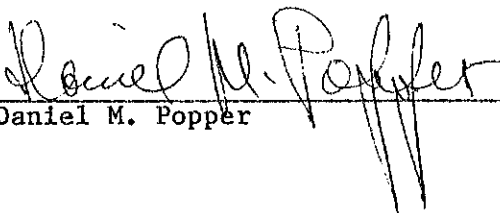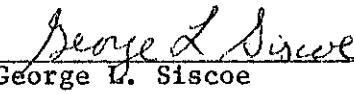
by

Allen Wayne Shafter

1983

The dissertation of Allen Wayne Shafter is approved.

_____
Mirek Plavec

_____
Daniel M. Popper

_____
George L. Siscoe

_____
John T. Wasson

_____
Roger K. Ulrich, Committee Chair

University of California, Los Angeles

1983

To my father

and the memory of my mother

TABLE OF CONTENTS

LIST OF TABLES

LIST OF FIGURES

ACKNOWLEDGMENTS

Throughout the course of my study at UCLA I have had the privilege of interacting with several astronomers who have had a great influence on the work presented here. I should like to begin by thanking Dan Popper who initially stimulated my interest in binary stars while I was assisting him with observations at Lick Observatory in June 1980. Recently, his comments have resulted in a significant improvement in this thesis. At the onset of my research, I was fortunate to meet Paula Szkody and Joe Patterson. I wish to take this opportunity to thank both of them for providing invaluable guidance during the early stages of my work with cataclysmic binaries. Since that time, my association with both of these astronomers has been very rewarding.

I am extremely grateful to my advisor, Roger Ulrich, for his support and advice during the course of this work. Although his primary field of interest is not cataclysmic binaries, his door was always open for numerous discussion on the subject. I have benefited from these discussions more, I'm sure, than he realized. In addition, I wish to express my gratitude for the financial support which he has generously provided during the last 3 years.

I wish to thank Mirek Plavec for several enlightening discussions, especially during the latter stages of this work. I am particularly grateful to him for bringing to my attention a recent preprint which turned out to be extremely useful in completing this work.

Steve Grandi, Mike Jura, and Ned Wright have provided useful discussions during the course of this work for which I am grateful.

ABSTRACT OF THE DISSERTATION

On the Masses of White Dwarfs in Cataclysmic Binaries

by

Allen Wayne Shafter

Doctor of Philosophy in Astronomy

University of California, Los Angeles, 1983

Professor Roger K. Ulrich, Chair

The indirect method of determining the masses of the white dwarfs

in cataclysmic binaries initially described by Warner has been

critically reexamined. Warner's method is based primarily on the

assumption that the quantity $K_1/(v_d \sin i)$ is a function only of the

mass ratio of the binary. In the above relationship K_1 is the velocity

semiamplitude of the white dwarf and $v_d \sin i$ is the projected circular

velocity of material in the accretion disk having the same specific

angular momentum as the material leaving the inner Lagrangian point.

The quantity $v_d \sin i$ can, in principle, be inferred from the emission

line profiles. I have calibrated the relationship by observing 11

cataclysmic binaries with directly determined mass ratios in order to

ascertain what position in the line profile best represents $v_d \sin i$.

This position has been parameterized by defining two quantities, f and

ξ. The quantity f is the fractional intensity of the emission line

normalized to the continuum intensity, and the quantity ξ is the fractional flux of the emission line. The calibration yields values of $\langle f \rangle = 0.30 \begin{smallmatrix} +0.07 \\ -0.06 \end{smallmatrix}$ and $\langle \xi \rangle = 0.58 \begin{smallmatrix} +0.09 \\ -0.07 \end{smallmatrix}$. I conclude that the method is useful and derive masses for 20 single lined cataclysmic binaries. In general, we find that the individual white dwarf masses are typically accurate to better than 30%. The radial velocity curves for 13 of the 20 systems, V794 Aql, KR Aur, V425 Cas, SY Cnc, YZ Cnc, CM Del, T Leo, V380 Oph, V442 Oph, SW UMa, UX UMa, TW Vir, and VW Vul, have been determined for the purpose of this study. By adopting the masses for the 20 single lined systems and those from the calibration systems, a weak correlation is found between the white dwarf mass and the orbital period of the binary. This trend is in the sense that the longer period systems appear to have, on the average, more massive white dwarfs. I discuss this result in the context of current theories of the evolutionary history of cataclysmic binaries. In addition, I find that the Z Camelopardalis and U Geminorum dwarf novae tend to contain higher mass white dwarfs than do the novalike variables. Finally, I briefly discuss the nature of a newly proposed class of cataclysmics, the VY Sculptoris systems.

I. INTRODUCTION

Cataclysmic Binaries (CBs)[1] are close binary systems consisting of a white dwarf and a near main sequence red companion (for a complete review see Warner 1976, Robinson 1976b). In these systems, the red dwarf (the secondary) fills its Roche lobe and transfers material through the inner Lagrangian point to the white dwarf (the primary) via an accretion ring or disk. In the vast majority of systems, the accretion disk is the dominant source of the system's luminosity in both the ultraviolet and visual regions of the spectrum. The disk is also responsible for the emission lines of Hydrogen and Helium which dominate the spectrum of most CBs during their quiescent state. The disk material is in Keplerian motion about the white dwarf and thus rotates differentially rather than as a solid body. This differential rotation Doppler broadens the emission lines to velocities which reach several thousand km s^{-1}.

The CBs are divided into several major classes depending on the amplitude and frequencies of their eruptions. These classes include: (1) Dwarf Novae (DN), (2) Novalike varibles (NL), (3) AM Herculis objects (AM Her), (4) Novae (N), and (5) Recurrent Novae (RN). The principal characteristics of each class are summarized in Table I which is a slight modification of Table 1 from Robinson (1976b).

At this point it seems appropriate to briefly review the general characteristics of each class.

---

[1] These systems are also referred to as Cataclysmic Variables.

1

(1) Dwarf Novae

The dwarf novae are characterized by eruptions on the order of 3-5 magnitudes, recurring on time scales of between ~ 10 to several hundred days. The average time interval between outbursts, which I will refer to as the mean outburst period is far from being strictly periodic. Consequently, there is no precise way to predict when a dwarf nova will erupt. However there does appear to be some correlation between the strength (i.e. the integrated energy output) of an eruption and the time interval since the previous eruption (Parenago and Kukarkin 1934).

Dwarf novae eruptions are caused by the liberation of gravitational potential energy as material falls into the potential well of the white dwarf. A quasi-periodic modulation of the accretion rate onto the white dwarf is responsible for the observed cyclic behavior between quiescent and outburst states. It is still a matter of debate as to where in the mass transfer process (from the secondary star to the surface of the white dwarf) this modulation takes place. Bath et al. (1974) advocate a variable mass transfer rate from the secondary star, and adopt the inner Lagrangian point (L_1) as the location where the mass transfer is modulated. Another theory, first proposed by Osaki (1974), assumes a constant mass transfer rate from the secondary star and relies on a hypothetical disk instability to modulate the accretion onto the white dwarf. There has been a recent explosion of accretion disk models by various authors which attempt to describe this instability (Faulkner and Lin 1983; Cannizzo, Wheeler, and Ghosh 1982; Hoshi 1979, 1981, 1982; Meyer and Meyer-Hofmeistser 1981).

Figure 10d shows spectra of the dwarf nova YZ Cnc during quiescence and outburst. The quiescent spectrum shows the distinctive Balmer and He I emission characteristic of an optically thin accretion disk. The outburst spectrum is almost continuous, showing Balmer absorption, and is characteristic of an optically thick accretion disk. We will return to the discussion of the effect of the mass transfer rate on the spectral characteristics of the disk in Section III.

There are three recognized subclasses of dwarf novae which have been created to distinguish between subtle differences in their outburst behavior. They include the U Geminorum, Z Camelopardalis, and SU Ursae Majoris subclasses. The U Geminorum subclass contains the "normal" dwarf novae, and their outburst behavior has already been described. The mean outburst period of U Geminorum type dwarf novae tends to be somewhat longer than the average for all dwarf novae.

The Z Camelopardalis subclass consists of dwarf novae which occasionally get "stuck" at a luminosity ~ 1 magnitude below their maximum brightness. These periods of sustained outburst are known as standstills and can last for an unpredictable length of time. It has been observed that the standstills almost always occur on the declining branch of an otherwise normal outburst. Recent disk models have attempted to explain the Z Camelopardalis phenomenon by postulating that the mass transfer rate for these systems is very close to the critical value above which disk instabilities of the type proposed by Osaki (1974) do not occur. Consequently, the "normal" or U Geminorium type dwarf novae have mass transfer rates below and the novalike variables have mass transfer rates above this critical value.

The last subclass of dwarf novae are known as the SU Ursae Majoris stars. These objects have the following properties which distinguish them from other dwarf novae.

(1) Supermaxima – outbursts of unusually long duration. The time interval between successive supermaxima appears to be more nearly constant than the interval between normal outbursts.

(2) Superhumps – periodic "humps" in the light curves during supermaxima which occur with a period that is typically 2 – 5% longer than the orbital period.

(3) Orbital periods which are among the shortest of all CBs for which orbital periods are known. In particular there are no known SU Ursae Majoris dwarf novae with orbital periods longer than 3 hours.

At the present time there is no generally accepted model for the SU Ursae Majoris behavior; however, a model proposed by Vogt (1980, 1982) seems promising. In his model, Vogt postulates the existence of an eccentric ring which surrounds the inner accretion disk during a supermaxium. If the line of apsides of this elliptical ring rotates with the beat period between the orbital period and the superhump periods, then the superhumps can be understood as arising from the varying energy which is released as the stream/eccentric ring impact point migrates around the ring. When the impact point is near the ring perihelion the maximum gravitational potential energy is released and the superhump occurs.

(2) Novalike Variables

The novalike variables constitute a class of cataclysmic binaries which display photometric and spectroscopic properties similar to dwarf novae at quiescence, but do not have well defined eruptions. It is possible that many novalike variables are classical novae with unrecorded eruptions or even dwarf novae with unusually long mean outburst periods. Some novalike variables such as UX UMa have spectra that resemble dwarf novae at outburst. It is also possible that some of these objects are Z Camelopardalis type dwarf novae in extended standstills.

Recently, a new class of novalike variables has begun to emerge; they are sometimes referred to as the VY Sculptoris stars or "anti-dwarf novae." These stars have a long term photometric behavior which is opposite to that of typical dwarf novae. They remain in what might be called an outburst state for many years and they occasionally fade in brightness by 3-5 magnitudes or more for relatively short periods of time before returning to their usual bright state. Spectroscopically, the high and low states of the VY Sculptoris stars are similar to the corresponding states for normal dwarf novae.

Because the VY Sculptoris classification has only recently begun to be widely used, the exact definition has not been generally agreed upon. For example, the original definition as proposed by Bond (1980) required that member objects have emission lines at maximum as well as minimum light and, in addition, that these objects exhibit He II emission as well. As we will see in the next section this definition includes most of the AM Herculis systems. Unfortunately, requiring member systems to

have He II emission excludes several systems which, as it turns out, are the best examples of the photometric behavior described in the VY Sculptoris definition. These systems are normally quite luminous and then suddenly fade to a quiescent state for a brief period of time before returning to maximum light. As a matter of fact, VY Scl itself is a good example of a system which exhibits the characteristic photometric behavior but does not have strong He II emission. It is my proposal, therefore, that the He II and the emission lines at maximum light criteria be dropped and the formal definition be primarily a photometric one. Furthermore, since the AM Herculis systems are such a well defined group, consisting of binaries which contain strongly magnetic white dwarfs and which do not contain accretion disks, it is likely that the process which produces the deep minimum of these systems is quite different from the process which produces the deep minimum of other systems. Consequently, I have opted to exclude the AM Herculis systems from our definition of the VY Sculptoris systems. With the revised, and less stringent, definition the following systems should be classified as VY Sculptoris objects: TT Ari, MV Lyr, KR Aur, V425 Cas, LX Ser, VZ Scl, and of course VY Scl itself.

It is unfortunate that VY Scl is unquestionably the least studied of the group. For example, it is the only one for which the orbital period is unknown. It is worth noting that all of the above systems have orbital periods between 3 and 4 hours. As I will discuss in detail in Section VI this is probably not just a coincidence and it is quite likely that the orbital period of VY Scl itself will be found to lie in this range as well.

(3) AM Herculis Objects

At the present time there are about a dozen AM Herculis objects known. These systems are in some respects similar to the novalike variables in that: (1) they do not show outbursts and (2) the well studied objects (i.e. AM Her, VV Pup, and AN UMa) have high and low states similar to the VY Sculptoris objects. However, the primary defining characteristic of the AM Herculis objects is not their outburst behavior, but rather the strong linear and circular polarization exhibited by these systems. The polarization is attributed to the relatively large magnetic field strength of the white dwarfs in these systems. This strong field alters the structure of the binary system in two principal ways. (1) It inhibits the formation of an accretion disk by constraining the accreting material to follow the field lines; thereby falling onto the magnetic poles of the white dwarf. (2) The field couples to the secondary star forcing the white dwarf into synchronous rotation with the binary orbital period.

In addition to the polarization, other observational properties characteristic of the AM Herculis stars include strong He II $\lambda 4686$ emission and a very optically thick Balmer decrement (i.e. Hβ is usually stronger than Hα). A review of the AM Herculis systems can be found in Chiapetti, Tanzi, and Treves (1980).

(4) Novae

The outburst of a classical nova is believed to be caused by a thermonuclear runaway on the surface of the white dwarf (Fujimoto 1982a, b; MacDonald 1982; Starrfield et al. 1974) rather than by accretion events as in dwarf novae. Models which are based on

thermonuclear runaways in the atmosphere of the white dwarf are the only ones which are capable of producing the observed outburst energy (10^{44} - 10^{45} ergs). Additional evidence for the explosive nature of novae outbursts is provided by the appearances of expanding shells of ejected material soon after a nova outburst. Thus, the outburst mechanisms of novae and dwarf novae are completely different, although the binary structure is essentially the same.

(5) Recurrent Novae

The outburst light curves of recurrent novae are similar to those of classical novae, the difference being that recurrent novae have a smaller outburst amplitude (4-7 mag, as opposed to 8-15 for typical novae). There are only about a half dozen CBs classified as recurrent novae, of which T CrB and V1017 Sgr are known to contain evolved secondaries. It is generally believed that all "true" recurrent novae contain evolved secondaries.

There are problems in differentiating long outburst period dwarf novae from recurrent novae. For example, VY Aqr has been considered a recurrent nova by Warner (1976); yet, there is no evidence for a giant secondary nor was there a detection of a circumbinary shell after its 1963 eruption. It is quite possible that VY Aqr is a long outburst period dwarf nova. Considering that all novae are probably recurrent and that the upper bound of the dwarf novae recurrence time is poorly known, it is my opinion that the recurrent novae classification should be redefined or abolished.

In view of the fact that nearly all cataclysmic binaries are short period binary stars consisting of a white dwarf and a late type main

sequence companion, it seems reasonable to inquire as to why they

exhibit so many different types of outburst behavior.

Four possibilities immediately come to mind:

(1) Differences in the magnetic field strength of the white dwarf.

(2) Differences in the mass transfer rate.

(3) Differences in orbital periods.

(4) Differences in the masses of the stars (particularly the white
dwarf).

We know that, at least in the case of the AM Herculis stars, (1) is of

paramount importance. But what about the other classes of CBs? The

differences between dwarf novae and novae can be qualitatively explained

by differences in the mass transfer rates. By assuming that the mass

transfer rate is higher in novae than dwarf novae, then the mass

required for a thermonuclear runaway on the surface of the white dwarf

is built up much more quickly in the case of novae.[1] This

interpretation predicts that after a sufficiently long time dwarf novae

should also show novae eruptions. If we adopt this interpretation then

differences in the mass transfer rate must also explain the absence of

dwarf novae type eruption in pre- and post-novae. The explanation for

this absence depends, of course, on which model of dwarf novae eruptions

one wishes to adopt. In the case of the Bath et al. (1974) model where

the mass transfer is modulated at the inner Lagrangian point, one can

_____

[1] It should also be pointed out that if the mass transfer rate is too
high then the accreted material will sustain a "controlled" nuclear
burning on the surface of the white dwarf and nova type eruptions are
not expected to occur (Fujimoto 1982a, b, MacDonald 1982).

9

account for the absence of dwarf novae eruptions in classical novae by postulating that novae have a constant mass transfer rate. On the other hand, preliminary calculations (Faulkner and Lin 1983; Cannizzo, Wheeler, and Ghosh 1982; Hoshi 1979, 1981, 1982) have shown that if the mass transfer rate is sufficiently high (as is presumably the case for novae) then the disk instabilities of the type proposed by Osaki (1974) will not occur.

Figure 1 shows a histogram of the available data on the orbital periods of the different classes of CBs. Some interesting correlations can be drawn from an inspection of this figure. For example there appears to be a statistically significant "gap" in the period distribution (usually referred to as the "period gap"). There are only two known CBs with orbital periods between 2 and 3 hours. Another interesting observation is that all novae and Z Camelopardalis type dwarf novae have orbital periods which are above the upper edge of the period gap; while, on the other hand, all SU Ursae Majoris type dwarf novae with known orbital periods lie below the period gap. The probability of this segregation occurring at random is infinitesimally small. Consequently, it follows that the outburst behavior is, in general, a function of the orbital period.

It should be pointed out that, although there seems to be some correlation between the orbital period and outburst behavior as described above, there are exceptions. For example, between orbital periods of 4 and 5 hours, there are a nova, a novalike variable, and a U Geminorum type dwarf nova. Clearly, a larger statistical sample of CBs with known orbital periods must be compiled before the final word

concerning possible correlations between period and outburst behavior will be in.

Nevertheless, it is obvious that there is a statistically significant gap in the period distribution between 2 and 3 hours, and to date there is no generally accepted explanation for its existence. However, there is a preponderance of recent models which have attempted to explain the period gap. Although the specific details of these models differ to varying degrees, they generally attribute the existence of the gap to various properties of the secondary star. For example, Robinson et al. (1981) have attempted to explain the absence of CBs with orbital periods between 2 and 3 hours by speculating that such systems have temporarily ceased mass transfer as a result of structural changes in the core of the secondary. Assuming that the secondary star fills its Roche lobe and that it obeys the mass radius relation for main sequence stars, we can express its mass (to a first approximation) as a function of the orbital period of the system

$$M_2 \sim 0.0751 \ P \ (hr)^{1.16}, \hspace{3cm} I.1$$

almost independently of the primary mass (Echevarria 1983). A period of 3 hours roughly corresponds to a secondary mass of 0.3 $M_\odot$. It is near this mass that the transition between a radiative and convective core occurs for main sequence stars. Robinson et al. point out that this coincidence may be related to the existence of the period gap. Robinson et al. go on to speculate that cataclysmic binaries with orbital periods near the gap should be "unstable" to occasional excursions to states of minimum or non-existent mass transfer. As mentioned earlier, there are

11

several systems which are known to exhibit this behavior of which six
have known orbital periods, all in the 3 - 4 hour range. Hence, there
is some observational support for the Robinson et al. hypothesis.

In the past year or so, there have been several attempts to
formulate a quantitative model which would explain the existence of the
gap (Paczynski and Sienewicz 1983; Rappaport, Verbunt and Joss 1983;
Spruit and Ritter 1983). We will not discuss these models in detail
here but will defer discussion to Section VI.

As previously mentioned, Figure 1 clearly suggests that there is a
relationship between the outburst behavior and the orbital period. It
is instructive to point out that in 1976, when only 27 orbital periods
were known and prior to the classification of the SU Ursae Majoris
systems, there was thought to be no correlation between outburst
behavior and the orbital period (or any other fundamental porperty of
binaries for that matter). In particular, Warner (1976) in his
comprehensive review article wrote, "...with the exception of recurrent
novae, the nature of the outbursts is independent of the binary period".
Since that time, with the discovery of many more orbital periods and
with a more elaborate classification scheme, we know that there is some
correlation between outburst behavior and orbital period.

At the present time, if we ask the question "Is there any
correlation between the outburst properties (or the orbital period) and
the mass of the white dwarf?", the situation is very similar to that
which existed in 1976 when one asked the analogous question concerning
possible correlations between outburst behavior and orbital period.
Namely, at the present time, there are not enough white dwarf masses

known of sufficient accuracy to answer such a question. This fact is not a reflection of any lack of effort on the part of the astronomers who have been working in this field, but rather an indication of the extreme difficulty involved in determining reliable masses for these systems. Fortunately, for statistical purposes it should be possible, by using the method outlined in this thesis, to make reasonable estimates of the white dwarf masses for many CBs. Even though the accuracy of the individual mass estimates may be poor (i.e. typically uncertainties of ~ 20 - 30%), from a statistical point of view it should be possible to determine if there is a general preference for the white dwarfs to be massive (> 1 $M_\odot$) as has been proposed by several authors (e.g. Warner 1973; Robinson 1976a), or whether there are a significant number of low mass white dwarfs as well. Paczynski (1983) has pointed out that, from an evolutionary standpoint, there should be low mass as well as high mass white dwarfs in cataclysmic binary systems. It would be of interest, then, to resolve the above discrepancy. In addition, it would be of considerable interest to establish or refute any possible correlation between the white dwarf mass and either the orbital period or outburst characteristics of the system. The existence of such a correlation is relevant to theoretical models of novae explosion which require massive white dwarfs (Fujimoto 1982a, b, MacDonald 1982), as well as to any models which postulate differences in white dwarf mass as a function of orbital period (e.g. Webbink 1979a, b).

In summary, it appears that a knowledge (albeit a somewhat inaccurate one) of the white dwarf masses would be of considerable interest in the study of CBs and, in particular, the evolutionary

history of these systems. With this quest in mind, I plunge ahead in Section II by describing an indirect method of estimating the white dwarf masses, which is essentially a modification of the one originally proposed by Warner (1973). Next, in Section III, I describe the calibration of the mass determination method using 11 systems with known and reasonably reliable mass ratios and discuss the errors associated with the calibration. After discussion of the calibration itself, I present the white dwarf masses for 20 single lined CBs along with masses for the calibration systems in Section IV. A discussion of the resulting masses in the context of the evolutionary history of CBs is reserved for Section V. The line profile observations which are used in the calibration and in the determination of mass ratios for the single lined systems are discussed in Appendix I. And finally, in Section VI, I briefly discuss the nature of a newly proposed class of CBs, the VY Sculptoris systems. Now, without further delay, let's turn to the discussion of the white dwarf mass determination method. I Hope the reader will be convinced that useful masses can be obtained for CBs by using the method which will now be described.

II. MASS DETERMINATION

A. Direct Methods

Before beginning to describe the procedures and the difficulties involved with estimating the masses of the component stars in a cataclysmic binary, I will briefly outline the essential steps necessary to determine the component masses for a detached spectroscopic binary. Since the velocities of the stars in a binary system are inversely proportional to their masses, we have $M_2/M_1 = q = K_1/K_2$ where K_1 and K_2 are the semiamplitudes of the radial velocity curves of the two stars. Consequently, the mass ratio can be directly obtained for a double lined spectroscopic binary. In order to determine M_1 and M_2 individually, we make use of Kepler's Third Law which yields the sum of the masses,

$$M_1 + M_2 = P (K_1 + K_2)^3/(2\pi G \sin^3 i), \qquad\qquad \text{II.1}$$

if the inclination (i) of the plane of the orbit to the plane of the sky is known. In general, $\sin i$ can only be determined for eclipsing systems. Therefore, the individual masses may only be "directly" determined for double lined eclipsing systems. We now turn to the discussion of determining masses for the specific case of cataclysmic binaries.

Although CBs are all close binary systems, a determination of the masses of the individual components, in particular the white dwarf, is difficult to obtain. This is primarily a consequence of the fact that the spectrum of either star is rarely directly observed. As we will see below, the spectrum of the red dwarf is usually only seen in the long period ($P \gtrsim 6$ hr) systems. The red dwarf may on occasion be detected

15

in shorter period systems if the mass transfer rate is extremely low, making the accretion disk relatively less luminous, or if the disk is eclipsed thereby reducing its flux relative to the red dwarf. In the case of the white dwarf, the spectrum is usually never seen except in rare occurences where the mass transfer rate drops to an infintesimal value or stops completely as in MV Lyr (Robinson et al. 1981). Even if white dwarf spectra were commonly observed, it would not be very helpful because the high surface gravity of the white dwarf broadens the lines making an accurate measurement of the radial velocity extremely difficult.

Fortunately the troublesome accretion disk surrounding the white dwarf, whose luminosity is responsible for drastically diluting the light from the less luminous stellar components, usually produces strong Balmer and He I emission lines which can be used to infer the motion of the white dwarf. The majority of CBs, then, are amenable to determination of a "single lined" spectroscopic orbit. The term "single lined" has been placed in quotations to indicate that the motion of the white dwarf is not directly measured, only inferred from the radial velocity variation of the emission lines formed in the disk which surrounds it. If sufficient care is exercised in the technique which is employed to extract the velocity from the emission lines, then in most cases, a reasonably accurate orbit for the white dwarf can be determined (see Apendix II).

Unfortunately, there is no way to indirectly measure the radial velocity of the red dwarf when it is not directly observed; and as mentioned above, it is usually only observed in the long period systems.

This is simply a consequence of the fact that the luminosity of the red dwarf is an increasing function of the orbital period of the system. For a Roche-lobe-filling main sequence star in a system with orbital period P, Echevarria (1983) finds that the absolute visual magnitude may be approximated by

$$M_v \cong 16.80 - 12.19 \log P. \qquad\qquad \text{II.2}$$

Typical CB luminosities (i.e. accretion disk luminosities) yield $M_v \cong 7.5$ (Warner 1976). Consequently, it turns out that the accretion disk luminosity is nearly equal to that of a Roche lobe filling main sequence star in a binary having a period of 5 - 6 hours.

Even in the long period systems where the secondary spectrum is visible, an accurate determination of K_2 is not always easy to obtain. Robinson (1983) has found that heating of the secondary due to irradiation by high energy photons from the accretion disk can cause an overestimation of K_2. This is due to the fact that the metals are ionized on the heated hemisphere of the secondary (the side facing the white dwarf). Since the radial velocity of the secondary is determined by measuring the radial velocities of the numerous absorption lines of these metals, the derived semiamplitude will be weighted heavily by contributions to the absorption spectrum from atoms on the far side of the secondary where the orbital velocity is greater than at the center of mass of the star. This effect is, as expected, much more pronounced when the accretion disk luminosity is high (i.e. when the mass accretion rate is above the quiescent level). Consequently, even if the system is only partially in outburst, the radial velocity of the secondary star in

a dwarf nova should not be measured if an accurate K value is desired.

In view of the above discussion it appears that masses may only be obtained for systems which (1) have a long enough period for the secondary to be detected, (2) have radial velocity curves for both components obtained while the system is at quiescence, and (3) are eclipsing so the orbital inclination is known. It is worth pointing out that sin i cannot always be easily specified even for eclipsing systems because the eclipse is sometimes of the disk rather than the white dwarf, allowing systems with i ~ 65 - 70° to eclipse (e.g. U Gem, Z Cam). Consequently, for the disk eclipsers, the eclipse profile must be analyzed and compared with theoretical models in order to get a reasonable estimate for the orbital inclination. In addition, considering that only ~20% of the known CBs have P ≥ 6 hours, it is easy to understand why so few reliable masses are known. In conclusion, it appears that if we are restricted to directly determined masses, then we are doomed to a poor knowledge of CB masses.

B. Indirect Methods

In spite of the failure of the direct method described above to be useful in determining the masses of the vast majority of CBs, there are two "indirect" methods which can potentially allow us to estimate the masses of virtually all known CBs. One method described by Robinson (1973, 1976a) allows one to determine the masses of CBs which have a known orbital period and either a known mass ratio or known orbital inclination and white dwarf (i.e. accretion disk) semiamplitude. The other method, described by Warner (1973), is essentially an extension of the Robinson method and can be applied to virtually all CBs with a

single lined spectroscopic orbit (i.e. with a knowledge of the semiamplitude of the white dwarf).

Both methods are based on two major assumptions: (1) the secondary star fills its critical Roche surface (a reasonable assumption since mass transfer is known to exist) and (2) the secondary star obeys the mass-radius relation for main sequence stars. This second assumption is somewhat uncertain, although the observational evidence to date seems to indicate that this is not a bad approximation for most systems with $2 < P(hr) < 8$ (Patterson 1983). Patterson has compared the masses and radii of the secondary stars observed in several CBs with both theoretical and empirical mass-radius relations for the lower main sequence. He found that, although the secondary stars were somewhat larger than the theoretical zero age main sequence stars of the same mass, they were consistent with the empirical zero age main sequence of Lacy (1977).

Because the Warner method is an extension of the Robinson method, we will begin by outlining the latter method. From Kepler's Third Law, we can immediately write

$$M_2 = 4\pi^2 a^3 [GP^2 (q + 1/q)]^{-1} \qquad\qquad II.3$$

where M_2 is the mass of the secondary, a is the separation between the center of the stars, P is the orbital period, and $q(\equiv M_2/M_1)$ is the mass ratio of the system. Assuming that the secondary star fills its Roche lobe, Paczynski (1971) and Plavec (1968) have shown that, to within an accuracy of $\sim 2\%$, R_2/a can be expressed as a function of q alone. From

Paczynski (1971), we have

$$R_2/a = \begin{cases} 0.38 + 0.2 \log q & 0.5 < q < 20 & \text{II.4a} \\ 0.462[q/(1 + q)]^{1/3} & 0 < q < 0.5. & \text{II.4b} \end{cases}$$

Robinson (1973, 1976a) adopted equation II.4a because he was only interested in long period systems where $M_2 > 0.7\ M_\odot$ and therefore $q \gtrsim 0.5$ for white dwarf masses less than the Chandrashekhar limit. Robinson further assumed a linear mass radius relation for the lower main sequence (i.e. $R/R_\odot = \beta\ M/M_\odot$). Using this mass-radius relation, solving equation II.4a for a and inserting this value into equation II.3, we obtain the following expression for the secondary mass (Robinson 1973a, 1976a equation 1):

$$(M_2/M_\odot) = [0.996 \times 10^{-8}\ P^2\ (q + 1/q)\ (0.38 + 0.2 \log q)^3]/\beta^3. \quad \text{II.5}$$

Consequently, with a knowledge of the mass ratio q, we can determine M_2 and then using q obtain M_1. Alternatively, if the orbital inclination is known, then the mass function allows us to obtain an independent expression for $M_2(q)$ if the period and semiamplitude of the primary can be measured. Specifically,

$$M_2 = [(1 + \frac{1}{q})^2/(\sin^3 i)]\ [(P\ K^3_1)/(2\pi G)]. \quad \text{II.6}$$

Equation II.6 in conjunction with equation II.5 allows one to solve for M_2 and hence for M_1.

In our analysis, we will make a few modifications to equation II.5. First, instead of simply adopting equation II.4a, we will adopt a more

general formula for R_2/a given in Eggleton (1983). We have

$$R_2/a = 0.49q^{2/3}/\left(0.6q^{2/3} + \ln(1 + q^{1/3})\right),$$ II.7

which is accurate to 1% for $0 < q < \infty$. Next, instead of adopting a linear mass-radius relation as Robinson does, we will adopt a power law expression

$$R_2/R_\odot = b(M/M_\odot)^x$$ II.8

(Faulkner 1971). Echevarria (1983) has determined values of b and x from a least squares fit of data on the masses and radii of 25 spectroscopic and visual binaries with main sequence components taken from Popper (1980). Echevarria (1983) finds

$$R/R_\odot = 1.057(\pm\ 0.024)(M/M_\odot)^{0.906(\pm 0.027)}.$$ II.9

Using this mass-radius relation and the expression for R_2/a given in equation II.7 and equation II.3 we can obtain an expression for M_2 as a function of the orbital period and the mass ratio of the system. After some algebra, we obtain:

$$M_2/M_\odot = \left[\frac{9.96 \times 10^{-10}\ (1 + 1/q)P^2q^2}{[0.6q^{2/3} + \ln(1 + q^{1/3})]^3}\right]^{0.582} \qquad P \lesssim 3\cdot10^4\ s$$ II.10

As an added bonus, equation II.10 allows us to derive an expression for the orbital inclination as a function of P, q, and K_1. Employing Kepler's Third Law and noting that $K_1 = (2\pi aq \sin i)/(P(1 + q))$ for

circular orbits, we find:

$$i = \sin^{-1}\left[\frac{(5.93 \times 10^{-3})\ K_1\ P\ (1 + q)}{q[P^2(1 + 1/q)]^{1/3}\left[\dfrac{(1 + 1/q)P^2q^2}{(0.6q^{2/3} + \ln(1 + q^{1/3}))^3}\right]^{0.194}}\right] \qquad \text{II.11}$$

or, in a more convenient form

$$i = \sin^{-1}\{3.79\ 10^{-3}\ K_1(\text{km s}^{-1})(1 + 1/q)^{2/3}\ P(\text{hr})^{-0.055}\ G(q)\} \qquad \text{II.12}$$

where $G(q) = [(q^2 + q)/(0.6q^{2/3} + \ln(1 + q^{1/3}))^3]^{-0.194}$,
and $G(q) \cong 1$ for $0.2 < q < 2$.

Equation II.12 is similar to the relation found by Warner (1976, equation 13). Warner's expression is somewhat simpler than ours because he adopted a linear relationship between the mass of the secondary and the orbital period which was independent of the mass ratio q. If we neglect our $G(q)$ and $P^{-0.055}$ terms (which are nearly unity over the relevant parameter space) then equation II.12 reduces to an expression which is nearly identical to equation 13 of Warner (1976). The only difference is that our constant $(3.79\ 10^{-3})$ is somewhat larger than Warner's due to our revised mass-radius relation for the secondary star.

In summary, the Robinson method is given by equation II.5, or, in more general and modified form, by equation II.10. Using this method, a knowledge of the orbital period of the system and the mass ratio q (either from a double lined radial velocity curve or from a single lined curve and the mass function if sin i is known) will result in the masses of the individual components.

Unfortunately, eclipsing systems (i.e. systems with known inclination) are quite rare and the mass ratio can only be directly measured in double lined systems, thereby requiring that the secondary spectra be visible. Because the secondary spectrum is, in general, only observable in systems with $P \gtrsim 6$ hours, the applicability of the Robinson method, while not as restrictive as the direct method, is, nevertheless, quite limited.

The other indirect method, first employed by Warner (1973), has the advantage of being applicable to essentially all CBs for which a single lined radial velocity curve can be obtained. As previously mentioned, the Warner method is essentially an extension of the method just described. In addition to an equation such as II.10, Warner makes use of an additional relation between the mass ratio (q) and two quantities which are, in principal, directly observable in single lined systems. We can derive such an expression by defining a radius in the accretion disk r_d where the orbiting material has the same specific angular momentum as the material spilling over from the secondary at the inner Lagrangian point. Namely,

$$v(r_d)r_d = 2\pi [f(q)]^2 a^2/P, \qquad\qquad\qquad II.13$$

where $f(q)$ is the distance from the center of the primary to the inner Lagrangian point in units of the binary separation, a, and is only a function of the mass ratio. A convenient formula for f, accurate to $\sim 1\%$ as deduced from the tables of Plavec and Kratchovil (1964), is

$$f(q) = 0.5 - 0.227 \log q. \qquad 0.1 \leqslant q \leqslant 10 \qquad II.14$$

For circular orbits, we may immediately write

$$P = (2\pi a_1 \sin i)/K_1. \qquad\qquad \text{II.15}$$

Combining equations II.13, II.14, and II.15, we find that

$$K_1/(v_d \sin i) = [f(q)]^{-2}[q/(1 + q)](r_d/a), \qquad\qquad \text{II.16}$$

where r_d/a is obtained from Kepler's Third Law and equation II.13. Specifically,

$$r_d/a = f^4 (1 + q). \qquad\qquad \text{II.17}$$

Combining this expression with equations II.14 and II.16 yields the desired result, namely

$$K_1/(v_d \sin i) = q(0.5 - 0.227 \log q)^2 \qquad\qquad \text{II.18}$$

where $v_d \sin i$ is the projected circular velocity in the accretion disk at the radius r_d. Equation II.18 is a powerful result. The left-hand side of equation II.18 consists exclusively of quantities which can potentially be derived from the emission lines originating in the accretion disk surrounding the white dwarf. Consequently, equation II.18 allows a determination of q without the detection of any lines from the secondary star. A simultaneous solution of equations II.10 and II.18 provide a determination of both M_1 and M_2. This is an important result because it opens up virtually every CB for which a single lined spectroscopic orbit can be determined, to an analysis for individual masses. Before we start celebrating, however, there is a major problem associated with this method which should be addressed and hopefully

ameliorated. The problem is concerned with how to reliably measure v_d sin i. A substantial portion of this thesis is concerned with the solution to this problem.

In principal, the quantity v_d sin i can be obtained from the line profiles of the emission lines originating in the disk. In the simplest possible disk, namely an infinitesimally thin ring containing material orbiting the white dwarf with velocity v_d, we would expect the emission line profile to have a full width of 2 v_d sin i. If the accretion rings in CBs had no viscosity then a straightforward determination of v_d sin i could easily be obtained from the emission line profiles. However, the viscosity is not negligible and acts to redistribute angular momentum within the ring. Although the exact nature of the viscosity is unknown (it is probably magnetic and/or turbulent) its effects are commonly observed. Accretion of material onto the surface of the central star results in observable X-rays and, in some systems (Novae), eventual thermonuclear runaways. In addition, eclipse observations reveal the outer radii of the disks to be typically 2 – 3 times larger than would be expected if the viscosity were negligible (Sulkanen, Brasure, and Patterson 1981). Finally, the emission line wings are quite extensive, indicating emission from a rapidly rotating region near the surface of the white dwarf.

The net effect of viscosity acting in the initial ring, then, is the production of a flattened accretion disk around the central gravitating body (i.e. the white dwarf). As expected, the emission line profile produced in such a disk is considerably more complicated than it is for a thin ring and is quite dependent on the radial emissivity

25

gradient of the disk. The radial emissivity gradient is, in turn, determined by the radial gradients of such quantities as the temperature, opacity, and optical depth, all of which are poorly known and undoubtedly vary from system to system. Consequently, there is no straightforward way to identify what part of the line profile best represents $v_d \sin i$ by using theoretical models of disk spectra. At the present time, we simply don't understand the physics of the accretion disks that well. Fortunately, this does not present a serious problem since, assuming Warner's method to be essentially valid, we should be able to empirically determine what part of the line profile best represents the quantity $v_d \sin i$. We begin by observing the emission line profiles of a number of systems with known and reasonably reliable mass ratios (i.e. double lined systems and/or single lined eclipsing systems). Then, working backwards, we compute $v_d \sin i$ for each observation using equation II.18. Finally, we locate the position in the observed line profile which has a velocity, $v_d \sin i$. In practice, this can be accomplished either by defining a simple parameter $f \equiv \left(I(v_d \sin i) - I_0 \right)/(I_{max} - I_0)$ which represents the fractional height of the emission line above the continuum (defined by I_0) where the width is equal to $2\, v_d \sin i$, or by inventing a somewhat more complicated parameter ξ, where we define (Shafter 1983b)

$$
\xi = 1 - \frac{\displaystyle\int_{-v_d \sin i}^{v_d \sin i} [I(v) - I(v_d \sin i)]\, dv}{\displaystyle\int_{-\infty}^{\infty} [I(v) - I_0]\, dv} .
\qquad \text{II.19}
$$

Simply stated, ξ represents the fraction of the total Hα line flux which is bounded by the continuum and the line $I = I(v_d \sin i)$.

The usefulness of Warner's method is dependent upon the existence of a universal value (or practically speaking, a narrow range of values) of the parameters f and ξ, as derived from the calibration systems, which can be assumed to be representative of the majority of CBs. In the next section, we will attempt to determine the canonical values of f and ξ.

III. THE CALIBRATION

A. The Systems

In order to determine representative values for the parameters f and ξ we have observed the Hα line profiles of every well studied CB north of declination $-30°$ which has a directly determined mass ratio (i.e. ones in which q has been determined from a double lined radial velocity study). There are 7 such systems: AE Aqr, Z Cam, EM Cyg, SS Cyg, U Gem, AH Her, and RU Peg. In addition Hα line profiles of four single lined eclipsing systems: DQ Her, LX Ser, RW Tri, and HT Cas were obtained for use in the calibration.

Before we proceed further with the discussion of the line profile observations, it is important to discuss some of the problems associated with performing the calibration. First of all, because CBs, and in particular dwarf novae, are photometrically and spectroscopically variable, we expect that the emission line strength and profile will be variable as well. If the variation is large and unpredictable, this could be a serious complication in our attempt to determine the apropriate values of f and ξ. With this problem in mind, whenever possible more than one observation was obtained for each calibration system in order to assess the degree of line profile variability characteristic of that system. A complete discussion of the variability will be presented later in this section. In the meantime, we turn to the discussion of the calibration systems themselves.

Table II lists all 11 calibration systems, the relevant orbital parameters for each system, along with the appropriate references to the literature. In cases where more than one radial velocity study exists

in the literature (e.g. SS Cyg, RU Peg, EM Cyg), we have determined mean values for K_1 and K_2 by combining the semiamplitudes from the various studies as described in Appendix III.

The mass ratios $q(\equiv M_2/M_1)$ and their 1σ errors were computed from the ratio of the semiamplitudes of the two components in the cases of the 7 double lined systems. The mass ratios for the single lined eclipsing systems were usually given explicitly in the source paper. In both cases, the 1σ errors in the semiamplitudes or individual masses were propagated to the mass ratio in the usual way (see Appendix IV). Once the mass ratios and their standard errors for each of the 11 systems were obtained, the required values of the parameter $v_d \sin i$ were computed. Rearranging equation II.18, we obtain

$$v_d \sin i = K_1/[q(0.5 - 0.227 \log q)^2].$$ III.1

The values of $v_d \sin i$ along with their 1σ errors (again see Appendix IV for the error propagation analysis) are presented in column 7 of Table II. Now that we have the required values of $v_d \sin i$ for the 11 calibration systems, we are ready to determine canonical values for the parameters f and ξ from our line profile observations. As mentioned earlier, we have obtained more than one observation of each calibration system, when possible, in order to study the consistency of the determinations of f and ξ for a given calibration system. The line profiles are presented in Figures 2a-ff where we have plotted the relative intensity as a function of wavelength. All observations were obtained by using the Robinson-Wampler Image Dissector Scanner. Since this instrument has a nearly linear response for the relatively low

counting rates which were encountered, the observed count rate is
assumed to be proportional to the intensity of the source (see
discussion in Appendix I). The dashed lines in Figures 2a-ff represent
the value of $v_d \sin i$ appropriate for the particular system.

B. Equivalent Width Variations

It has long been recognized that the strength of the emission lines
relative to the continuum (i.e. the equivalent width of the line) in a
CB is a function of the luminosity of the system. Before we determine
the canonical values of f and ξ, it is worth spending a little time to
explore why this is the case and to predict what effect a change in a
particular system's luminosity (or alternatively in the equivalent width
of Hα) will have on the derived values of f and ξ. In order to make
such a prediction we need to briefly review how the emission lines are
produced. According to the current accretion disk models (Mayo,
Wickramasinghe, and Whelan 1980; Tylenda 1980; Williams 1980), the low
excitation optical emission lines such as the Balmer and He I lines are
formed in the outer, relatively cool regions of the disk which is
optically thin in the continuum and optically thick in the lines. The
continuum, on the other hand, is produced in the inner optically thick
regions of the disk. The high excitation lines such as He II $\lambda4686$ and,
in the ultraviolet, C IV $\lambda1550$, N V $\lambda1240$, and He II $\lambda1641$ are believed
to be produced in an extended disk corona which is powered by the high
energy photons originating in the inner disk and disk/white dwarf
boundary layer (e.g. see Jameson, King, and Sherington 1980). There is
some evidence from time resolved spectroscopy of eclipsing systems which
indicates that the He II $\lambda4686$ line may originate in the inner disk

region itself (Williams and Ferguson 1982). Since the luminosities of the component stars are not expected to be time variable, any changes in the system luminosity must arise from changes in the disk luminosity. The disk luminosity is directly proportional to the mass transfer rate through the disk. Therefore, for a given orbital period, the higher the system luminosity, the higher the mass transfer rate. This results in the interface between the optically thick inner part of the disk and the optically thin outer disk moving outward to a larger disk radius. Consequently, the ratio of continuum to line flux increases (i.e. the equivalent width decreases) as the luminosity (i.e. mass transfer rate) increases. Because the disk is rotating differentially (the gas is in Keplerian motion around the white dwarf), the line width is dependent on the disk radius where the line is formed. We expect that when the optically thick/optically thin interface is displaced to larger radii as is the case when the luminosity increases, that the line width will decrease as well as the equivalent width.

We are now able to predict, in light of the qualitative disk structure described above, what effect an increase in the system's luminosity will have on the resulting value of f and ξ for a given $v_d \sin i$. If the system is above its quiescent luminosity, we expect that we will have to measure further out in the line wings to reach the required value of $v_d \sin i$ because the line width will be somewhat less than it is at quiescence. Measuring further out in the line wings corresponds to smaller values of the parameters f and ξ. Put simply, we predict that $f(EW)$ and $\xi(EW)$ will be increasing functions of the equivalent width of the lines.

We should stress the point that the above conclusion is based on the assumption that the entire Balmer emission line flux originates in the main body of the disk. If, on the other hand, a significant, narrow component of the emission is produced in a lower velocity region such as the hot spot or in the vicinity of L_1, it is possible that an increase in the strength of this narrow component would cause the line width (for a fixed value of f or ξ) to decrease as the equivalent width increases. Obviously, in this case we would propose quite a different prediction, namely tht f(EW) and ξ(EW) will be decreasing functions of the equivalent width of the emission lines. After computing the values of f and ξ for the individual line profile measurements, we will determine which of these two predictions is correct for a given system.

C. The Values of f and ξ

We are now ready to present the values of f and ξ as determined from the individual line profile observations. For the reasons just described, we have kept track of the equivalent width for each line profile. In addition, we have made an attempt to correct for the effects of instrumental broadening of the emission lines by adjusting the values of $v_d \sin i$ as follows: If $(v_d \sin i)_c$ is the corrected velocity then

$$(v_d \sin i)_c \cong \left[(v_d \sin i)^2 + (R(\text{HWHM}))^2 \right]^{1/2} \qquad \text{III.1}$$

where R is the resolution of the data in km s^{-1}. We have assumed that the line profiles are essentially Gaussian in the line core, and that $2 v_d \sin i$ is approximately the FWHM of the emission line. The correction procedure proved to make little difference in our

computations since $2 v_d \sin i \gg R$ (FWHM).

Table IIIA shows the derived values of f and ξ and the measured equivalent widths for the 32 line profile observations of the 11 calibration systems. We have included the $\pm 1\sigma$ errors for each value of f and ξ. Note that the errors are <u>not</u> symmetrical about the mean value of f or ξ in Table IIIB. This is not surprising considering that the line profiles are nearly Gaussian and the width of a Gaussian is a non-linear function of both its fractional height (f) and its fractional area (ξ).

Before we combine the individual values of f and ξ for the different systems to determine the canonical values of these parameters, we first consider the individual values for each system in order to see if our prediction of how f and ξ vary with the equivalent width is borne out. Figure 3 shows a plot of f versus the equivalent width (EW), for all of the calibration systems with multiple observations. The equivalent width for a given system has been normalized to the maximum equivalent width for that particular system. The value of f has also been normalized to its value at the maximum equivalent width (i.e. $f_{max} = f(EW = EW_{max})$.

By referring to Figure 3, it is obvious that there is no well defined relationship between the equivalent width and the derived values of f. The novalike variables AE Aqr and LX Ser seem to indicate that the general trend is for the line width to slightly decrease, for a given value of f, as the equivalent width increases. The value of f seems to be relatively independent of the equivalent width for the dwarf novae SS Cyg and U Gem. Only the dwarf nova RU Peg seems to indicate a

33

decrease in the value of f as the equivalent width decreases. We conclude that the mechanisms behind our two predictions desribed earlier tend to cancel each other out for relatively small equivalent width variations. Of course, if the equivalent width was much smaller than EW_{max}, as would be expected if a dwarf novae were in outburst, then we would expect our first prediction to hold and the derived value of f to be much too small. I have deliberately avoided dwarf novae in outburst in the calibration, so this effect is not demonstrated in Figure 3. In any case, it appears that f is not strongly dependent on EW for $EW/EW_{max} > 0.5$.

I have combined the 32 individual values of f and ξ from the 11 calibration systems following the analysis presented in Appendix V. The resulting grand canonical values for f and ξ are as follows:

$$\langle f \rangle = 0.30 \begin{array}{l} + .07 \\ - .06 \end{array}$$

$$\langle \xi \rangle = 0.58 \begin{array}{l} + .09 \\ - .07 \end{array}.$$

These values are a major result of this dissertation. They describe where to measure $v_d \sin i$ in order to estimate the mass ratio of single lined CBs.

D. The Relationship Between f and ξ

At this point it is worth pausing for the moment and taking time to explore the relationship between the parameters f and ξ. In particular, the following questions immediately come to mind.

34

(1) Which, if either, parameter is preferable to employ when determining $v_d \sin i$?

(2) Is there any significance to the fact that the errors associated with ξ are somewhat larger?

(3) What do the actual values of $f = 0.30$ and $\xi = 0.58$ reveal about the line profiles of the calibration systems?

We can address the latter two questions by exploring the functional relationship between f and ξ for a couple of simple examples. For the simplest possible line profile, namely a rectangle, it is obvious that $f = \xi$. But what about a more realistic profile, such as a Gaussian? In this case, after some algebra, we find that

$$\xi(f) = 2Q(\sqrt{-2 \ln f}) + \sqrt{2/\pi} \; f\sqrt{-2 \ln f} \qquad \text{III.2}$$

where $Q(x) = (1/\sqrt{2\pi}) \int_x^\infty e^{-t^2/2} \, dt$.

This functional relationship is shown graphically in Figure 4. It is interesting to note that $\xi(f = 0.30) = 0.49$ and not 0.58. This disagreement is not alarming; it simply means that the line profiles are not strictly Gaussian. The flux in the line wings is noticeably stronger than that which would be expected for a Gaussian profile. This excess flux is precisely what the values of f and ξ indicate. The parameter ξ is larger than what is predicted if the lines were Gaussian because of the excess flux in the line wings. Again referring to Figure 4, we see that the slightly larger error in ξ is a natural consequence of the fact that the slope of the curve is slightly greater than 1 in the region of interest.

Because of the fact that there is no significant difference between the errors of f and ξ, it appears that neither parameter is preferred over the other. From a practical standpoint, however, each parameter has its own advantages and disadvantages. For example, the measurement of f requires an accurate measurement of the peak intensity of the emission line; this measurement can be complicated by the effect of a strong sharp S-wave component in the line profiles. The measured value ξ, on the other hand, is sensitive to the precise identification of the continuum level. Whenever possible, both parameters should be measured to assure that neither one of the sources of error described above is adversely affecting the determination of v_d sin i.

E.   Demonstration of the Calibration

Before we proceed to the next section and compute the mass ratios of several single lined CBs, it is of considerable interest to know how accurately our values of $\langle f \rangle$ and $\langle \xi \rangle$, in conjunction with equation II.18, can predict the mass ratios of the calibration systems themselves! The resulting comparison of the observed values of $K_1/(v_d$ sin i) with those predicted using the directly determined mass ratios would provide a good illustration of the usefulness of equation II.18. With this quest in mind, we have measured v_d sin i for all 32 line profile observations of the 11 calibration systems. We have measured each profile twice using both $\langle f \rangle$ and $\langle \xi \rangle$. The weighted means and variances for the 11 calibration systems were then computed via an analysis analogous to that presented in Appendix IV. Figure 5 demonstrates the consistency of the resulting values of v_d sin i computed from $\langle f \rangle$ and from $\langle \xi \rangle$. Armed with the assurance provided by

Figure 5, I have computed the mean value of $\langle v_d \sin i \rangle$ for each calibration system based on the values derived from $\langle f \rangle$ and $\langle \xi \rangle$. The solid lines shown in Figures 2a-ff represents the appropriate value of $\langle v_d \sin i \rangle$ for each calibration system. Next, in Figure 6, I have plotted the resulting value of $K_1/\langle v_d \sin i \rangle$ as a function of the known value of $F(q)$, where, from equation II.14, $F(q) = q(0.5 - 0.227 \log q)^2$. The observed variation of $K_1/\langle v_d \sin i \rangle$ with $F(q)$ can be directly compared with the solid line which is the expected theoretical relationship, namely that these two quantities are equal. The observed correlation of $K_1/(v_d \sin i)$ with $F(q)$ is undeniable. In particular, a correlation analysis reveals that the relationship between these two parameters is characterized by a correlation coefficient of $R = 0.92$. The vertical error bars reflect the errors both in K_1 and in $\langle v_d \sin i \rangle$. For the reader who prefers more transparent units for the abscissa of Figure 6, we have plotted the observed value of $K_1/(v_d \sin i)$ versus q in Figure 7. The error bars have been omitted from this figure in order to make the comparison between the observed points and the theoretical relationship more obvious. Because Figures 6 and 7 represent a major conclusion of this work, it is worth reviewing both figures once again and noting how well the observed values of $K_1/\langle v_d \sin i \rangle$ follow the theoretical relationships.

IV. MASS ESTIMATES FOR SINGLE LINED CATACLYSMIC BINARIES

A. The Mass Ratios

Now that we have determined the canonical values for the parameters f and ξ we may proceed to estimate the mass ratios for several single lined CBs. Table IV lists 20 systems for which single lined radial velocity curves and Hα line profile observations are available. This list includes all single lined systems known which have reasonably well determined semiamplitudes and which are not believed to contain strongly magnetic white dwarfs. Such systems (e.g. the AM Her stars) do not have fully developed accretion disks and therefore $v_d \sin i$ cannot be measured from the emission line width.

Of the 20 systems in Table IV, the radial velocity curves for 13 of them have been determined by the author for the purpose of this study. The radial velocities were measured by using the method outlined in Appendix II. After measuring the velocities, I have made a non-linear least squares fit to a circular orbit of the form

$$V(t) = \gamma + K_1 \sin [2\pi(t - t_0)/P] \qquad\qquad IV.1$$

I have plotted the radial velocities as a function of orbital phase in Figures 8a-q. For systems having a sufficiently large number of observations, I have co-added the individual spectra into ten phase bins. Then, as described in Appendix II, I have remeasured the velocities of the ten co-added spectra in an attempt to determine the best value of K_1.

In order to minimize systematic errors, the Hα line profiles for all of the systems from Table IV were obtained by using the same

38

instrumentation, the Robinson-Wampler Image Dissector Scanner. For the 13 systems whose radial velocity curves were obtained by the author, I have simply summed the spectra used in the radial velocity study after correcting for orbital motion. In cases where the radial velocity observations were obtained on different observing runs, or if the equivalent width changed significantly during the same run, the spectra from each of the different nights were summed separately. For the remaining 9 systems, measurements of the Hα line profile were obtained as many times as possible by using the highest dispersion which was available at the time. The integration time, dispersion, etc. for each line profile measurement are presented in Appendix I (summary of observations), and the line profiles are shown in Figures 9a-m. As was the case for the calibration systems, the relative intensity has been plotted as a function of wavelength. In addition, because many of the 13 systems for which I have determined orbital periods are relatively obscure, low dispersion spectra of each of these systems are shown in Figures 10a-m. These figures are meant primarily to provide the reader with a knowledge of the general spectral character of each system. The equivalent widths of the prominent emission lines are summarized in Table V. With the exception of the VY Sculptoris system KR Aur, which was experiencing one of its rare minima, the ultrashort period systems have the strongest emission lines. The accretion disks in the systems have extensive optically thin regions indicating low mass transfer rates in agreement with the conclusion of Patterson (1983).

We can estimate mass ratios for all 20 single lined systems using equation II.18. The value of v_d sin i for a given system has been

determined based on our canonical values of $\langle f \rangle$ and $\langle \xi \rangle$. In cases where there are multiple line profile measurements for the same system, we can compute $v_d \sin i$ for each line profile observation using both $\langle f \rangle$ and $\langle \xi \rangle$. I have corrected for instrumental broadening as described in Section III. We can then compute the weighted mean of the individual $v_d \sin i$ measurements for both $\langle f \rangle$ and $\langle \xi \rangle$. The error analysis parallels that found in Appendix V. Finally, we can compute the grand mean $\langle v_d \sin i \rangle$ for each system by combining the values derived using $\langle f \rangle$ and $\langle \xi \rangle$. The value of $\langle v_d \sin i \rangle$ and the resulting value of the mass ratio, q, for each system is presented in Table IV. The error in the mass ratio has been determined from the errors in K_1 and $\langle v_d \sin i \rangle$ in the usual way (see Appendix IV). In order to determine if the line width is a function of orbital phase, we have measured $v_d \sin i$ for TW Vir and SW UMa at several different orbital phases. As can be seen by referring to Figures 9a-m, it is apparent that the line width is not significantly affected by orbital phase.

B. Discussion of the Mass Ratios

Several authors have claimed a correlation between the mass ratio and the orbital period of the binary. For example, Warner (1973) argued that $q \propto P$ based on 9 systems. Subsequently, Ritter (1976) in a criticism of Warner's analysis, suggested that $q \cong$ constant $\cong 1$ based only on systems with directly determined mass ratios. More recently, Bruch (1982) has suggested a non-linear relationship between q and P. In order to determine if our much larger and more homogeneous data base is consistent with any of the above interpretations, I have plotted the mass ratios for the 20 single lined systems and the 11 calibration

systems in Figure 11. In addition, I have included the mass ratios of

OY Car, Z Cha, and AM Her. Vogt (1980) and Vogt et al. (1981) have

determined mass ratios of 0.2 ± 0.07 and 0.15 ± 0.06 for Z Cha and

OY Car respectively, while Ritter (1980a, 1980b) has found

$q = 0.46 \pm 0.07$ and 0.4 ± 0.06 for these two systems. The

determinations of both authors were based on an analysis of the eclipse

light curves. The discrepancies between the mass ratios for each system

were due to the different times of ingress and egress of the white dwarf

that were adopted by the two authors. For the purposes of Figure 11, I

have adopted the mean of the two determinations for both systems. It

should be pointed out that if the secondary is not on the main sequence,

then the mass ratios of these two systems will be lower limits. The

mass ratio for AM Her has been adopted from Young, Schneider, and

Shectman (1981c).

The first impression which is immediately obtained from an

inspection of Figure 11 is the lack of any striking correlation. There

does, however, appear to be a general tendency for the longer period

systems to have a slightly larger value of q. In addition, Figure 11

shows the best fit linear least squares line which demonstrates the

apparent trend of q with orbital period. The purpose of showing this

line is not to imply a functional relationship between q and P. It is

meant as a comparison of our results with those of Warner (1973) and

Ritter (1976). The relatively large scatter about this line prohibits

us from unequivocally confirming or denying Warner's or Ritter's

interpretations. Our results seem to suggest that if a relationship

exists at all, it is probably intermediate between the ones suggested by

41

these authors. In particular, in view of my results, it appears that while there may be a correlation between the mass ratio and orbital period, it is <u>much weaker</u> than the relationship proposed by Warner. The solid line presented in Figure 11 is described by:

$q = 0.06 \ P(hr) + 0.4.$

Given the mass ratios presented above, we can compute the white dwarf masses if we have estimates of the secondary masses. As outlined in Section II, M_2 can be computed if the mass ratio and orbital period are known, and if we make the assumption that it is a main sequence star. Using equation II.10, we can compute the masses of the secondary stars for the 20 single lined systems as well as the 11 calibration systems. The results are presented in Table VI. The errors have been computed based on the errors associated with P and q and with the mass radius relations (for the details of the error propagation see Appendix IV.) The errors are, in general, quite small due to the high accuracy for which most of the orbital periods are known and because of the weak dependence of M_2 on the relatively uncertain values of q. For completeness, I have also included an estimate of the orbital inclination, i, as computed from equation II.12. The error estimates for the inclinations have been computed in the usual way (again see Appendix IV). The inclinations tend to be very uncertain for $i > 60°$ because of the steepness of the arcsin(x) function as the argument approaches unity. Nevertheless, our estimates of the inclination based on equation II.12 are consistent with independently known inclinations. In particular, known eclipsing systems have $i > 60°$ with the exception of UX UMa and PG1012-029. Our estimates for the inclinations of these

two systems are obviously too small; however, their 1σ errors are quite

large and do include the independently estimated inclinations. I

predict that future observations may show CM Del to be an eclipsing

system.

C. The White Dwarf Masses

We are finally in a position to estimate the masses of the white

dwarfs for the systems with available mass ratios. The white dwarf

masses and their 1σ errors are presented in Table VI. As in the case of

the mass ratios, I have plotted M_1 as a function of orbital period in

Figure 12. I have plotted the masses below the period gap (i.e.

$P < 2.5$ hr) as upper limits because of the possibility that the

secondaries are degenerate in these ultrashort period systems. Again,

there is no striking correlation with orbital period. However, there

appears to be a weak correlation suggesting that M_1 is an increasing

function of orbital period. This trend can be seen more clearly in

Figure 13, where I have grouped the masses into regions: (A) The

ultrashort period group ($P(hr) < 3$), (B) the short period group

($3 < P(hr) < 6$), and (C) the long period systems ($6 < P(hr) < 10$).

Considering that M_2 is highly correlated with the orbital period and

that $q \cong$ constant the trend shown in Figure 12 and 13 is not unexpected.

In fact, we can use the relationship between M_2 and P (equation II.10)

along with the suggested $q - P$ relationship from Figure 11 to predict

how M_1 should depend on P. In particular, with the aid of equation

II.10, we can derive the following expression for $M_1(P)$:

43

$$M_1(P) = \frac{\left[\dfrac{9.96 \times 10^{-10} \left(1 + 1/(aP + b)\right)P^2 (aP + b)^2}{\left(0.6 (aP + b)^{2/3} + \ln[1 + (aP + b)^{1/3}]\right)^3}\right]^{0.582}}{(aP + b)}. \qquad \text{IV.2}$$

In the previous equation I have adopted $a = 0.06$ and $b = 0.40$, based on the solid line from Figure 11.

I have plotted this function in Figure 12. If q was directly proportional to P (i.e. if $b = 0$) then $M_1(P) \cong$ constant. This was the conclusion drawn by Warner (1973). As mentioned earlier, while our results are not in violent disagreement with Warner's conclusion, there does seem to be a general trend for M_1 to increase with orbital period. Again, I emphasize that the curve drawn in Figure 12 is not meant to imply a strict functional relationship between M_1 and P. It has only been included to illustrate the general trend which apparently exists between these two quantities. In addition, Warner (1973) concluded that M_1 was not only constant but that the white dwarf masses were clustered near 1 $M_\odot$. Referring to Table VI, we see that the majority of CBs have white dwarf masses <u>less</u> than 1 $M_\odot$. The mean of all 35 white dwarf masses is $\langle M_1 \rangle = 0.65 \pm 0.27\ M_\odot$; a value consistent with the average for field white dwarfs (Weideman 1975; Koester, Schulz, and Weidemann 1979). I have deliberately excluded indirectly determined masses obtained by other workers from Figure 12. This was done in order to increase the possibility of detecting any trends with orbital period in the event that our masses were systematically different from those of other workers. We can, however, make a comparison of our masses with the few available masses from the literature.

The number of mass estimates available in the literature is somewhat limited primarily because of the fact that radial velocity curves were not available for 13 of the systems until the present study. The masses estimated by other workers are included in Table VII. In general, the agreement with our results is reasonably good. Our masses tend to be somewhat smaller because of the fact that we have adopted a new and more reliable mass-radius relation for the secondary given in Echevarria (1983).

In general, our results tend to be more in line with the conclusions of Ritter (1976) who found that $q \cong$ constant and proposed that M_1 was proportional to P. As we will see in the next section, a general trend toward large white dwarf masses for longer period CBs is consistent with the evolutionary history of these binaries. Before we leave this section, I wish to emphasize that (although the individual masses are not known with high precision) from a statistical standpoint, I feel confident that the general trend for the average white dwarf mass to increase as a function of orbital period , as shown in Figure 13, is supported by the results of this dissertation.

V. DISCUSSION OF THE WHITE DWARF MASSES

A. Review of Cataclysmic Binary Evolution

> "The discovery of the binary nature of DQ Her not
> only provides us with the possibility of obtaining
> direct information regarding the physical make-up of an
> old nova but also raises several interesting questions
> concerning the evolution of a nova: Has the present
> binary system existed since the original formation of
> the stars, or did a single star undergo fission during
> the nova stage in 1934? If it has existed as a binary
> system since the formation of the stars we encounter
> another problem. If the current ideas of stellar
> evolution are correct, then we should expect that at one
> stage in its development the nova component must have
> been a red giant. Since the shortness of the period
> indicates that the stars are very close together, during
> the red giant phase the companion star would have had to
> revolve deep within the expanded photosphere of the nova
> component.[4] It is to be hoped that an examination of
> plates taken before the 1934 nova outburst may establish
> whether or not the star was a binary at that time."

[4] I am indebted to Dr. W. Baade for this suggestion.

-- Walker (1954).

We begin this section by briefly describing the currently

acceptable scenario for the evolutionary history of CBs (following

Paczynski 1983). It is generally believed that CBs evolve from binary

systems having orbital periods of several months to years which have

mass ratios significantly different from unity. In these initially

widely separated systems, the more massive component evolves from the

main sequence and expands to become a red giant or supergiant before

filling its critical Roche surface. By this time, the evolved component

has developed a massive degenerate core and a convective envelope.

After the red giant component fills its Roche lobe, a phase of rapid

mass transfer begins in which material from the red giant is transferred

via L_1 to the secondary component, which is a low mass main sequence star. Because the mass losing star is the more massive component and has a convective envelope, the mass transfer occurs on a convective or even dynamical time scale (Paczynski, Ziolkowski, and Zytokow 1969; Lauterborn and Weigert 1972; Paczynski and Sienkiewicz 1972). As a result, an extended envelope develops around the secondary; the binary eventually evolves to a contact configuration and finally, a common envelope engulfs the degenerate core and the main sequence secondary. As the two compact cores transfer angular momentum to the extended envelope, they gradually spiral in toward a shorter period and smaller separation. Finally, the envelope is lost and we are left with a very short period binary consisting of the degenerate primary and a low mass dwarf (Ostriker 1973; Eggleton 1976; Paczynski 1976; Ritter 1976; Taam, Bodenheimer, and Ostriker 1978; Meyer and Meyer-Hofmeister 1979; Livio, Saltzman, and Shaviv 1979; Livio 1982). There are several examples of such systems which are thought to have recently emerged from the common envelope stage of evolution and are now the nuclei of planetary nebulae: UU Sge (Bond, Liller, and Mannery 1978), V477 Lyr = Abell 46 (Grauer and Bond 1981), VW Pyx (Bond 1981), BD+50° 2869 = NGC 6826 (Noskova 1982), and Abell 41 (Grauer and Bond 1983). Subsequent to the planetary nebula phase described above, the primary settles down to become a white dwarf, the late type dwarf component settles down to an equilibrium radius appropriate for its mass, and the system becomes a short period detached binary. Examples of such systems are V471 Tau = BD+16° 516 (Nelson and Young 1970; Young and Capps 1971), HZ 9 (Lanning and Pesch 1981), GK Vir = PG 1431+01 (Green et al. 1978), UX CVn = HZ 22 (Young, Nelson,

47

and Mielbrecht 1972; Young and Wentworth 1982), BE UMa (Ferguson et al. 1981) and Case 1 (Lanning and Pesch 1981; Lanning 1982). Finally, after a sufficiently long time, as a result of angular momentum loss from the system, the secondary component contacts its critical Roche surface and mass transfer ensues giving rise to a cataclysmic binary. If at this time the mass losing secondary is more massive than the white dwarf (as would be the case for a low mass white dwarf in a long period system) then a stage of rapid mass transfer on a thermal time scale will occur until the mass ratio is reversed. This phase of rapid mass transfer should be relatively short lived; we should not expect to see many systems in this evolutionary state.

After reversal of the mass ratio, mass loss from the secondary will result in an increase of the binary separation and a subsequent increase in the radius of the secondary's Roche lobe. Consequently, mass transfer in the system must be driven by angular momentum loss from the system which more than compensates for the effects of the changing mass ratio.

The mechanisms of angular momentum loss appropriate for CBs have just recently begun to be well established. Gravitational radiation will act as a sink of angular momentum and shorten the orbital period on a time scale of $\sim 10^{10}(P/4 \text{ hrs})^{1.44}$ years (Patterson 1983) and is consequently only important for the ultrashort period systems (Paczynski and Sienkiewcz 1981, 1983; Rappaport, Joss and Webbink 1982; Taam 1983). For the longer period systems, it appears that angular momentum loss is due to a stellar wind which is magnetically coupled to the secondary. This phenomenon, known as "magnetic braking", has recently been the

subject of considerable interest in evolutionary models for CBs
(Eggleton 1976; Whyte and Eggleton 1980; Verbunt and Zwaan 1981; Taam
1983; Paczynski and Sienkiewicz 1983; Patterson 1983; Spruit and Ritter
1983; Rappaport, Verbunt, and Joss 1983). We will return to the
discussion of magnetic braking in Section VI in the discussion of the
VY Sculptoris phenomenon.

In view of the evolutionary scenario described above, it is natural
to expect that CBs with relatively massive white dwarf components
originated as relatively long period, extreme mass ratio systems. It is
only in these relatively long period systems that the red giants are
able to grow high mass degenerate cores. In particular, calculations by
Webbink (1979b) have shown that initially short period, low mass systems
(region IIIa in his Figure 3) will interact tidally before the
degenerate core has grown to critical mass for helium ignition.
Consequently, these systems should give rise to CBs containing low mass
(0.18 – 0.46 $M_\odot$) helium white dwarfs. The longer period systems (region
IIIb) interact after the primary has reached the asymptotic giant branch
and, as a result, leave more massive (0.56 – 1.4 $M_\odot$) carbon–oxygen white
dwarfs. In terms of the traditional notation (cf. Kippenhahn and
Weigert 1967; Lauterborn 1970) the low mass helium and the relatively
large mass carbon–oxygen white dwarfs are a result of Case B and Case C
evolution, respectively.

More recently, Law and Ritter (1983) have pointed out that the mass
spectrum of Case C white dwarfs should be shifted to slightly smaller
masses than the spectrum of white dwarfs formed in single stars.
Because of the fact that the average mass of field white dwarfs is less

49

than 0.65 $M_\odot$ (Weidemann 1975; Koester, Schulz, and Weidemann 1979), Law and Ritter have argued that the massive ($> 1 M_\odot$) white dwarfs found in some long period CBs must be formed via evolutionary scenario other than Case C. These authors propose that the massive white dwarfs are formed via Case BB mass transfer. In Case BB evolution, a Helium star is formed as an intermediate product after a first stage of non-conservative Case B mass transfer. Then, for a certain range of masses, the helium star becomes a red giant during its shell burning phase and can therefore reduce its mass below the Chandrashekhar limit in a second stage of Case B mass transfer (Delgado and Thomas 1981).

Webbink (1979a) has proposed that the scarcity of CBs with orbital periods between 2 and 3 hours (the period gap) is a consequence of the discontinuity in core masses (for stars of a given total mass) between the tip of the giant branch and asymptotic giant branch stars of the same radius. Assuming that this dichotomy in core mass is preserved through the subsequent common envelope evolution, Webbink argues that CBs below the gap should contain low mass helium white dwarfs, while those above the gap should contain more massive carbon-oxygen white dwarfs.

Webbink's explanation for the period gap has fallen into disfavor because of recent observational studies of ultrashort period systems which indicate that $M_1 > 0.6 M_\odot$ for some systems. However, the evidence for massive white dwarfs in ultrashort period systems is not particularly overwhelming. For example, Vogt (1982) and Vogt et al. (1981) studied Z Cha and OY Car and found $M_1 = 0.85$ and $0.95 M_\odot$, respectively, while Ritter (1980a, 1980b) found $M_1 = 0.35$ and $0.3 M_\odot$ for

the same two systems. In addition, as we have already alluded to, our ignorance of the structure of the secondary component makes mass estimates for the ultrashort period systems extremely treacherous business significantly more so than for the long period systems. The possibility that the secondaries in the ultrashort period systems are low mass degenerates renders all calculations of M_1, which are based on the assumption of a main sequence secondary, upper limits. With this in mind, it is difficult to reject Webbink's hypothesis outright until more reliable masses are available for the ultrashort period systems.

In any event, regardless of whether high mass white dwarfs are discovered among the ultrashort period objects, the basic trend for the mean white dwarf mass to increase with orbital period is a natural consequence of the evolutionary scenario which we have presented. As already pointed out, stable long term mass transfer can only be sustained if the accreting white dwarf is the more massive component. Since the secondary mass is very nearly proportional to the orbital period, we would expect that the average white dwarf mass should increase with orbital period as is observed (see Figure 13). I wish to emphasize that this statement is not necessarily in agreement with the conclusion of Webbink (1979a, b). I am not proposing that all ultrashort period systems should contain helium white dwarfs, only that long period systems should not. While it may be true that the majority of systems which form in the ultrashort period regime contain low mass white dwarfs, as Webbink suggests, it is conceivable that the longer period systems could evolve to shorter periods and invade the ultrashort period regime with their carbon-oxygen white dwarfs. The evolution of

51

CBs toward shorter periods will be discussed in greater detail in Section VI.

B. Correlations of White Dwarf Mass with Eruption Characteristics?

At this point, it would be interesting to explore the possibility that a correlation may exist between outburst behavior and the mass of the white dwarf. As we have already pointed out in Section I there are correlations between outburst behavior and orbital period. Consequently, it seems reasonable to expect that the white dwarf masses may be segregated with respect to the different classes of CBs. Unfortunately, our attempts at exploring possible correlations are hampered by ignorance of the overall outburst behavior of several of the systems for which we have determined white dwarf masses. In addition, we have not determined masses for any AM Herculis objects and we have only two mass determinations for old novae. Nevertheless, we will forge ahead and concentrate on identifying possible correlations between the two classes for which we have a relatively large statistical sample: the dwarf novae (and their subclasses) and the novalike variables.

By adopting the white dwarf masses presented in Table VI, I have determined the averages for the masses of the various classes of CBs. The results are presented in Table VIII. In computing the average mass for a given class, I have excluded any systems whose classifications are highly uncertain. These systems are identified by a "?" next to their classification in Table VI. Although we must be wary of any conclusions drawn from Table VIII because of the relatively small sample size within a given class, a few general statements can be made. To begin with, it is obvious that our results do not indicate any significant differences

between the masses of the white dwarfs in the U Geminorum and the Z Camelopardalis subclasses of the dwarf novae. In addition, we find no indication of any variation in masses among the novalikes. There are only two general segregations which are evident. Firstly, it appears that the dwarf novae (excluding the SU UMa systems, whose masses are highly uncertain) contain white dwarfs which are, in general, more massive than the novalikes. This is primarily a consequence of the fact that the novalikes tend to have shorter orbital periods than typical U Geminorum and Z Camelopardalis systems. Secondly, the SU Ursae Majoris systems have white dwarf masses which seem to be smaller than other dwarf novae. There is nothing surprising about either one of these segregations. They are both consequences of the weak dependence of the average white dwarf mass on orbital period.

It has long been theorized that novae should contain relatively large mass white dwarfs. Recent models of novae require white dwarf masses in excess of 1 $M_\odot$ (Fujimoto 1982a, b; MacDonald 1982). It is unfortunate that our sample of CBs only contains two classical novae. As a consequence, we cannot make any meaningful statements from an observational point of view. I only point out that for both novae, V603 Aql and DQ Her, I have estimated masses of 0.66 and 0.62 $M_\odot$ respectively. These values are typical of the mean mass found for all systems: $\langle M_1 \rangle = 0.65 \pm 0.27 \; M_\odot$. Furthermore, as mentioned earlier, both values are consistent with the best estimate of the average mass of field white dwarfs (Weidemann 1975; Koester, Schulz, and Weidemann 1979).

VI. COMMENTS ON THE NATURE OF THE VY SCULPTORIS SYSTEMS

As described in the initial discussion in Section I, the orbital periods of the VY Sculptoris systems appear to be confined to a fairly narrow range adjacent to the period gap. We can strengthen this conclusion by determining the orbital periods of two additional CBs which exhibit the characteristics of VY Sculptoris systems, KR Aur and V425 Cas. The orbital periods of these two systems are 3.9 and 3.6 hours, respectively. In addition, Schaefer and Patterson (1982) and Sherington, Bailey, and Jameson (1983) have reported that the novalike variable VZ Scl has recently faded to a deep minimum characteristic of the VY Sculptoris systems. The orbital period of VZ Scl (P = 3.3 hrs) has been known for quite some time (Krzeminski 1966), and in view of its recently reported minimum, it is not surprising that it lies in the 3 - 4 hour range.

Based on the observed period distribution (see Figure 1e), the probability that the six VY Sculptoris systems would be found in the 3 - 4 hour bin by coincidence is $\sim 2 \times 10^{-4}$. This result is based on the assumption that the distribution presented in Figure 5 is representative of the actual period distribution of CBs. It is likely that selection effects render this assumption invalid (Robinson 1982). For example, it is more difficult to discover novalike variables than typical dwarf novae because the former objects do not have the frequent outbursts which aid in their discovery. In addition, it is usually more difficult to determine the orbital periods of the longer period systems, especially if photometry is used to search for the period. Consequently, with the discovery of a considerable number of new

novalike variables (and potential VY Sculptoris objects) with periods > 4 hrs, it may turn out that our conclusion about the period distribution of VY Sculptoris objects is erroneous. Nevertheless, based on the presently available data, this possibility seems somewhat unlikely and we conclude that there must be a physical explanation for the preference of these systems to have orbital periods between 3 and 4 hours.

Assuming the above statement to be correct, we are confronted with the task of supplying an explanation (at least a speculative one) for the nature of the VY Sculptoris systems. In particular, it would be interesting to know why the systems tend to cluster near the period gap. As described in Section I, Robinson et al. (1981) have proposed an explanation for the existence of the period gap by speculating that systems with orbital periods between $\sim 2 - 3$ hours have temporarily ceased mass transfer as a result of structural changes within the core of the secondary star which cause it to shrink and detach from its Roche lobe. In particular, they pointed out that systems with orbital periods between $2 - 3$ hours should have secondaries with masses of $0.2 - 0.3$ $M_\odot$. This is precisely the mass range where the core of the star is expected to make the transition from radiative to convective. Robinson et al. went on to speculate that systems near the boundaries of the period gap will be subject to episodes of sporadic mass transfer as they evolve into and out of the gap. This provides a natural explanation for the VY Sculptoris phenomena.

Unfortunately, there were a few unanswered questions pertaining to the Robinson et al. (1981) explanation. Namely these authors were

55

unable to establish specifically how a change in core structure from radiative to convective could cause a cessation of mass transfer. Indeed, such a transition in core structure may increase the stellar radius, not decrease it (Faulkner 1976). Nevertheless, these authors predicted that future evolutionary calculations of CBs would reveal the cessation of mass transfer within the period gap. As described below, the recent calculations by D'Antona and Mazzitelli (1982), Rappaport, Verbunt, and Joss (1983), Spruit and Ritter (1983), and Taam (1983) seem to support the prediction of Robinson et al.

As indicated in the previous section, recent calculations of CB evolution have incorporated magnetic braking as the dominant mechanism of angular momentum loss for systems with orbital periods on the long side of the period gap. In their recent paper, Spruit and Ritter (1983) have proposed that the transition from a radiative to a convective core may result in a decrease in the magnetic field generation within the secondary, and hence a decrease in the rate of angular momentum loss from the system. According to these authors, if the decrease in the angular momentum loss rate occurs sufficiently rapidly, the mass transfer will also be reduced allowing the secondary to shrink back to its equilibrium radius (while the secondary is transferring material, its radius is larger than its equilibrium radius if the time scale for mass loss is shorter than its Kelvin-Hemholtz time scale). If the rate at which the secondary star shrinks to its equilibrium radius is larger than the rate at which the radius of the Roche lobe decreases (due to the reduced rate of angular momentum loss), then the mass transfer will cease altogether until the Roche lobe eventually reaches the equilibrium radius. At this

time, mass transfer will be initiated at a lower rate dictated by the reduced angular momentum loss. As argued by Spruit and Ritter, this scenario offers a natural explanation for the period gap.

It seems reasonable to assume that there might be several abrupt low amplitude fluctuations in the magnetic field strength (and hence the angular momentum loss rate) as the secondary begins its transition to a fully convective state. If such is the case, then the model of Spruit and Ritter may offer an explanation for the VY Sculptoris phenomena.

Patterson (1983) has expressed his doubts as to whether the VY Sculptoris systems are related to the period gap. In order to support his view, Patterson has proposed three definitions which can be used to describe the behavior of the VY Sculptoris objects. (1) They have $\dot{M} < 10^{-11}$ $M_\odot$/yr at minimum light, (2) Their mean mass transfer rate, $\langle\dot{M}\rangle < 10^{-10}$ $M_\odot$/yr, and (3) The amplitude of their brightness variations, $\Delta M_V > 5$ mag. He then goes on to compare the period distribution of the objects within these three classes with the period distribution of all CBs. He concludes that the distributions in (1), (2), and (3) are no more strongly clumped near the period gap than is the overall distribution of all CBs.

From my perspective, this conclusion is not surprising considering that none of his three definitions adequately describe the VY Sculptoris behavior. His definitions (1) and (3) are individually incomplete, while his definition (2) is irrelevant. If we adopt a correct single definition, by combining Patterson's partial definitions (1) and (3) and include an additional requirement that these objects spend the majority of their time in a state of high mass transfer and only occasionally

fade to minimum light, then we find that the periods of member systems tend to fall in the 3 - 4 hour range. If our speculation concerning the connection between the VY Sculptoris objects and the period gap are correct, then all of these systems will eventually fade to a deep minimum for an extended period of time until they reinitiate mass transfer and emerge below the gap.

Patterson (1983) does point out an interesting fact that two apparently normal dwarf novae TU Men (P = 2.8 hrs) and YZ Cnc (P = 2.1 hrs) define the boundaries of the period gap. Neither of these objects has been known to exhibit any of the characteristics of the VY Sculptoris objects. However, while it may raise a few eyebrows, this apparent inconsistency is not in serious conflict with our basic conclusions. I simply propose that objects which do show the characteristics of the VY Sculptoris systems, as described by my definition, tend to have orbital periods between 3 - 4 hours. I have not demanded that all objects in this period range exhibit this behavior. It may take awhile before these two systems are observed to exhibit VY Sculptoris characteristics (after all VZ Scl and TT Ari have only recently announced their membership). Nevertheless, we will have to await the discovery of many more novalikes (hopefully including more VY Sculptoris systems) before we can be assured that selection effects have not conspired against our apparent understanding of the period distribution of these systems.

Finally, I would like to stress that my conclusion concerning the tendency for the VY Sculptoris systems to clump near the upper edge of the period gap is not dependent upon the validity of the hypothesis put

forth by Spruit and Ritter (1983) (see also D'Antona and Mazzzitelli 1982; Rappaport, Verbunt, and Joss 1983). Robinson et al. (1981) have predicted that a connection between the period gap and the VY Sculptoris systems will be found. I have simply indicated that the models of Spruit and Ritter (1983) can potentially provide the connection which Robinson et al. were seeking.

VII. SUMMARY

A. Goals

A calibrartion has been made of an indirect method for estimating the mass ratios of cataclysmic binaries initially described by Warner (1973). The method is based on the assumption that the quantity $K_1/(v_d \sin i)$ is a function solely of the mass ratio of the system. The quantity $v_d \sin i$ is the projected circular velocity of material in the accretion disk having the same specific angular momentum as the particles leaving the inner Lagrangian point. This quantity can potentially be extracted from the profiles of the emission lines originating in the disk. The precise location in the emission line profile which represents $v_d \sin i$ is unknown and may vary from system to system. Consequently, this position must be calibrated <u>empirically</u> using systems with directly determined mass ratios. In order to specify an arbitrary velocity in an emission line profile, I have chosen to parameterize the line profiles by using two parameters. The first parameter, f, is simply the fractional intensity of the line normalized to the continuum intensity. The second parameter, ξ, was defined to be the fractional flux of the line normalized to the continuum flux. The usefulness of Warner's method of determining the mass ratios is dependent on the existence of a universal value, or more likely, a relatively small range of values of the parameters f and ξ which will yield the appropriate values of $v_d \sin i$ for the majority of CBs.

The purpose of this thesis was twofold. First, to determine the general usefulness of the method by calibrating it by using systems with directly determined mass ratios. In particular my goal was to establish

values of the parameters f and ξ for the calibration systems and then using the distribution of these values to ascertain the general validity of the method.

During the course of my analysis, I have tried to pay careful attention to the error analysis in order to obtain as quantitative an estimate as possible of the accuracy which can be expected by using the method outlined in Section II. In this analysis, I have implicitly adopted the philosophy that "Even a poorly known quantity can be a useful one if a reliable estimate of the magnitude of its uncertainty is specified".

The second purpose, assuming the initial calibration analysis revealed the method to be useful, was to estimate the white dwarf masses for a large number of single lined cataclysmic binaries and look for correlations with orbital period and with outburst behavior.

B. Results

By using the 11 systems with directly determined mass ratios, I have determined values of $0.30 \begin{smallmatrix} + & 0.07 \\ - & 0.06 \end{smallmatrix}$ and $0.58 \begin{smallmatrix} + & 0.09 \\ - & 0.07 \end{smallmatrix}$ for the parameters f and ξ, respectively. The relatively small 1σ errors for these two parameters have provided confidence that the method is useful. In particular, by referring to Figures 6 and 7, it is obvious that the quantity $K_1/\langle v_d \sin i \rangle$ is indeed strongly correlated with the mass ratio of the system. Satisfied with the calibration, the mass ratios of 20 single lined CBs were computed. Then using the assumption that the secondary stars were on the main sequence, we have computed the white dwarf masses for these 20 systems (for the ultrashort period systems I have adopted the mass of the secondary as an upper limit due to the

possibility that it may be partially degenerate).

I have arrived at the following principal conclusions based on the white dwarf masses for the 20 single lined systems, the 11 calibration systems, and 3 systems (OY Car, Z Cha, and AM Her) from the literature.

(1) As indicated in Figures 12 and 13 there appears to be a general trend for the average white dwarf mass to increase with increasing orbital period. Such a trend is consistent with the currently popular scenario for the evolution of CBs. I acknowledge that the observed trend is very weak and is only evident because of our large statistical sample. I have not meant to imply that one could use the observed trend to estimate the mass of any individual system with known orbital period.

(2) I find no evidence for any systematic difference between the masses of U Geminorum and Z Camelopardalis type dwarf novae. This is not very surprising since the mean orbital periods for the two classes in our sample were 0.23 and 0.26 days for the U Geminorum and Z Camelopardalis systems respectively.

(3) There does appear to be a systematic difference between the masses of the novalike variables and the dwarf novae (excluding the SU Ursae Majoris systems) in the sense that the dwarf novae are somewhat more massive. We find that $\langle M_1 \rangle = 0.58$ $M_\odot$ for the novalikes and $\langle M_1 \rangle = 0.84$ $M_\odot$ for the dwarf novae. This is a result of the fact that most known novalikes seem to have a preference for orbital periods which are shorter than for typical U Geminorum and Z Camelopardalis systems.

(4) As expected, from the orbital period distribution, the SU Ursae Majoris systems contain lower mass white dwarfs on the average than the longer period dwarf novae (see Figure 13).

(5) Although I have only computed white dwarf masses for two classical novae, V603 Aql ($M_1 = 0.66 \pm 0.27\ M_\odot$) and DQ Her ($M_1 = 0.61 \pm 0.09\ M_\odot$), their masses are consistent with the mean mass of all the CBs in our sample $\langle M_1 \rangle = 0.65 \pm 0.27\ M_\odot$.

Finally, I have discussed the nature of the VY Sculptoris systems and argued that they form a homogeneous subgroup of the novalike variables with orbital periods which are strongly clumped in the 3 - 4 hour range. The suggestion put forth by Robinson et al. (1981), namely that the VY Sculptoris systems are in the process of aborting mass transfer in preparation for their trek through the period gap, has gained some support through the observational results presented here and through the recent theoretical work of D'Antona and Mazzitelli (1982) and Spruit and Ritter (1983).

Appendix I

OBSERVATIONS AND REDUCTION PROCEDURES

All observations reported in this thesis were obtained by using the
Robinson-Wampler Image Dissector Scanner (IDS) (Robinson and Wampler
1972) either at the Cassegrain focus of the Lick 3m or the Mt. Lemmon
1.5m. Both low and high resolution observations were obtained for most
systems. All observations have been divided by the spectrum of a
tungsten lamp in order to remove channel-to-channel irregularities and
have been placed on a wavelength scale by comparison with the spectrum
of a He-Hg-Ar-Ne lamp.

The low resolution observations were made of the 13 single lined
systems for which we have determined radial velocity curves. These
observations cover a typical wavelength range of 3800 - 7000 Å at a
resolution of ~ 11 Å FWHM. These observations were intended to study
the general spectral character of the object and to determine the
optical energy distribution. The low dispersion observations have been
reduced to absolute fluxes by calibration with standard stars observed
by Stone (1977).

The high dispersion observations cover ~ 1000 Å centered on Hα
These observations were obtained for two specific reasons: (1) to be
used in a radial velocity study, and/or (2) to be used in the
determination of the quantity of $v_d \sin i$ (see Section II). It was not
necessary to reduce the high dispersion observations to a flux scale so,
for all line profile observations presented here, I have simply plotted
the observed count rate (divided by the continuum lamp) as a function of
wavelength. Since the IDS is a nearly linear detector for the low count

rates which were encountered, the count rate has been assumed to be proportional to intensity (a suitable "dead time" correction has been applied to the raw instrumental count rate in order to correct for any low level saturation of the detector).

For the radial velocity studies, I have chosen to limit the velocity measurements to the Hα line for the following reasons: (1) The Hα line has the largest wavelength shift for a given velocity and, in most cases, the largest equivalent width of all the Balmer lines; (2) The comparison lamps available at Mount Lemmon have a significantly higher density of lines near Hα than they do shortward of 6000 Å. Consequently, the wavelength calibration is more accurate for Hα than for the higher Balmer lines.

For the high-resolution observations, a reciprocal dispersion of 0.66 Å per channel was obtained by using a 1200 line mm^{-1} grating in first order. The IDS is oversampled by approximately a factor of 6; consequently, the resulting instrumental resolution is ~ 4 Å FWHM. The accuracy of the velocity measurements, however, is not limited by the instrumental resolution directly. In particular, I have found that the IDS readouts are stable to at least 0.1 channel. At the wavelength of Hα, this corresponds to a velocity error of ~ 3 km s^{-1} which allows small velocity shifts to be easily measured.

The IDS, being a Cassegrain instrument, also suffers from wavelength displacements as a function of telescope position. Fortunately, these shifts were empirically found to be a smoothly varying and easily calibratable function of the telescope hour angle. I have found that, by taking comparison spectra at sufficiently frequent

65

intervals (approximately every half-hour), the error introduced by the varying telescope position can be corrected to an accuracy comparable to the readout error. Consequently, the accuracy of the radial velocity measurements is, in general, determined by the quality of the data and by the line measuring technique, rather than by instrumental limitations.

I now present a summary of all observations which were used in this work. The following table contains the relevant information on these observations.

Table AI.1

SUMMARY OF OBSERVATIONS

(A) Low Resolution Observations (11 Å FWHM)

Spectral Coverage = 3800 − 6800 Å

Object	Julian Date JD 2,440,000+	Integration Time (min)	Sky Condition
RX And	4605(01-Jan-81)	32	clear
V603 Aql	5533(18-Jul-83)	8	clear
V794 Aql	4751(27-May-81)	32	ptly cldy
KR Aur	4970(01-Jan-82)	40	thin cirrus
SS Aur	4612(08-Jan-81)	32	thin cirrus
V425 Cas	5224(12-Sep-82)	16	clear
WW Cet	4872(25-Sep-81)	32	clear
SY Cnc	4605(10-Jan-81)	32	clear
YZ Cnc	4610(06-Jan-81)	80	thin cirrus
YZ Cnc	4612(08-Jan-81)	32	clear
CM Del	4751(27-May-81)	8	ptly cldy
T Leo	5002(02-Feb-82)	32	clear
V380 Oph	5465(11-May-83)	48	clear
V442 Oph	5085(26-Apr-82)	24	cirrus
PG1012-029	5465(01-May-83)	16	clear
SW UMa	5465(11-May-83)	48	clear
UX UMa	4613(09-Jan-81)	32	clear
TW Vir	5465(11-May-83)	32	clear
VW Vul	4876(29-Sep-81)	48	clear

(B) <u>High Resolution Line Profile Observations of Calibration Systems</u>

Resolution = 4 Å FWHM, Spectral Coverage ~ 6000 - 7000 Å

Object	JD 2,440,000+	Int. Time (min)
AE Aqr	5168(18-Jul-82)	16
	5463(09-May-83)	8
	5532(17-Jul-83)	8
	5533(18-Jul-83)	8
Z Cam	5427(03-Apr-83)	16
HT Cas	5376(11-Feb-83)	24
EM Cyg	5168(18-Jul-82)	32
	5178(28-Jul-82)	16
SS Cyg	5163(13-Jul-82)	8
	5286(13-Nov-82)	48
	5287(14-Nov-82)	48
	5330(27-Dec-82)	16
	5332(29-Dec-82)	16
	5532(17-Jul-83)	4
U Gem	5330(27-Dec-82)	24
	5378(13-Feb-83)	40
	5463(09-May-83)	16
	5464(10-May-83)	24
AH Her	4528(04-Apr-83)	16
DQ Her	5463(09-May-83)	24
	5533(18-Jul-83)	16
RU Peg	5167(17-Jul-82)	16
	5178(28-Jul-82)	8
	5330(27-Dec-82)	8
	5332(29-Dec-82)	16
	5532(17-Jul-83)	8
	5533(18-Jul-83)	8
LX Ser	5463(09-May-83)	24
	5464(10-May-83)	16
	5532(17-Jul-83)	48
	5533(18-Jul-83)	16
RW Tri	5330(27-Dec-82)	32

(C) <u>Line Profile Observations of Single Lined Systems</u>

Object	JD 2,440,000+	Int. Time (min)	Resolution (FWHM)
RX And	4605(01-Jan-81)	32	11
	5376(11-Feb-83)	16	4
V603 Aql	5532(17-Jul-83)	8	4
	5533(18-Jul-83)	4	4
SS Aur	4610(06-Jan-81)	32	11
	4612(08-Jan-81)	32	11
	5377(12-Feb-83)	4	4
WW Cet	4607(03-Jan-81)	2x 16	4
	4608(04-Jan-81)	2x 16	4
YZ Cnc	4607(03-Jan-81)	2x 48	4
	4608(04-Jan-81)	2x 32	4
	4609(05-Jan-81)	2x 16	4
EX Hya	5378(13-Feb-83)	16	4
PG1012-029	5463(09-May-83)	24	4
	5464(10-May-83)	16	4
WZ Sge	5163(13-Jul-82)	8	4
UX UMa	4610(06-Jan-81)	80	11
	4613(09-Jan-81)	32	11

(D) Radial Velocity/Line Profile Observations

Resolution = 4 Å FWHM, Spectral Coverage = ~ 6000 – 7000 Å

Object	JD 2,440,000+	Time Base of Observations	Number of Spectra
V794 Aql	5165(15-Jul-82)	5	11
KR Aur	4973(04-Jan-82)	4	14
	4993(24-Jan-82)	2	6
	4996(27-Jan-82)	2	6
	5000(31-Jan-82)	5.5	18
	5001(01-Feb-82)	2	6
	5001(01-Feb-82)	2	6
	5001(01-Feb-82)	0.5	2
	5002(02-Feb-82)	0.5	2
	5002(02-Feb-82)	1	4
V425 Cas	5224(12-Sep-82)	7.2	18
	5225(13-Sep-82)	8.2	11
	5226(14-Sep-82)	8.9	12
SY Cnc	5377(12-Feb-83)	3.3	11
	5378(13-Feb-83)	7.4	9
	5381(16-Feb-83)	4.0	10
YZ Cnc	4993(24-Jan-82)	3.1	10
	4994(25-Jan-82)	4.6	14
CM Del	5171(21-Jul-82)	5.4	11
T Leo	4973(04-Jan-82)	2.6	17
	4993(24-Jan-82)	2.5	16
	4994(25-Jan-82)	3.4	21
	4995(25-Jan-82)	5.3	24
	4996(27-Jan-82)	0.4	4
	5000(31-Jan-82)	1.1	8
	5089(30-Apr-82)	5.6	31
V380 Oph	5464(10-May-83)	4.5	14
V442 Oph	5162(12-Jul-82)	4.7	15
	5163(13-Jul-82)	4.7	8
SW UMa	5330(27-Dec-82)	1.8	12
	5376(11-Feb-83)	7	43
	5377(12-Feb-83)	8.2	18
	5378(13-Feb-83)	1.2	8

70

(D) <u>Radial Velocity/Line Profile Observations</u> (continued)

Resolution = 4 Å FWHM, Spectral Coverage = ~ 6000 - 7000 Å

Object	JD 2,440,000+	Time Base of Observations	Number of Spectra
UX UMa	5376(11-Feb-83)	2.2	8
	5377(12-Feb-83)	3.5	9
	5378(13-Feb-83)	1	4
	5381(16-Feb-83)	5	8
TW Vir	4996(27-Jan-82)	1.7	6
	4997(28-Jan-82)	3.0	8
	5080(31-Jan-82)	3.6	7
	5087(28-Apr-82)	5.6	14
	5088(29-Apr-82)	3.8	8
VW Vul	5163(13-Jul-82)	5.1	8

Appendix   II

ON MEASURING THE RADIAL VELOCITY OF WHITE DWARFS

IN CATACLYSMIC BINARIES[1]

It is notoriously difficult to determine the velocity semiamplitude

of the white dwarf in a cataclysmic binary (Smak 1970). This is a

result of the fact that spectral features arising in the photosphere of

the white dwarf are rarely, if ever, seen in the spectra of these

systems. The motion of the white dwarf must be inferred from radial

velocity variations of the broad emission lines which originate in the

surrounding accretion disk. This task would not pose any particular

problem if the disk emissivity was axially symmetric. Unfortunately,

this is usually not the case, primarily because of enhanced emission in

the vicinity of the shock front (hot spot) where the interstar mass

transfer stream impacts the disk. The challenge, then, is to measure

the velocity of the emission lines by using a method which is

insensitive to contamination from the hot spot. The purpose of this

paper is twofold: (1) to review a simple method of measuring the

velocity of emission lines in cataclysmic binaries and (2) to remind the

reader of the disastrous consequences which can arise if care is not

exercised when measuring the emission line velocities.

It is generally agreed that the best method to determine the radial

velocity of the white dwarf is to employ a line measuring technique

which is mainly sensitive to the motion of the line wings. The high

---

velocity emission line wings are presumably formed in the inner parts of the accretion disk near the white dwarf and thus should reflect its motion with the highest reliability. One such method was outlined by Schneider and Young (1980). Here, I discuss a preliminary analysis of this method and conclude by applying it to the dwarf nova T Leo.

As pointed out by Schneider and Young, the wavelength, λ, of an emission line in a spectrum $S(\Lambda)$ can be found by solving the equation:

$$\int_{-\infty}^{\infty} S(\Lambda) \, G(\lambda - \Lambda) \, d\Lambda = 0, \qquad\qquad \text{A.II.1}$$

where $G(x) = \exp[-(x-\underline{a})^2/2\sigma^2] - \exp[-(x+\underline{a})^2/2\sigma^2]$.

Generally speaking, this method consists of convolving $S(\Lambda)$ with two identical Gaussian bandpasses whose centroids have a separation of $2\underline{a}$. Equation 1 is satisfied and the wavelength of the spectral feature is determined when the counts in each bandpass are equal. The choice of the parameters $\underline{a}$ and σ can be chosen to suit the characteristics of the spectra being analyzed (i.e., the emission line width and the signal-to-noise ratio of the data). This method has the advantage that the entire velocity profile of the line can be mapped out by varying $\underline{a}$.

In general, I have found that the value of the semiamplitude (K_1), which is derived from a fit of the resulting velocity points to a sinusoid, is a strong function of the parameter $\underline{a}$ (Shafter 1983b; Shafter and Szkody 1984). This dependence is easy to understand when the emission line profiles are asymmetrical and this asymmetry is a function of orbital phase. In most cases, the line asymmetry can be attributed to emission from the hot spot and/or the interstar mass transfer stream. As pointed out by Smak (1970), contamination by the

73

hot spot results in a measured semiamplitude which is spurious; usually smaller than the true value of K_1. In the simplest model, the maximum velocity amplitude of the emission from the hot spot is equal to the rotational velocity at the outer edge of the accretion disk. This velocity is much smaller than the Keplerian velocity at the inner edge of the disk where the extreme line wings are formed. Consequently, K_1 should increase as one measures further out in the line wings, where the contamination from the hot spot is less pronounced (i.e. $K_1(\underline{a})$ should be an increasing function of $\underline{a}$).

As an example, I have employed the above analysis in a radial velocity study of the dwarf nova T Leo (Shafter and Szkody 1984). I have co-added 121 individual 8 minute spectra of T Leo synchronously with the 84.7 minute orbital period and summed them into 10 phase bins. I then measured the velocities of the 10 Hα emission lines using 11 different values of the parameter $\underline{a}$. The result is shown in Figure AII.1. As expected, the value of K_1 increases with increasing $\underline{a}$. I argue that the best estimate of the semiamplitude is determined by increasing the value of $\underline{a}$ until the fractional error (σ_K / K_1) in the resulting semiamplitude begins to sharply increase. At this point, the velocity measurements are beginning to be dominated by noise in the continuum rather than by flux in the line wings. In some, but not all, cases, this point will correspond to the maximum value of K_1. The best estimate of K_1 for T Leo is indicated by the dashed line in Figure AII.1. The resulting radial velocity curve is shown in Figure AII.2.

An example which dramatically illustrates the importance of restricting the velocity measurements to the extreme line wings is provided by a comparison of the radial velocity curves presented in Figures AII.2 and AII.3. As described above, the curve presented in Figure AII.2 was derived by using equation AII.1, with $\underline{a}$ = 21 Å. While, for purposes of comparison, the curve presented in Figure AII.3 was derived from measurements of the centroid of the entire Hα emission line from the 10 co-added spectra. By simply measuring the centroid of the line, I have deliberately made no attempt to avoid contamination from the hot spot or from any other non-orbital mass motions. Although the curves shown in Figures AII.2 and AII.3 were derived from measurements from the same 10 spectra, the difference is striking. It is clear that failing to restrict the measurements to the extreme line wings can result in not only a poor fit of the velocity points to a circular orbit, but also a serious underestimation of the semiamplitude.

Although I believe that the line measuring technique outlined in equation AII.1 is particularly effective, I have not intended to imply that it is the only method, nor that it is necessarily the best method of estimating the radial velocity of the white dwarf in a cataclysmic binary. For example, other line measuring techniques which are frequently employed, such as fitting a Lorentzian profile (Gilliland 1982) or a high order symmetric polynomial (Stover, Robinson, and Nather 1981) to the line wings, may potentially be as effective as the method presented here. However, the important point is that, regardless of the line measuring technique used, a special effort should be made to assure that one is measuring as far out in the line wings as is practically

possible. I believe that the best way to accomplish this is to construct a diagnostic diagram analogous to the one presented in Figure AII.1. The diagnostic diagram is a useful tool for assessing the degree of hot spot contamination and for determining the best estimate of K_1 which can be extracted from the available data.

Figure AII.1. The diagnostic diagram for the dwarf nova T Leo.
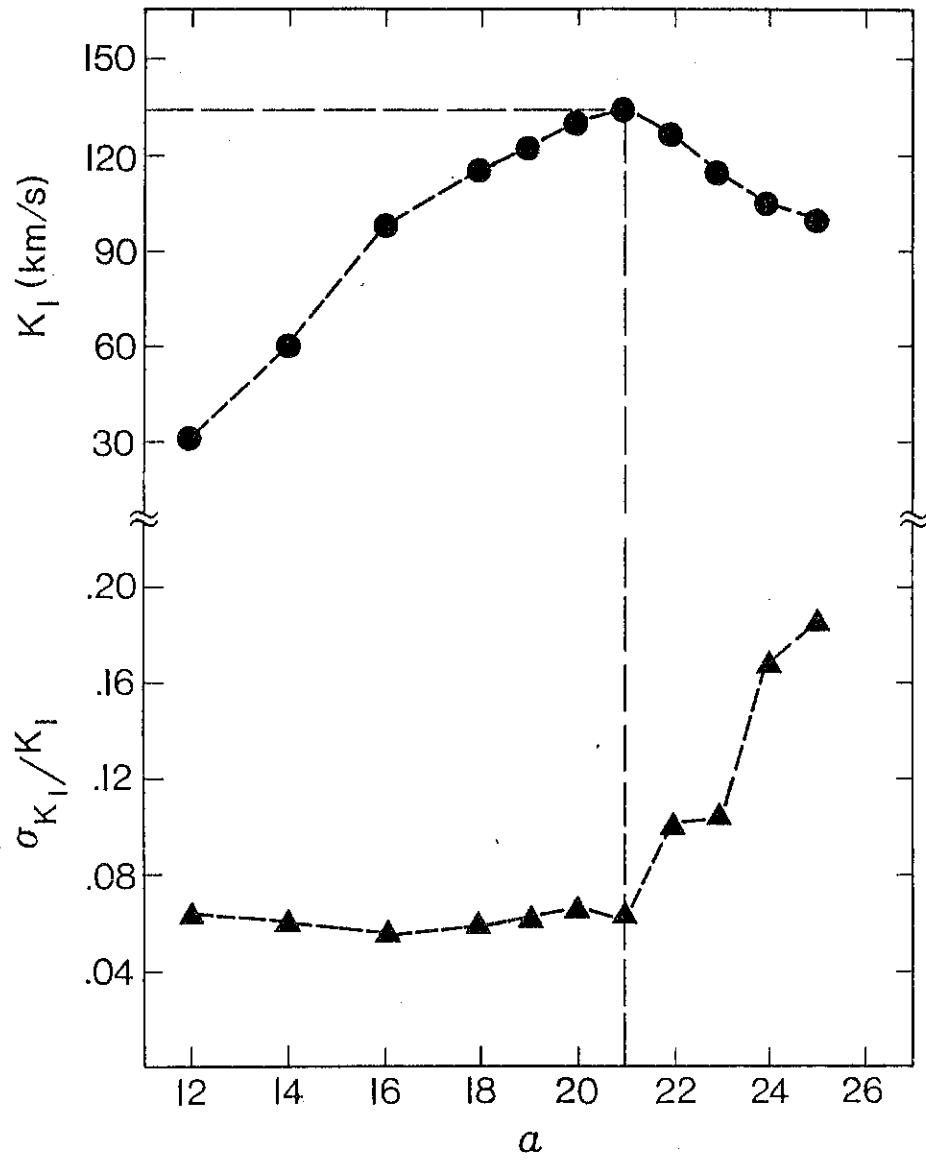
Figure AII.1

Figure AII.2. The radial velocity curve for T Leo. The velocities were
measured using equation AII.1 with $\underline{a}$ = 21 Å and σ = 1 Å.

Figure AII.2

80
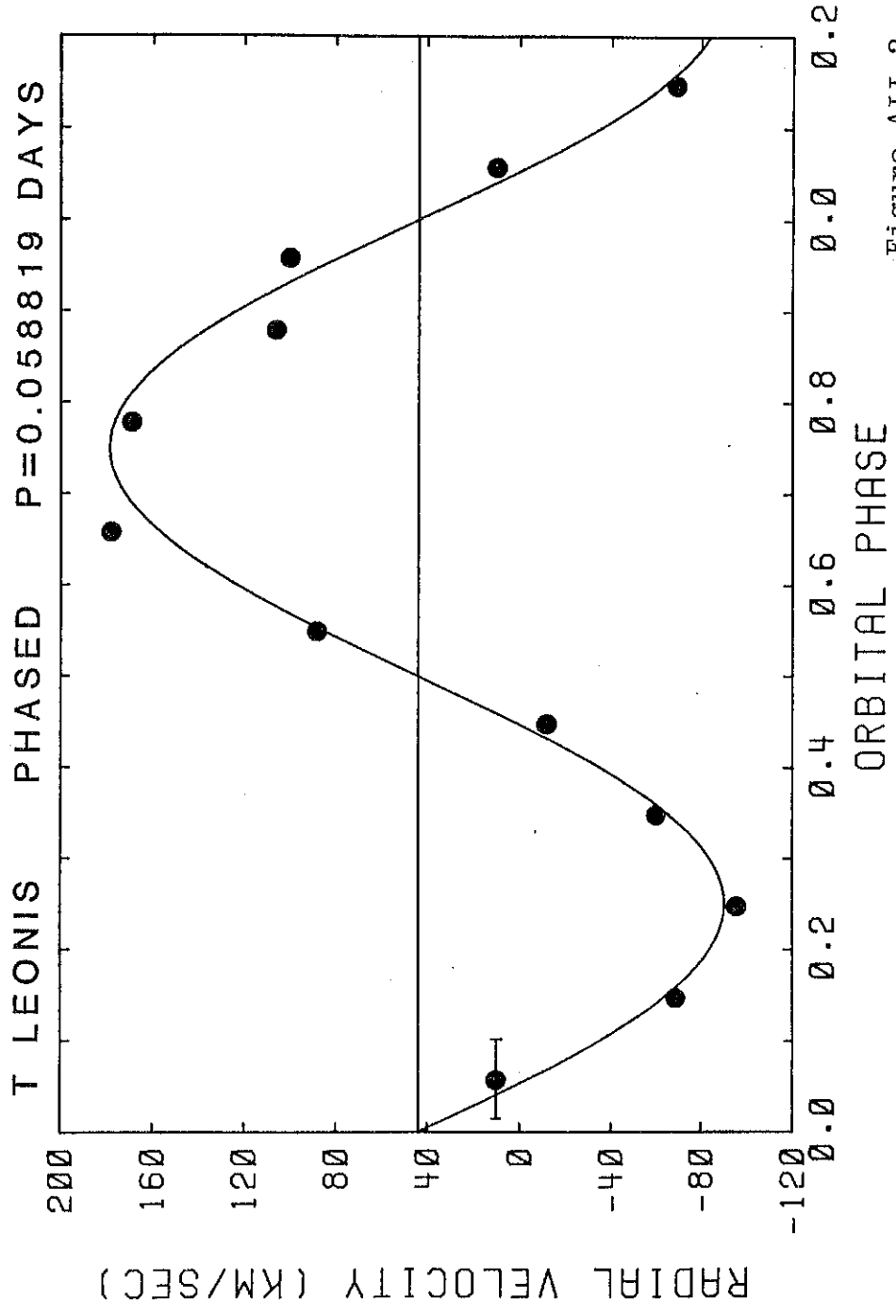
Figure AII.3. The radial velocity curve for T Leo. The velocities were
measured from the centroid of the entire Hα emission
line. Note the poor fit and low semiamplitude compared
with Figure AII.2.

Figure AII.3

82
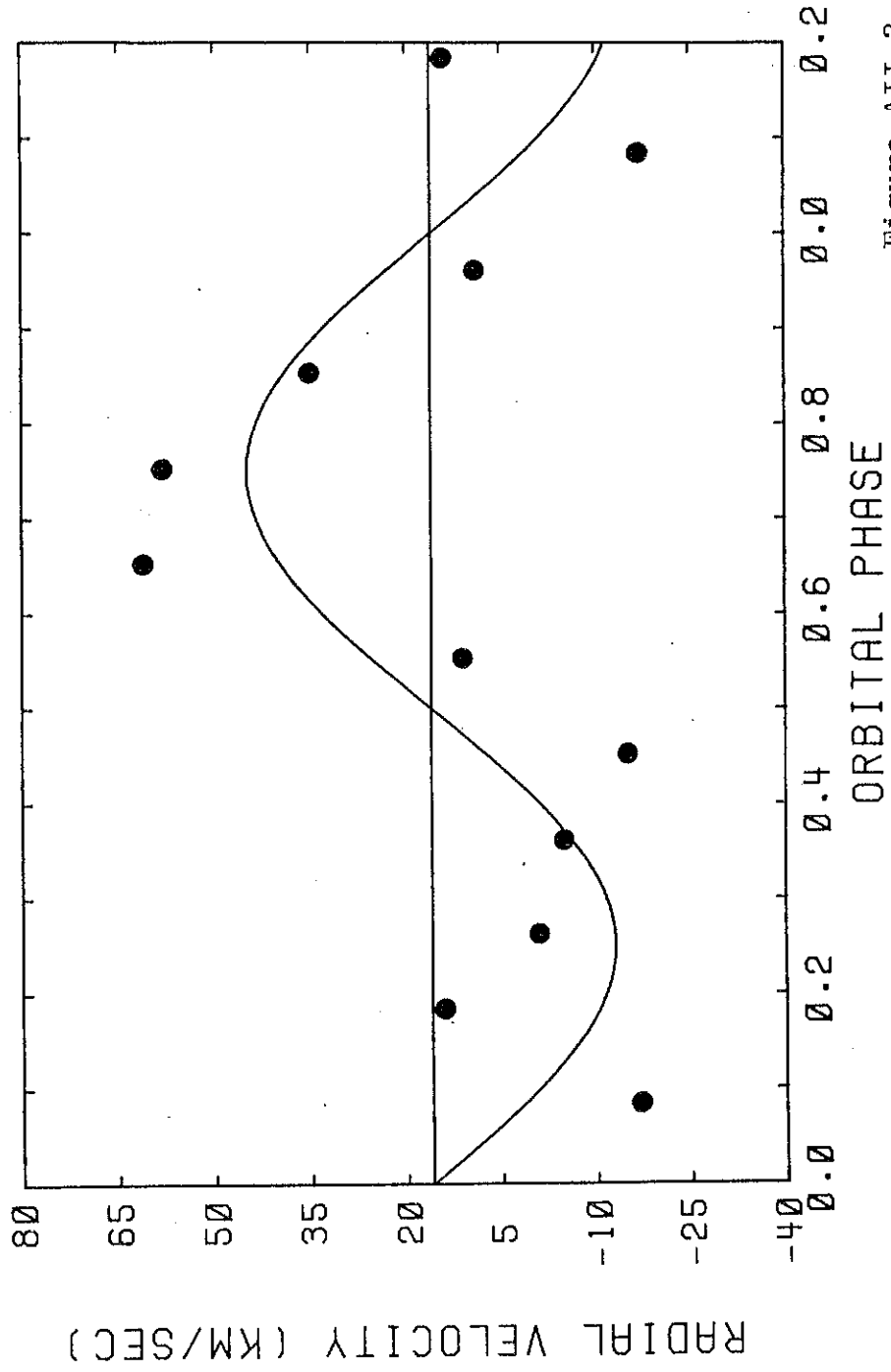
Appendix III

ANALYSIS TO DETERMINE THE SEMIAMPLITUDES OF THE CALIBRATION SYSTEMS

For calibration systems which have multiple determinations of the semiamplitude of the component stars, I have adopted the mean values for K_1 and K_2 using the following weighting scheme:

$$W_{ij} = (1/\sigma_{K_{ij}})^2 (N_{ij}), \qquad\qquad\qquad \text{A.III.1}$$

where $i = 1$ for K_1 and $i = 2$ for K_2 and j refers to the particular radial velocity study. The factor N_{ij} is an arbitrary weighting factor which I have assigned based on my assessment of the quality of the radial velocity study. In particular I have defined the following three classes:

N = 1:   Poor determination – (photographic plates having poor time resolution, velocity measurements not restricted to line wings, etc.).

N = 2:   Fair determination – (good quality plates with high time resolution, measurements restricted to line wings, or digital spectra with attempt to restrict measurements to line wings).

N = 3:   Good determination – (digital spectra, secondary spectra subtracted before K_1 determined, K_2 determined by cross correlation, study undertaken during quiescence).

The weighting factor, then, is simply a combination of the arbitrary quality factor N and the $1/\sigma_K^2$ factor which represents the accuracy of

the fit of the radial velocity measurements to a circular orbit. Note

that if systematic effects (due to poor observational techniques and

inadequate reduction procedures) were not important then I would simply

weight by the $(1/\sigma_K^2)$ factor.

The mean values of K_1 and K_2 for a given system are then determined

in the usual way

$$\langle K_1 \rangle = \frac{\sum\limits_{j} W_{ij} K_{ij}}{\sum\limits_{j} W_{ij}}. \qquad\qquad \text{A.III.2}$$

For the SS Cyg system, for which there are the largest number of

independent radial velocity studies, we can compute a sample variance as

follows:

$$(S_{K_1})^2 = \frac{\sum\limits_{j} W_{ij} (K_{ij} - \langle K_1 \rangle)^2}{\sum\limits_{j} W_{ij}}. \qquad\qquad \text{A.III.3}$$

This variance is an "external" variance and represents the spread among

the different K values from the various radial velocity studies. That

is, it is an estimator of the <u>systematic</u> errors which are involved in

determining the semiamplitudes. For the SS Cyg system, the five radial

velocity studies summarized in Table AIII.1, yield values of

$\langle K_1 \rangle = 94$ km s^{-1} and $\langle K_2 \rangle = 145$ km s^{-1}. The errors as given by equation

A.III.3 are $S_{K_1} = 8$ km s^{-1} and $S_{K_2} = 14$ km s^{-1}.

Unfortunately, all of the calibration systems, with the exception

of SS Cyg, have less than three independent radial velocity studies.

For these systems, it is not possible to estimate the errors in K_1 and

K_2. The formal 1σ errors quoted in the literature reflect the error of the fit of the velocity points to a circular orbit, and do <u>not</u> include possible systematic effects. As we have just seen in the case of SS Cyg, such errors do exist and it seems reasonable to expect that they exist in the determination of K values for other systems as well. Since SS Cyg is the brightest and most well studied (for orbital element determination) CB, it hardly seems fair to adopt S_{K_1} of 8 km s^{-1} while at the same time adopting an error of 5 km s^{-1} for a relatively poorly studied system, such as DQ Her. In order to correct this apparent inequity, I will henceforth adopt a standard systematic error of 8 km s^{-1} for K_1 and 14 km s^{-1} for K_2 based on the SS Cyg system. It is my feeling that, while for rare cases this may be an overestimate, in most cases it will be a very conservative estimate of the systematic error involved in determining K_1 and K_2. This is particularly true in the case of systems where the radial velocity determinations were relatively poor and were assigned weights of N = 1 or 2.

The systematic error described above is independent of the formal fit error quoted in the literature, and consequently the final error for the K values for a particular system is simply given by

$$\Sigma_{\langle K_i \rangle} = [(\sigma_{K_i})^2 + (S_{K_i})^2]^{1/2}, \qquad\qquad \text{A.III.4}$$

where σ_{K_i} is the formal error derived from the fit of the velocity measurements to a sinusoid and, as mentioned earlier, S_{K_i} is 8 km s^{-1} and 14 km s^{-1} for i = 1 and 2, respectively. The adopted values for $\langle K_i \rangle$ and $\Sigma_{\langle K_i \rangle}$ for the 11 calibration systems are presented in Table 2.

Before we leave this topic, I wish to make one final comment. For the reader who may feel uncomfortable with assigning systematic errors, consider the following points:

(1) Remember that the K_1 values are derived from the emission lines originating in the disk. We are not "directly" measuring the white dwarf velocity. There are undoubtedly systemtic errors in using the emission line velocities to infer the white dwarf velocity, but the magnitude of phase errors and the ways to correct for them are unknown.

(2) The K_2 values are dependent upon the disk luminosity as described by Robinson (1983).

(3) As demonstrated in Appendix II the K values can be extremely strong functions of the line measuring techniques used to extract the individual velocity points.

In view of these points it seems that the least we can do is adopt S_{K_1} = 8 km s^{-1} and S_{K_2} = 14 km s^{-1}. As we will see shortly, the absolute errors of the K values are not crucial to determining the canonical values of the parameters f and ξ. It is the relative errors of K_1 and K_2 from one calibration system to another that are of interest in determining these two parameters. The absolute errors of K_1 and K_2 will be mainly reflected in the standard errors of f and ξ.

Table AIII.1

RADIAL VELOCITY STUDIES OF SS CYG

Authors	K_1	K_2	q	N
Cowley, Crampton, and Hutchings (1980)	118±8	120±6	0.98	2
Joy (1956)	122±24	114±19	1.08	1
Kiplinger (1979)	85±4	164:	0.52:	2
Stover et al. (1981)	90±2	153±2	0.59	3
Walker (1981)	107±3	123±3	0.87	2

Appendix IV

PROPAGATION OF ERRORS

We begin with the usual formula for the propagation of errors. If $Q = f(a,b,\ldots)$ then:

$$\sigma_Q = \left[\left(\frac{\partial Q}{\partial a}\right)^2 \sigma_a{}^2 + \left(\frac{\partial Q}{\partial b}\right)^2 \sigma_b{}^2 + \ldots \right]^{1/2}. \qquad \text{A.IV.1}$$

During the course of our analysis we needed to determine errors in the following quantities:

(A) The mass ratio of a calibration system, q:

$$q = K_1/K_2 \qquad \text{A.IV.2}$$

From equation A.IV.1 we find

$$\sigma_q = \left[\left(\sigma_{K_1}/K_2\right)^2 + \left((K_1\sigma_{K_2})/(K_2)^2\right)^2 \right]^{1/2}. \qquad \text{A.IV.3}$$

(B) The line width, $v_d \sin i$, for a calibration system:

$$v_d \sin i = K_1/\left(q(0.5 - 0.227 \log q)^2\right). \qquad \text{A.IV.4}$$

From equation A.IV.1 we find

$$\sigma_{v_d} \sin i = \left[\left(1/(qX^2)\right)^2 \sigma_{K_1}^2 + \left(2K_1 q^{-1}X^{-3}(0.099/q)\right. \right. \qquad \text{A.IV.5}$$
$$\left. \left. - K_1 q^{-2}X^{-2}\right)^2 \sigma_q{}^2 \right]^{1/2},$$

where for convenience we have defined:

$$X = (0.5 - 0.227 \log q). \qquad \text{A.IV.6}$$

C) The indirect mass ratio, q, for the single lined systems

The master equation,

$$K_1/(v_d \sin i) = q(0.5 - 0.227 \log q)^2, \qquad\qquad \text{A.IV.7}$$

cannot be solved analytically for q. Nevertheless, we note that

the quantities $\dfrac{\partial q}{\partial K_1}$ and $\dfrac{\partial q}{\partial v_d \sin i}$ needed in equation A.IV.1 can

simply be computed as follows:

$$\frac{\partial q}{\partial K_1} = \left[\frac{\partial K_1}{\partial q}\right]^{-1} \qquad\qquad \text{A.IV.8}$$

and $\quad \dfrac{\partial q}{\partial v_d \sin i} = \left[\dfrac{\partial v_d \sin i}{\partial q}\right]^{-1}. \qquad\qquad \text{A.IV.9}$

Then from equation A.IV.1, the following nasty expression for σ_q

emerges:

$$\sigma_q = \left[\, [v_d \sin i(X^2 + (0.045 \log q - 0.227))]^{-2}\sigma_{K_1}^2 + \qquad \text{A.IV.10}\right.$$
$$\left. [-2K_1 q^{-1} X^{-3}(-0.099/q) - K_1 q^{-2} X^{-2}]^{-2} \, (\sigma_{v_d} \sin i)^2\right]^{1/2},$$

where X is defined in equation A.IV.6.

(D) The secondary mass, M_2:

$$\frac{M_2}{M_0} = \left[\frac{GM_\odot}{4\pi^2 R_\odot{}^3 \beta^3}\left(1 + \frac{1}{q}\right)P^2 \frac{0.118q^2}{\left(0.6q^{2/3} + \ln(1 + q^{1/3})\right)^3}\right]^{1/(3\alpha-1)}, \qquad \text{A.IV.11}$$

where, as described in the text, β and α are constants in the

empirical mass-radius relation for main sequence stars.

From equation A.IV.1, we find the following monster equation:

$$\sigma_{M_2} = \left[\left(\frac{\partial M_2}{\partial P}\right)^2 \sigma_P{}^2 + \left(\frac{\partial M_2}{\partial q}\right)^2 \sigma_q{}^2 + \left(\frac{\partial M_2}{\partial \alpha}\right)^2 \sigma_\alpha{}^2 + \left(\frac{\partial M_2}{\partial \beta}\right)^2 \sigma_\beta{}^2 \right]^{1/2}, \qquad \text{A.IV.12}$$

where, after redefining $X = M_2{}^{(3\alpha-1)}$, we find:

$$\frac{\partial M_2}{\partial P} = \frac{2X}{P(3\alpha - 1)} X((2-3\alpha)/(3\alpha-1)), \qquad \text{A.IV.13}$$

$$\frac{\partial M_2}{\partial q} = \frac{CP^2}{\beta^3(3\alpha - 1)} X((2-3\alpha)/(3\alpha-1)) \frac{2qZ^3 - 3q^2Y + Z^3 - 3qY}{Z^4}, \qquad \text{A.IV.14}$$

where for convenience we have defined

$$C = \frac{GM_\odot}{4\pi^2 R_\odot{}^3} = 1.00 \times 10^{-8} \text{ sec}^{-2}, \qquad \text{A.IV.15}$$

$$Y = 0.4 \ q^{-1/3} + q^{-2/3} \left(3(1 + q^{1/3})\right)^{-1}, \qquad \text{A.IV.16}$$

and

$$Z = 0.6q^{2/3} + \ln(1 + q^{1/3}). \qquad \text{A.IV.17}$$

Finally we find

$$\frac{\partial M_2}{\partial \alpha} = [-3/(3\alpha - 1)^2] \ X^{1/(3\alpha-1)} \ \ln(X), \qquad \text{A.IV.18}$$

and

$$\frac{\partial M_2}{\partial \beta} = - \frac{3X}{(3\alpha - 1)\beta} X((2-3\alpha)/(3\alpha-1)). \qquad \text{A.IV.19}$$

90

(E) The orbital inclination, i:

$$i = \sin^{-1}\left(3.79 \times 10^{-3}\ P^{-0.055}\ K_1\ (1 + 1/q)^{2/3}\ G(q)\right) \qquad \text{A.IV.20}$$

From equation A.IV.1, we find that

$$\sigma_i = \left[\left(\frac{\partial i}{\partial K_1}\right)^2 (\sigma_K)^2\ +\ \left(\frac{\partial i}{\partial q}\right)^2 (\sigma_q)^2\ +\ \left(\frac{\partial i}{\partial P}\right)^2 (\sigma_P)^2\right]^{1/2}, \qquad \text{A.IV.21}$$

where

$$\frac{\partial i}{\partial K} = \frac{X}{K_1\sqrt{1 - X^2}}, \qquad \text{A.IV.22}$$

and

$$\frac{\partial i}{\partial q} = -\ \frac{(2.53 \times 10^{-3})\ P^{-0.055}\ K_1\ (1 + 1/q)^{-1/3}\ G(q)}{q^2\ \sqrt{1 - X^2}}. \qquad \text{A.IV.23}$$

In equation A.IV.23

$$X = 3.79 \times 10^{-3}\ P^{-0.055}\ K_1\ (1 + 1/q)^{2/3}\ G(q), \qquad \text{A.IV.24}$$

and I have assumed that

$$\frac{\partial G(q)}{\partial q} = 0. \qquad \text{A.IV.25}$$

Since the orbital periods are generally known to high accuracy and i is almost independent of P, we have also set $\left(\frac{\partial i}{\partial P}\right)^2 \sigma_P^2 = 0.$

Appendix V

DETERMINATION OF THE CANONICAL VALUES OF f AND ξ

In cases where we have more than one line profile observation for a given system, we can immediately combine the individual f and ξ values to determine their weighted means and associated errors. For the ith observation of the jth system, we can write

$$\langle X_j \rangle = \frac{\sum\limits_i w_{ij} X_{ij}}{\sum\limits_i w_{ij}}, \qquad\qquad \text{A.V.1}$$

where $w_{ij} = \left(\dfrac{2}{\sigma_{ij}(+) + \sigma_{ij}(-)} \right)^2$,

and X represents either f or ξ. The error associated with $\langle X_j \rangle$ will <u>not</u> be given simply by the variance of the individual f and ξ values from this mean $\langle X_j \rangle$. This is because of the fact that the errors σ_{ij} are <u>not</u> measurement errors but are intrinsic errors due to the finite uncertainties in the q values for the calibration systems. In other words, no matter how many observations of the line profile of a particular system are available, this intrinsic error cannot be diminished. However, the error in $\langle X \rangle$ (i.e. the standard <u>error of the mean</u> of X) can be reduced if a large number of observations are available. The final error of $\langle X \rangle$, then, is a sum of two independent errors: the standard error of the mean (which is reduced for large numbers of observations), and the RMS intrinsic error of the various observations (which is independent of the number of observations). The RMS error will be different for the (+) and (-) errors because of the

92

non-linear transformation between $v_d \sin i$ and the parameters f or ξ. If s represents the sign of the RMS error (either (+) or (−)) then for the jth system we have

$$\Sigma\langle X_j\rangle, s = \left((\sigma_m)_j^2 + RMS^2_{j,s}\right)^{1/2}, \qquad\qquad A.V.2$$

$$\text{where} \quad (\sigma_m)_j^2 = \frac{\sum\limits_i w_{ij}\,(X_{ij} - \langle X_j\rangle)^2}{N \sum\limits_i w_{ij}}.$$

The results for $\langle X_j\rangle$ and $\Sigma\langle X_j\rangle, s$ are presented in Table IIIA.

In order to determine the appropriate method to employ in combining the values of $\langle X_j\rangle$, we need to know if the individual $\langle X_j\rangle$ values are Gaussian distributed. This question can be answered by testing the goodness of fit of the $\langle X_j\rangle$ values with a Gaussian distribution. Since there are only 11 calibration systems, the appropriate statistical test to employ is the Kolomogorov-Smirnov test as opposed to a standard χ^2 test. As the null hypothesis we will adopt the following: The sample distribution is Gaussian. The results of the Kolomogorov-Smirnov test indicate a level of significance of 0.92. Consequently, we have a 92% chance of making an error if we reject the null hypothesis. We can assume that the individual $\langle X_j\rangle$ values are Gaussian distributed.

Finally we may compute the grand canonical values for f and ξ from the $\langle f_j\rangle$ and $\langle \xi_j\rangle$ values from the 11 calibration systems. We proceed in a straightforward way by simply computing the weighted mean and variance, using the reciprocal of the individual variances for each calibration system as the weighting factor for that system. It is

important to remember that the final probability distributions for f and ξ will be skewed so that the standard error will consist of 2 components: $\Sigma(+)$ and $\Sigma(-)$.

If the weighting factor for the jth system is

$$w_j = \left[\frac{2}{\Sigma_{\langle X_j \rangle,+} + \Sigma_{\langle X_j \rangle,-}}\right]^2 , \qquad \text{A.V.3}$$

then

$$\langle X \rangle = \frac{\sum\limits_{j} w_j \langle X_j \rangle}{\sum\limits_{j} w_j} , \qquad \text{A.V.4}$$

and the (+) and (−) standard errors are given by

$$\Sigma_{\langle X \rangle,+} = \frac{\sum\limits_{j'} w_j (\langle X_j \rangle - \langle X \rangle)^2}{\sum\limits_{j'} w_j} , \qquad \langle X_j \rangle > \langle X \rangle \qquad \text{A.V.5}$$

and

$$\Sigma_{\langle X \rangle,-} = \frac{\sum\limits_{j=1}^{j-j'} w_j (\langle X_j \rangle - \langle X \rangle)^2}{\sum\limits_{j=1}^{j-j'} w_j} , \qquad \langle X_j \rangle < \langle X \rangle \qquad \text{A.V.6}$$

where j' is the number of systems with $\langle X_j \rangle < \langle X \rangle$.

Using the values for $\langle X_j \rangle$ and $\Sigma_{\langle X_j \rangle,+}$ and $\Sigma_{\langle X_j \rangle,-}$ from Table 3, we find that

$$\langle f \rangle = 0.30,$$

$$\Sigma_{\langle f \rangle,+} = 0.07,$$

$$\Sigma_{\langle f \rangle,-} = 0.06,$$

and

$$\langle \xi \rangle = 0.58,$$

$$\Sigma_{\langle \xi \rangle,+} = 0.09,$$

$$\Sigma_{\langle \xi \rangle,-} = 0.07.$$

Table I

THE CLASSES OF CATACLYSMIC BINARIES

Eruption Characteristics

Class	Amplitude (mag)	Energy (ergs)	Recurrence time
Novae	9- >14	10^{44}–10^{45} or more	Only one eruption
Recurrent novae	7-9	10^{43}–10^{44}	10-100 years
Dwarf novae			
(a) U Gem	2-6	10^{38}–10^{39}	15-500 or more days
(b) Z Cam	2-5	10^{38}–10^{39}	10-50 days
(c) SU UMa	2-5	10^{38}–10^{39}	10-200 days
Novalike	--	--	No eruptions
AM Her	--	--	No eruptions

Table II

CALIBRATION SYSTEMS**

Star	Class	Period (days)	K_1* (km s^{-1})	K_2* (km s^{-1})	q	$v_d \sin i$ (km s^{-1})	$\sigma_{v_d} \sin i$ (km s^{-1})	Ref.
(A) Double Lined Systems								
AE Aqr	NL	0.41165	135(9)	159(14)	0.85(09)	596	56	1
Z Cam	ZC	0.28984	137(12)	193(22)	0.71(10)	677	84	2
EM Cyg	ZC	0.29091	181(12)	135(14)	1.34(17)	608	60	3,4
SS Cyg	UG	0.27513	94(8)	145(14)	0.65(08)	491	57	5,6,7,8,9
U Gem	UG	0.17691	137(11)	283(21)	0.48(05)	871	92	10,11
AH Her	ZC	0.25811	130(14)	170(24)	0.76(14)	616	97	12
RU Peg	UG	0.3708	94(8)	121(15)	0.78(12)	438	56	17,13
(B) Single Lined Eclipsing Systems								
HT Cas	UG?	0.07365	115(10)		0.31(07)	979	172	14,15
DQ Her	N	0.19362	149(10)[†]		0.71(10)	737	82	16,17,18
LX Ser	VY	0.15843	172(15)		0.88(19)	744	118	19
RW Tri	NL	0.23188	197(11)		1.31(23)	671	78	20

* Errors in K_1 and K_2 include the 8 and 14 km s^{-1} systematic errors (see Appendix III). K_1 for EM Cyg is the weighted mean of 5 values given by Stover, Robinson, and Nather. K_1 and K_2 for SS Cyg have been computed as described in Appendix III.

† We have adopted the K_1 value of Greenstein and Kraft (1959) because the smaller value given by Hutchings, Cowley, and Crampton (1979) is inconsistent with a mass ratio of 0.71 subject to the condition that DQ Her is an eclipsing system.

**The numbers in parenthses are the 1σ errors.

References to Table II

1. Chincarini and Walker (1981)

2. Robinson 1973b

3. Robinson 1974

4. Stover, Robinson, and Nather (1981)

5. Cowley, Crampton, and Hutchings (1980)

6. Joy (1956)

7. Kiplinger (1979)

8. Stover et al. (1980)

9. Walker (1981)

10. Stover (1981a)

11. Wade (1981)

12. Horne (1983)

13. Stover (1981b)

14. Young, Schneider, and Shectman (1981a)

15. Patterson (1981)

16. Young and Schneider (1980)

17. Greenstein and Kraft (1959)

18. Hutchings, Cowley, and Crampton (1979)

19. Young, Schneider, and Shectman (1981b)

20. Kaitchuck, Honeycutt, and Schlegel (1983)

Table III

THE CALIBRATION

(A) Individual Line Profile Observations

Star	Date	f	$\sigma_f(-)$	$\sigma_f(+)$	ξ	$\sigma_\xi(-)$	$\sigma_\xi(+)$	EW(Å)
AE Aqr	18-Jul-82	0.28	0.04	0.06	0.48	0.05	0.07	41
	09-May-83	0.16	0.04	0.06	0.33	0.07	0.09	80
	17-Jul-83	0.22	0.04	0.03	0.50	0.05	0.04	94
	18-Jul-83	0.26	0.03	0.03	0.52	0.04	0.03	40
HT Cas	11-Feb-83	0.41	0.13	0.22	0.71	0.17	0.26	175
Z Cam	03-Apr-83	0.27	0.05	0.08	0.55	0.06	0.09	36
EM Cyg	18-Jul-82	0.15	0.07	0.06	0.25	0.13	0.11	10
	28-Jul-82	0.50	0.20	0.18	0.75	0.23	0.19	12
SS Cyg	13-Jul-82	0.35	0.07	0.07	0.64	0.07	0.06	49
	13-Nov-82	0.34	0.08	0.07	0.59	0.10	0.08	19
	14-Nov-82	0.34	0.09	0.10	0.62	0.10	0.09	30
	27-Dec-82	0.33	0.08	0.11	0.55	0.10	0.13	19
	29-Dec-82	0.46	0.11	0.11	0.70	0.11	0.10	23
	17-Jul-83	0.45	0.07	0.08	0.71	0.07	0.07	34
U Gem	27-Dec-82	0.42	0.12	0.15	0.62	0.13	0.14	65
	13-Feb-83	0.40	0.09	0.24	0.60	0.09	0.22	58
	09-May-83	0.39	0.11	0.14	0.61	0.14	0.16	122
	10-May-83	0.35	0.06	0.16	0.60	0.07	0.17	103
AH Her	04-Apr-83	0.27	0.08	0.16	0.56	0.11	0.19	13
DQ Her	09-May-83	0.36	0.09	0.09	0.60	0.11	0.11	38
	18-Jul-83	0.46	0.23	0.10	0.69	0.02	0.09	43
RU Peg	17-Jul-82	0.26	0.07	0.06	0.57	0.09	0.06	14
	28-Jul-82	0.38	0.08	0.09	0.68	0.09	0.08	18
	27-Dec-82	0.36	0.04	0.11	0.65	0.04	0.09	18
	29-Dec-82	0.40	0.05	0.07	0.68	0.06	0.07	19
	17-Jul-83	0.38	0.07	0.07	0.66	0.07	0.06	23
	18-Jul-83	0.35	0.07	0.07	0.66	0.07	0.06	17
LX Ser	09-May-83	0.23	0.05	0.12	0.48	0.07	0.17	59
	10-May-83	0.24	0.08	0.06	0.43	0.11	0.07	66
	17-Jul-83	0.28	0.12	0.12	0.52	0.18	0.16	61
	18-Jul-83	0.21	0.08	0.07	0.45	0.14	0.10	129
RW Tri	27-Dec-83	0.32	0.06	0.03	0.57	0.08	0.03	33

Table III

THE CALIBRATION

(B) <u>System Averages</u>

Star	$\langle f \rangle$	$\Sigma_{\langle f \rangle,-}$	$\Sigma_{\langle f \rangle,+}$	$\langle \xi \rangle$	$\Sigma_{\langle \xi \rangle,-}$	$\Sigma_{\langle \xi \rangle,+}$
AE Aqr	0.24	0.04	0.05	0.49	0.06	0.07
Z Cam	0.27	0.05	0.08	0.55	0.06	0.09
HT Cas	0.41	0.13	0.22	0.71	0.17	0.26
EM Cyg	0.19	0.18	0.17	0.37	0.29	0.27
SS Cyg	0.37	0.09	0.09	0.65	0.10	0.09
U Gem	0.38	0.10	0.18	0.61	0.11	0.18
AH Her	0.27	0.08	0.16	0.56	0.11	0.19
DQ Her	0.43	0.08	0.11	0.67	0.09	0.10
RU Peg	0.35	0.07	0.08	0.65	0.07	0.07
LX Ser	0.23	0.09	0.10	0.46	0.13	0.13
RW Tri	0.32	0.06	0.03	0.57	0.08	0.03

Table IV

SINGLE LINED SYSTEMS**

Star	Class	Period (days)	K_1‡ (km s^{-1})	$\langle v_d \sin i \rangle$ (km s^{-1})	q	Ref.*
RX And	ZC	0.21154(5)	99(14)	689(89)	0.42(12)	1
V603 Aql	N	0.1385(7)	37(9)	249(32)	0.44(18)	2
V794 Aql	NL	0.23(2)	96(21)	531(88)	0.60(25)	3
KR Aur	VY	0.16280(3)	90(10)	503(78)	0.59(17)	4
SS Aur	UG	0.18059	72(14)	558(80)	0.36(13)	5
V425 Cas	NL	0.1496(4)	50(9)	386(62)	0.36(13)	6
WW Cet	ZC	0.159(7)	129(16)	642(71)	0.70(19)	7
SY Cnc	ZC	0.380(1)	86(9)	320(49)	1.13(35)	3
YZ Cnc	SU	0.0864(2)	77(11)	522(75)	0.44(13)	8
CM Del	NL	0.162(6)	155(24)	740(73)	0.75(22)	3
EX Hya	NL?	0.06823	90(29)	938(80)	0.23(11)	9
T Leo	SU?	0.058819	135(11)	673(69)	0.70(15)	10
V380 Oph	NL	0.16(1)	100(14)	541(72)	0.62(19)	3
V442 Oph	NL	0.1406(6)	158(19)	675(79)	0.90(25)	11
PG1012-029	NL	0.13494	144(30)	598(65)	0.94(40)	12
WZ Sge†	SU?	0.056688	30(8)	1179(48)	0.04(01)	13,14
SW UMa	UG?	0.056743	47(8)	704(57)	0.14(04)	15
UX UMa	NL	0.19667	157(10)	595(73)	1.1(25)	8
TW Vir	UG	0.18267(7)	88(9)	596(91)	0.44(12)	3
VW Vul	UG?	0.0731(7)	97(11)	546(67)	0.58(15)	3

* The reference refers to the source of the radial velocity study.

† The K_1 velocity for WZ Sge is poorly known. It has been assumed to be 30 km s^{-1} based on the results of Brunt (1982) and Kraft (1964)

**The numbers in parenthses are the 1σ errors of the least significant digit(s).

‡ The quoted errors include the probable systematic error of 8 km s^{-1}.

References to Table IV

1. Hutchings and Thomas (1982)

2. Kraft (1964)

3. Shafter (1983a)

4. Shafter (1983b)

5. Kraft and Luyten (1965)

6. Shafter and Ulrich (1983)

7. Kraft and Luyten (1965)

8. This work

9. Cowley, Hutchings, and Crampton (1981)

10. Shafter and Szkody (1984)

11. Szkody and Shafter (1983)

12. Penning et al. (1983)

13. Brunt (1982)

14. Krzeminski and Kraft (1964)

15. Shafter (1983c)

Table V

EQUIVALENT WIDTHS OF PRINCIPAL OPTICAL EMISSION LINES

Star	Hδ	Hγ	HeI λ4471	HeII λ4686	Hβ	HeI λ4922	HeI λ5015	HeI λ5876	Hα	HeI λ6678
V794 Aql	41	37	11	12	52	6	7	12	63	9
KR Aur	65	85	21	9	113	8	13	42	122	–
V425 Cas	4	4	–	27	10	1	2	4	22	3
SY Cnc	–	–	–	–	2	–	–	1	8	–
YZ Cnc	26	34	9	–	41	4	3	14	56	8
CM Del	–	–	–	2	1	–	–	–	11	–
T Leo	35	37	8	–	62	3	5	20	87	8
V380 Oph	–	8	3	–	9	1	3	3	28	2
V442 Oph	6	6	–	6	8	–	–	2	20	–
SW UMa	21	37	5	–	52	4	6	15	138	8
TW Vir	39	46	12	7	57	8	9	15	70	13
VW Vul	61	81	22	–	114	9	6	35	144	18

103

Table VI

ORBITAL ELEMENTS

Star	Class	P	q	M_2	M_1	i*
		(A) Calibration Systems				
		(i) Double lined				
AE Aqr	NL	0.41165	0.85(09)	0.74(06)	0.87(12)	49(6)
Z Cam	ZC	0.28984	0.71(10)	0.70(03)	0.99(15)	57(11)
EM Cyg	ZC	0.29091	1.34(17)	0.76(03)	0.57(08)	63(10)
SS Cyg	UG	0.27513	0.65(08)	0.66(03)	1.02(13)	37(5)
U Gem	UG	0.17691	0.48(05)	0.39(02)	0.81(09)	~90(39)
AH Her	ZC	0.25811	0.76(14)	0.62(03)	0.82(16)	51(12)
RU Peg	UG	0.3708	0.78(12)	0.94(04)	1.21(19)	33(5)
		(ii) Single lined eclipsing				
HT Cas	UG?	0.07365	0.31(07)	0.19(02)	0.61(12)	~90
DQ Her	N	0.19362	0.71(10)	0.44(02)	0.62(09)	70(17)
LX Ser	VY	0.15843	0.88(19)	0.36(02)	0.41(09)	~90
RW Tri	NL	0.23188	1.31(23)	0.58(03)	0.44(08)	82(42)
		(B) Single Lined Systems				
RX And	ZC	0.21154(5)	0.42(12)	0.48(03)	1.14(33)	51(19)
V603 Aql	N	0.1385(7)	0.44(18)	0.29(02)	0.66(27)	17(7)
V794 Aql	NL	0.23(2)	0.60(25)	0.53(07)	0.88(39)	39(17)
KR Aur	VY	0.16280(3)	0.59(17)	0.35(02)	0.59(17)	38(10)
SS Aur	UG	0.18059	0.36(13)	0.39(02)	1.08(40)	38(16)
V425 Cas	VY	0.1496(4)	0.36(13)	0.31(02)	0.86(32)	25(9)
SY Cnc	ZC	0.380(1)	1.13(35)	1.10(05)	0.89(28)	26(6)
WW Cet	ZC	0.159(7)	0.70(19)	0.35(03)	0.50(14)	55(18)
YZ Cnc	SU	0.0864(2)	0.44(13)	0.17(02)	0.39(12)	38(12)
CM Del	NL	0.162(6)	0.75(22)	0.36(03)	0.48(15)	73(47)
EX Hya	NL?	0.068234	0.23(11)	0.13(01)	0.57(27)	~90
T Leo	SU?	0.058819	0.70(15)	0.11(01)	0.16(04)	65(19)
V380 Oph	NL	0.16(1)	0.62(19)	0.36(04)	0.58(19)	42(13)
V442 Oph	NL	0.1406(6)	0.90(25)	0.31(02)	0.34(10)	67(27)
PG1012−029	NL	0.1344	0.94(36)	0.30(02)	0.32(12)	56(26)
WZ Sge	SU	0.056688	0.04(01)	0.03(01)	0.75(3)	78
SW UMa	UG?	0.056743	0.14(04)	0.10(01)	0.71(22)	45(18)
UX UMa	UG	0.19667	1.10(25)	0.47(03)	0.43(10)	57(12)
TW Vir	UG	0.18267(7)	0.44(12)	0.40(02)	0.91(25)	43(13)
VW Vul	UG?	0.0731(7)	0.58(15)	0.14(01)	0.24(06)	44(12)

* Note the values of i quoted here are computed via equation II.12, and are based on values of q and K_1 presented in this work. For inclinations greater than ~60° the estimates are very uncertain due to the steepness of the arcsin(x) function as x approaches unity.

Table VII

COMPARISON OF MASSES*

Star	This Work		From Ritter (1982)	
	M_2	M_1	M_2	M_1
(A) Calibration Systems				
AE Aqr	0.74(06)	0.87(12)	0.70(10)	0.9(1)
Z Cam	0.70(03)	0.99(15)	0.86(10)	1.17(10)
HT Cas	0.19(02)	0.61(12)	0.19(02)	0.53(10)
EM Cyg	0.76(03)	0.57(08)	0.75(10)	0.55(05)
SS Cyg	0.66(03)	1.02(13)	0.80(10)	1.33
U Gem	0.39(02)	0.81(09)	0.56(06)	1.18(15)
DQ Her	0.44(02)	0.62(09)	0.32(03)	0.45(05)
RU Peg	0.94(04)	1.21(19)	1.14	1.47:
LX Ser	0.36(02)	0.41(09)	0.35(03)	0.40(08)
RW Tri	0.58(03)	0.44(08)	0.40(10)	0.4
(B) Single Lined Systems				
RX And	0.48(03)	1.14(33)	0.65:	1.0:
V603 Aql	0.29(02)	0.66(27)	0.4:	0.9:
SS Aur	0.39(02)	1.08(40)	0.6:	0.9:
EX Hya	0.13(01)	0.57(27)	0.19(05)	1.4:
PG1012-029	0.30(02)	0.32(12)	0.33(06)	0.58(20)
WZ Sge	0.03(01)	0.75(31)	0.04:	0.7:
UX UMa	0.47(03)	0.43(10)	0.35(25)	0.3(2)

*The numbers in parenthses are the 1σ errors. A colon indicates an uncertain value.

Table VIII

WHITE DWARF MASSES BY CLASS OF CATACLYSMIC BINARY

	Number of Systems	Average Mass
Dwarf Novae:		
U Gem	7	0.87 ± 0.27
Z Cam	6	0.82 ± 0.25
SU UMa	4	$<0.49 \pm 0.18$
Novalikes:		
UX UMa	7	0.55 ± 0.24
VY Scl	3	0.62 ± 0.23

REFERENCES

Bath, G. T., Evans, W. D., Papaloizov, J., and Pringle, J. E. 1974 M.N.R.A.S. 169, 447.

Bond, H. E. 1980, paper presented at the Fifth Annual Workshop on Cataclysmic Variables and Related Objects, University of Texas, Austin, Texas.

_____ 1981, paper presented at the Santa Cruz Workshop on Cataclysmic Variables.

Bond, H. E., Liller, W., and Mannery, E. J. 1978 Ap.J. 223, 252.

Bruch, A. 1982 P.A.S.P. 94, 916.

Brunt, C. 1982, paper presented at the Leicester Workshop on Cataclysmic Variables.

Cannizzo, J. K., Wheeler, J. C., and Ghosh, P. 1982 Ap.J. (Letters) 260, L83.

Chiapetti, L., Tanzi, E. G., and Treves, A. 1980 Space Sci. Rev. 27, 3.

Chincarini, G., and Walker, M. F. 1951 Astron. Astrophys. 104, 24.

Cowley, A. P., Crampton, D., and Hutchings, J. B. 1980 Ap.J. 241, 269.

Cowley, A. P., Hutchings, J. B., and Crampton, D. 1981 Ap.J. 246, 489.

D'Antona, F., and Mazzitelli, I. 1982 Ap.J. 260, 722.

Delgado, A. J., and Thomas, H. C. 1981 Astron. Astrophys. 96, 142.

Echevarria, J. 1983, preprint.

Eggleton, P. P. 1976 IAU Symp. No. 73, p. 209.

_____ 1983 Ap.J. 268, 368.

Faulkner, J. 1971 Ap.J. (Letters) 170, L99.

_____ 1976, in I.A.U. Symposium No. 73, The Structure and Evolution of Close Binaries, ed. P. Eggleton, S. Mitton, and J. Whelan (Dordrecht: Reidel), p. 193.

Faulkner, J., and Lin, D. 1983 AAS Meeting, Boston.

Ferguson, D. H., Liebert, J., Green, R. F., McGraw, J. T., and Spinrad, H. 1981 Ap.J. 251, 205.

Fujimoto, M. Y.   1982a Ap.J. 257, 752.

           1982b Ap.J. 257, 767.

Gilliland, R.L.: 1982, Astrophys. J. 254, pp.653-657.

Grauer, A. D., and Bond, H. E.   1981 P.A.S.P. 93, 388.

           1983, preprint.

Green, R. F., Richstone, D. O., and Schmidt, M.   1978 Ap.J. 224, 892.

Greenstein, J. L., and Kraft, R. P.   1959 Ap.J. 130, 99.

Horne, K.   1983, private communication.

Hoshi, R.   1979 Prog. Theor. Phys. 61, 1307.

           1981 Prog. Theor. Phys. Suppl. 70, 181.

           1982 Prog. Theor. Phys. 67, 179.

Hutchings, J. B., Cowley, A. P., and Crampton, D.   1979 Ap.J. 232, 500.

Hutchings, J. B., and Thomas, B.   1982 P.A.S.P. 94, 102.

Jameson, R. F., King, A. R., and Sherington, M. R.   1980 M.N.R.A.S. 191, 559.

Joy, A. H.   1956 Ap.J. 124, 317.

Kaitchuck, R. H., Honeycutt, R. K., and Schlegel, E. M.   1983 Ap.J. 267, 239.

Kiplinger, A. L.   1979 A.J. 84, 655.

Kippenhahn, R., and Weigert, A.   1967 Z. Astrophys. 66, 58.

Koester, D., Schulz, H., and Weidemann, V.   1979 Astron. Astrophys. 76, 262.

Kraft, R. P.   1964 Ap.J. 139, 457.

Kraft, R. P., and Luyten, W. J.   1965 Ap.J. 142, 1041.

Krzeminski, W.   1966 I.B.V.S. #160.

Krzeminski, W., and Kraft, R. P.   1964 Ap.J. 140, 921.

Lacy, C.   1977 Ap.J. Suppl. 34, 479.

Lanning, H. H.   1982 Ap.J. 253, 752.

108

Lanning, H. H., and Pesch, P. 1981 Ap.J. 244, 280.

Lauterborn, D. 1970 Astron. Astrophys. 7, 150.

Lauterborn, D., and Weigert, A. 1972 Astron. Astrophys. 18, 294.

Law, W. Y., and Ritter, H. 1983 Astron. Astrophys. 123, 33.

Livio, M. 1982 Astron. Astrophys. 105, 37.

Livio, M., Saltzman, J., and Shaviv, G. 1979 M.N.R.A.S. 188, 1.

MacDonald, J. 1982, preprint.

Mayo, S. K., Wickramasinghe, D. T., and Whelan, J. A. J. 1980
    M.N.R.A.S. 193, 793.

Meyer, F., and Meyer-Hoffmeister, E. 1979 Astron. Astrophys. 78, 167.

Nelson, B., and Young, A. 1970 P.A.S.P. 82, 699.

Noskova, R. I. 1982 Astron. Tsirk. No. 1128.

Osaki, Y. 1974 Pub. Astr. Soc. Jap. 26, 429.

Ostriker, J. P. 1973, private communication to B. Paczynski.

Paczynski, B. 1965 Acta Astron. 15, 197.

_____ 1971 Ann. Rev. Astr. Ap. 9, 183.

_____ 1976 IAU Symp. No. 73, p. 75.

_____ 1983 in Cataclysmic Variables and Low-Mass X-ray
    Binaries, ed. D. Q. Lamb and J. Patterson (Dordrecht: Reidel).

Paczynski, B., and Sienkiewicz, R. 1972 Acta Astron. 22, 73.

_____ 1981 Ap.J. (Letters) 248, L27.

_____ 1983 Ap.J. 268, in press.

Paczynski, B., Ziolkowski, J., and Zytkow, A. 1969 in Mass Loss from
    Stars, ed. M. Hack (Dordrecht: Reidel).

Parenago, P.P., and Kukarkin, B. V. 1934 Variable Star Bulletin IV No.
    8, 44.

Patterson, J. 1981 Ap.J. Suppl. 45, 517.

_____ 1983 Ap.J. Suppl. in press.

Penning, W. R., Ferguson, D. H., McGraw, J. T., Liebert, J., and Green, R. F. 1983, preprint.

Plavec, M. 1968 Adv. Astr. Ap. 6, 202.

Plavec, M., and Kratochvil, P. 1964 Bull. Astron. Inst. Czechoslovakia 15, 165.

Popper, D. M. 1980 Ann. Rev. Astr. Ap. 18, 115.

Rappaport, S., Joss, P. C., and Webbink, R. F. 1982 Ap.J. 254, 616.

Rappaport, S., Verbunt, F., and Joss, P. C. 1983 Ap.J. submitted.

Ritter, H. 1976 M.N.R.A.S. 175, 279.

_____ 1980a Astron. Astrophys. 85, 362.

_____ 1980b Astron. Astrophys. 86, 204.

_____ 1982 Catalogue of Cataclysmic Binaries, Low-Mass X-Ray Binaries and Related Objects, Second Edition.

Robinson, E. L. 1973a Ap.J. 180, 121.

_____ 1973b Ap.J. 186, 347.

_____ 1974 Ap.J. 193, 191.

_____ 1976a Ap.J. 203, 485.

_____ 1976b Ann. Rev. Astr. Ap. 14, 119.

_____ 1982, to appear in IAU Colloquium No. 72: Cataclysmic Variables and Related Objects.

_____ 1983, private communication.

Robinson, E. L., Barker, E. S., Cochran, A. L., Cochran, W. D., and Nather, R. E. 1981 Ap.J. 251, 611.

Robinson, L. B., and Wampler, E. J. 1972 P.A.S.P. 84, 161.

Schaefer, B., and Patterson, J. 1982 IAU Circ. No. 3756.

Schneider, D. P., and Young, P. 1980 Ap.J. 238, 946.

Shafter, A. W. 1983a I.B.V.S. #2377.

_____ 1983b Ap.J. 267, 222.

_____ 1983c I.B.V.S. #2354.

Shafter, A. W. 1983d in Cataclysmic Variables and Low-Mass X-ray Binaries, ed. D. Q. Lamb and J. Patterson (Dordrecht: Reidel).

Shafter, A. W., and Szkody, P. 1984 Ap.J. in press.

Shafter, A. W., and Ulrich, R. K. 1982 B.A.A.S. 14, 880.

Smak, J.: 1970, Acta Astronomica 20, 311.

Sherington, M. R., Bailey, J., and Jameson, R. F. 1983, preprint.

Spruit, H. C., and Ritter, H. 1983, preprint.

Starrfield, S., Sparks, W. M., and Turan, J. W. 1974 Ap.J. 192, 647.

Stone, R. P. S. 1977 Ap.J. 213, 767.

Stover, R. J. 1981a Ap.J. 248

_____ 1981b Ap.J. 249, 673.

Stover, R. J., Robinson, E. L., and Nather, R. E. 1981 Ap.J. 248, 696.

Stover, R. J., Robinson, E. L., Nather, R. E., and Montemayor, T. J. 1980 Ap.J. 240, 597.

Sulkanen, M. E., Brasure, L. W., and Patterson, J. 1981 Ap.J. 244, 579.

Szkody, P., and Shafter, A. W. 1983 P.A.S.P. 95, 509.

Szkody, P., Shafter, A. W., and Cowley, A. P. 1984 Ap.J. in press.

Taam, R. 1983, preprint.

Taam, R. E., Bodenheimer, P., and Ostriker, J. P. 1978 Ap.J. 222, 269.

Tylenda, R. 1981 Acta Astr. 31, 127.

Verbunt, F., and Zwaan, C. 1981 Astron. Astrophys. 100, L7.

Vogt, N. 1980 Astron. Astrophys. 88, 66.

_____ 1982 Ap.J. 252, 653.

Vogt, N., Schoembs, R., Krzeminski, W., and Pederson, H. 1981 Astron. Astrophys. 94, L29.

Wade, R. A. 1981 Ap.J. 246, 215.

Walker, M. F. 1954 P.A.S.P. 66, 230.

_____ 1981 Ap.J. 248, 256.

Warner, B.   1973 M.N.R.A.S. 162, 189.

_____   1976, in I.A.U. Symposium No. 73, The Structure and Evolution of Close Binaries, ed. P. Eggleton, S. Mitton, and J. Whelan (Dordrecht: Reidel), p. 85.

Webbink, R. F.   1979a, in IAU Colloquium N. 46, Changing Trends in Variable Star Research, ed. F.M. Bateson, J. Smak, and I.H. Urch (Hamilton, New Zealand: U. of Waikato Press).

_____   1979b, in I.A.U. Colloquium No. 53, White Dwarfs and Variable Degenerate Stars, ed. H.M. Van Horn and V. Weidemann (University of Rochester: New York), p. 426.

Weidemann, V.   1975, in Problems in Stellar Atmospheres and Envelopes, ed. B. Baschek, W.H. Kegel, and G. Traving (Berlin: Springer-Verlag), p. 173.

Whyte, C. A., and Eggleton, P.   1980 M.N.R.A.S. 190, 801.

Williams, R.   1980 Ap.J. 235, 939.

Williams, R. E., and Ferguson, D. P.   1982 Ap.J. 257, 672.

Young, A., and Capps, R. W.   1971 Ap.J. (Letters) 166, L81.

Young, A., and Wentworth, S. T.   1982 P.A.S.P. 94, 815.

Young, A., Nelson, B., and Mielbrecht, R.   1972 Ap.J. 174, 27.

Young, P., and Schneider, D. P.   1980 Ap.J. 238, 955.

Young, P., Schneider, D. P., and Shectman, S. A.   1981a Ap.J. 245, 1035.

_____   1981b Ap.J. 244, 259.

_____   1981c Ap.J. 245, 1043.

Figures la–g. Histograms of the orbital periods less than 10 hours for

the various classes of CBs. The background distribution

is the overall distribution for all known CBs with

orbital periods between 1 and 10 hours.
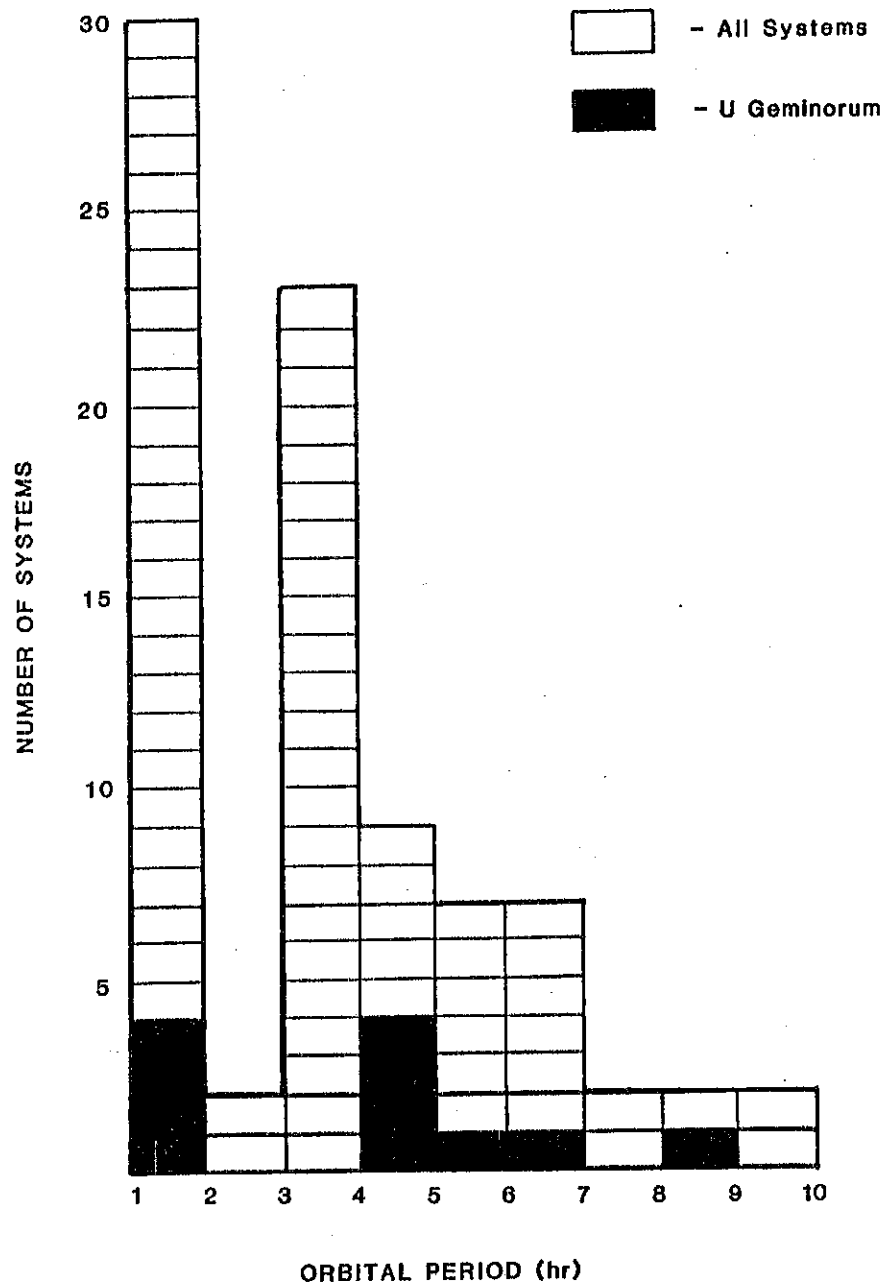
Figure 1a
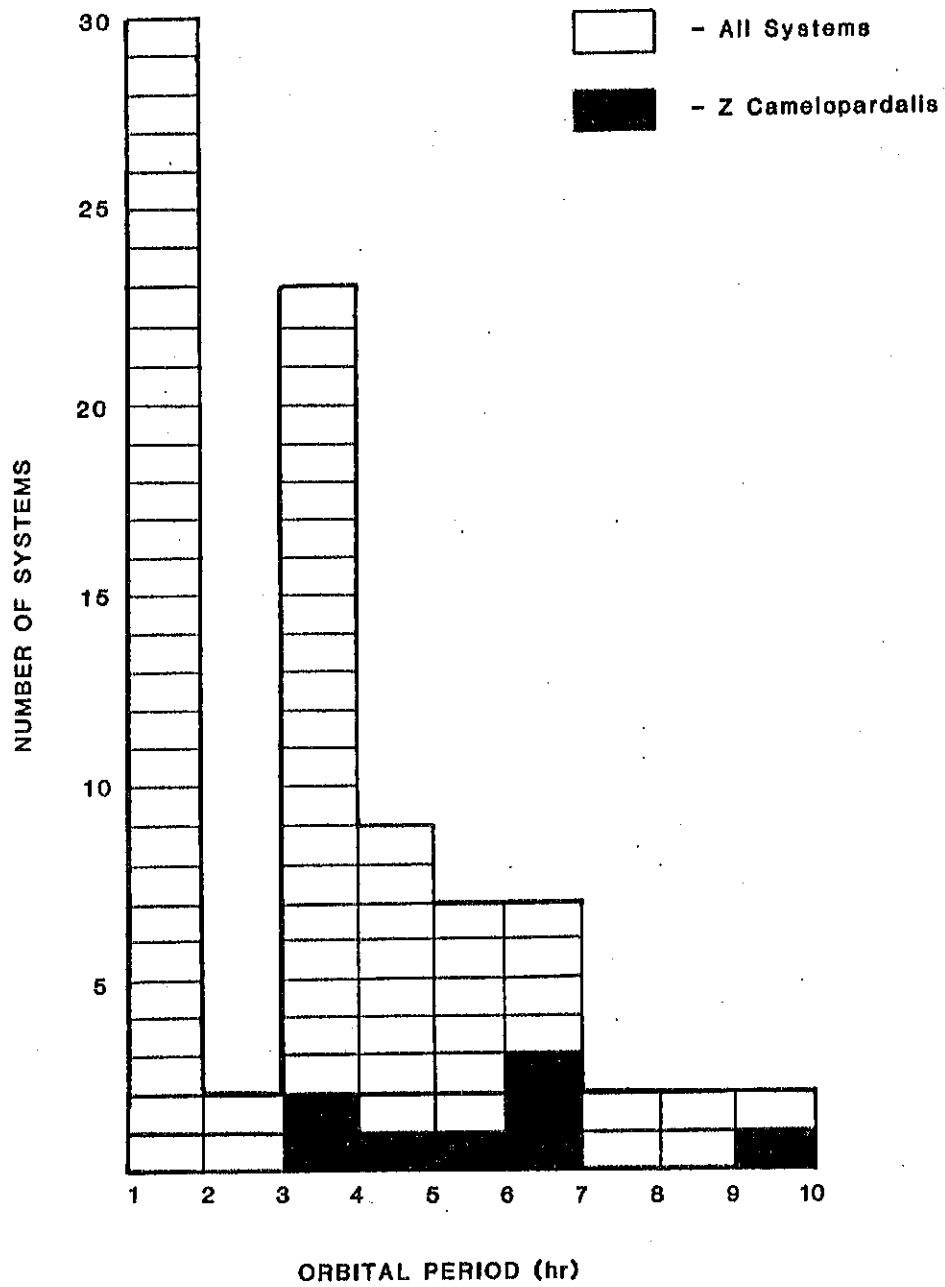
Figure 1b
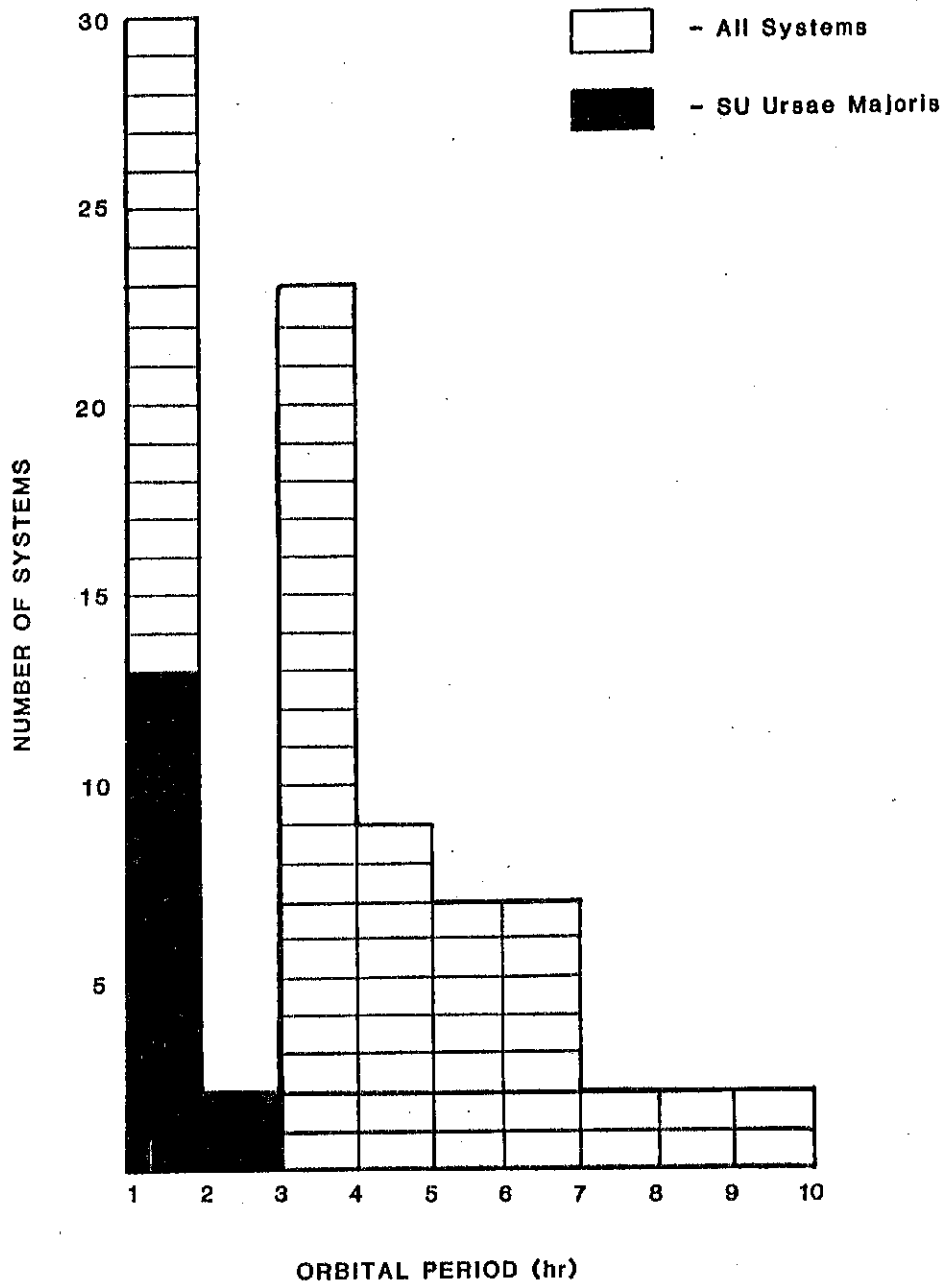
Figure 1c
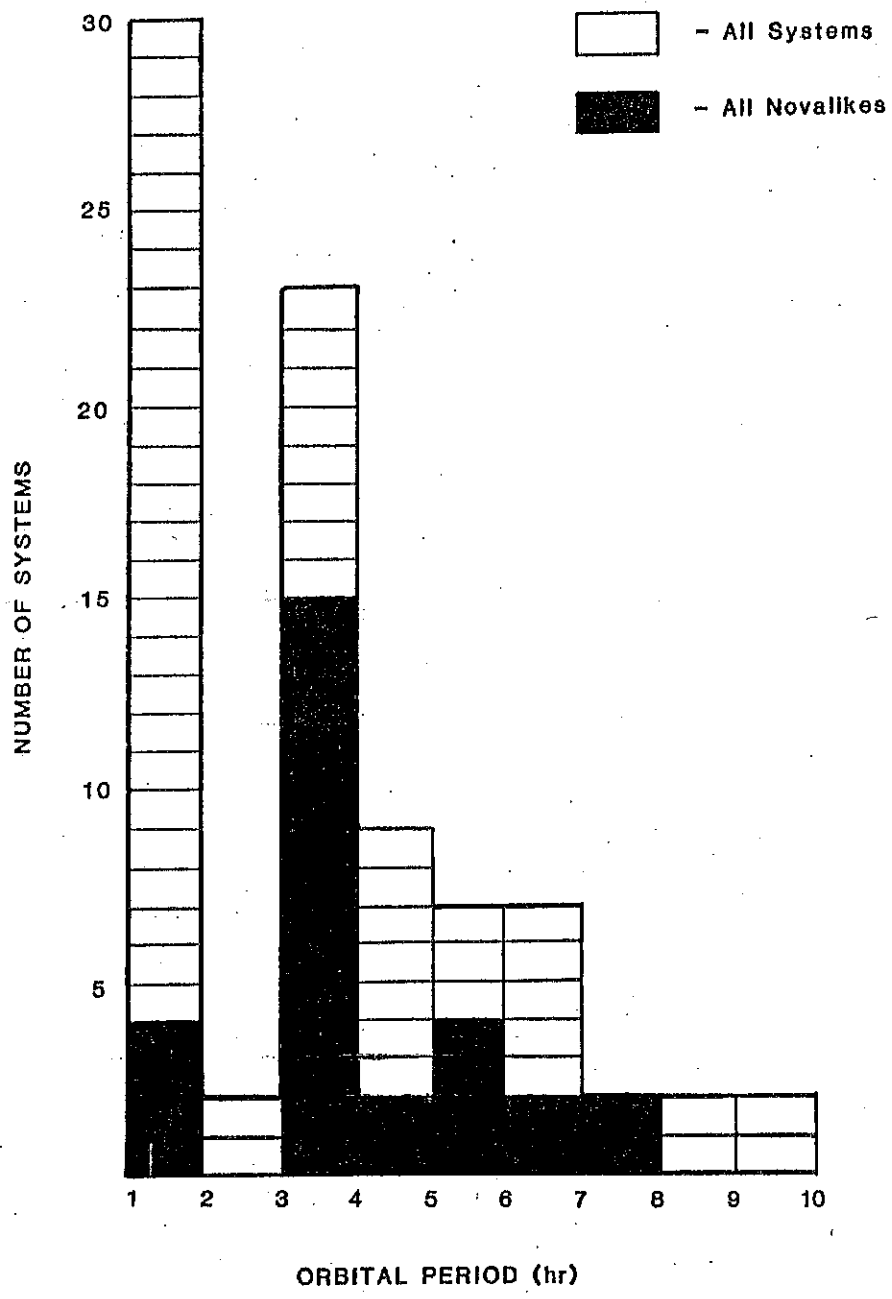
Figure 1d
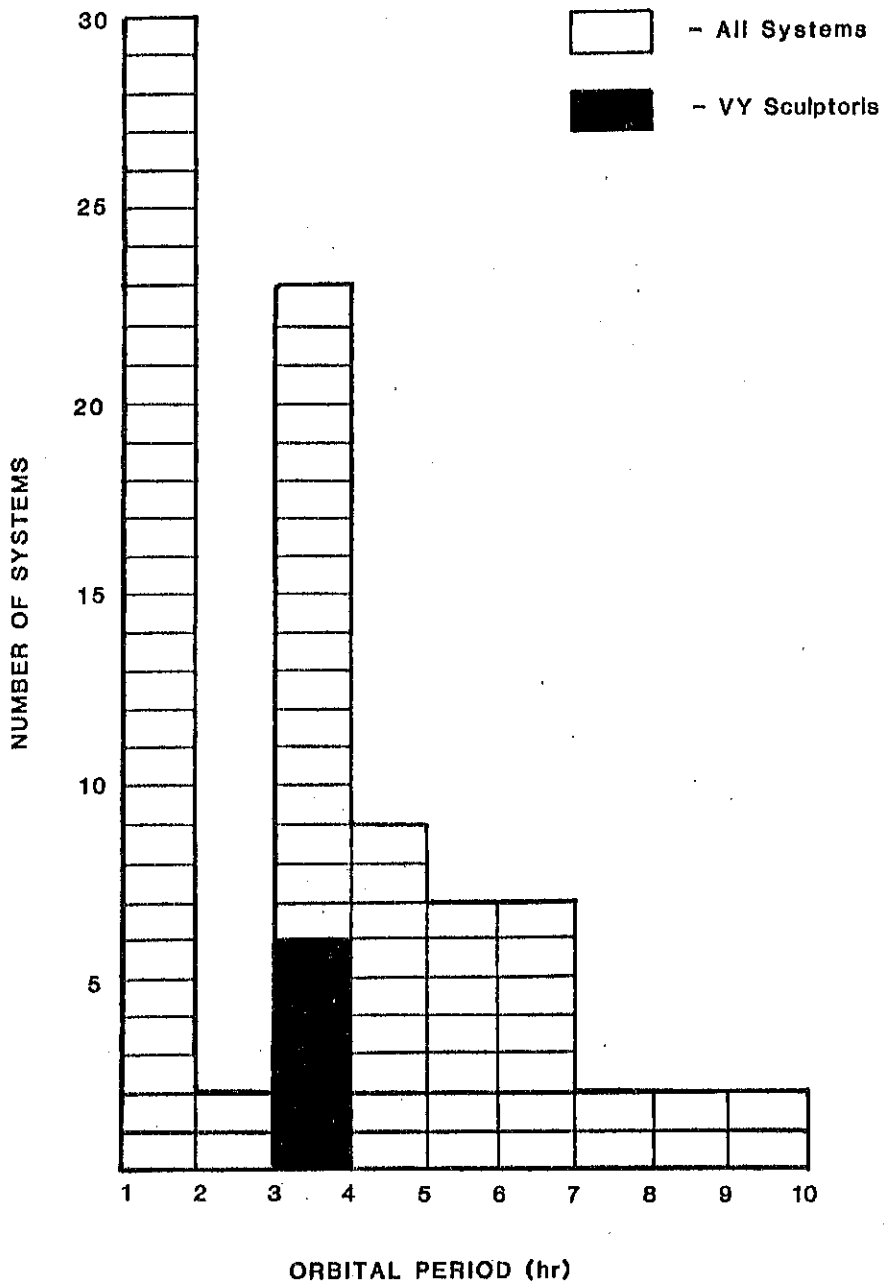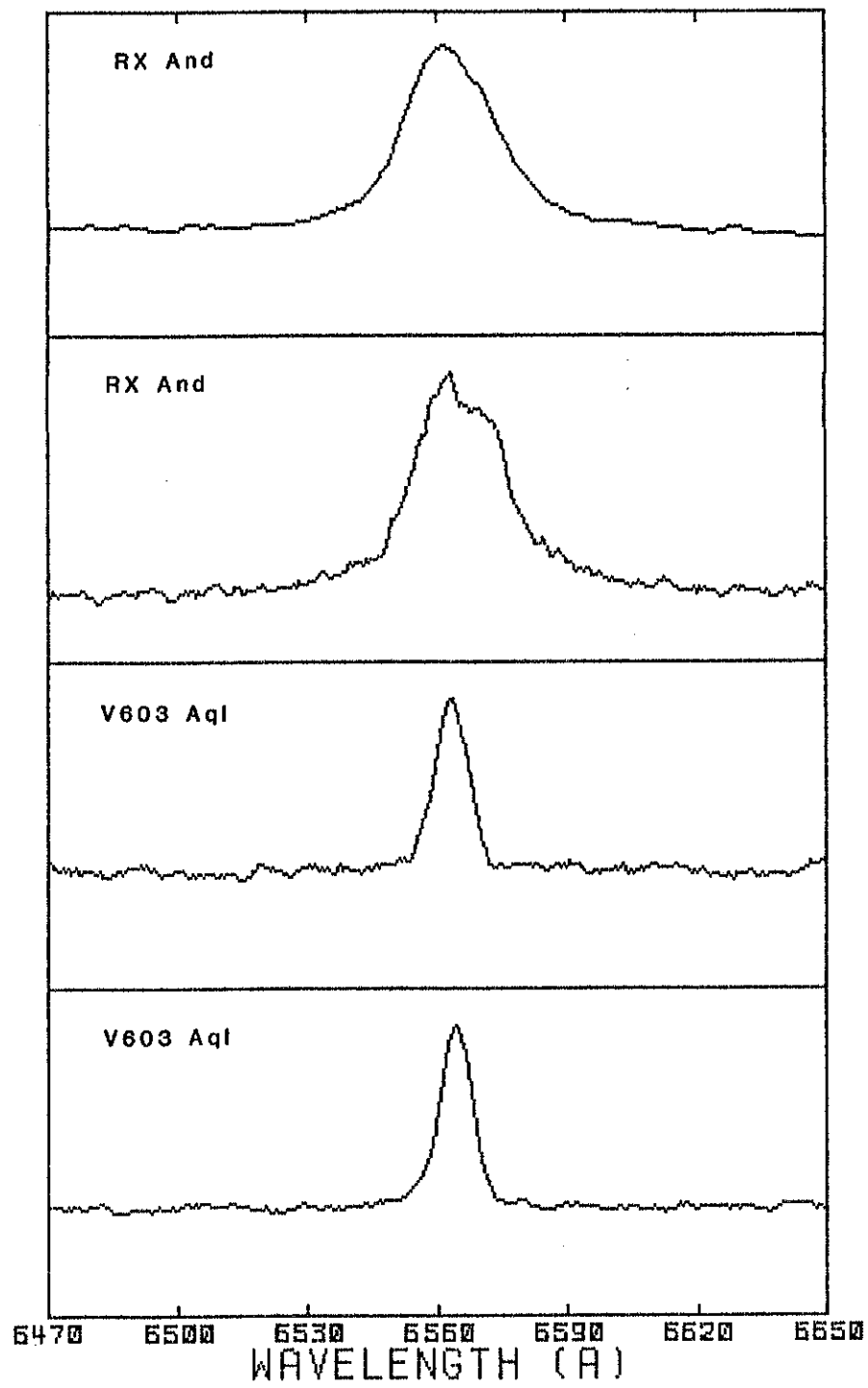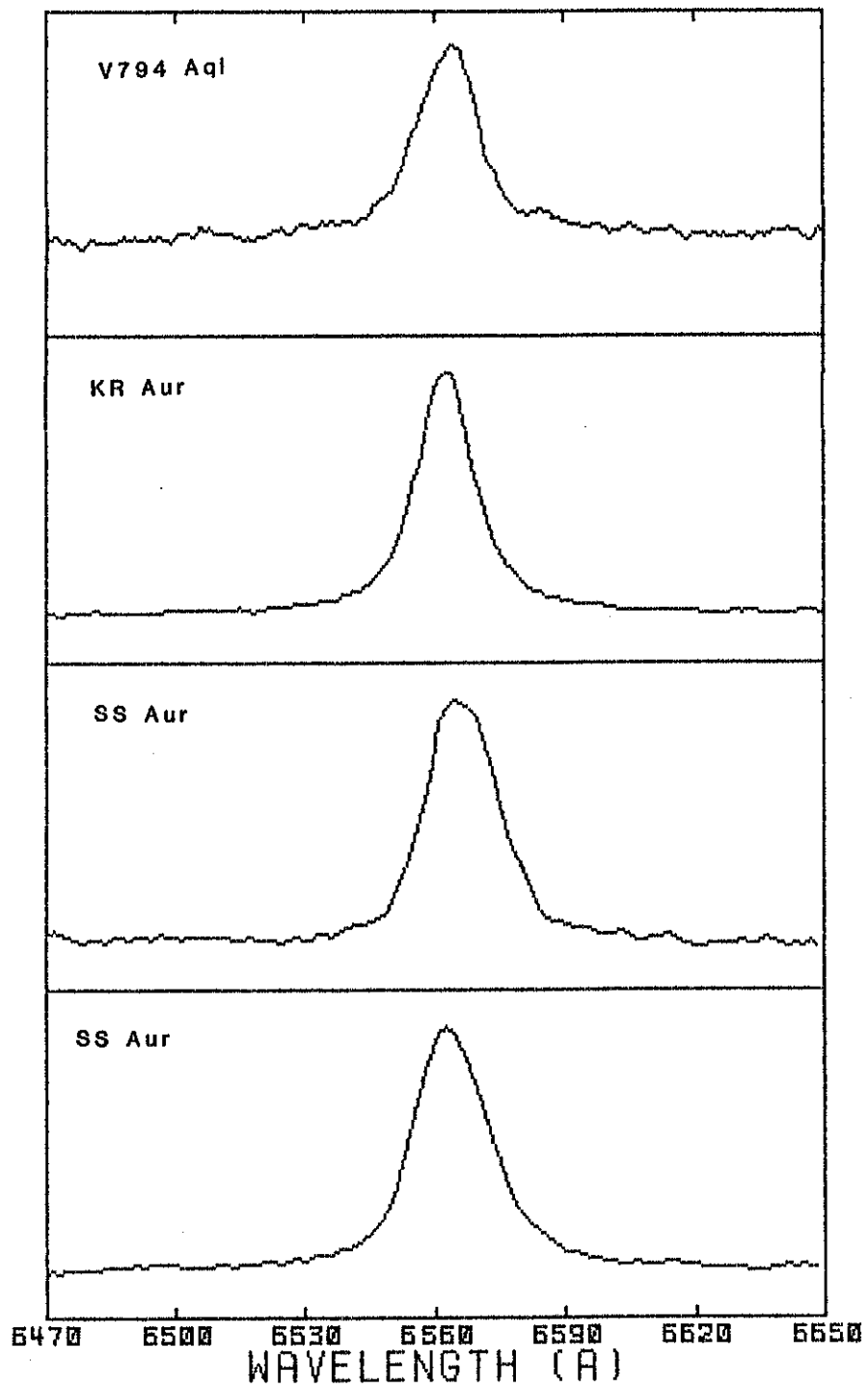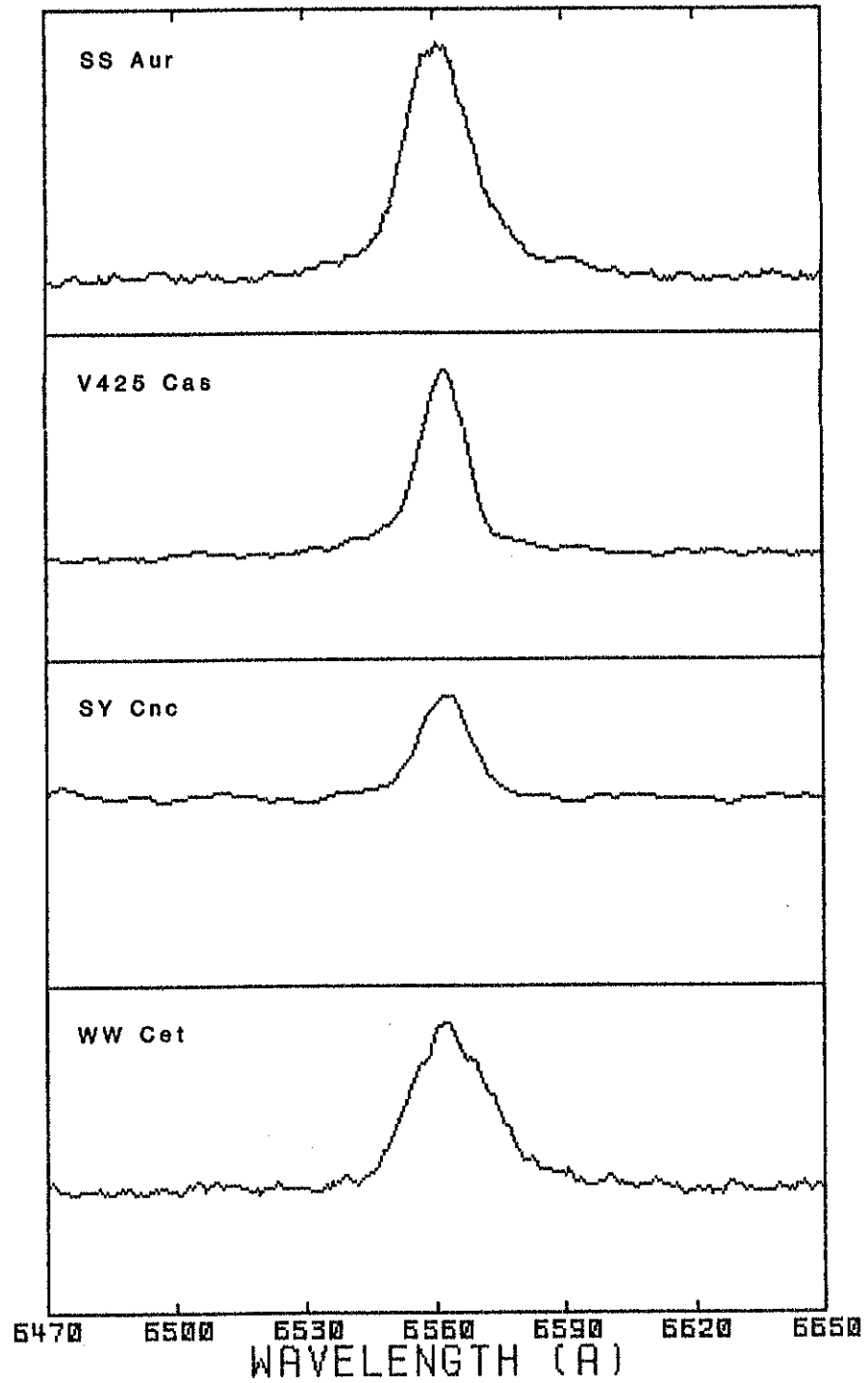
Figure 1e
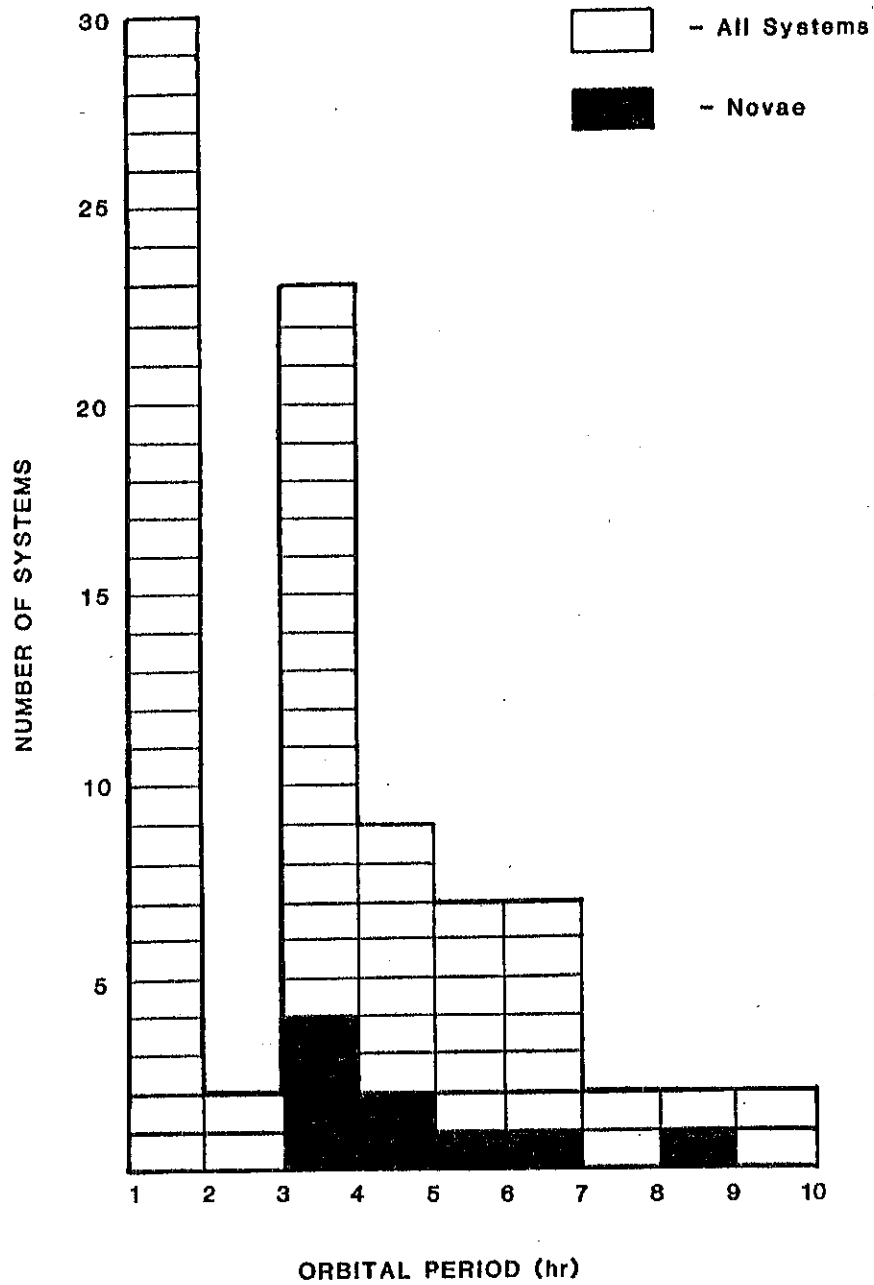
Figure 1f
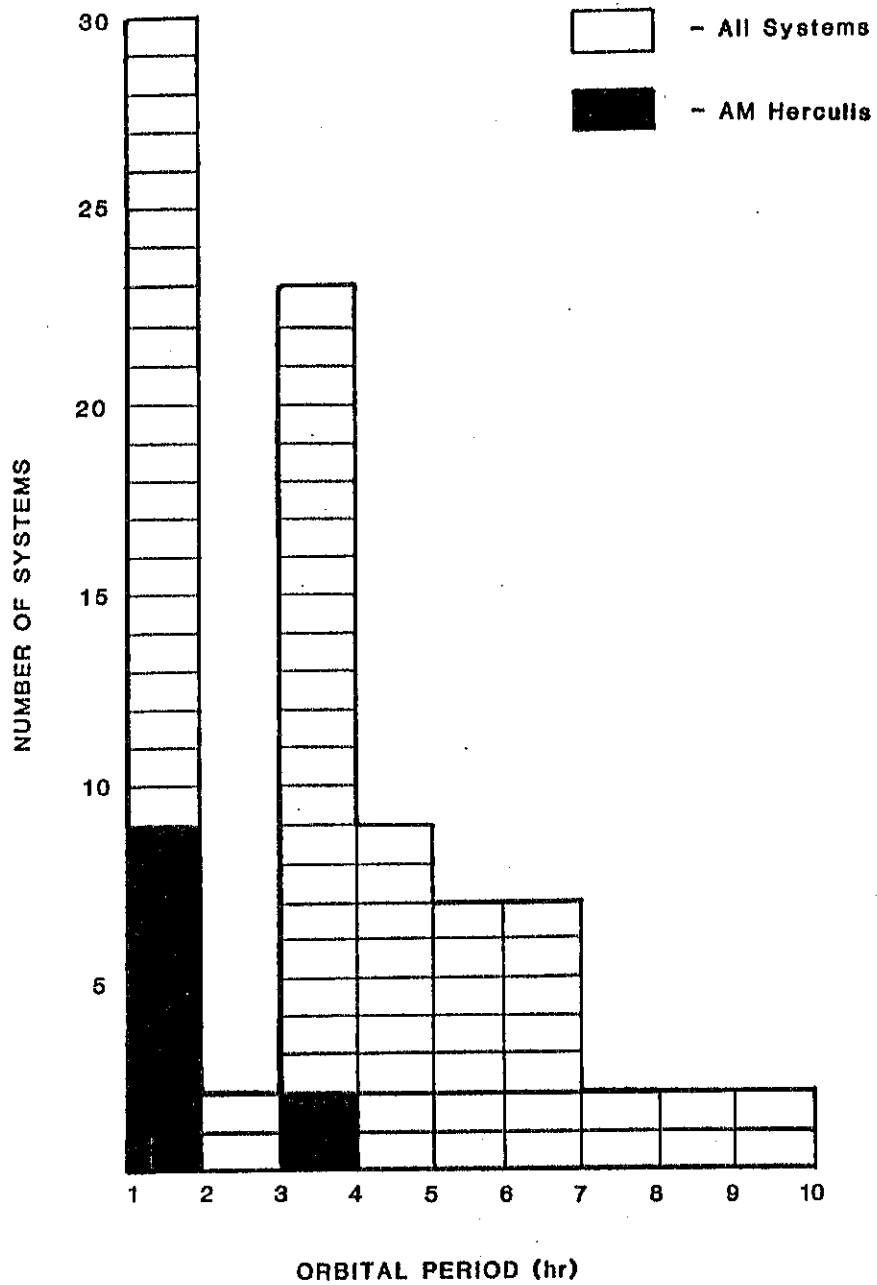
Figure 1g

Figures 2a-ff.   The Hα line profiles of the systems used in the

calibration.   The dashed line represents the value of

v_d sin i which has been derived from the known mass

ratio of the system via equation II.18.   The solid line

represents the value of v_d sin i defined by the

canonical value of the parameter $\langle f \rangle$ (= 0.30).

Figure 2a

122

Figure 2b

AE AQUARII   17-JUL-83 UT

WAVELENGTH (A)
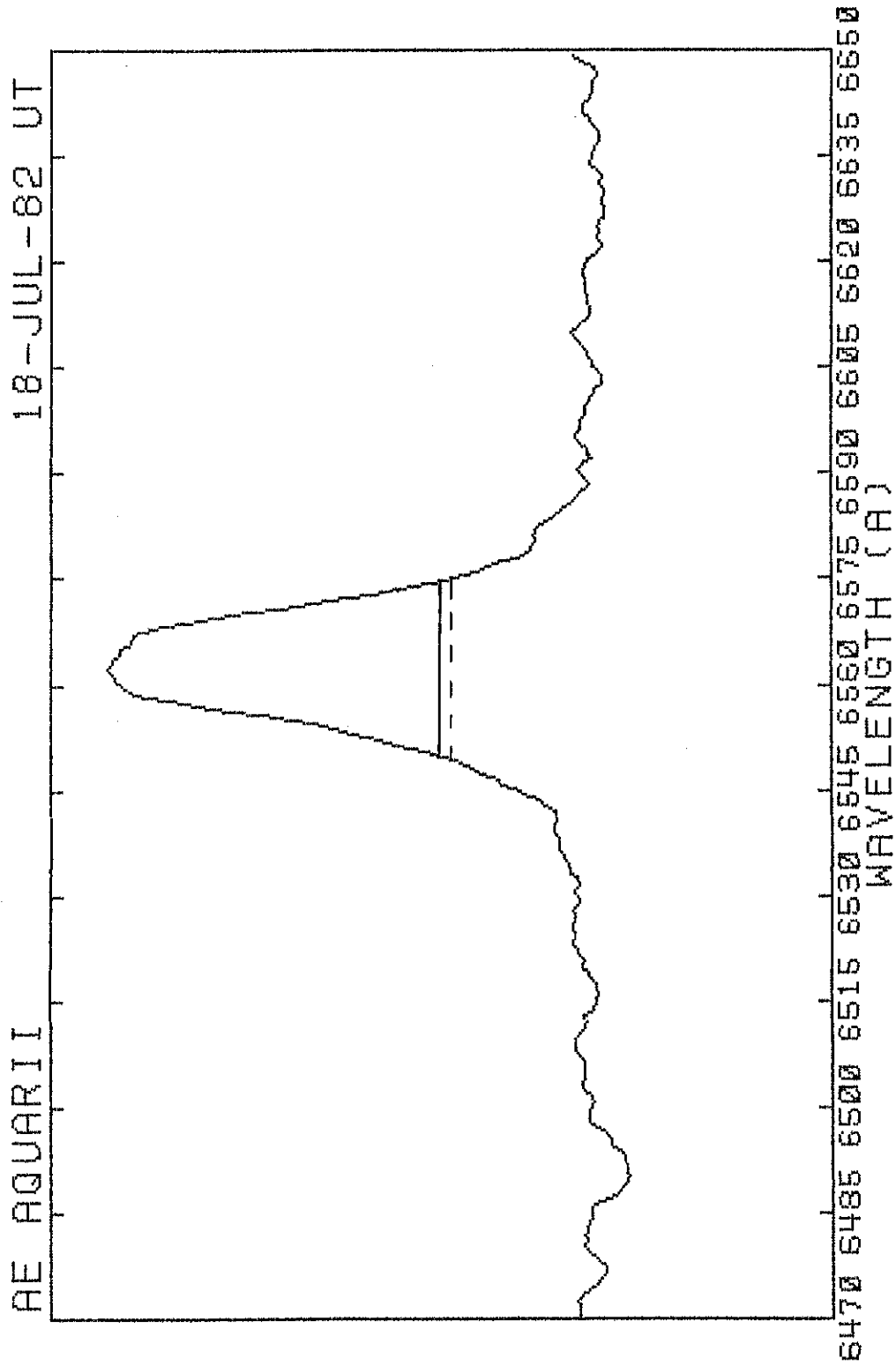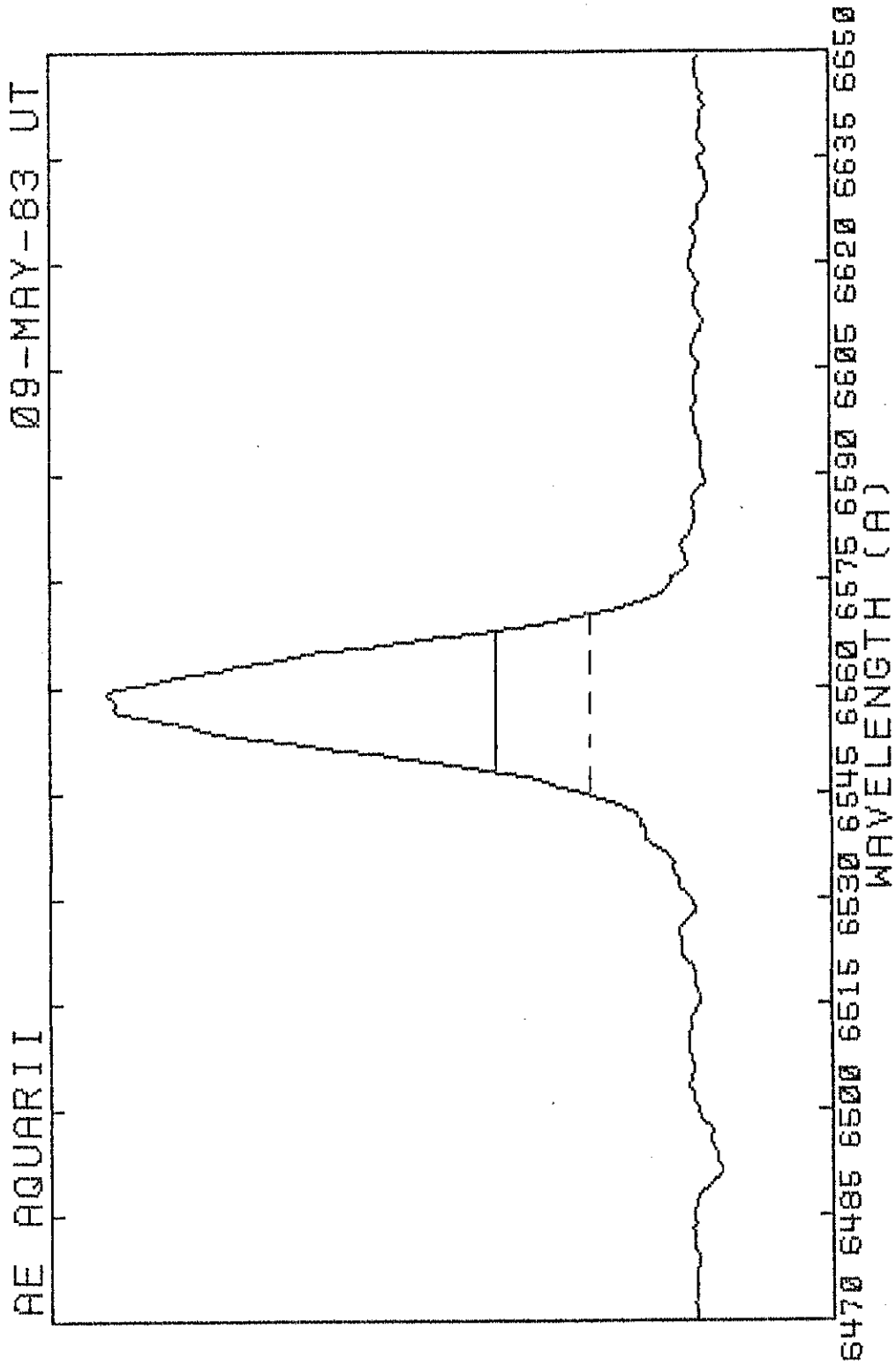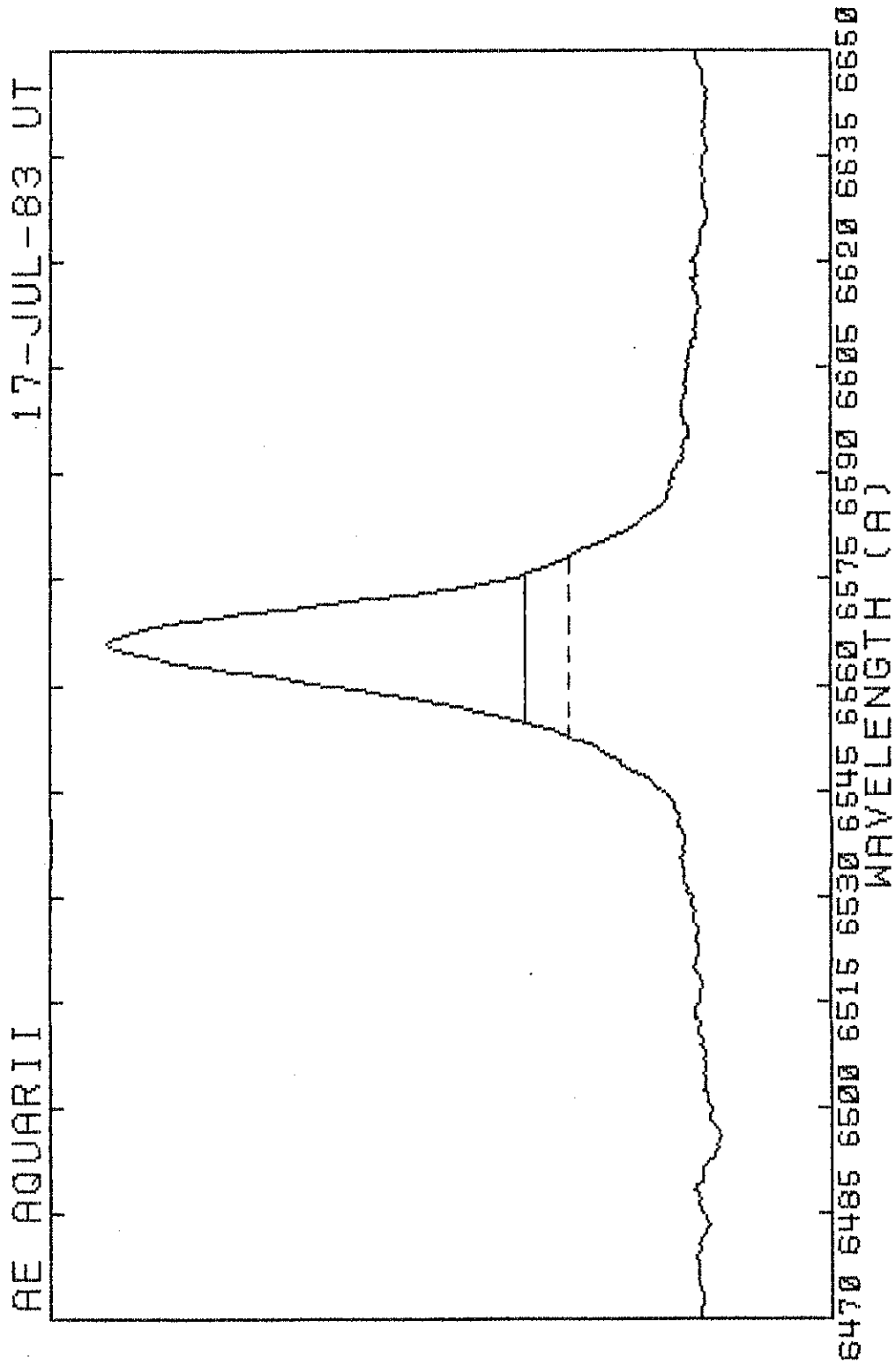
Figure 2c

Figure 2d

Figure 2e
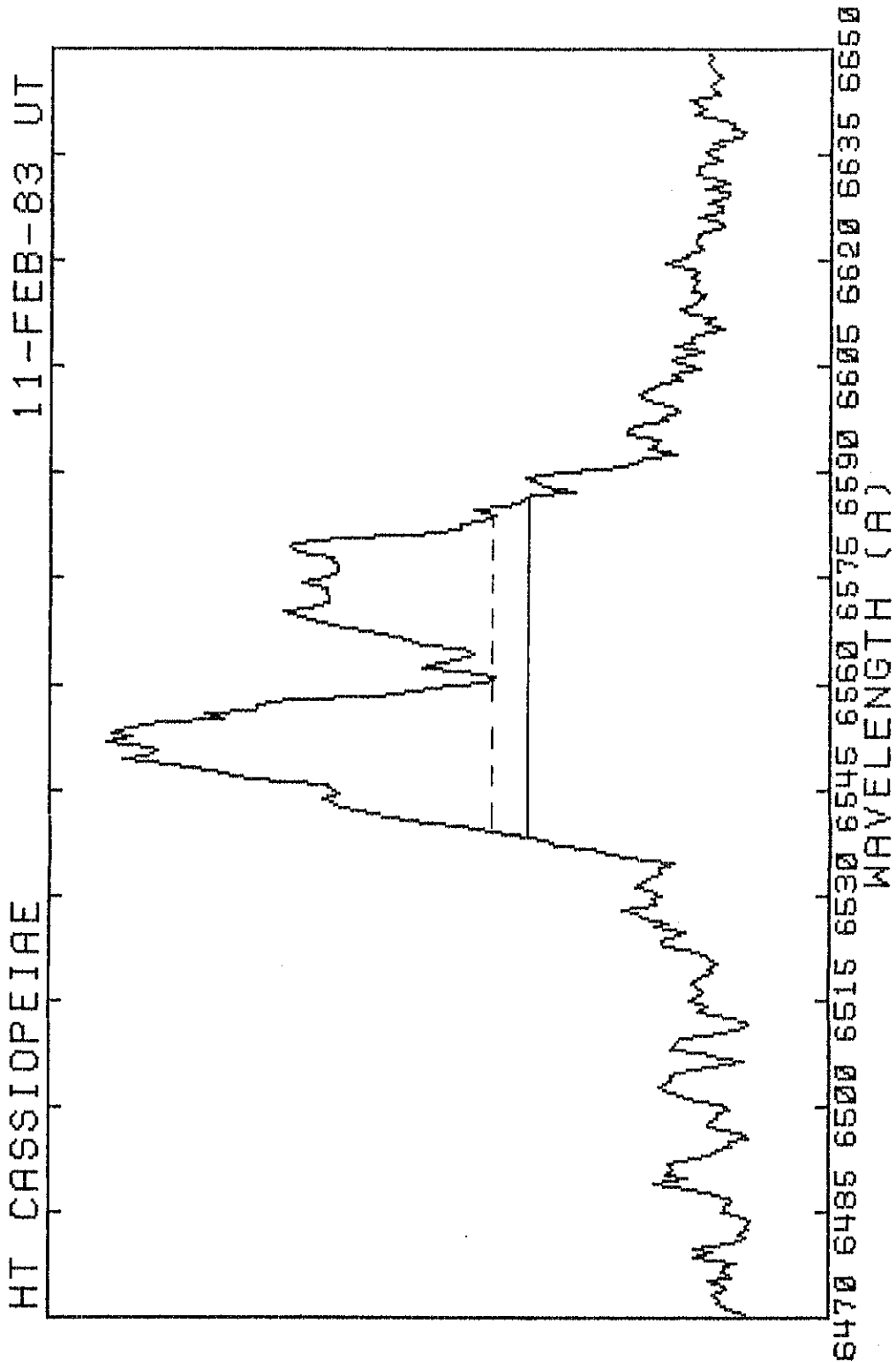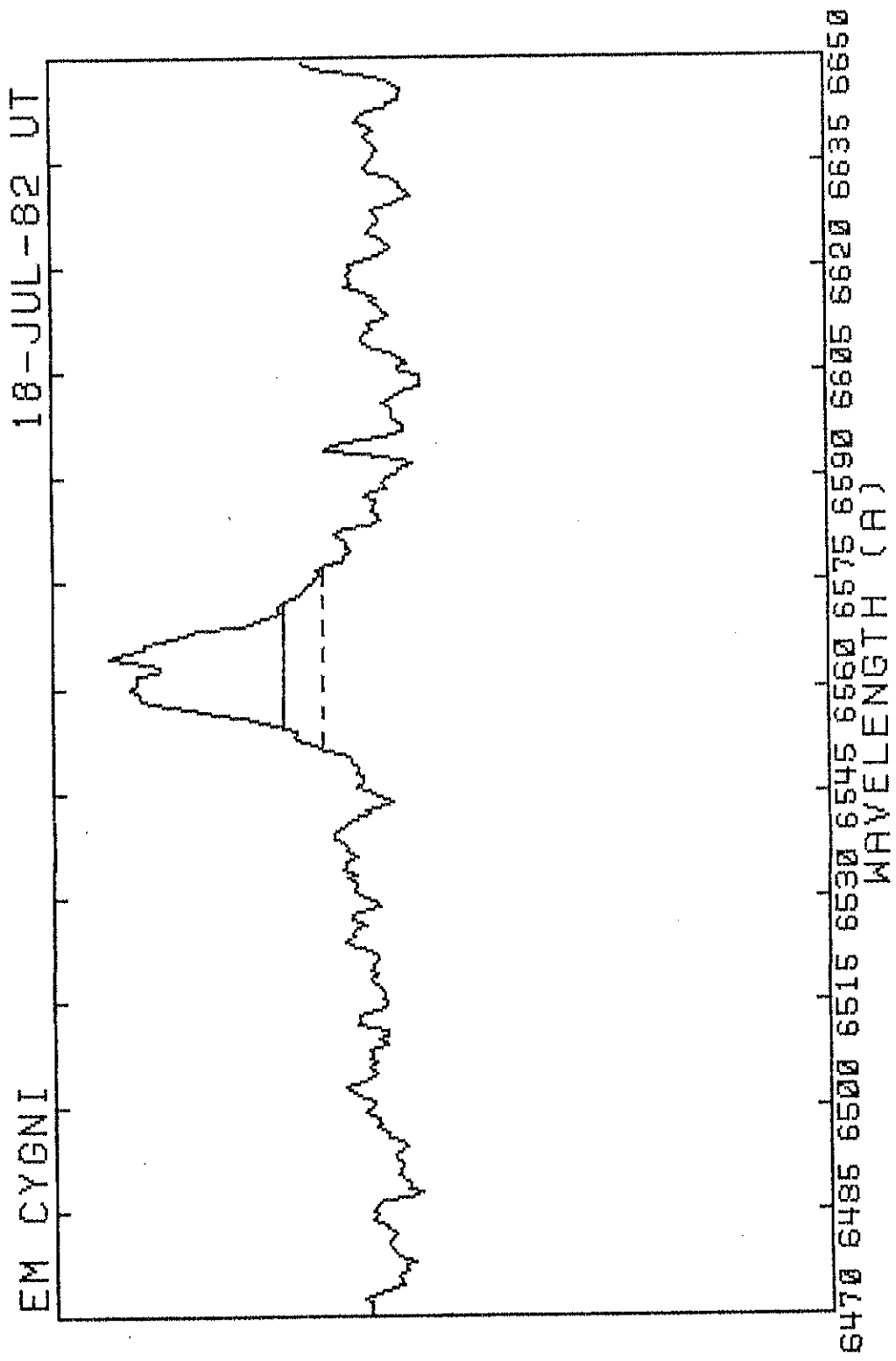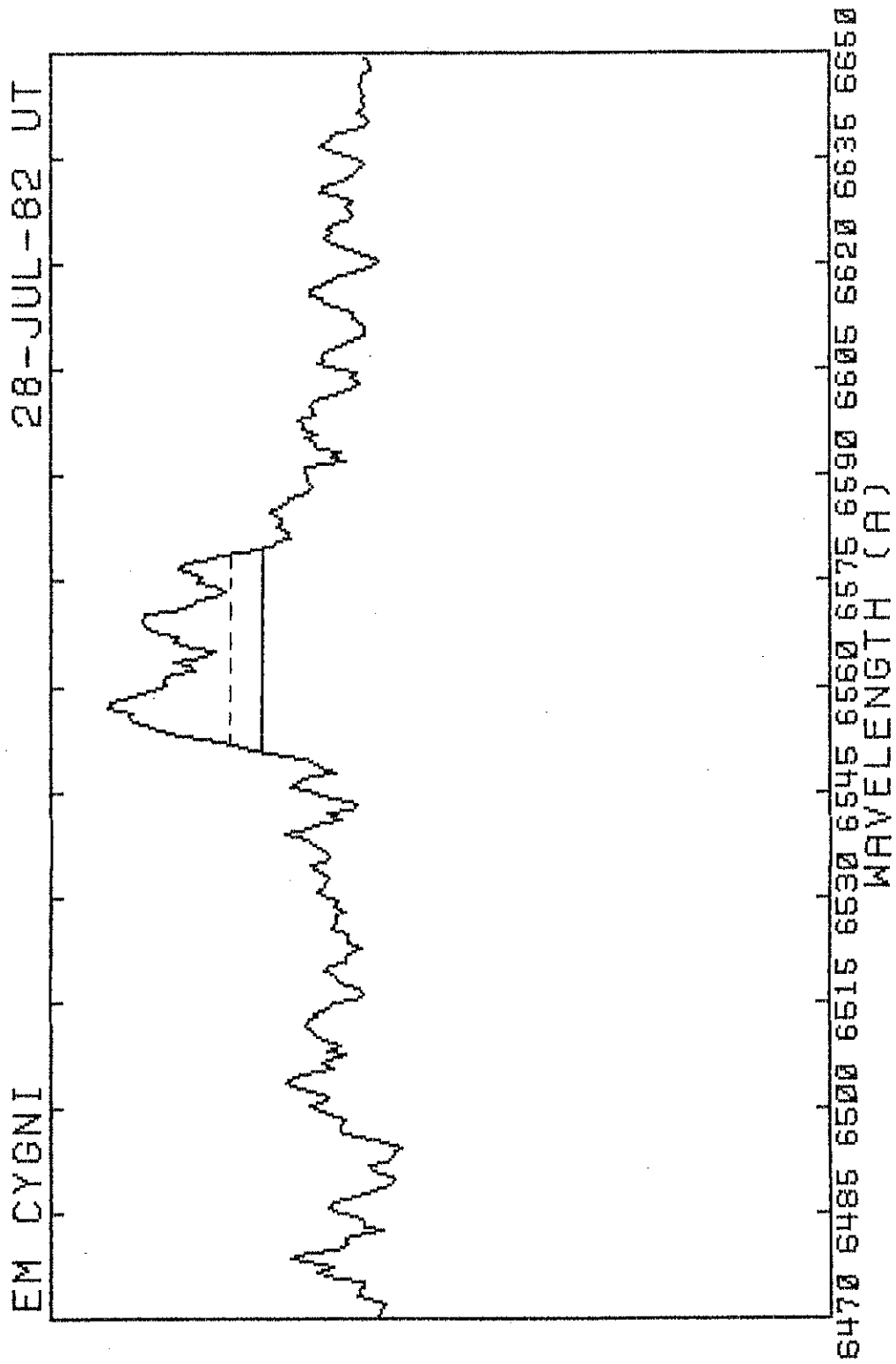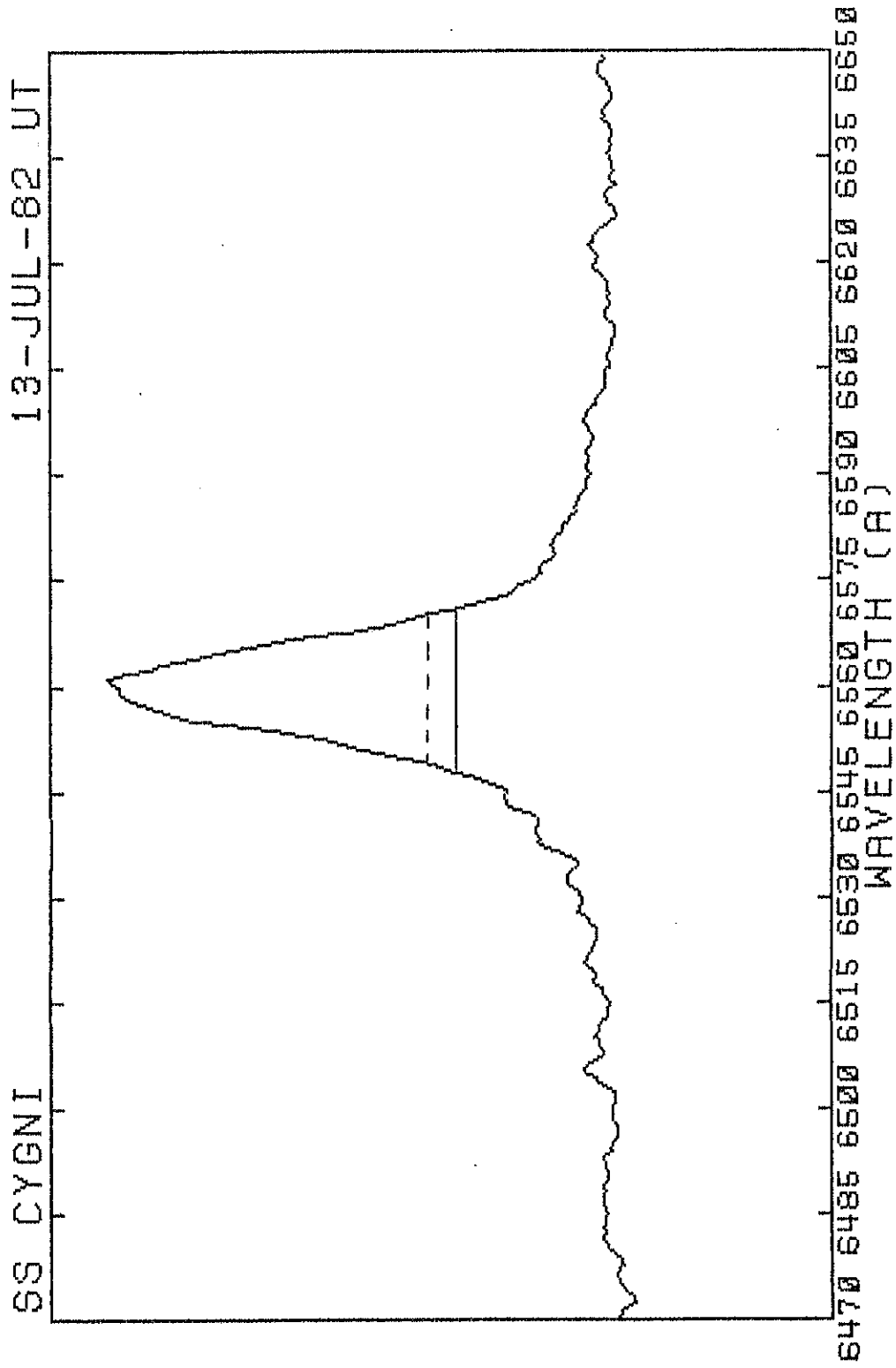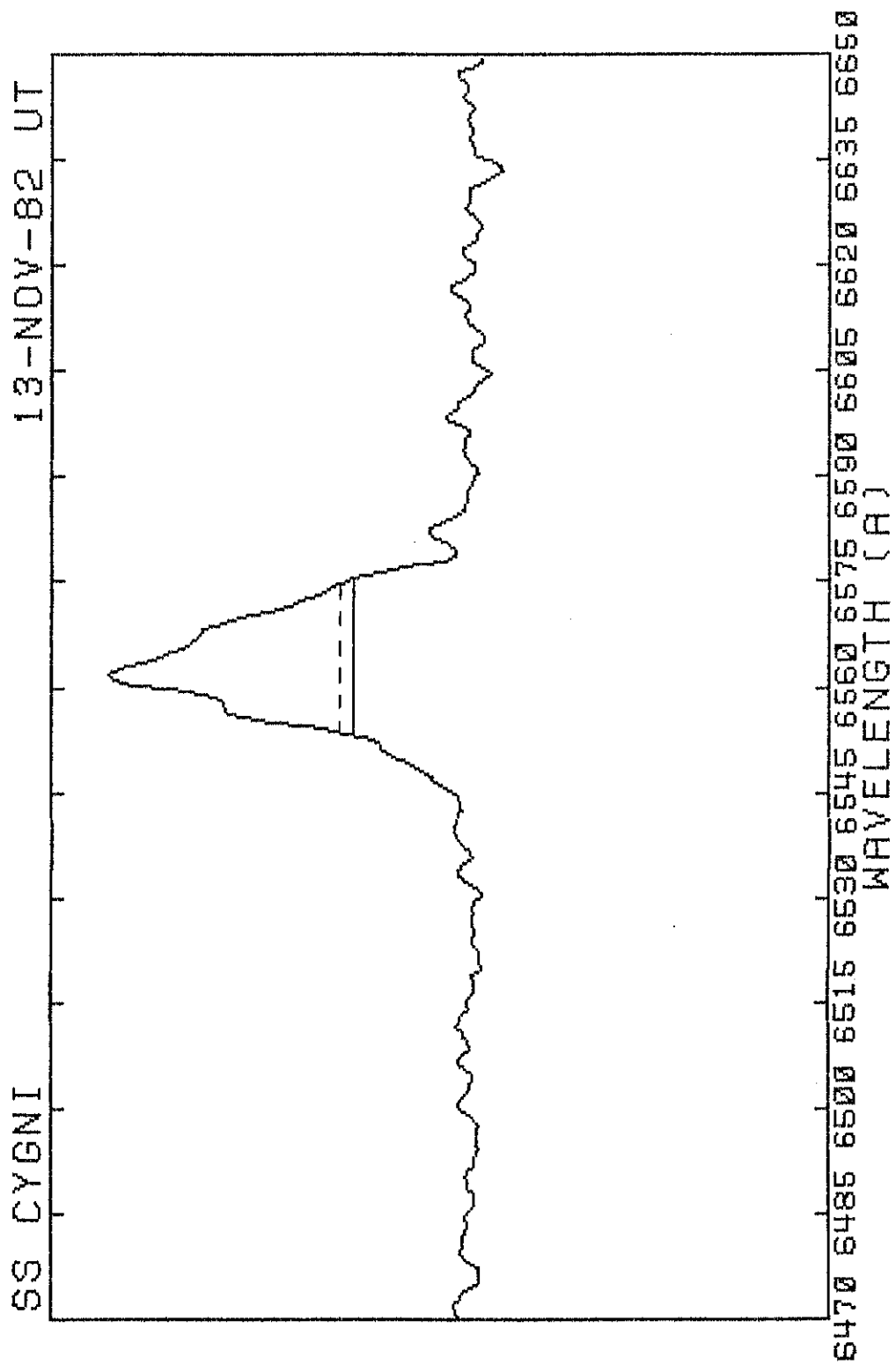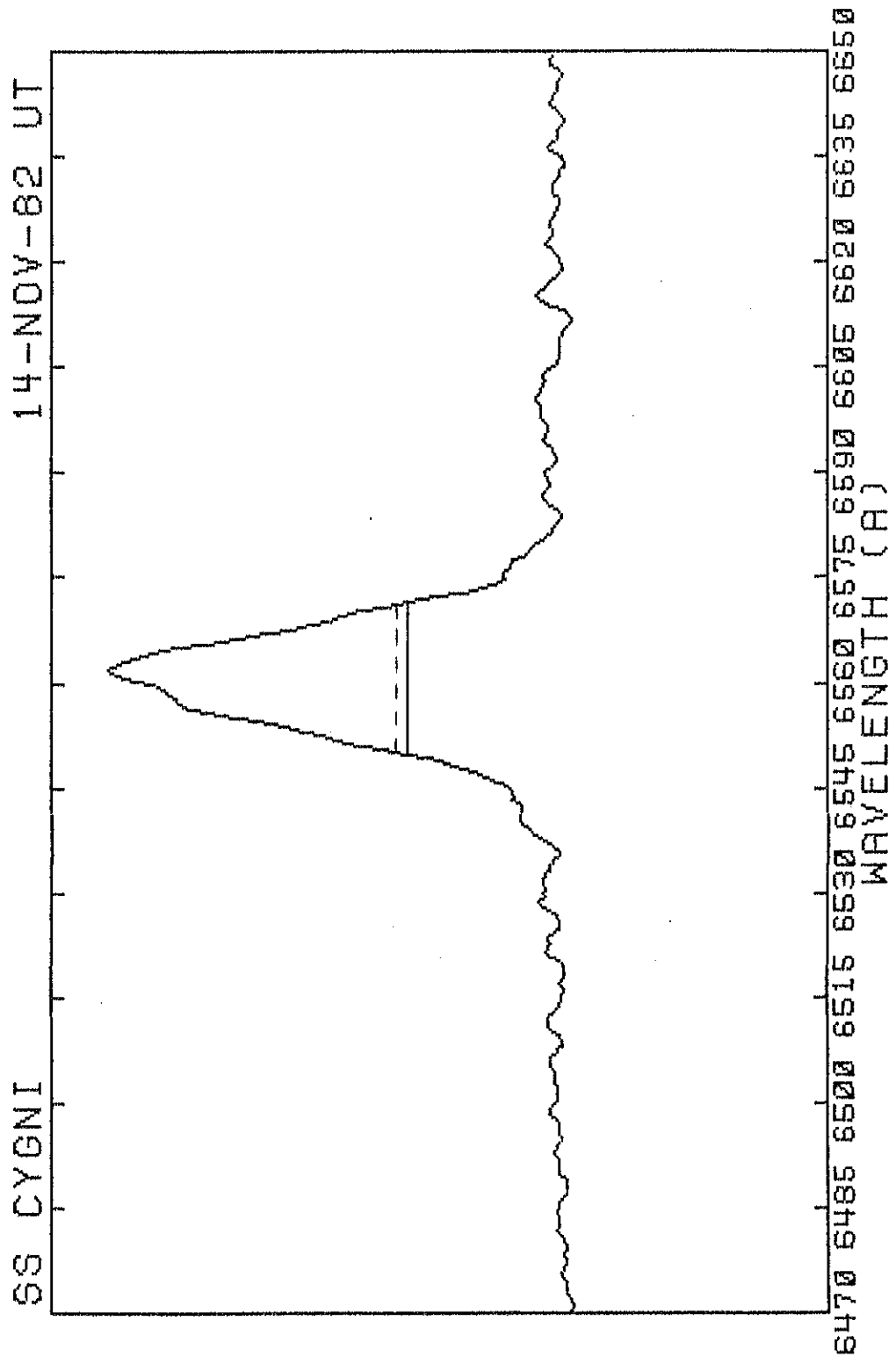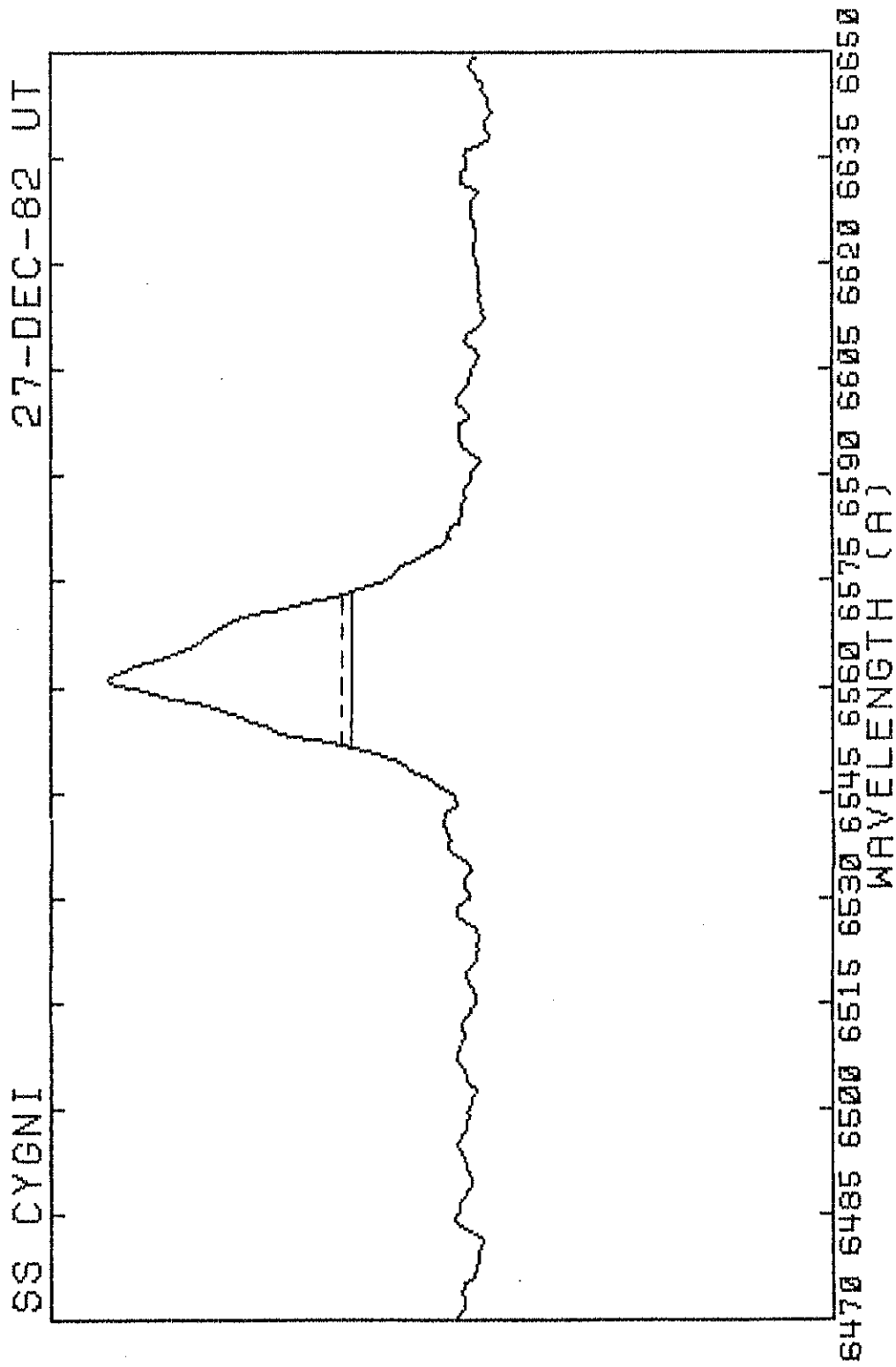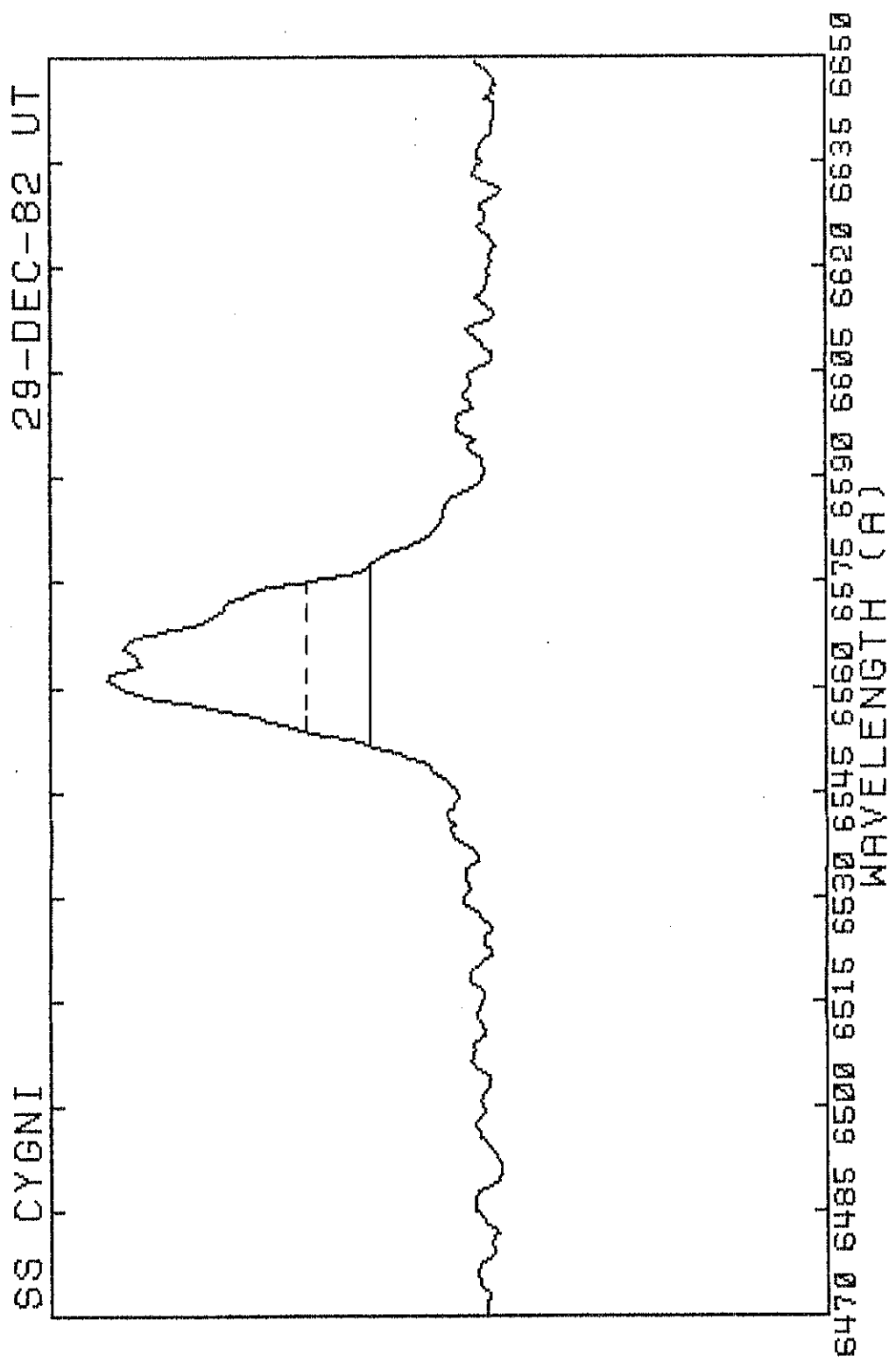
Z CAMELOPARDALIS   03-APR-83 UT

WAVELENGTH (A)

6470 6485 6500 6515 6530 6545 6560 6575 6590 6605 6620 6635 6650

126

Figure 2f

Figure 2g

Figure 2h

129

Figure 21

130

Figure 2j

131

Figure 2k

Figure 2 1

SS CYGNI   27-DEC-82 UT

WAVELENGTH (A)

Figure 2m

134

Figure 2n

Figure 2o

136

Figure 2p

137

Figure 2q

138

Figure 2r

Figure 2s

140

Figure 2t

Figure 2u

142

Figure 2v

143

Figure 2w

144

Figure 2x

145

Figure 2y

146

Figure 2z

147

Figure 2aa

148

Figure 2bb

LX SERPENTIS   09-MAY-83 UT

WAVELENGTH (A)

Figure 2cc

150

LX SERPENTIS   17-JUL-83 UT

Figure 2dd

WAVELENGTH (A)

Figure 2ee

152

Figure 2ff

RW TRIANGULI   27-DEC-82 UT

WAVELENGTH (A)
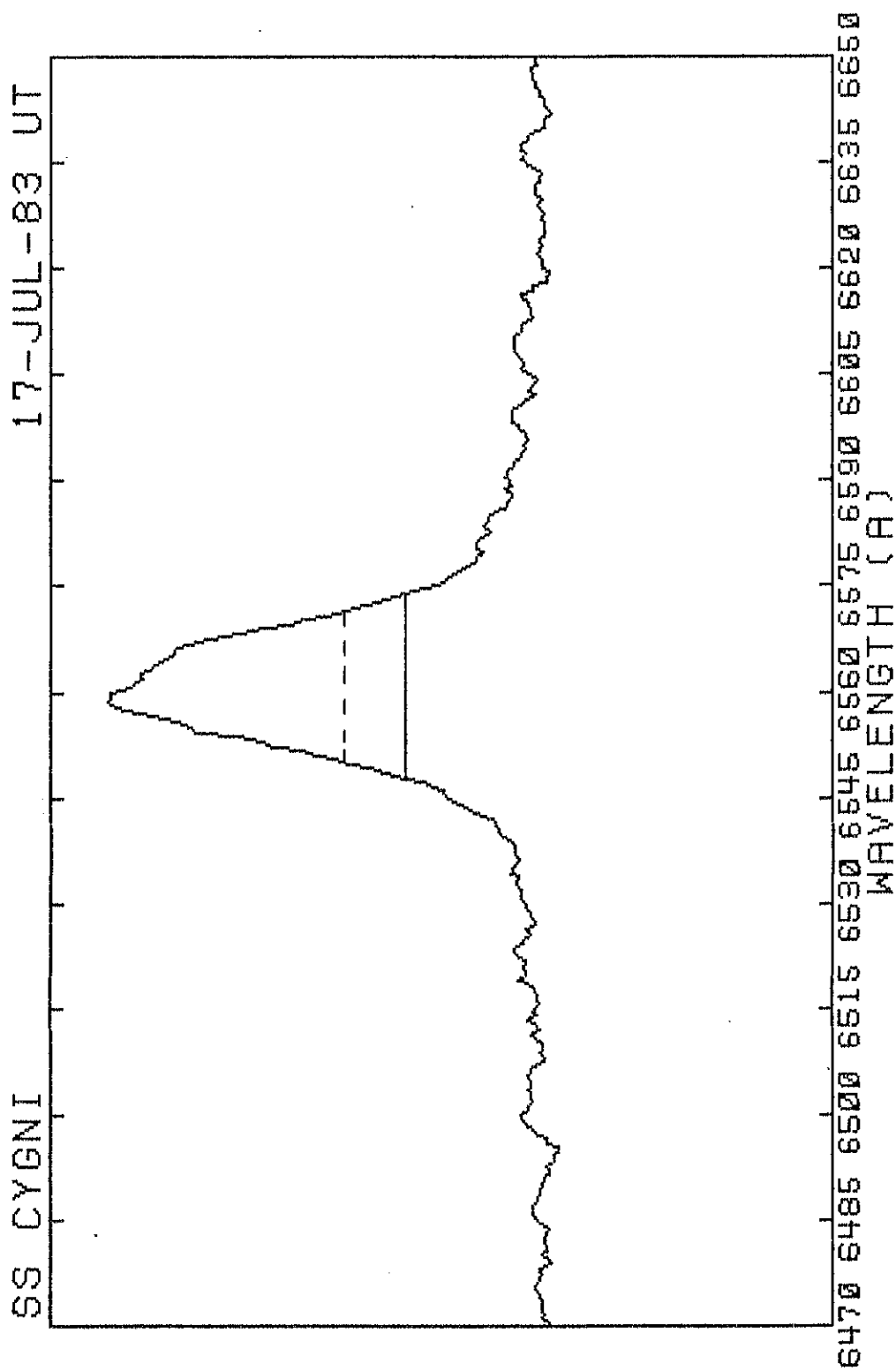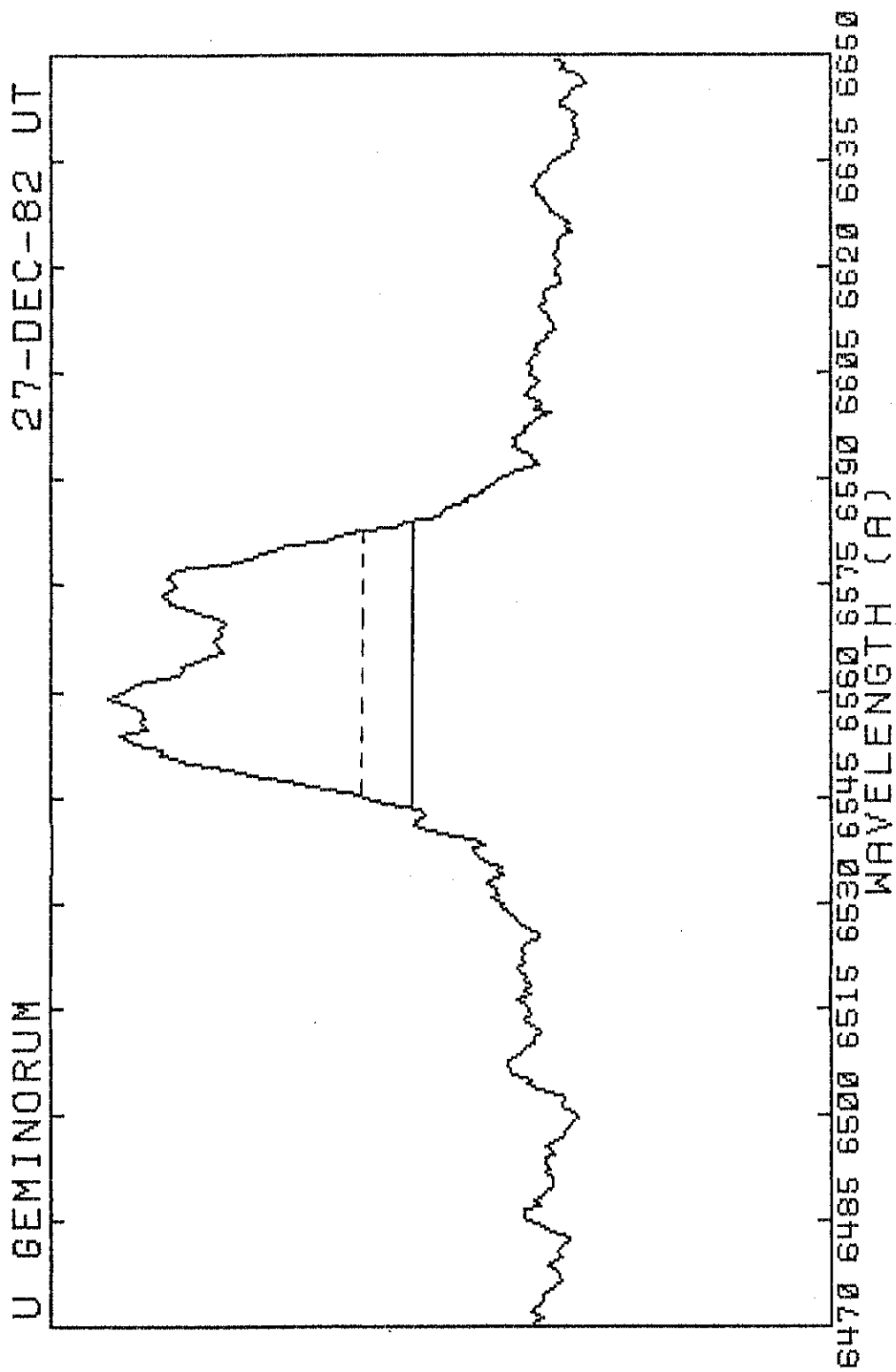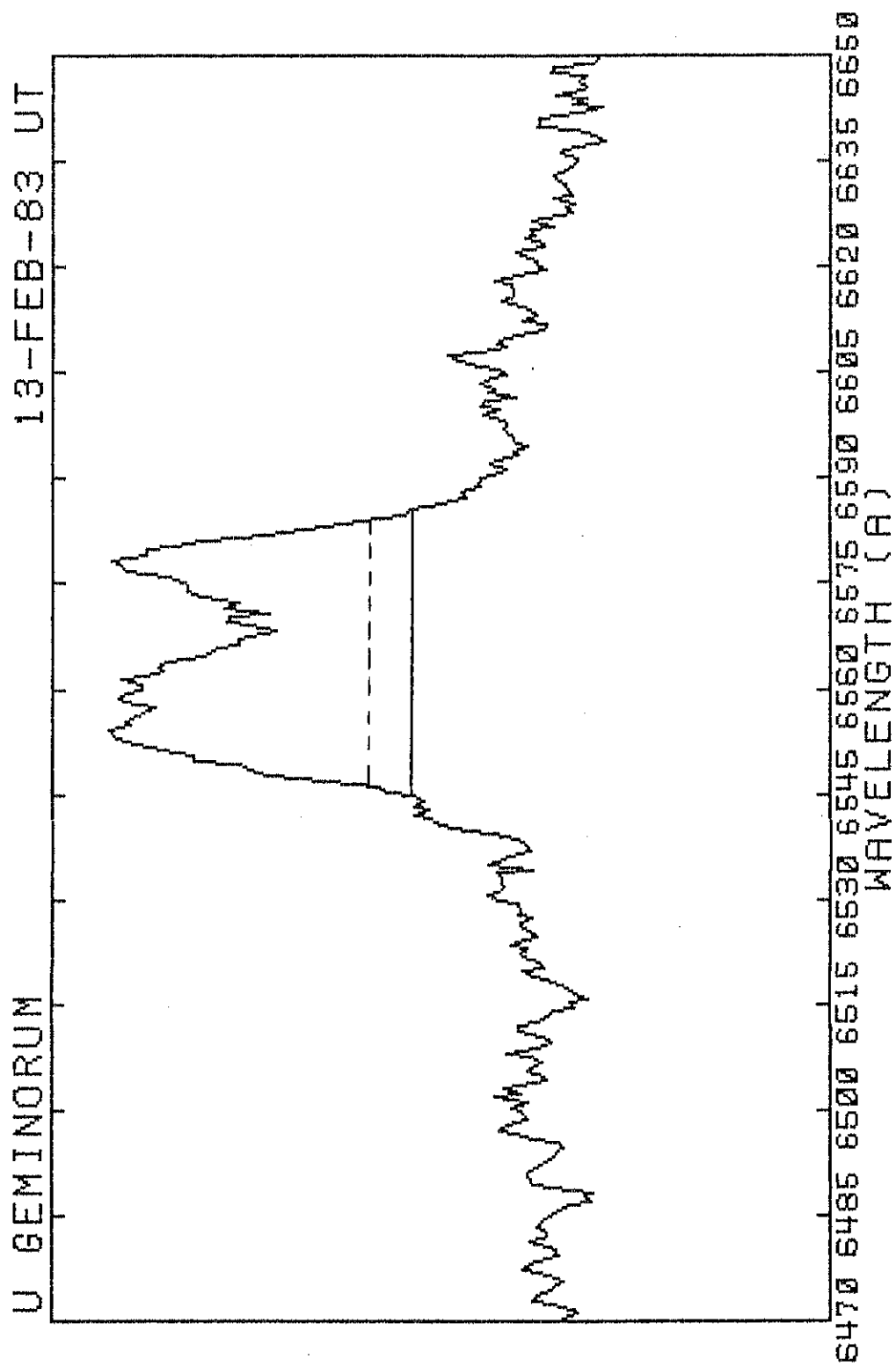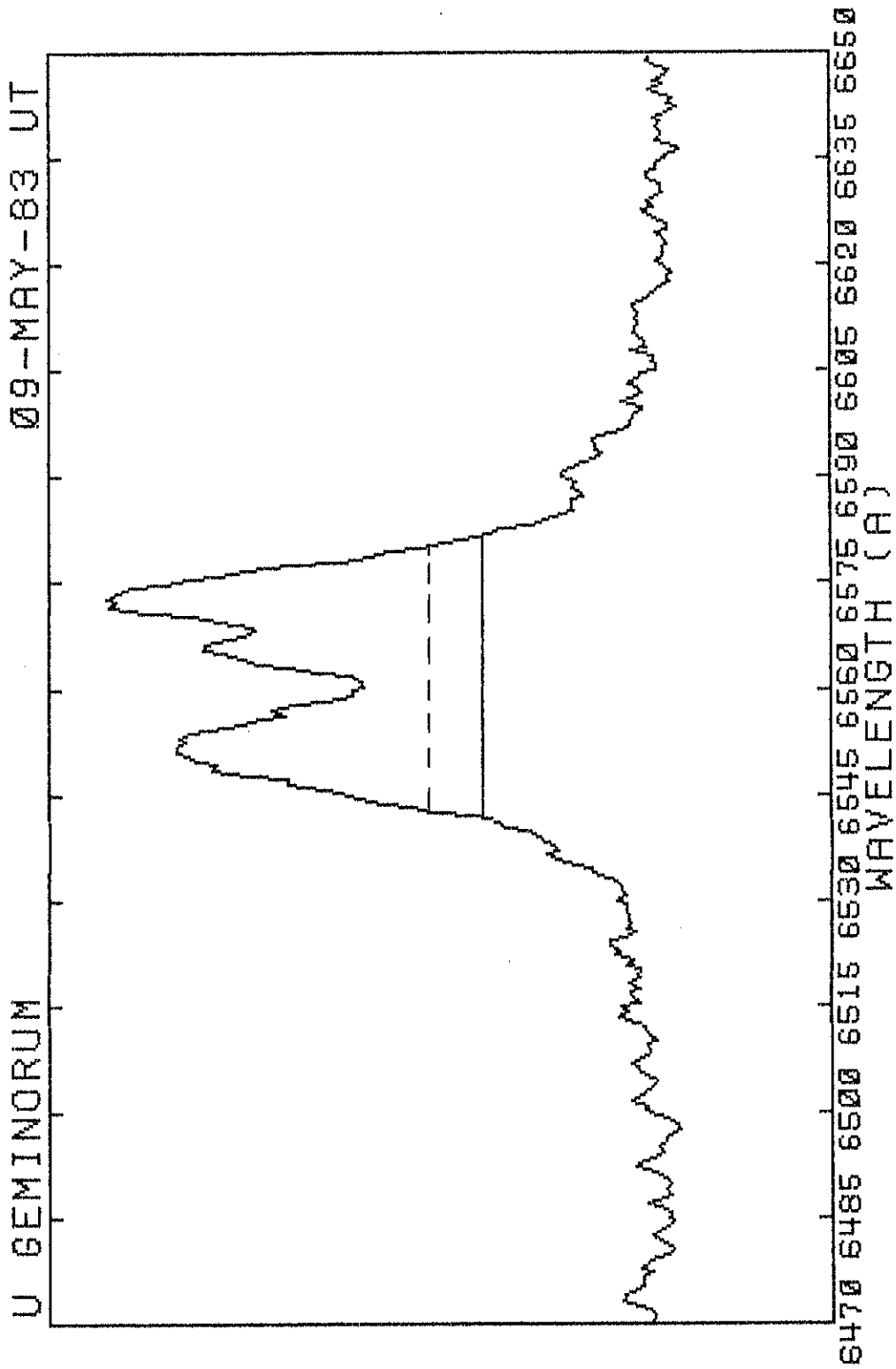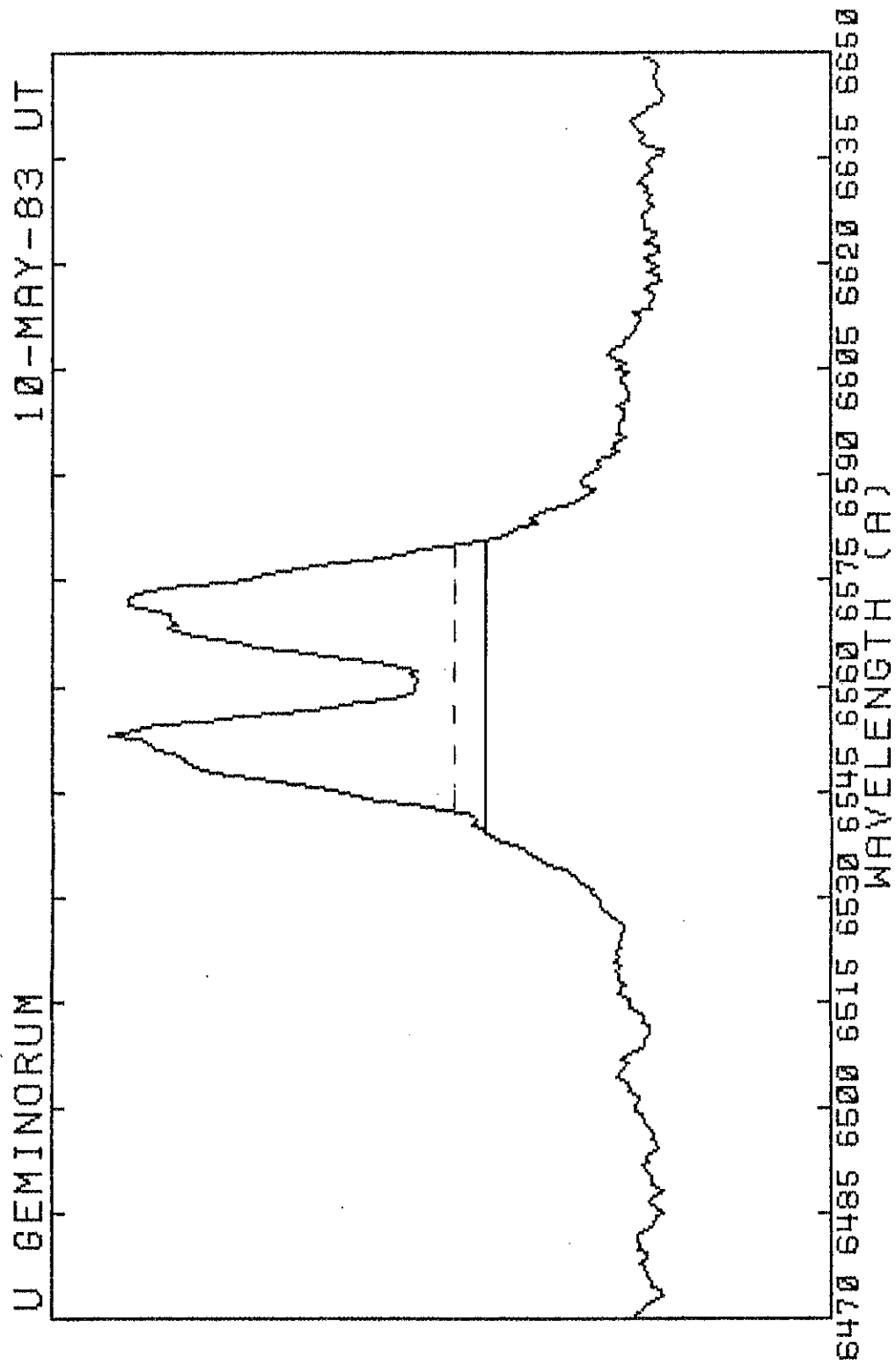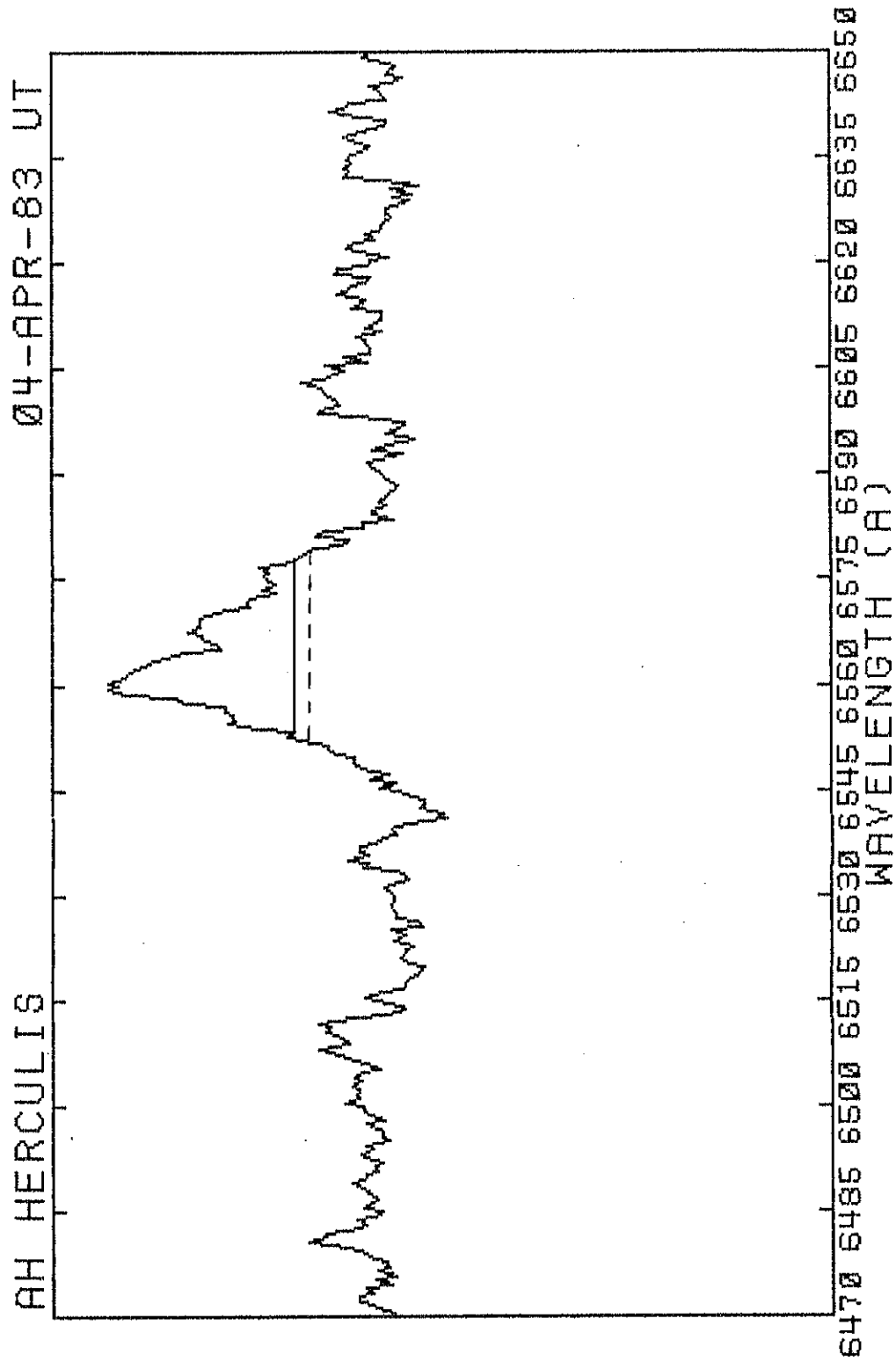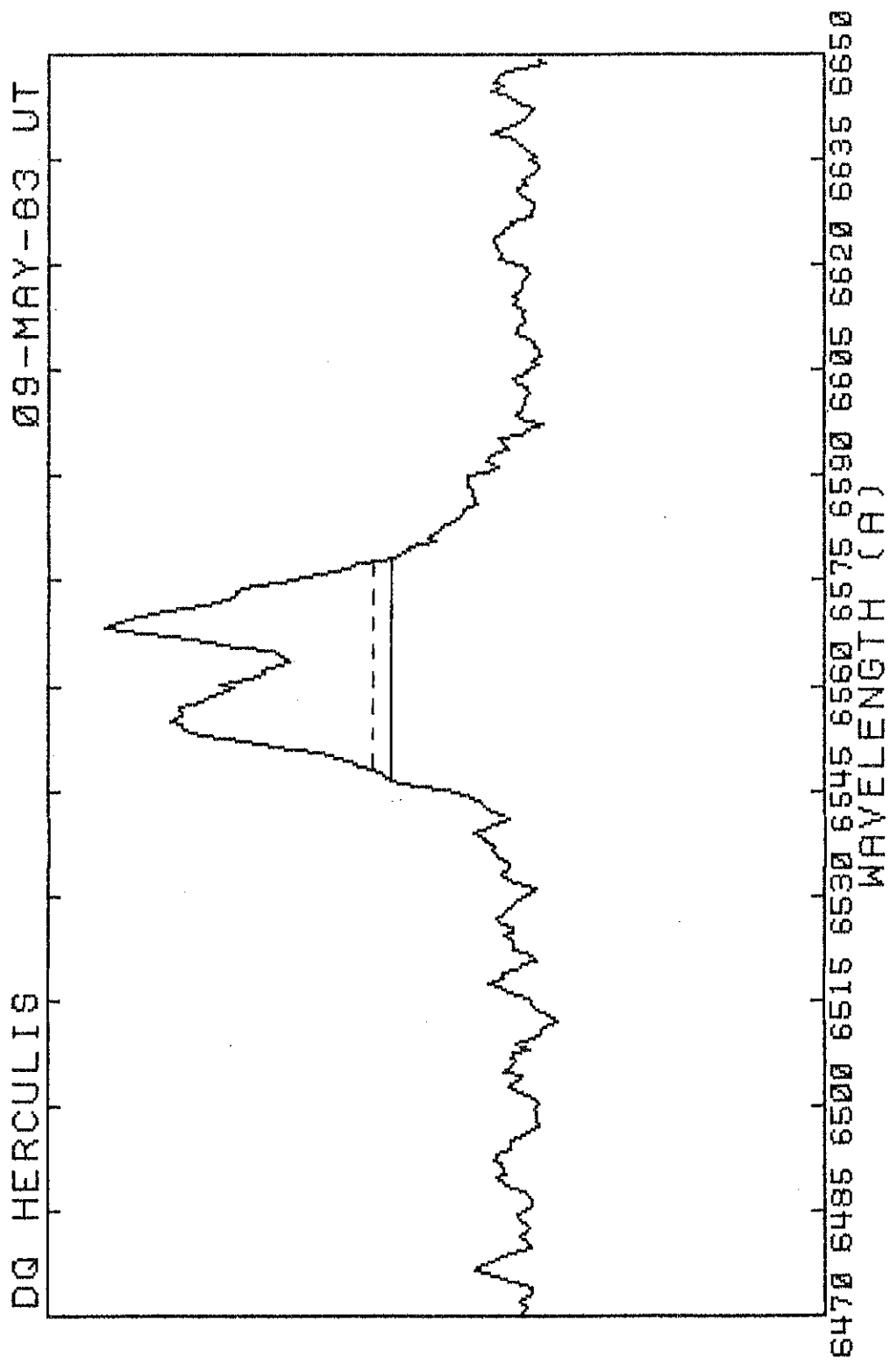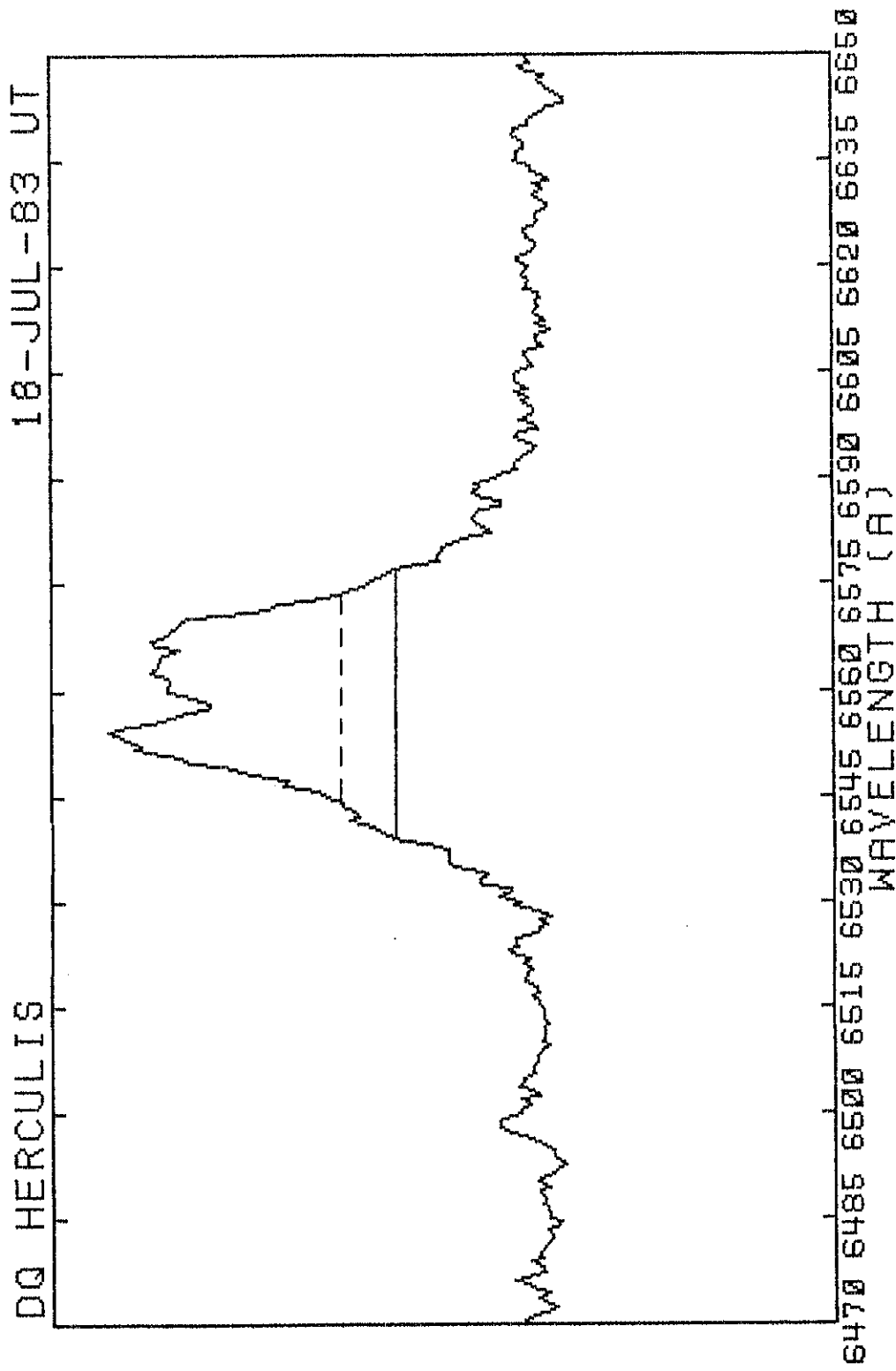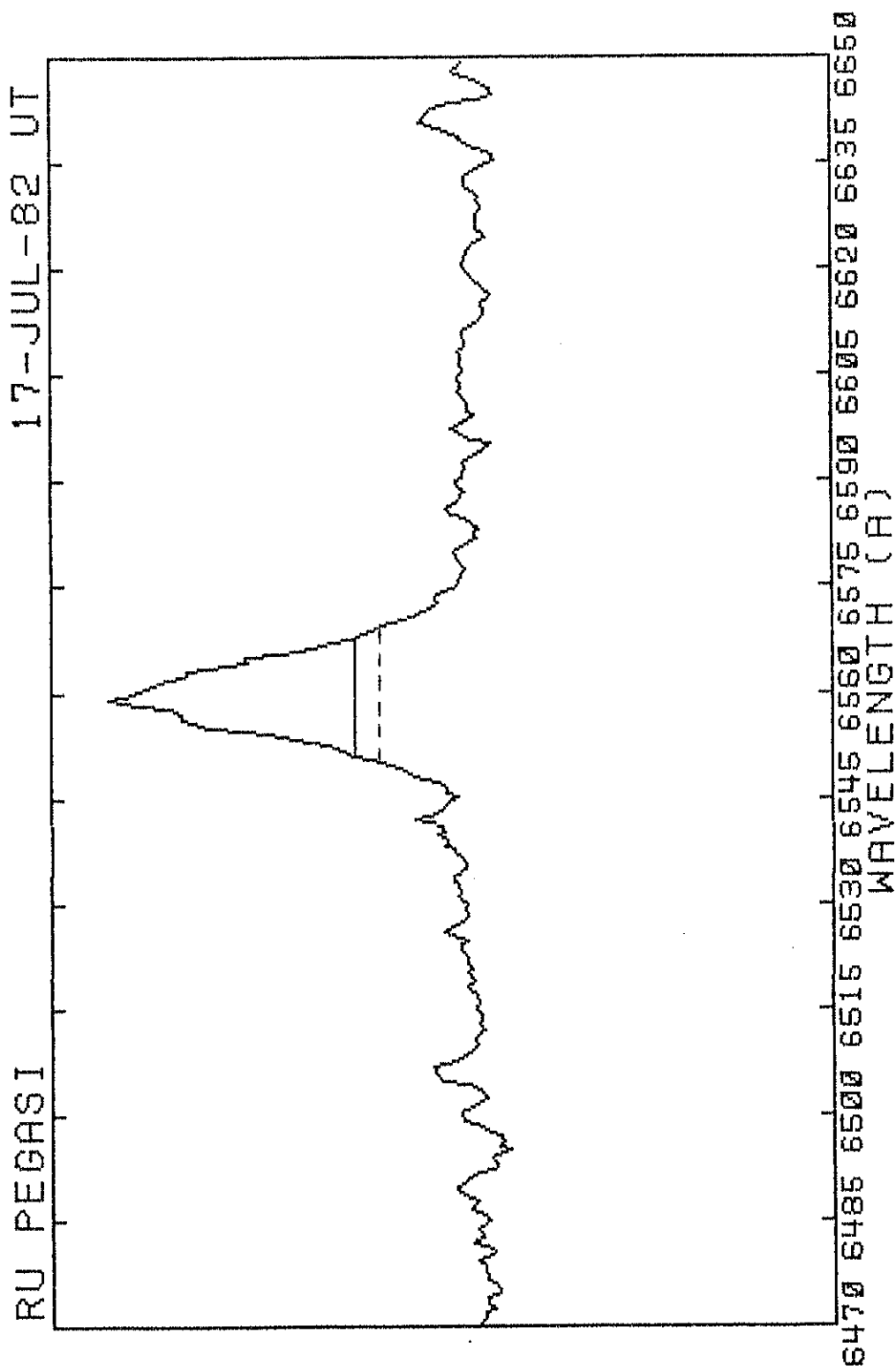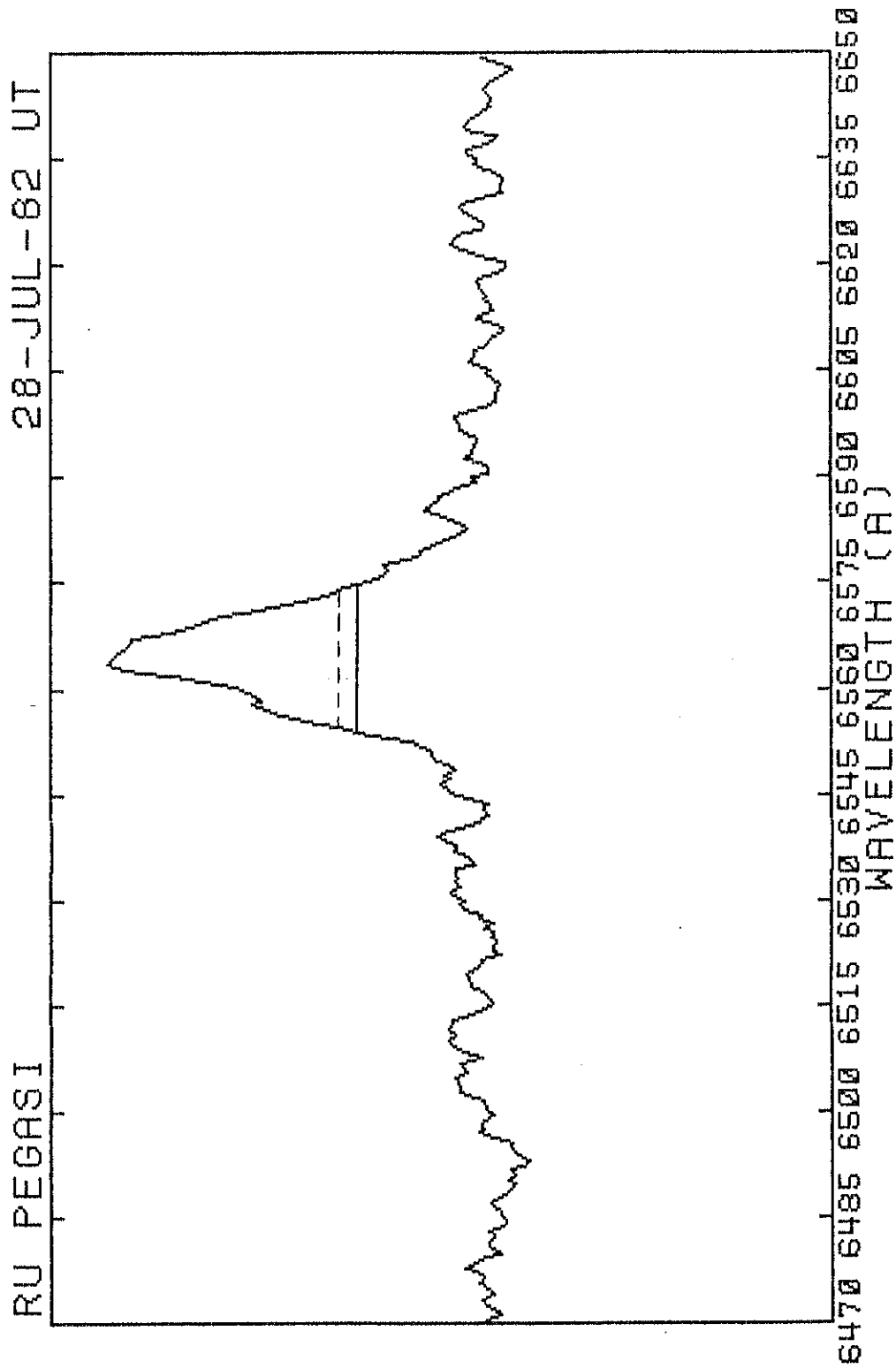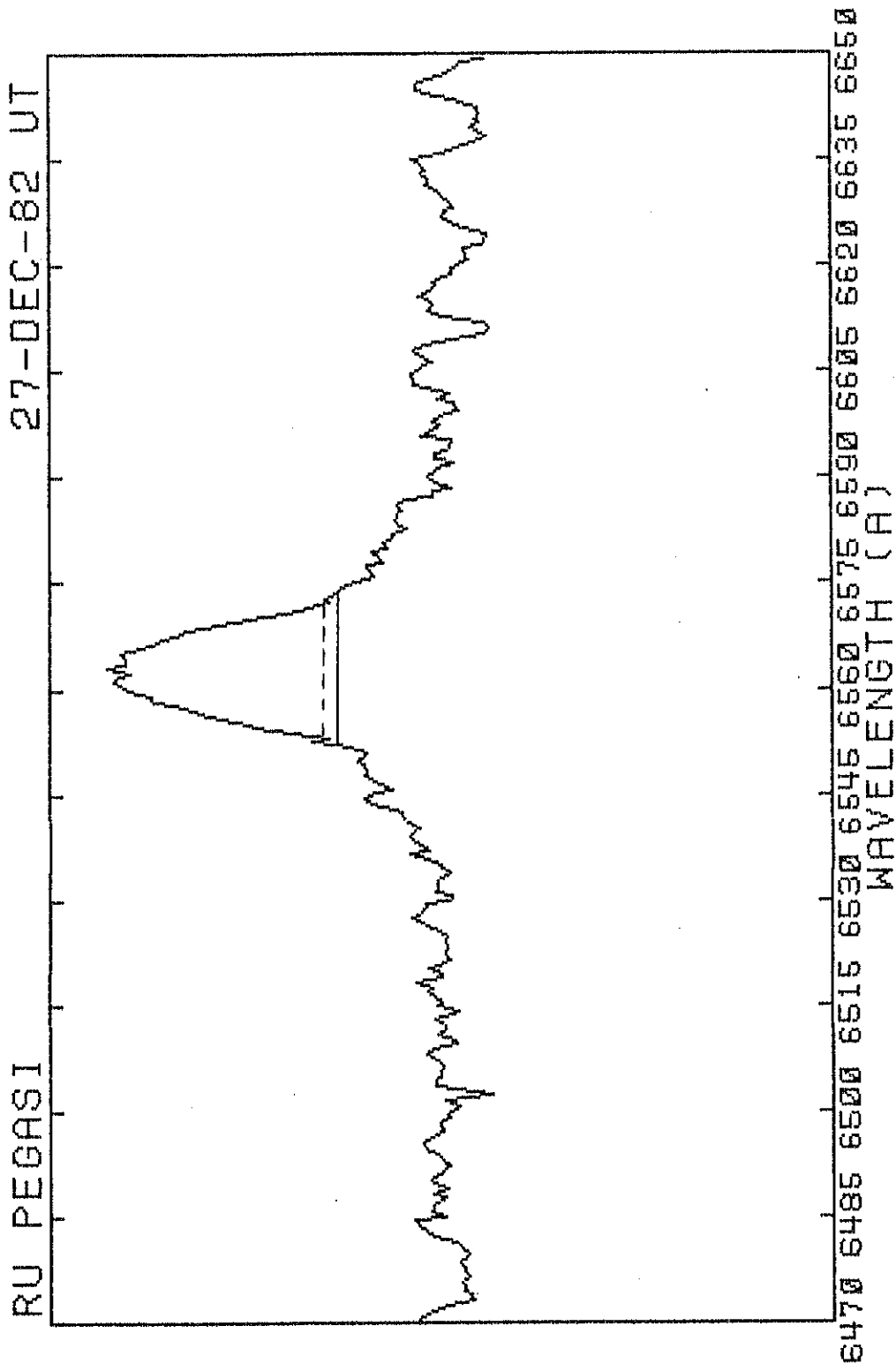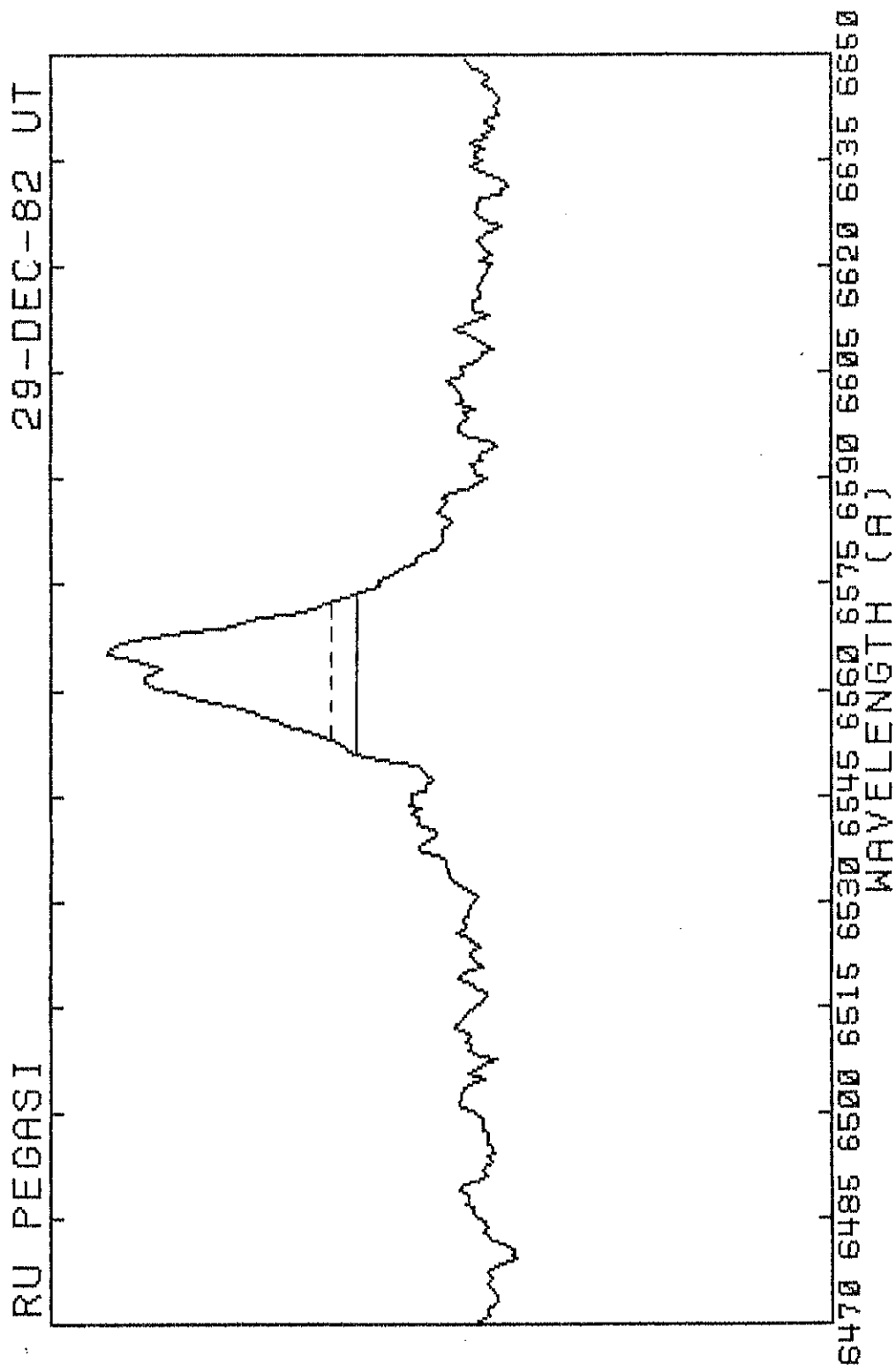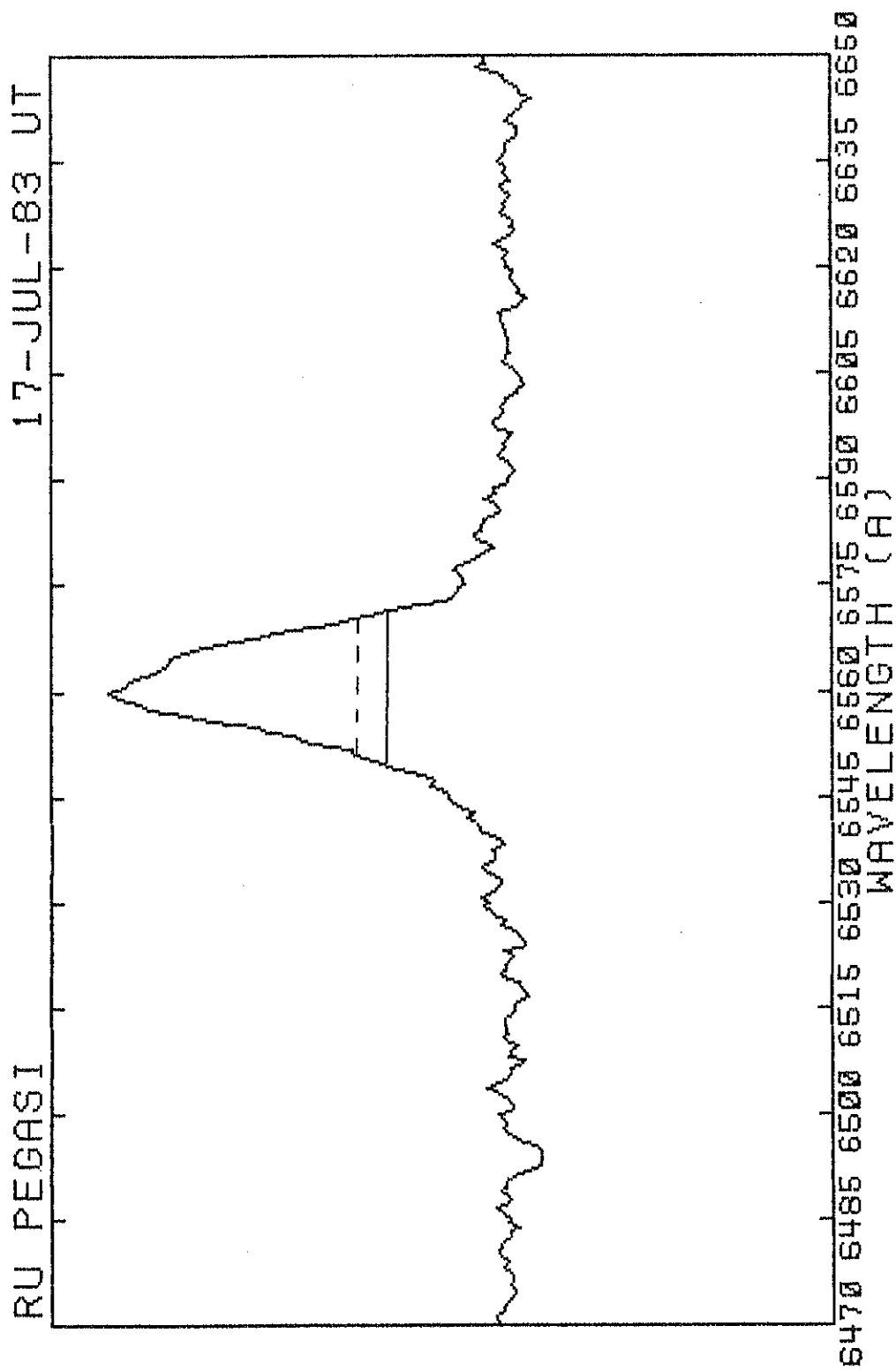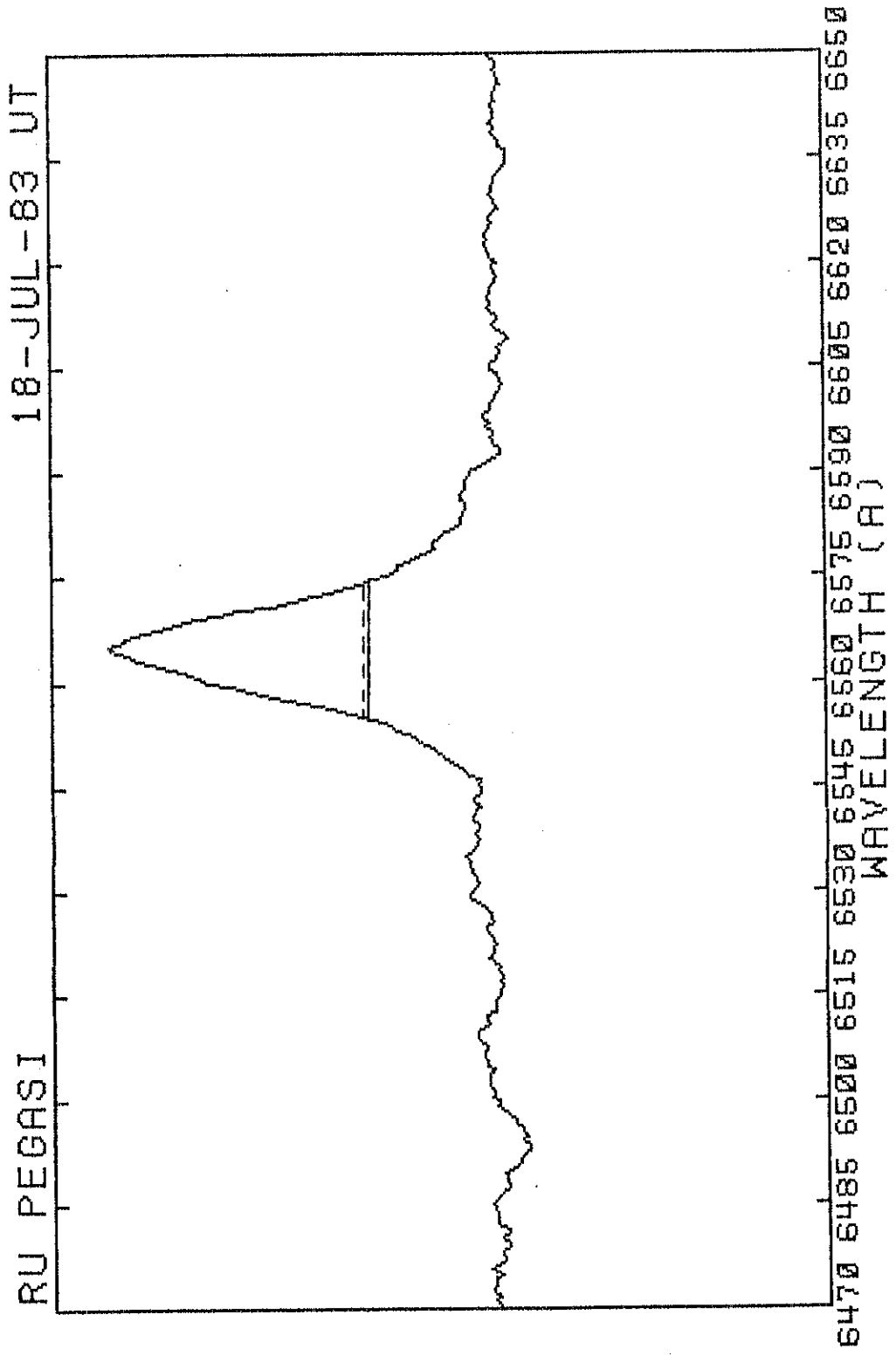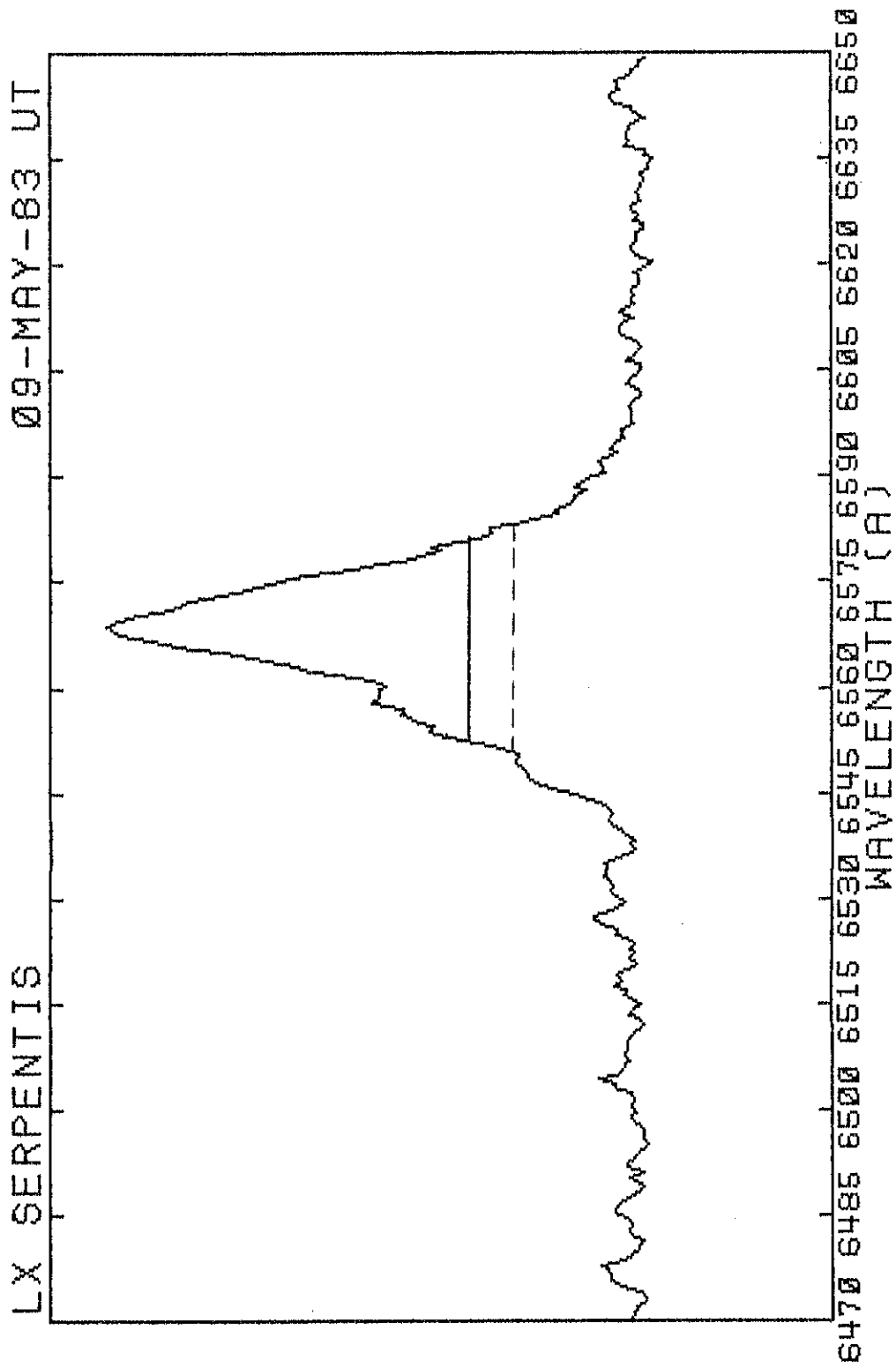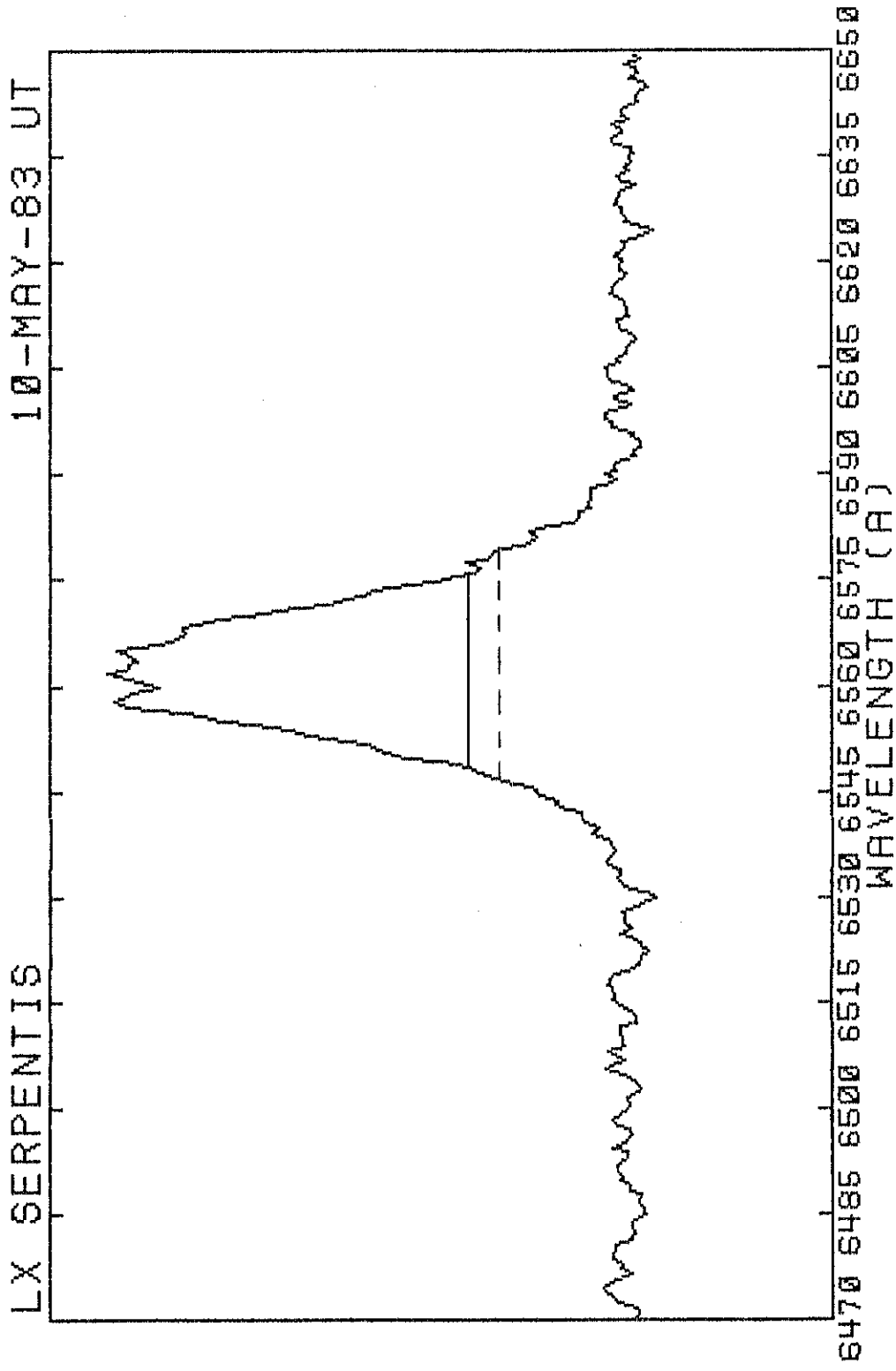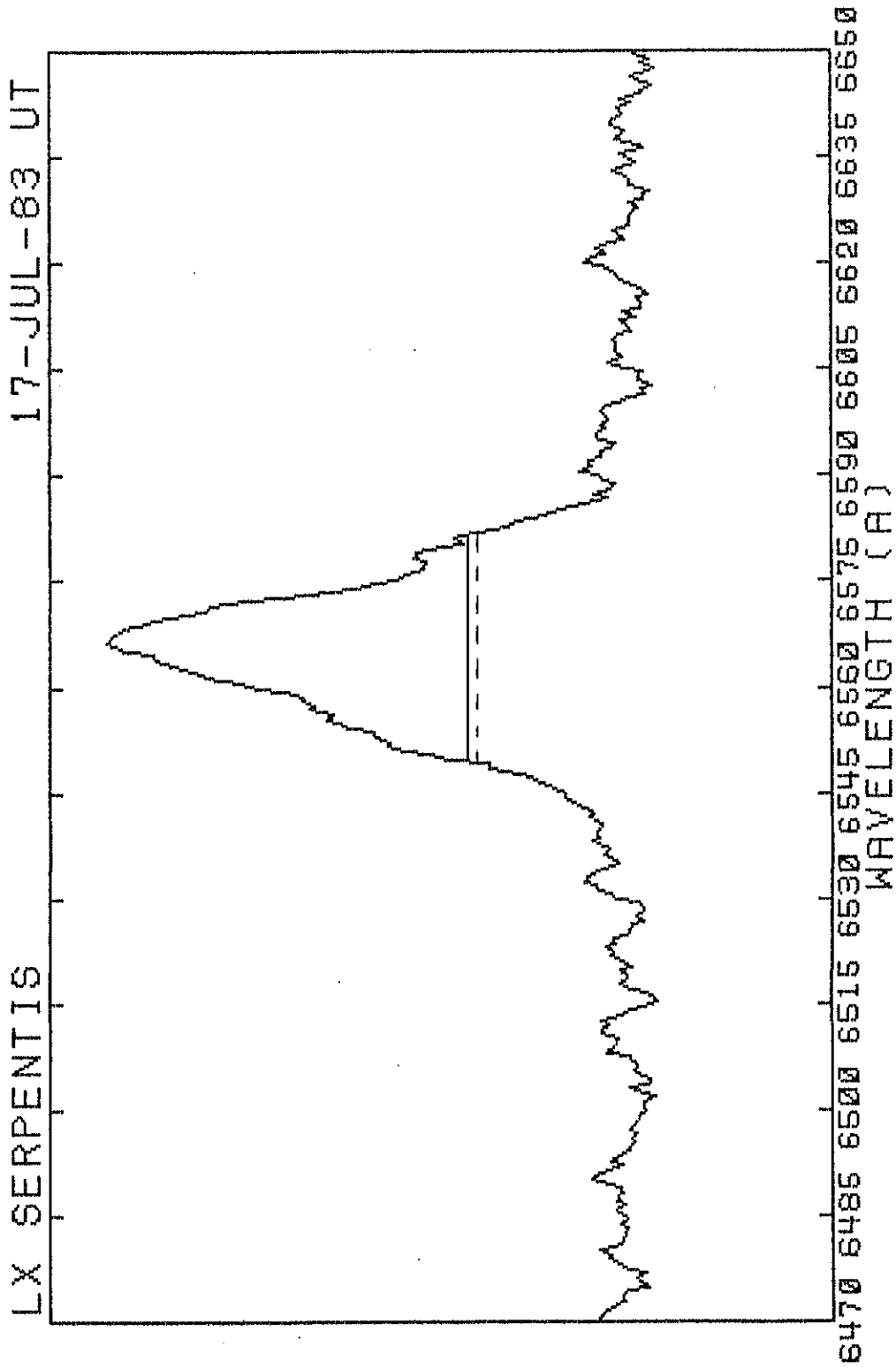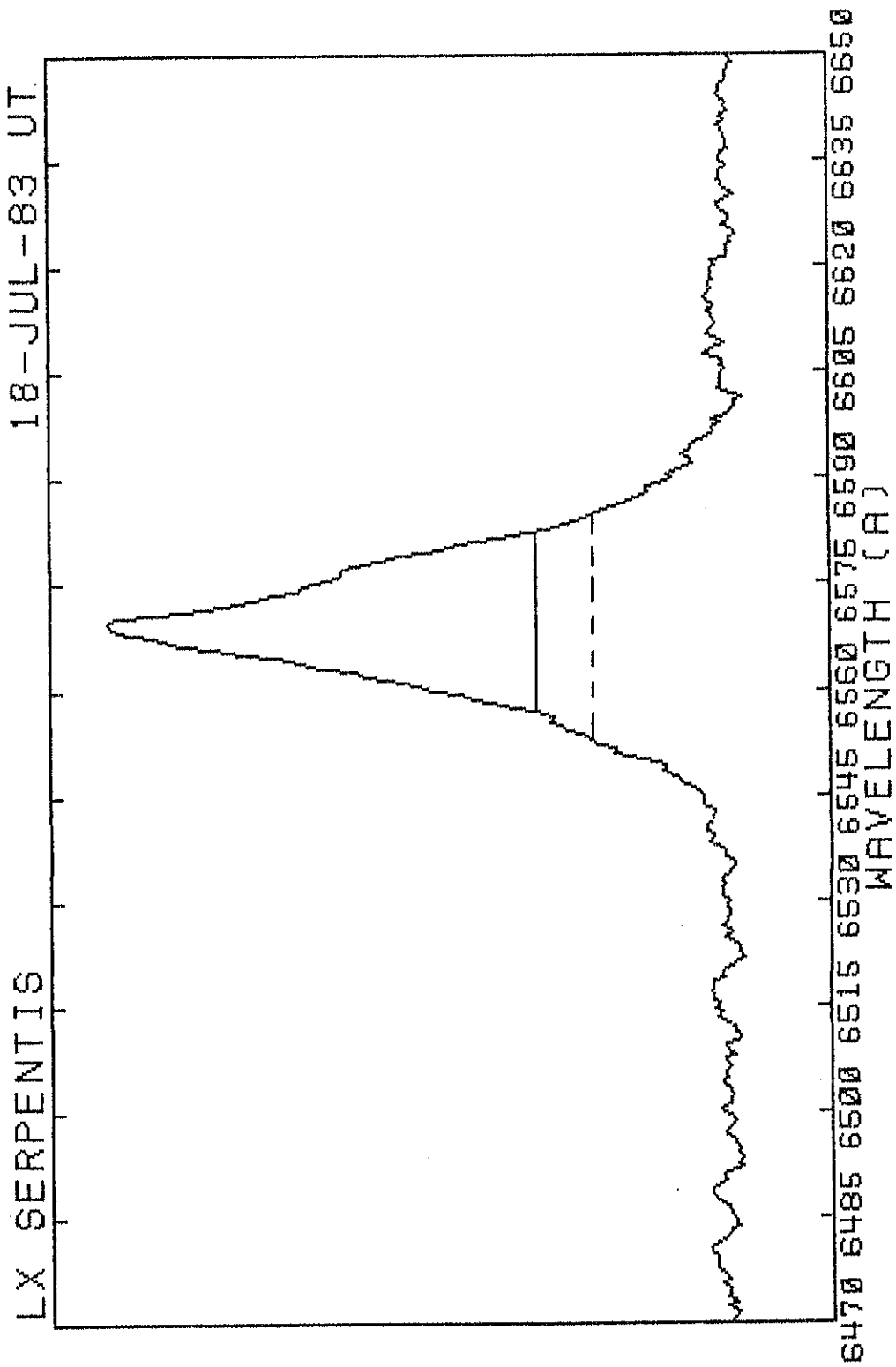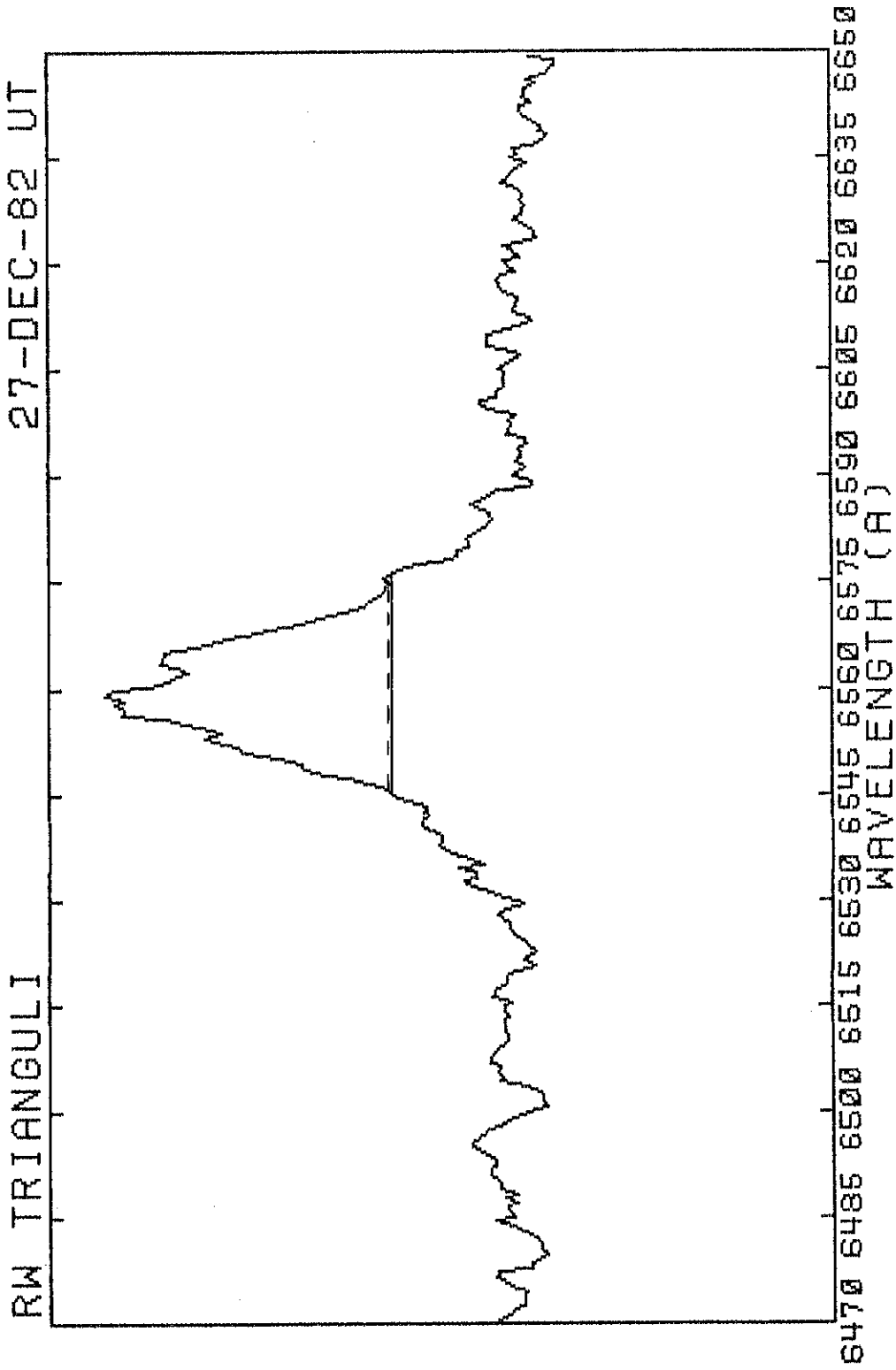
Figure 3. The value of the parameter f as a function of the equivalent width of the Hα emission line. The horizontal line represents the locus that systems would follow if the value of the parameter f derived from a given $v_d \sin i$ was independent of the equivalent width of the emission line. Key: AE Aqr: star, SS Cyg: diamond, U Gem: triangle, RU Peg: cross, and LX Ser: box.

Figure 3

155
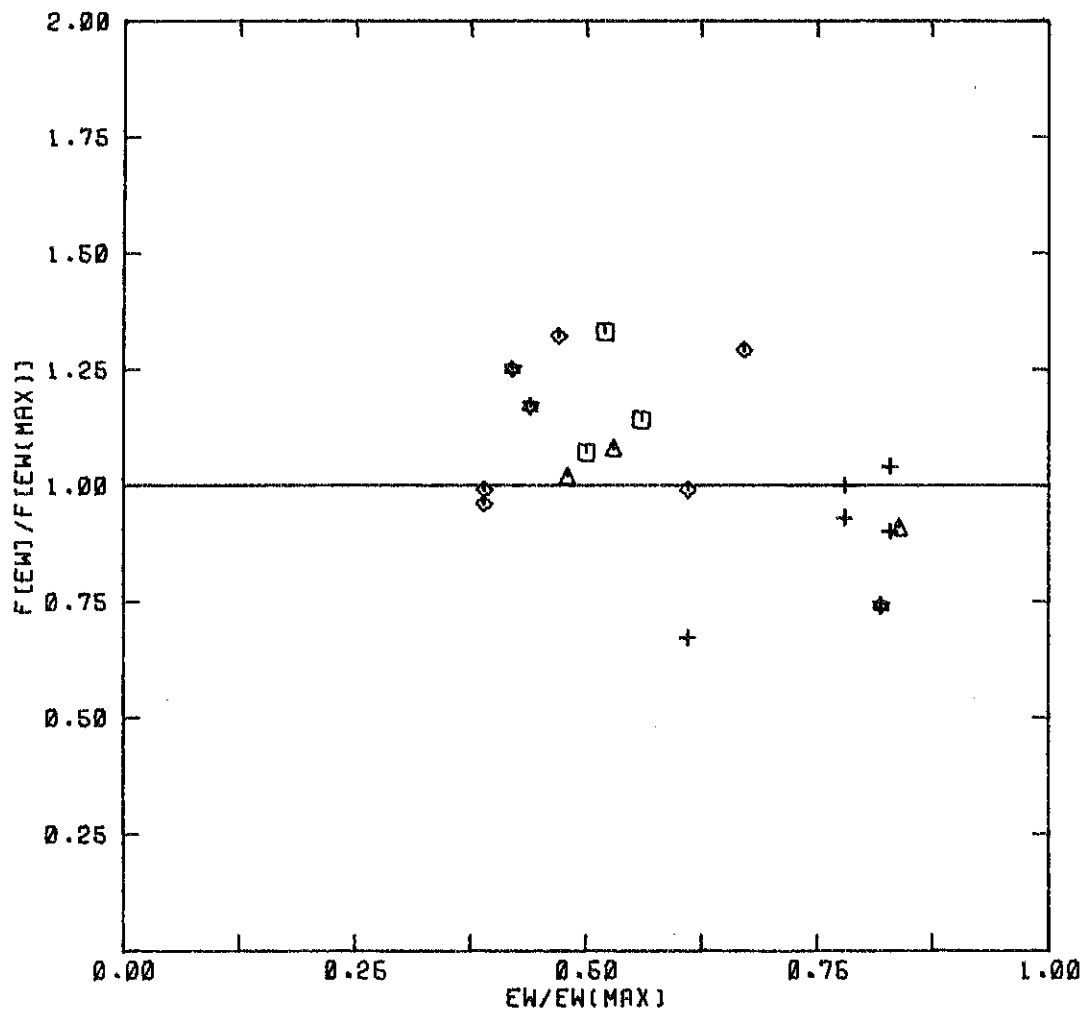
Figure 4. The functional relationship between the parameters f and ξ
for a Gaussian line profile. The straight line (f = ξ) has
been included for comparison.

Figure 4

157
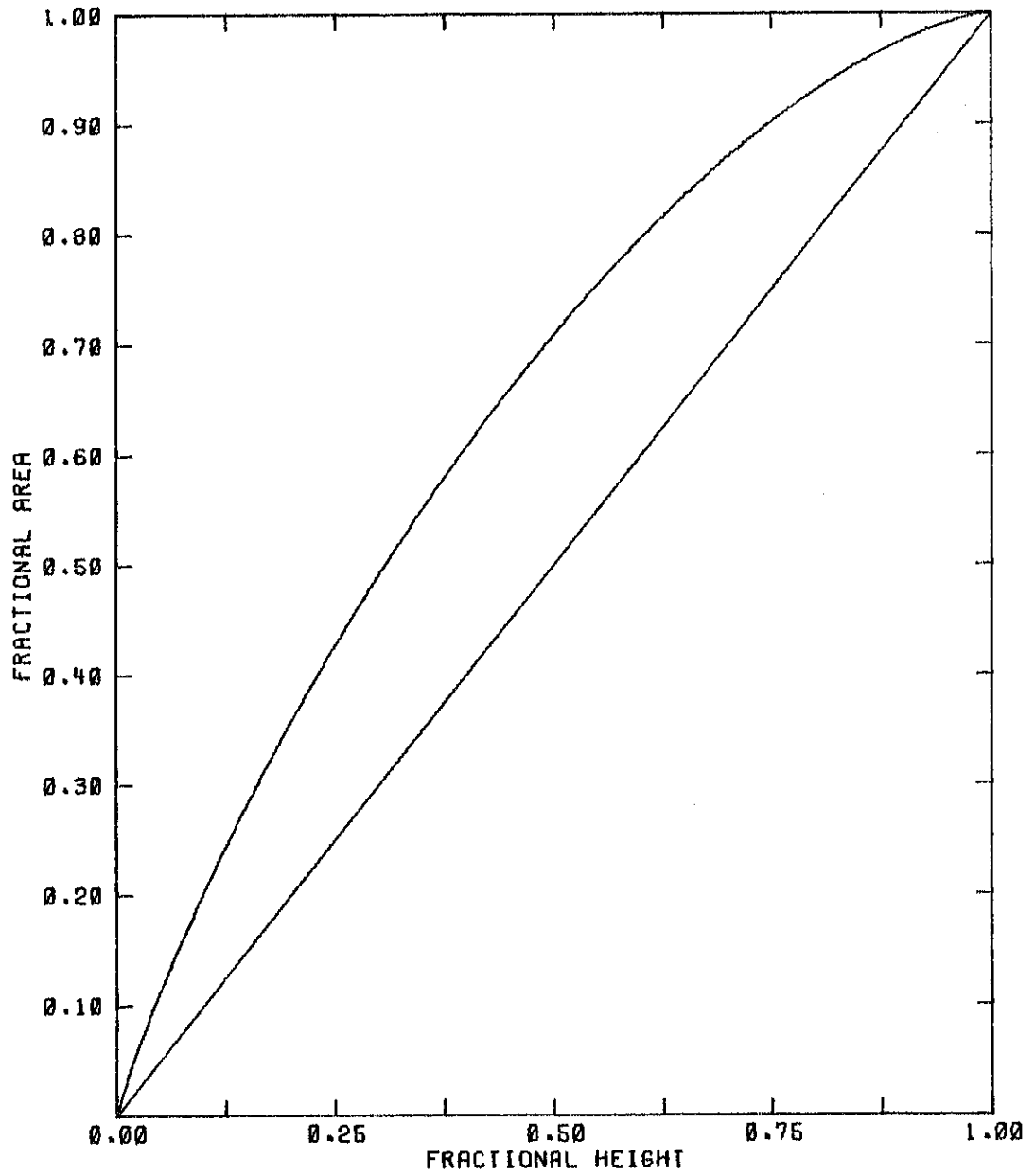
Figure 5. The values of $v_d \sin i$ for the 11 calibration systems computed using $\langle \xi \rangle = 0.58$ are compared with the values computed using $\langle f \rangle = 0.30$. The figure demonstrates the consistency of the two parameters.

158
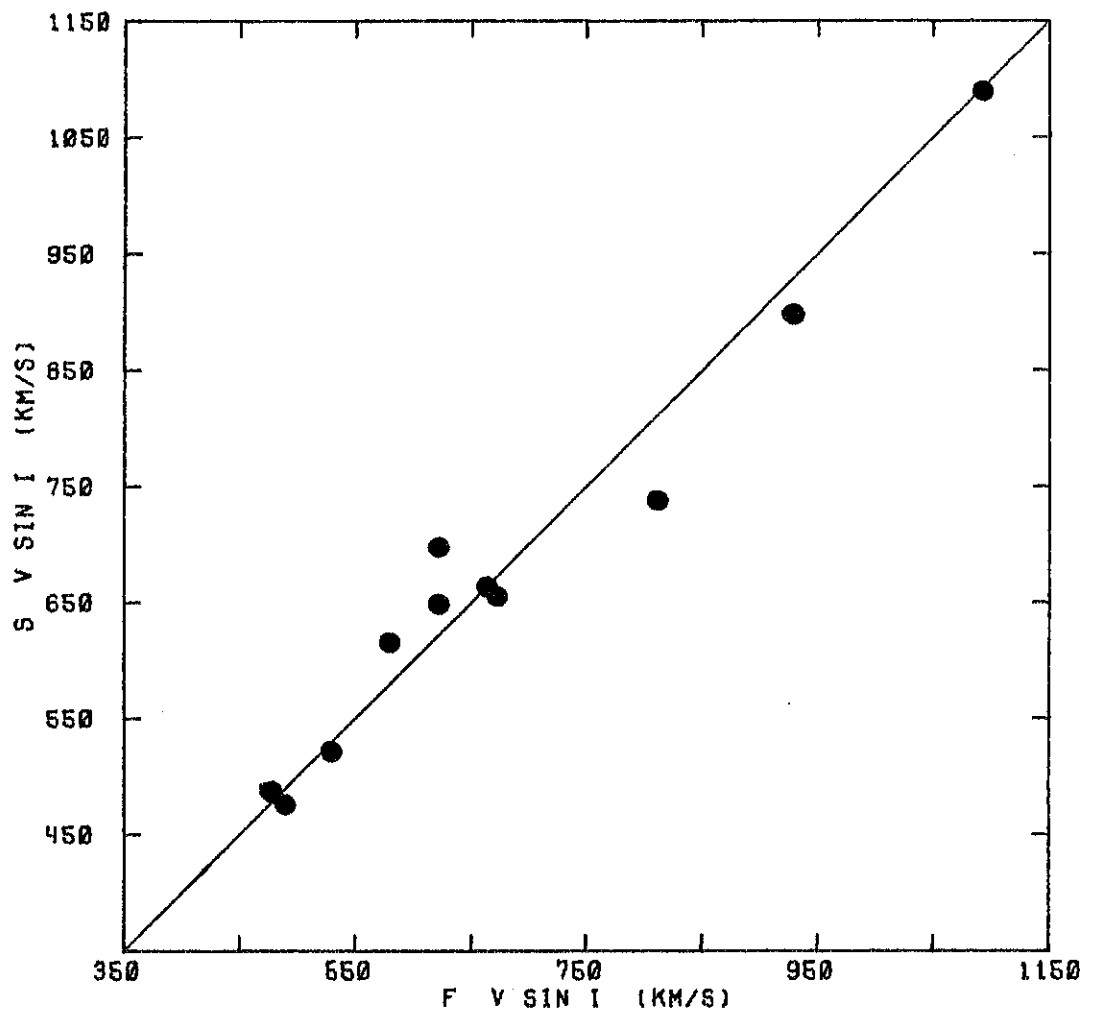
Figure 5

Figure 6. The comparison of the theoretical and the observed variation

of $K_1/\langle v_d \sin i\rangle$ with $F(q)$ for the 11 calibration systems.

The solid line represents the theoretical relationship,

namely that $K_1/(v_d \sin i) = F(q)$. The observed points have

been determined based on our canonical values of $\langle f\rangle$ and

$\langle \xi\rangle$.
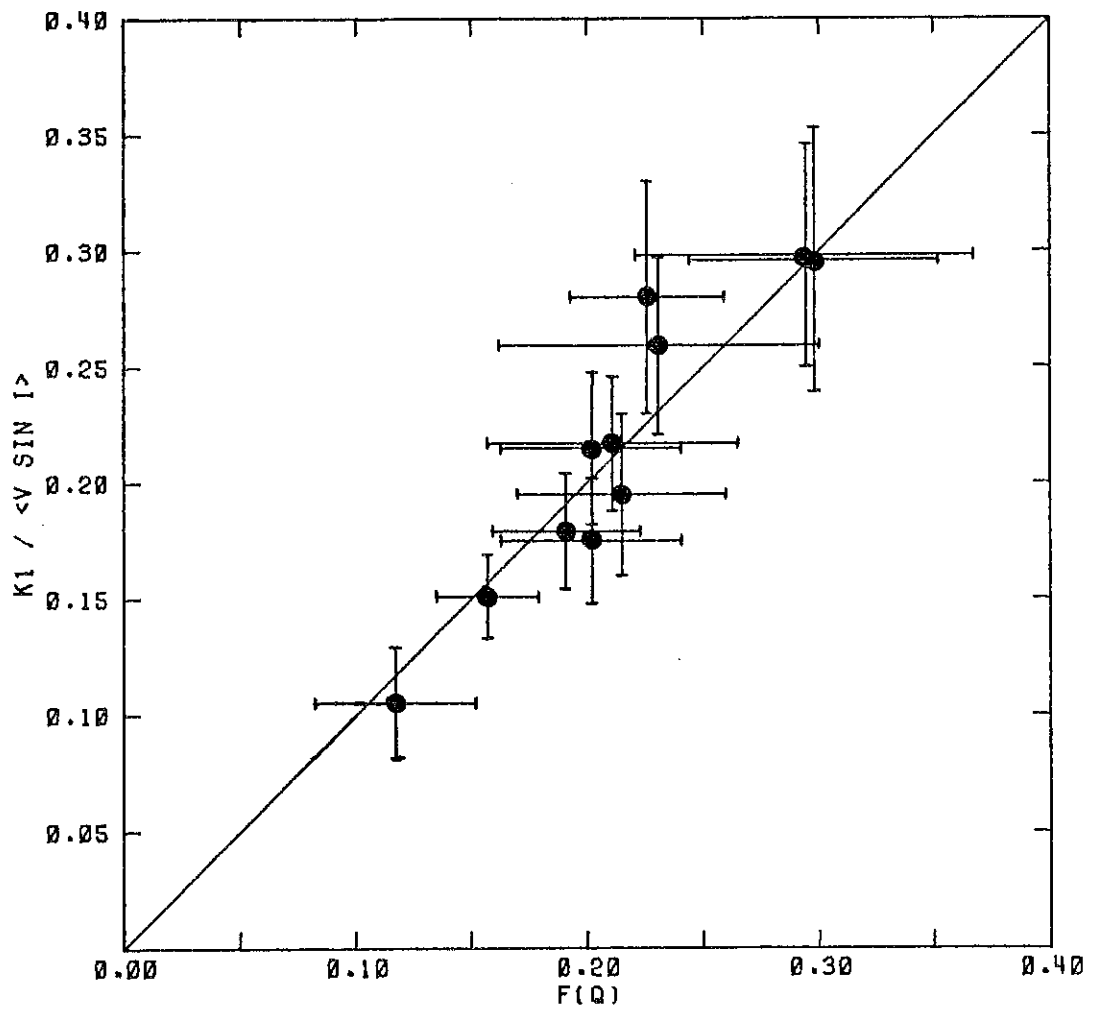
Figure 6

Figure 7. The comparison of the theoretical and the observed variation of $K_1/\langle v_d \sin i\rangle$ with the mass ratio, q. The solid line has been computed from equation II.18.

Figure 7

163
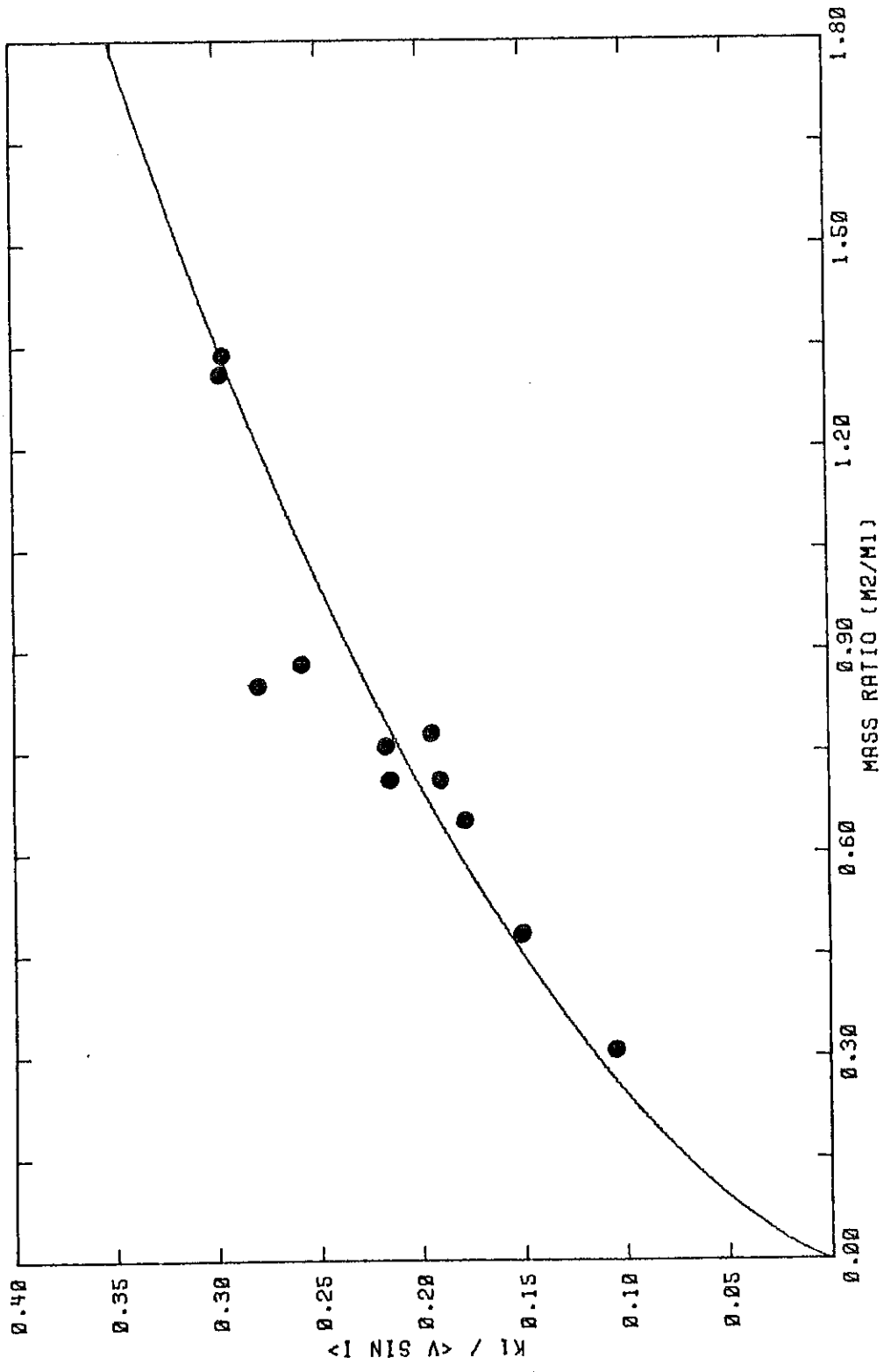
Figures 8a-q. The radial velocities derived from measurements of the Hα emission lines have been plotted as a function of orbital phase for the 13 systems with previously unknown orbital periods. Also included is UX UMa whose period was known but whose radial velocity curve was not. The open circles in the radial velocity curve of YZ Cnc were not used in the orbital solution.
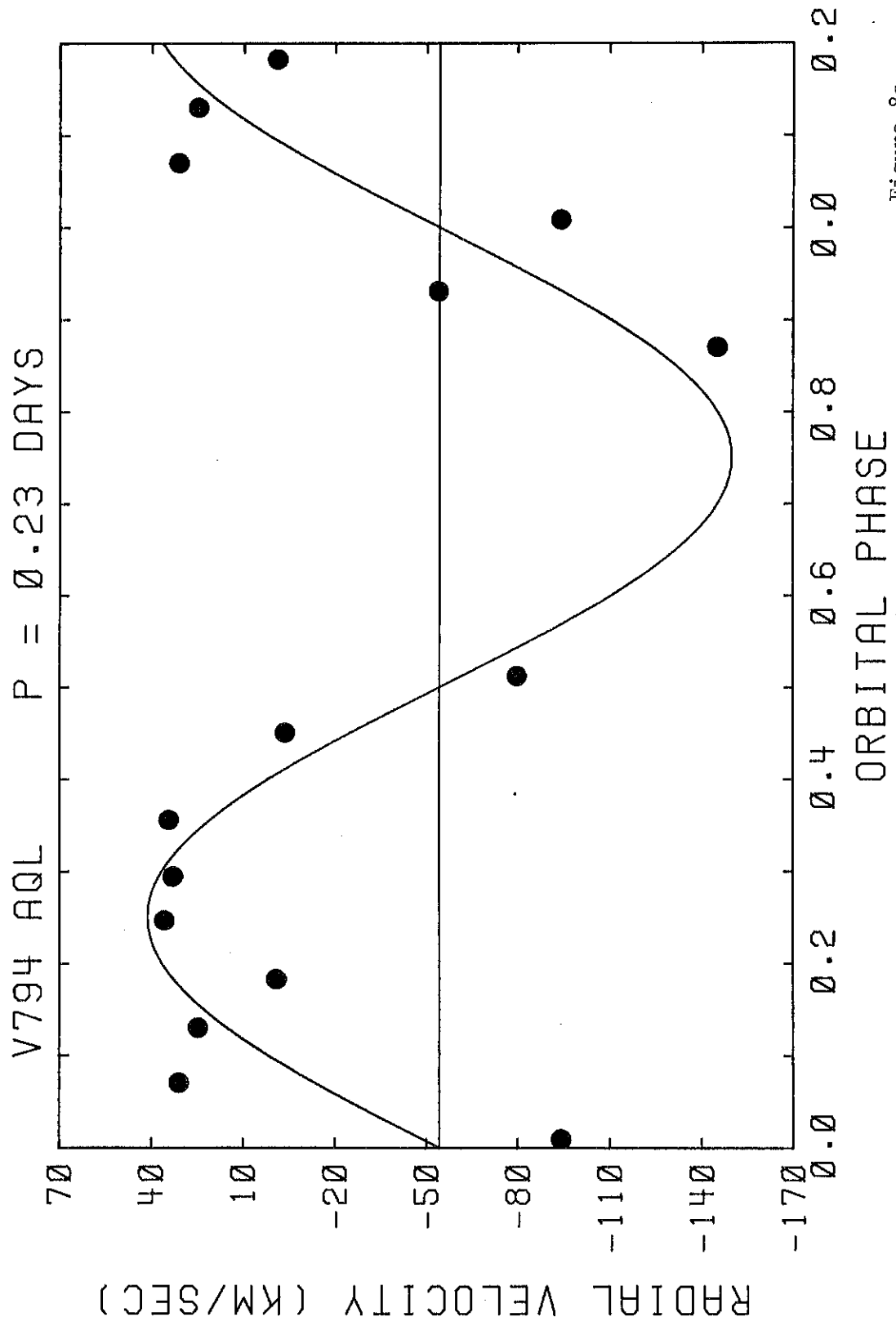
Figure 8a
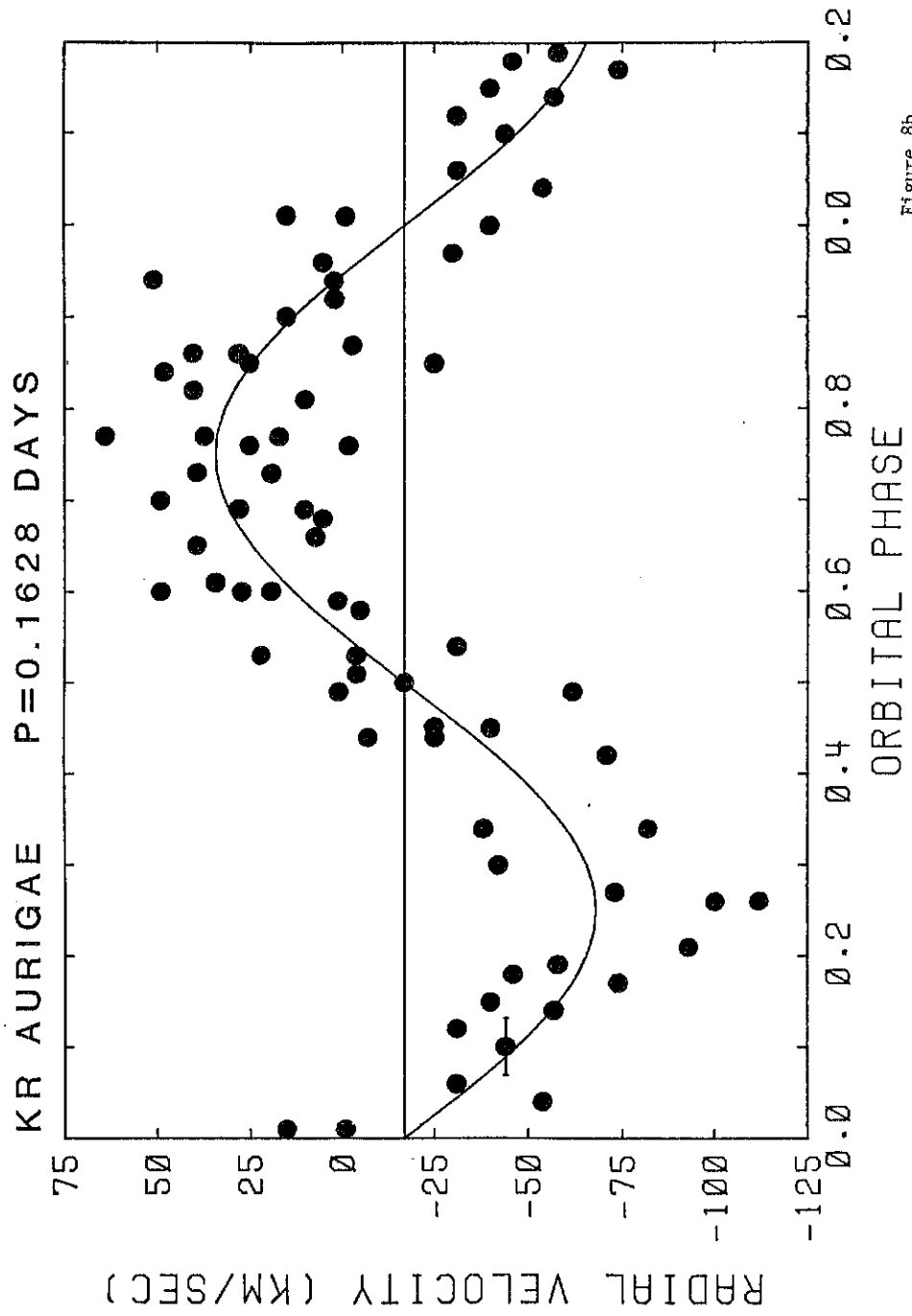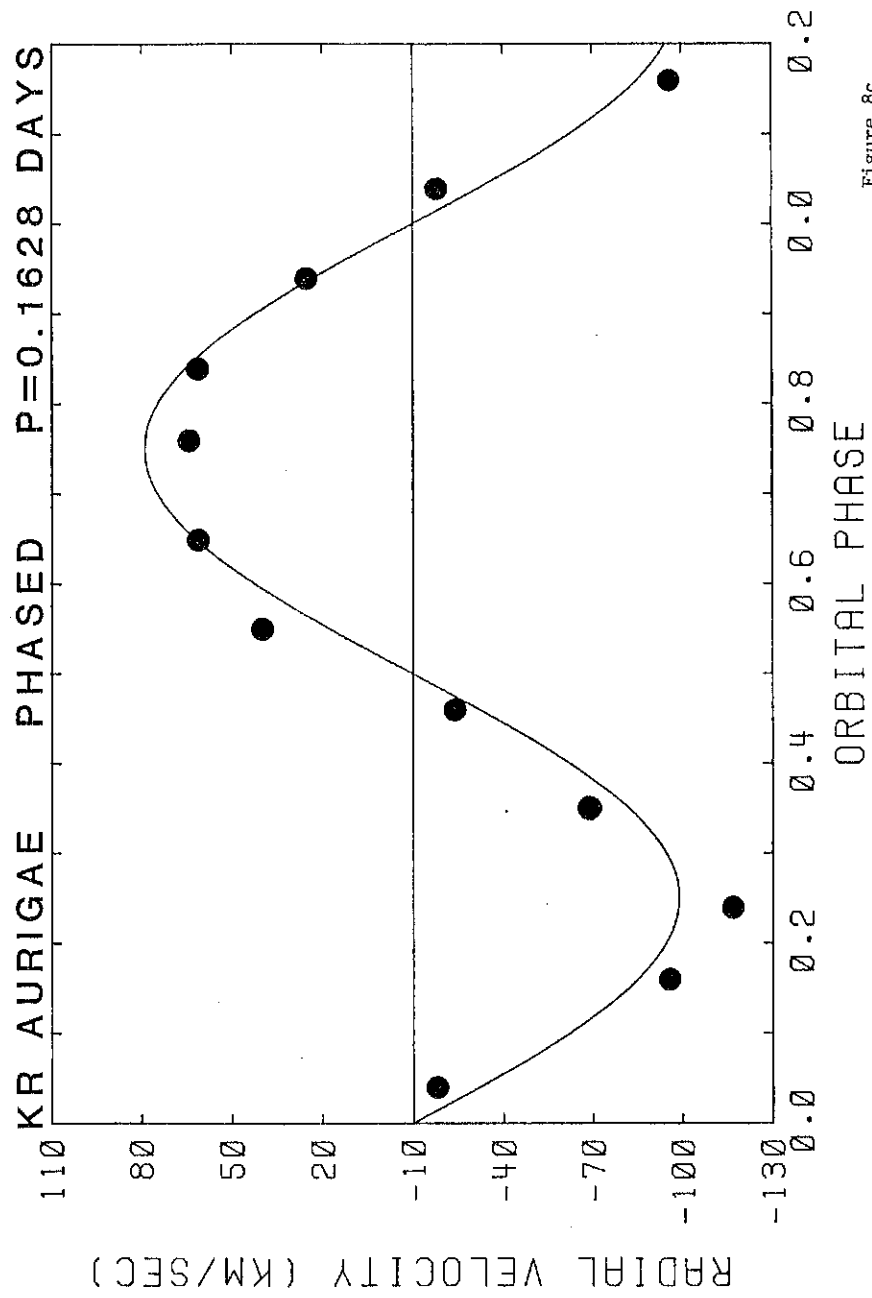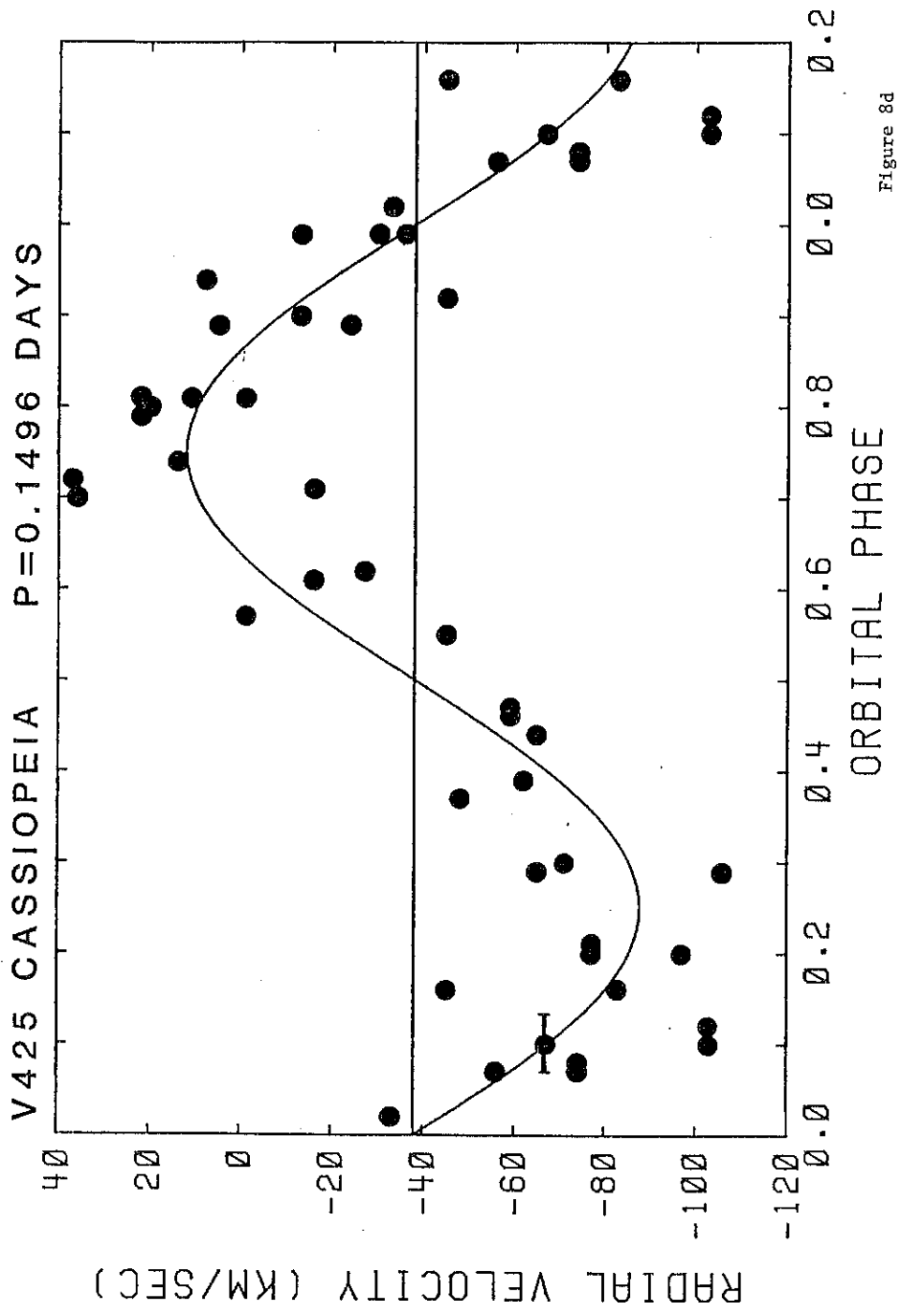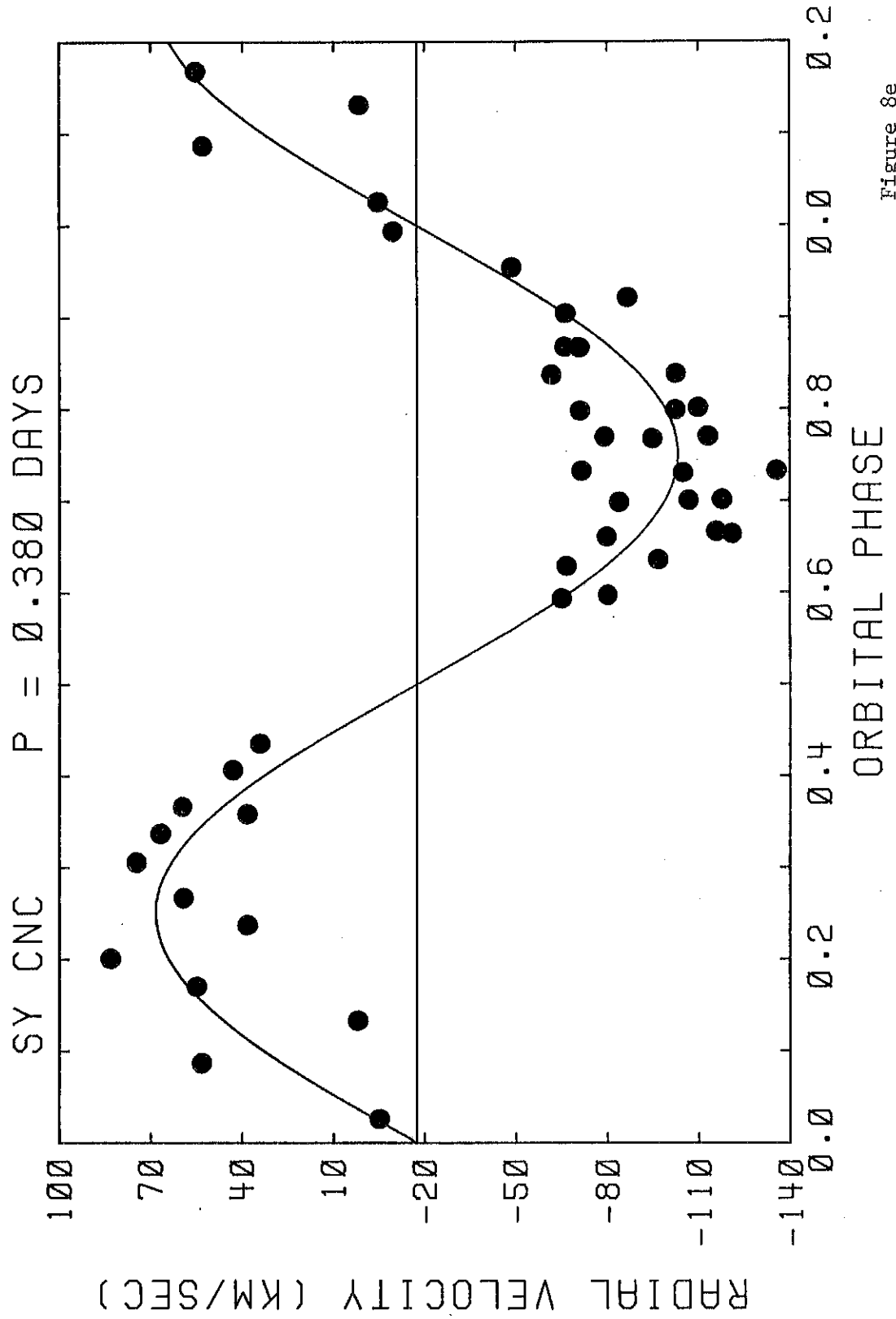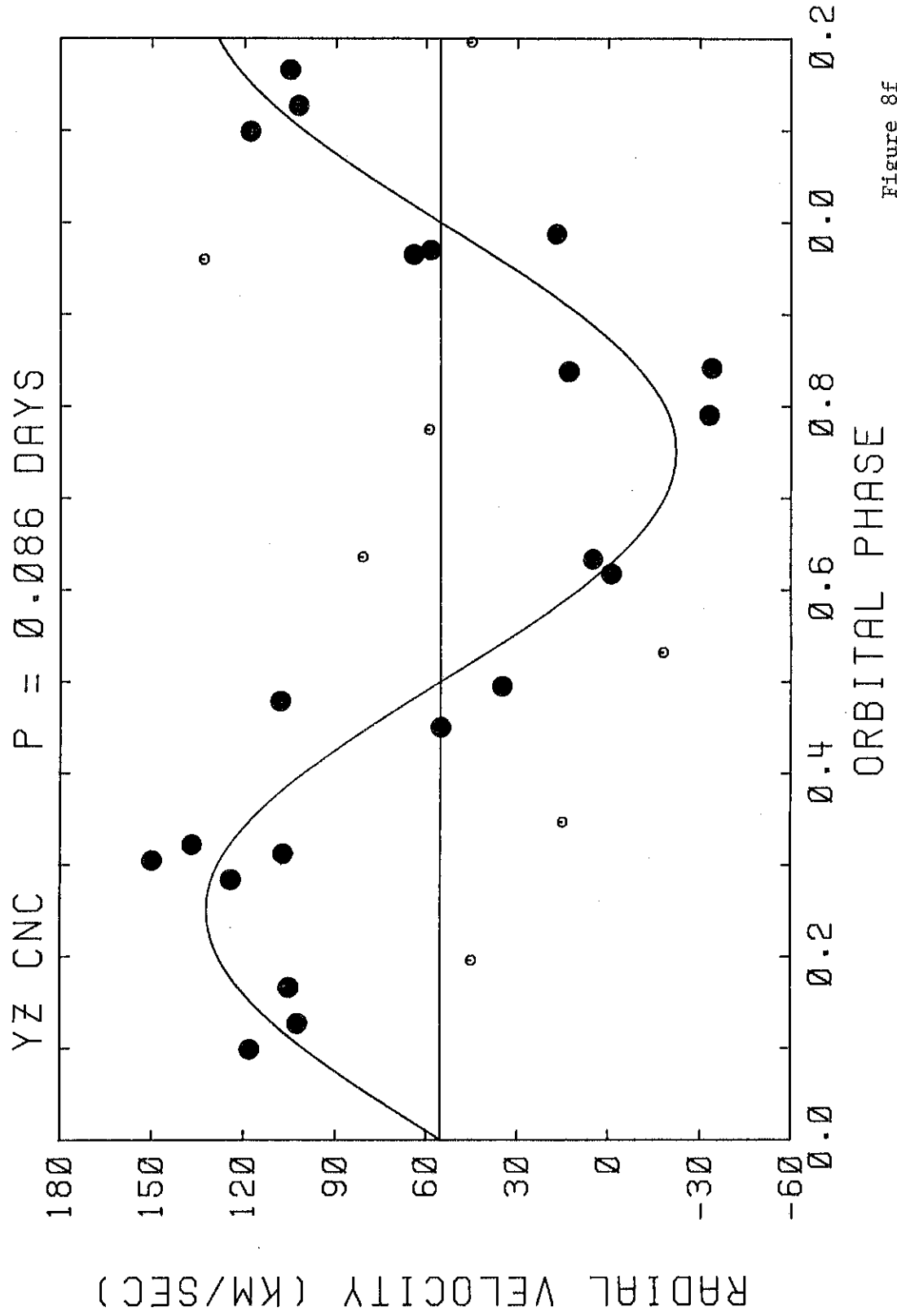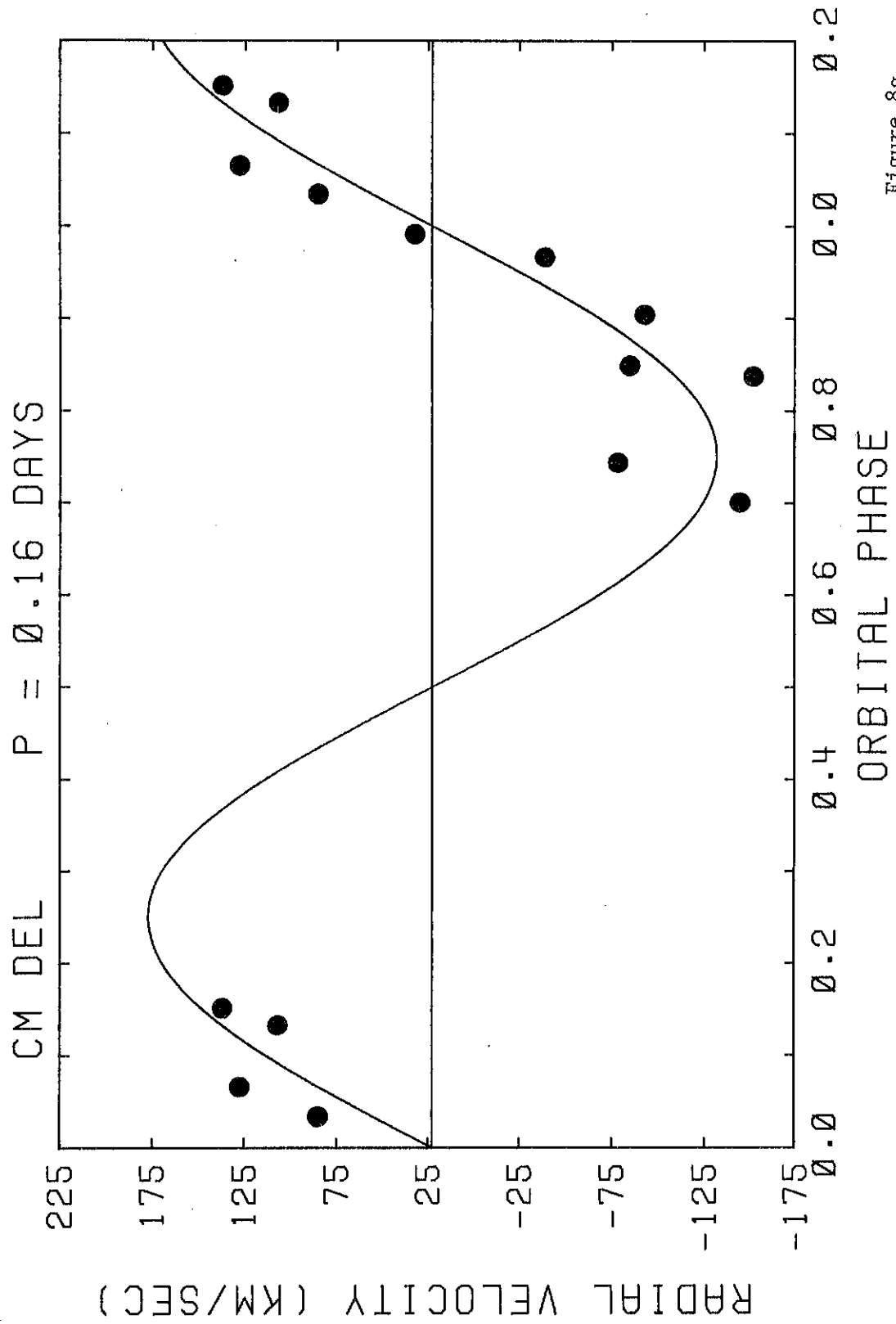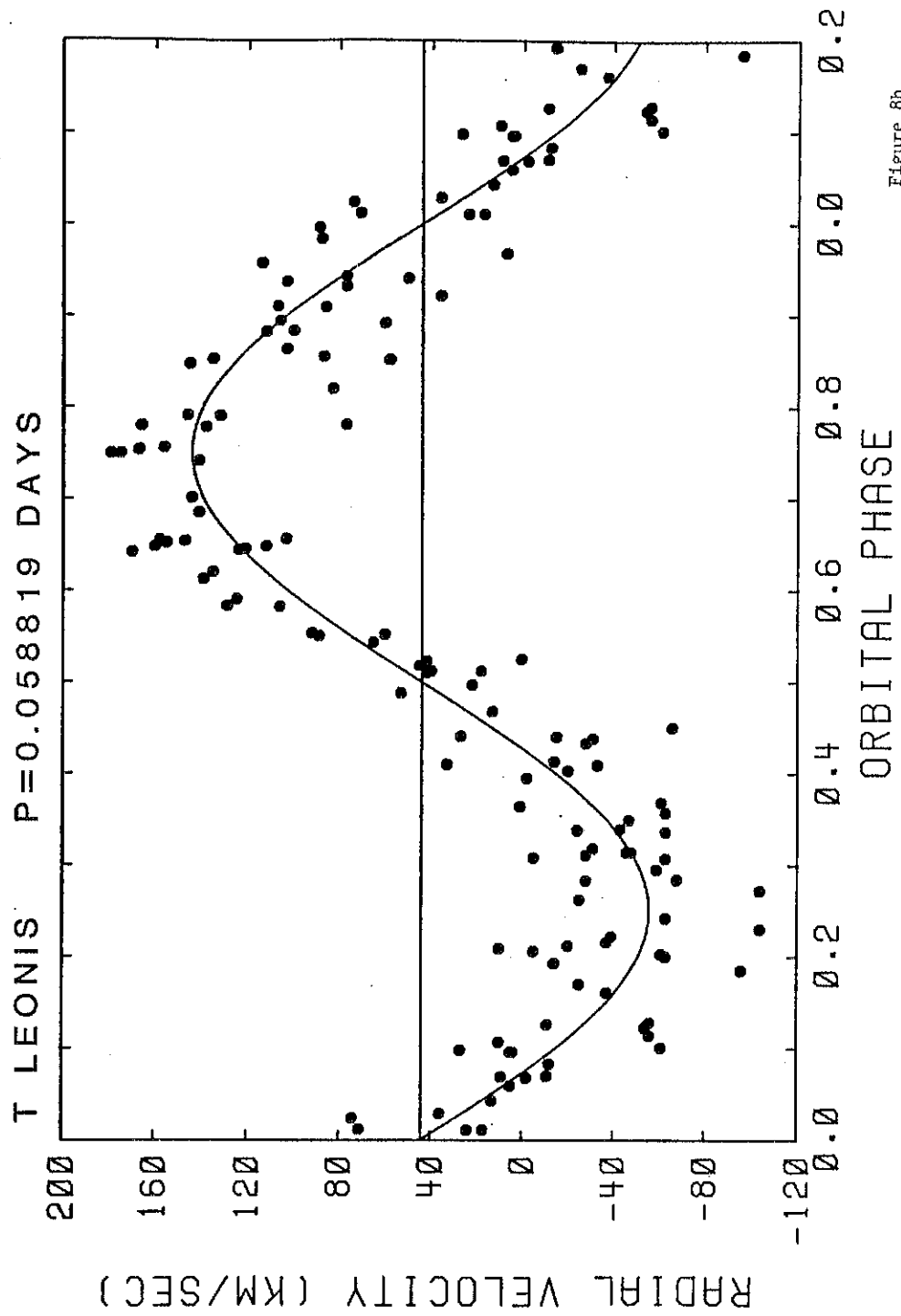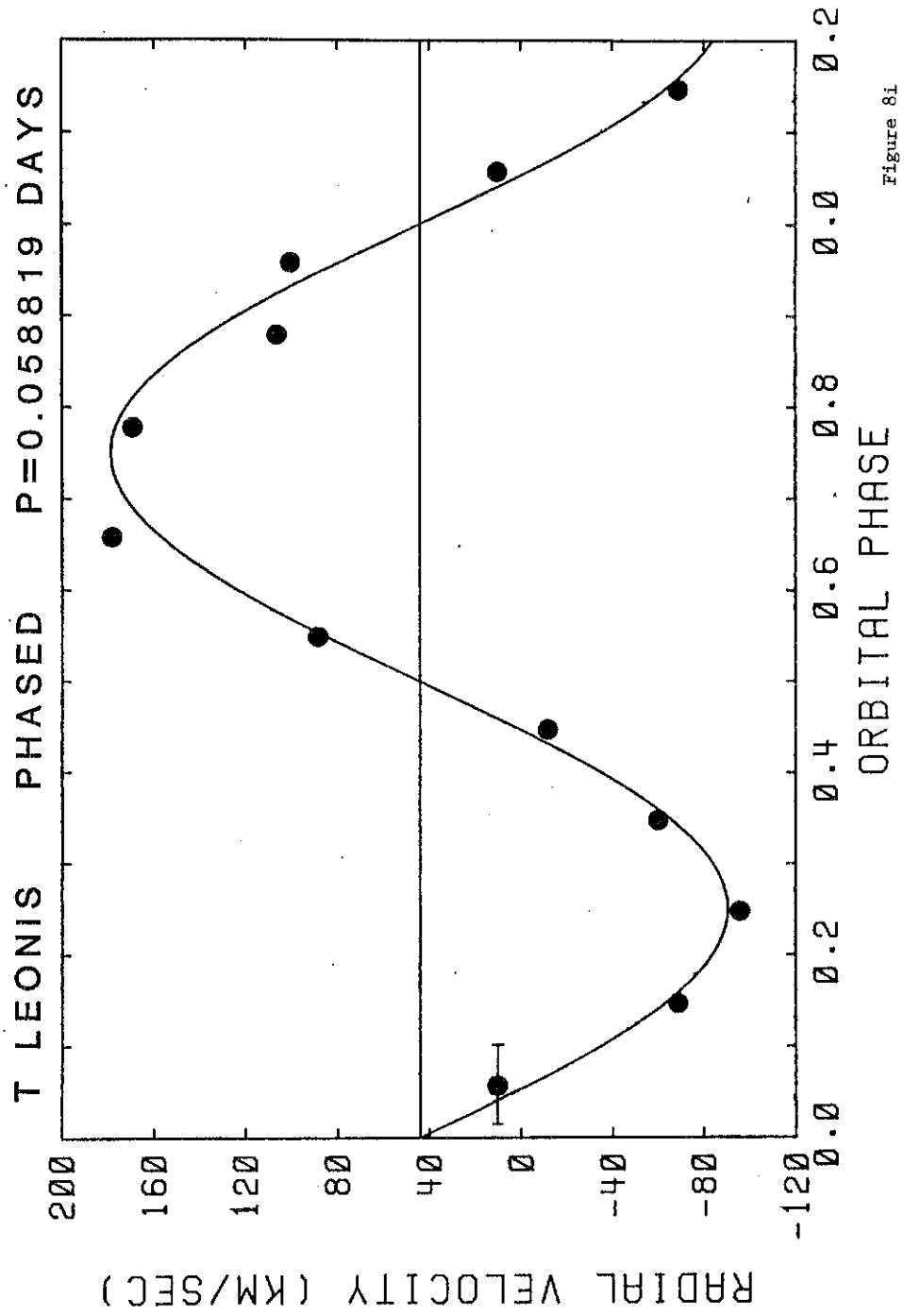
165

Figure 8b

KR AURIGAE   P=0.1628 DAYS

RADIAL VELOCITY (KM/SEC)

ORBITAL PHASE

166

Figure 8c

KR AURIGAE   PHASED   P=0.1628 DAYS

RADIAL VELOCITY (KM/SEC)

ORBITAL PHASE

167

Figure 8d

168

Figure 8e

SY CNC   P = 0.380 DAYS

RADIAL VELOCITY (KM/SEC)

ORBITAL PHASE

169

Figure 8f

170

CM DEL   P = 0.16 DAYS

Figure 8g

RADIAL VELOCITY (KM/SEC)

ORBITAL PHASE

171

Figure 8h

172

Figure 8i

Figure 8j

174

V442 OPHIUCHI   P=0.1406 DAYS

ORBITAL PHASE

RADIAL VELOCITY (KM/SEC)

Figure 8k

Figure 8L

176

SW UMA   PHASED P = 0.05974 DAYS

RADIAL VELOCITY (KM/SEC)

ORBITAL PHASE

Figure 8m

177

Figure 8n

178

Figure 8o

179

Figure 8p

180

VW VUL   P = 0.073 DAYS

RADIAL VELOCITY (KM/SEC)

ORBITAL PHASE
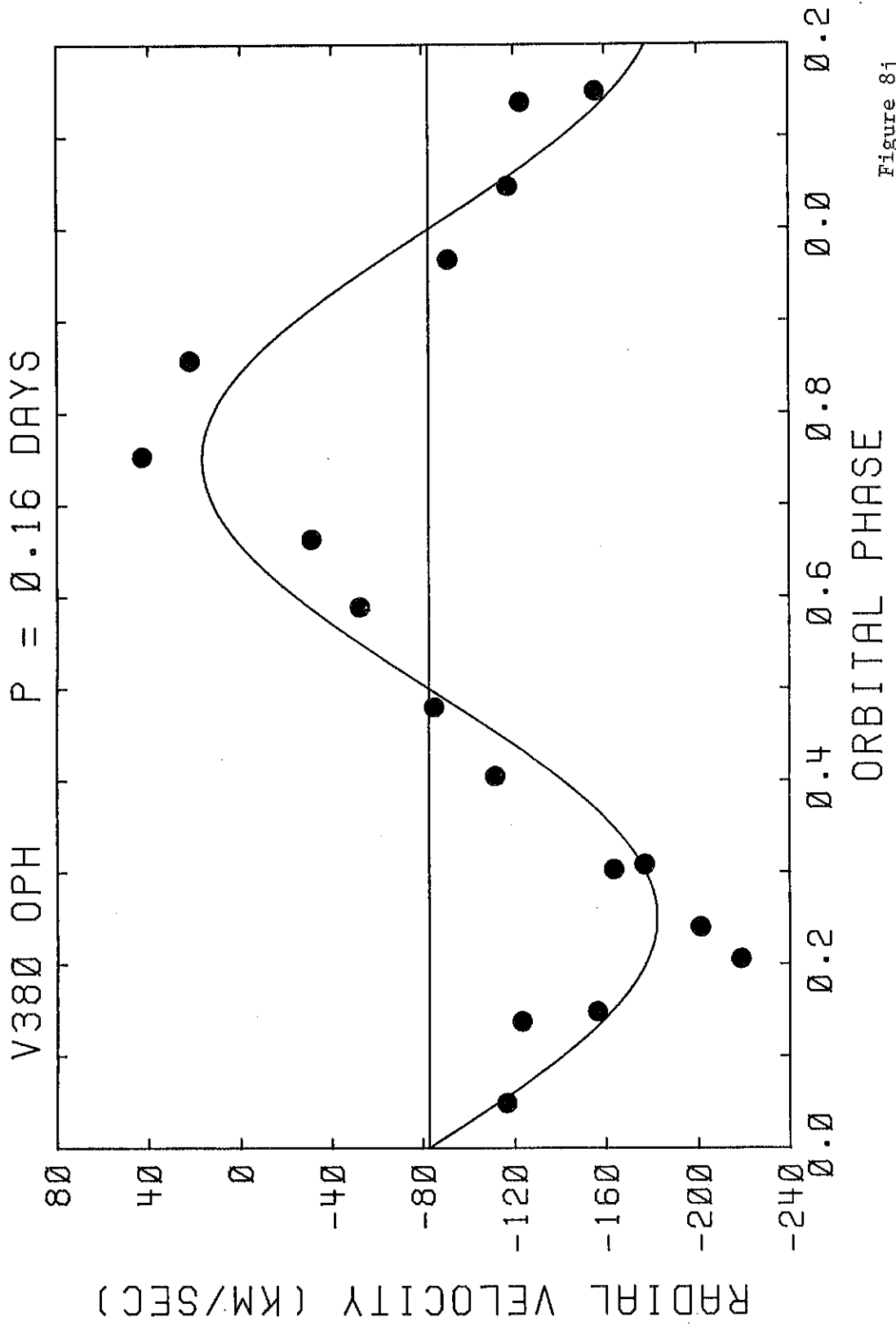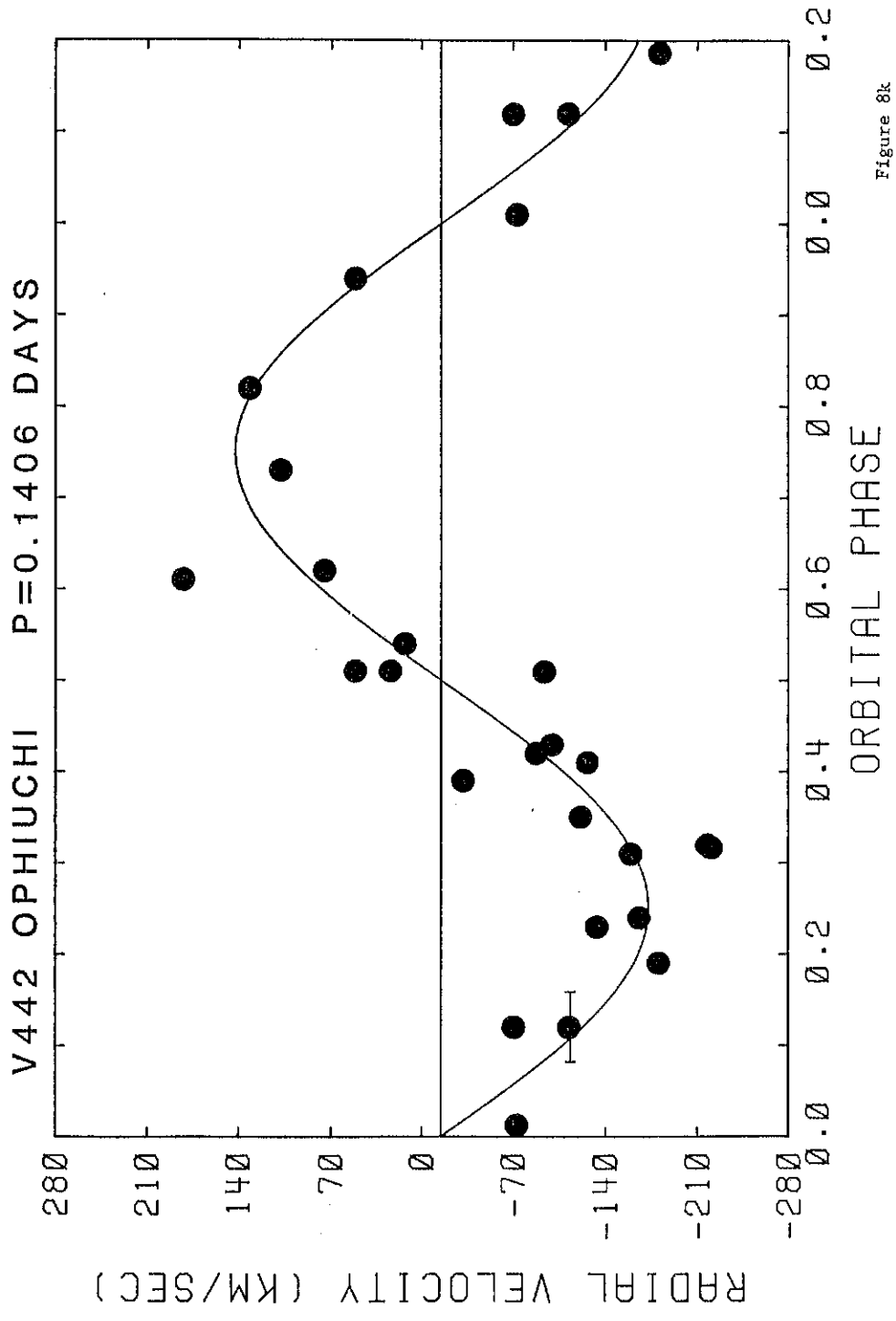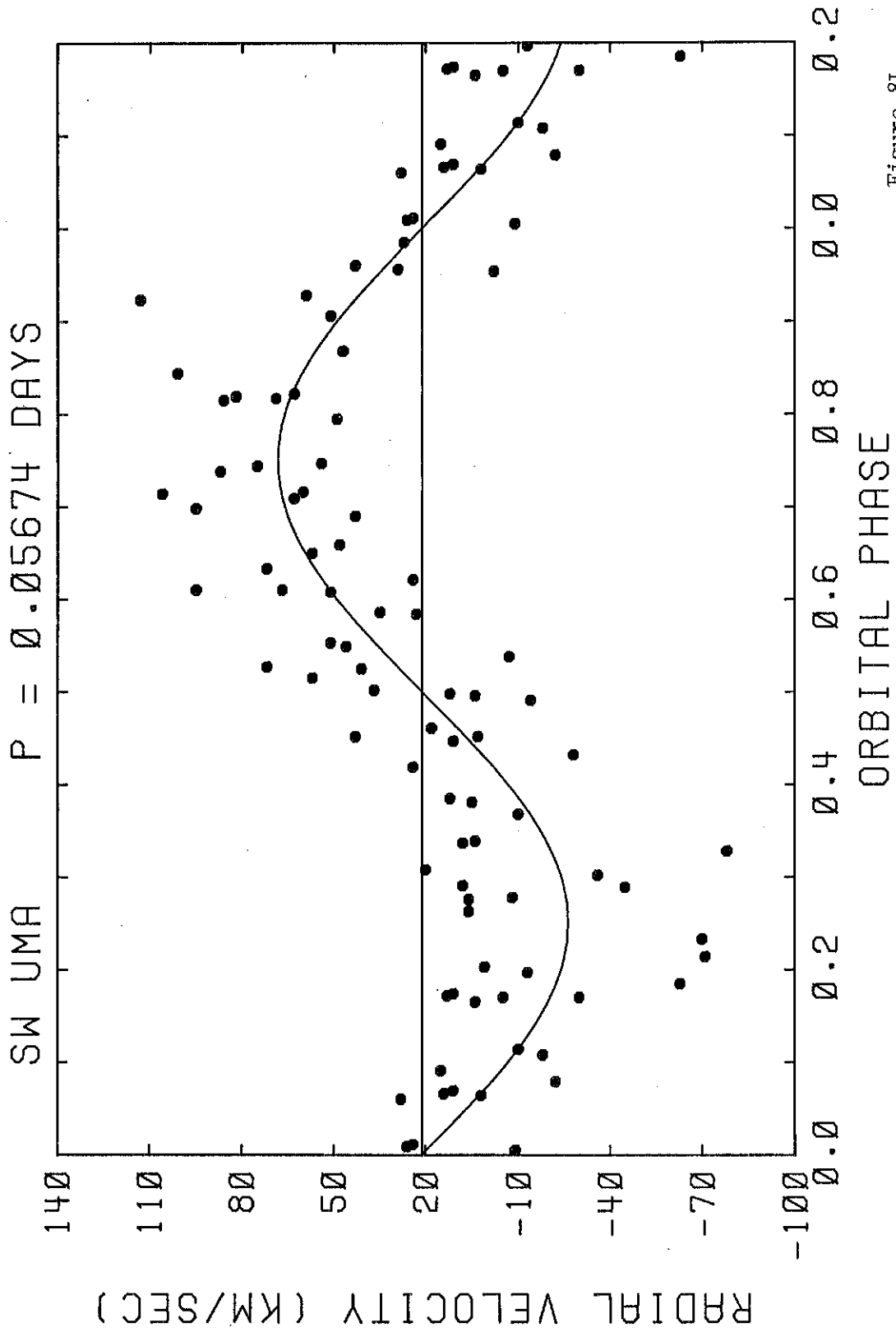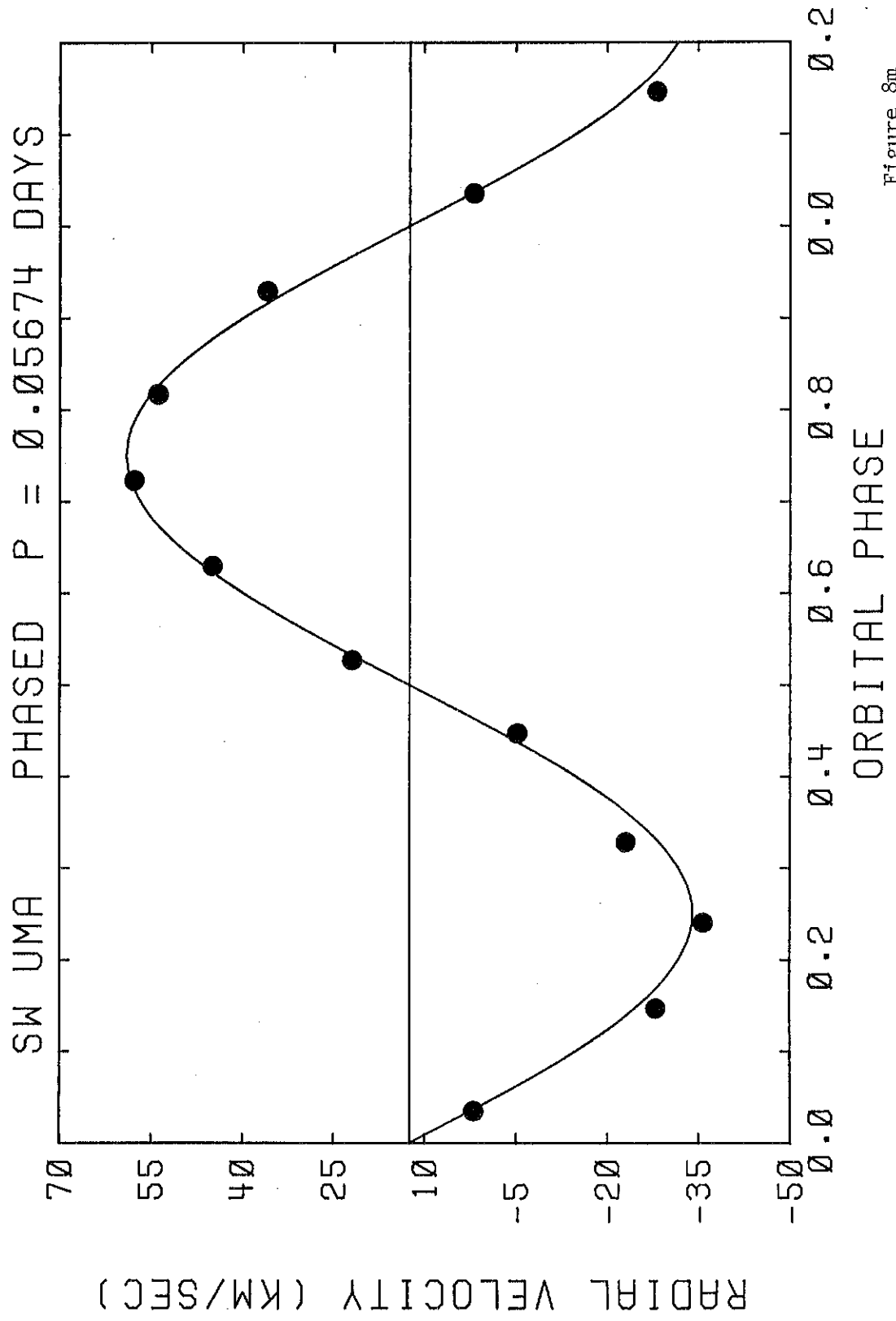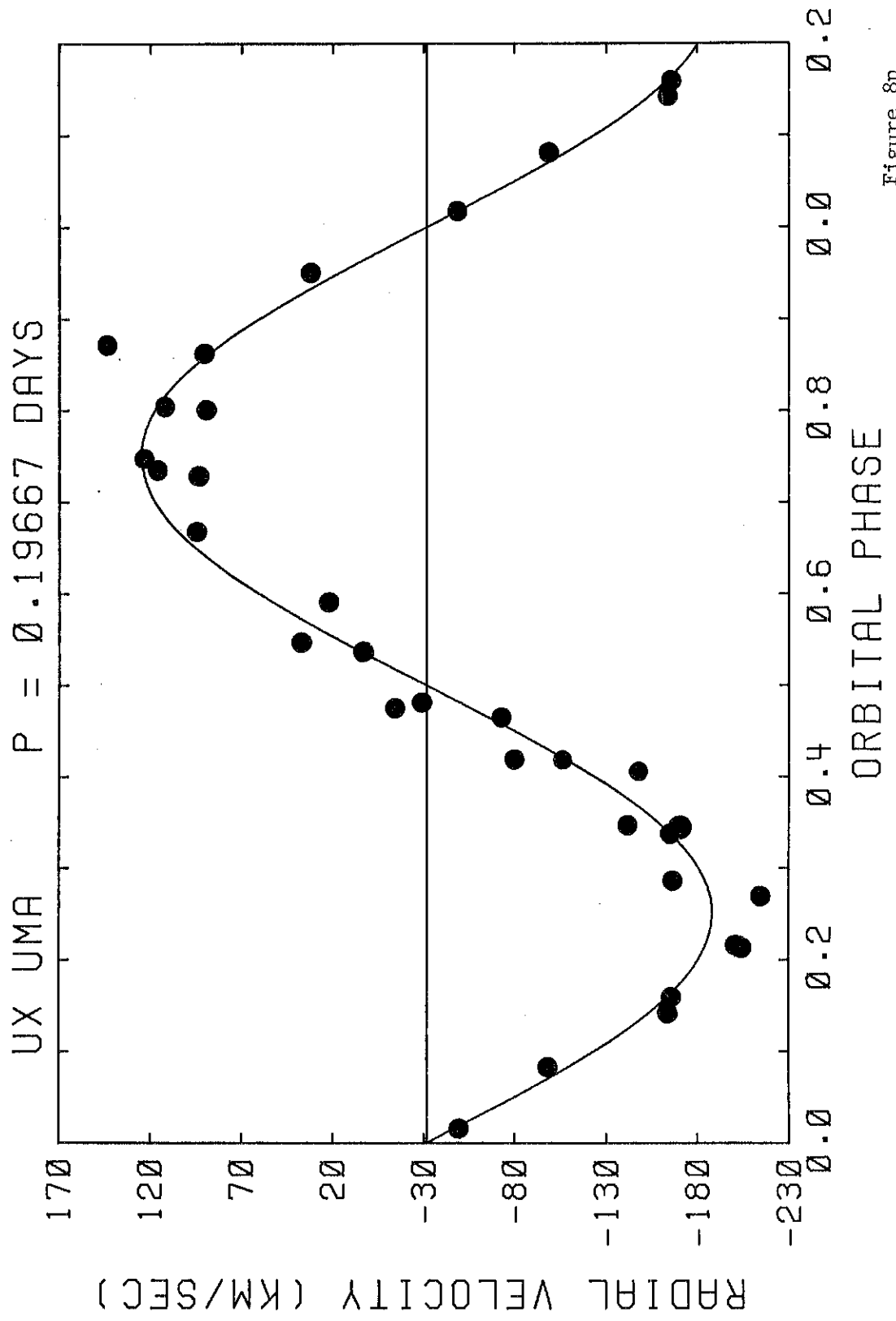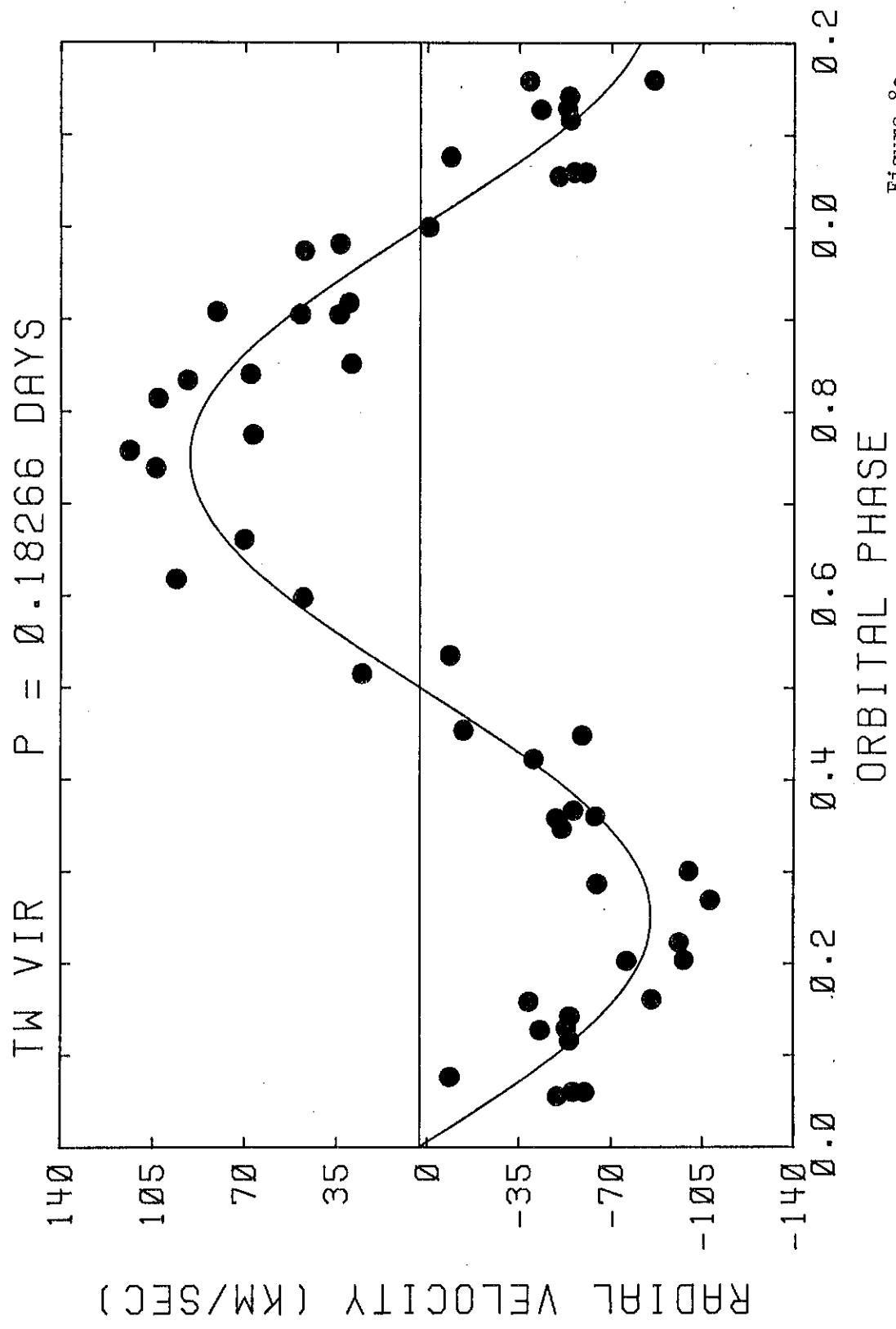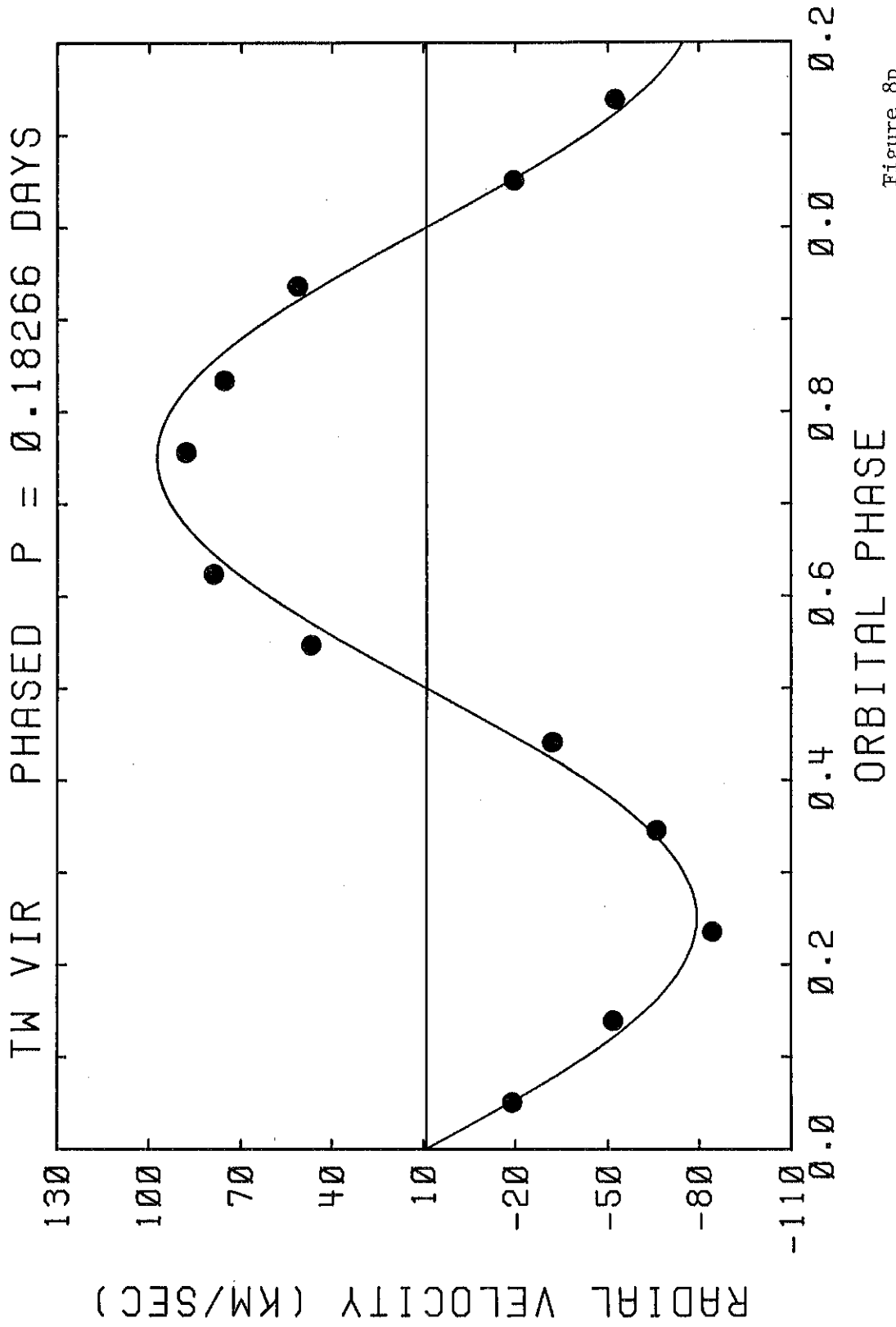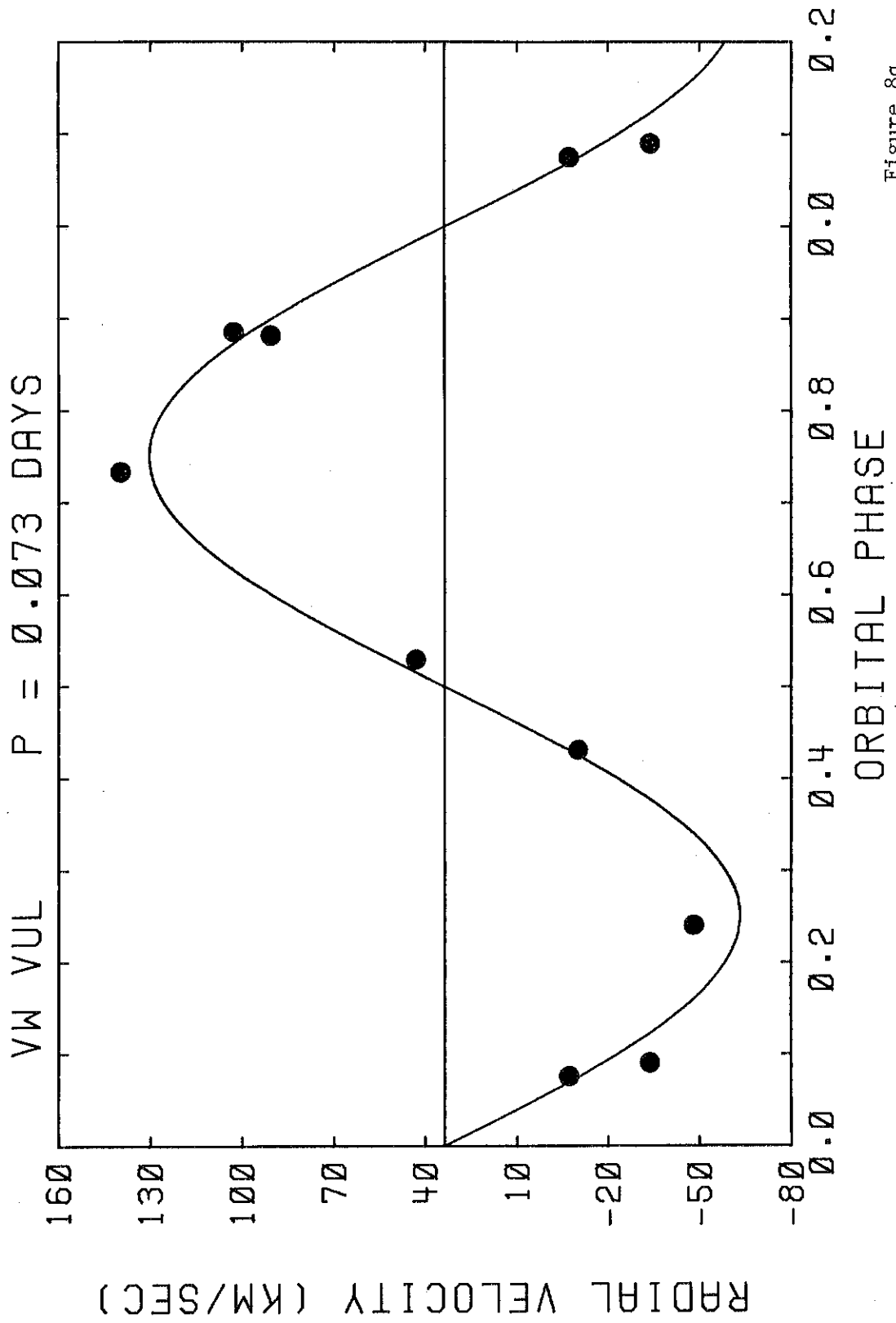
Figure 8q

Figures 9a-m.   The Hα line profiles of the 20 systems with single lined radial velocity curves.   The line profiles were used to determine v_d sin i and hence q for these systems.   For objects with multiple line profile observations, the profiles have been shown in chronological order.   The orbital phases for SW UMa and TW Vir have been indicated to demonstrate the lack of any obvious phase dependent line width variations.

RX And

RX And

V603 Aql

V603 Aql

WAVELENGTH (A)

Figure 9a

183

Figure 9b

Figure 9c

185

Figure 9d
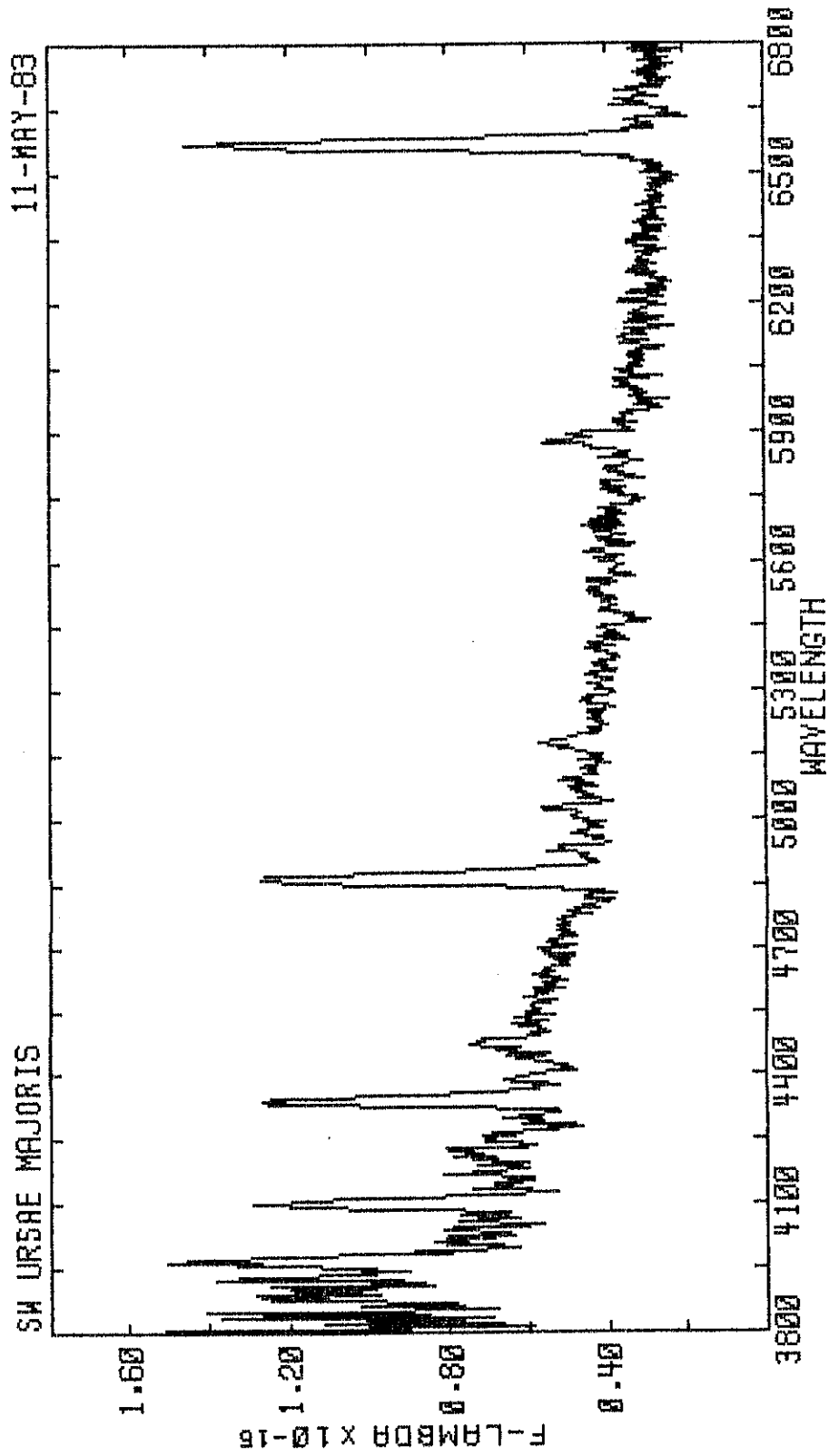
186
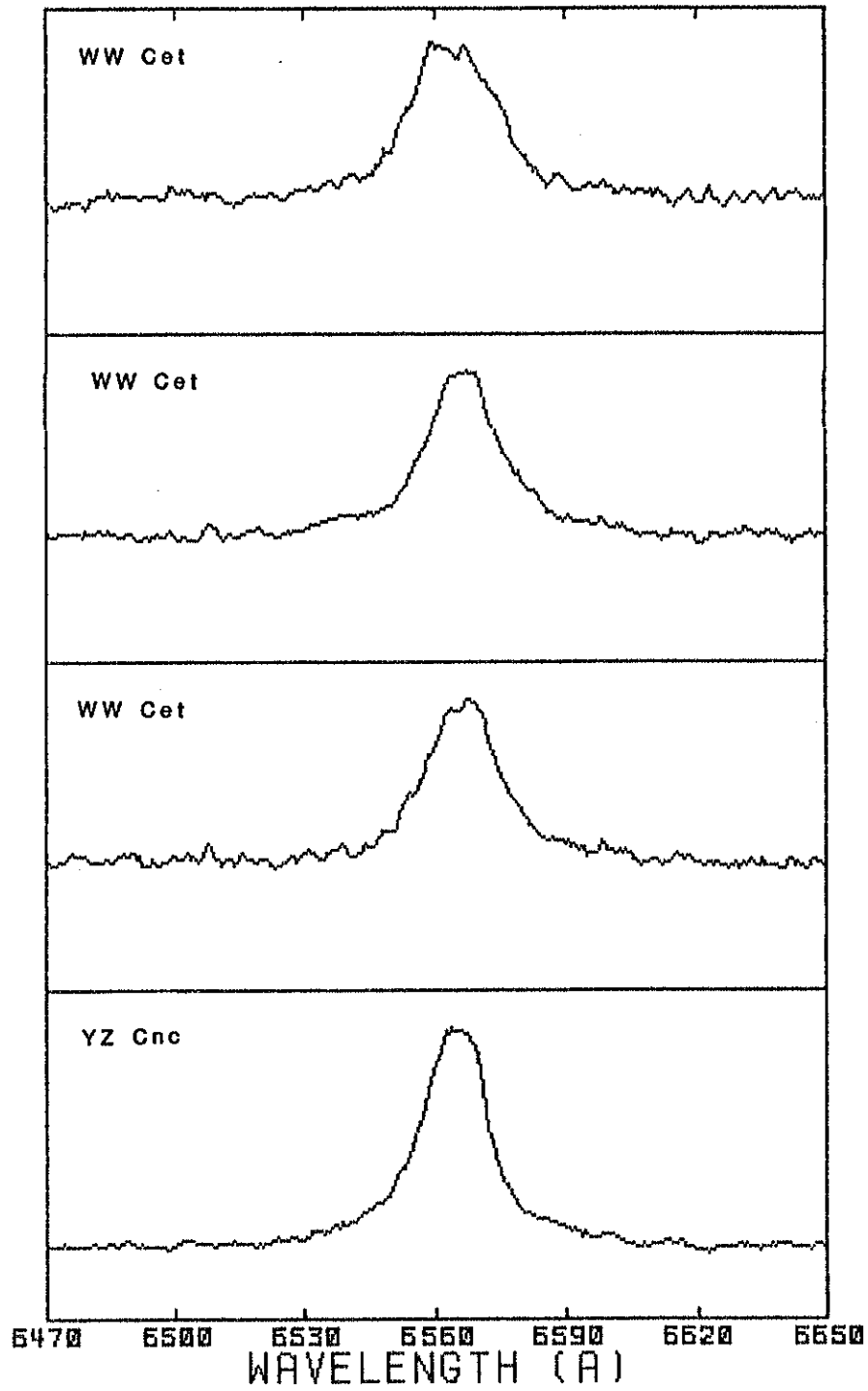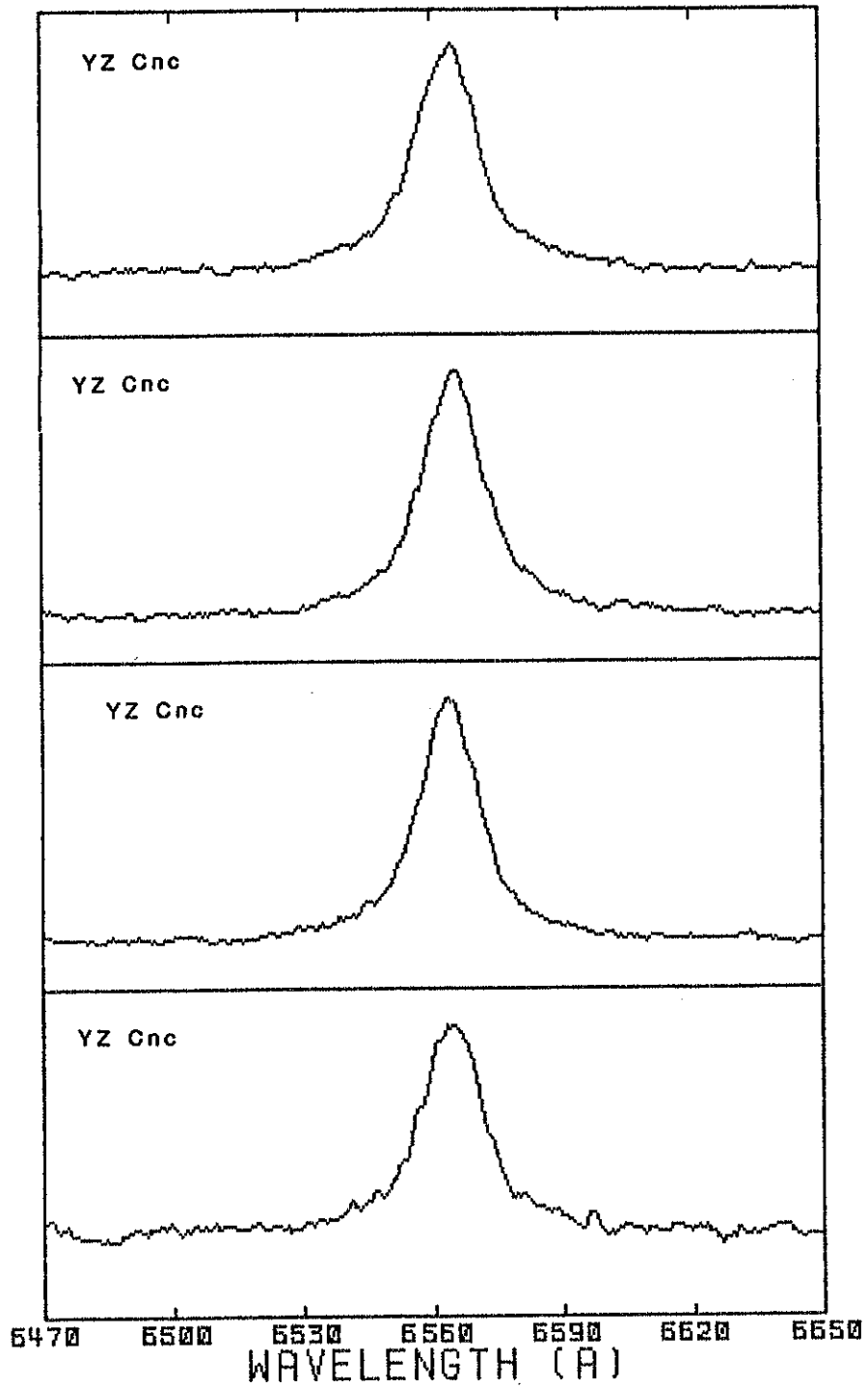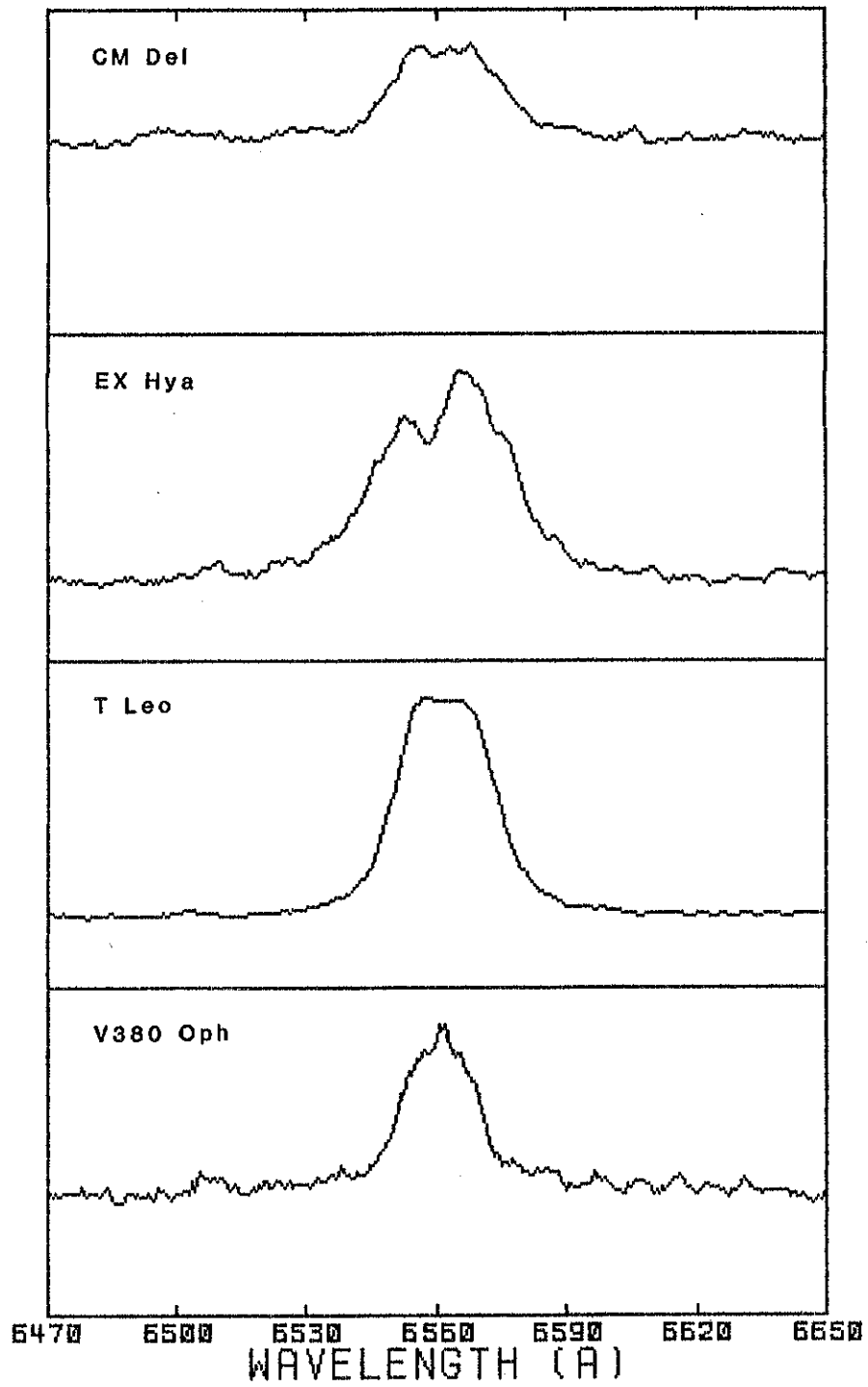
Figure 9e

Figure 9f

Figure 9g

189
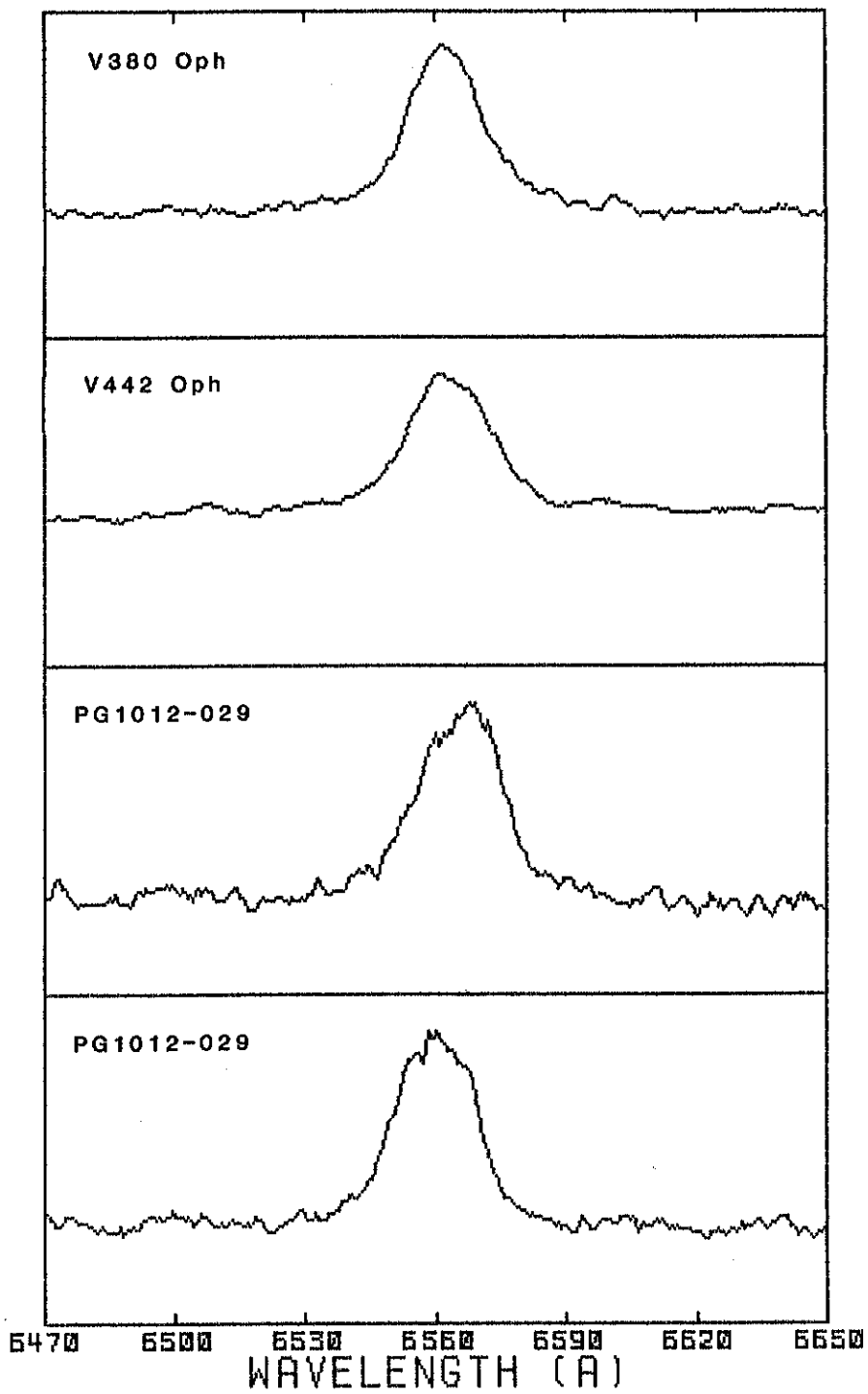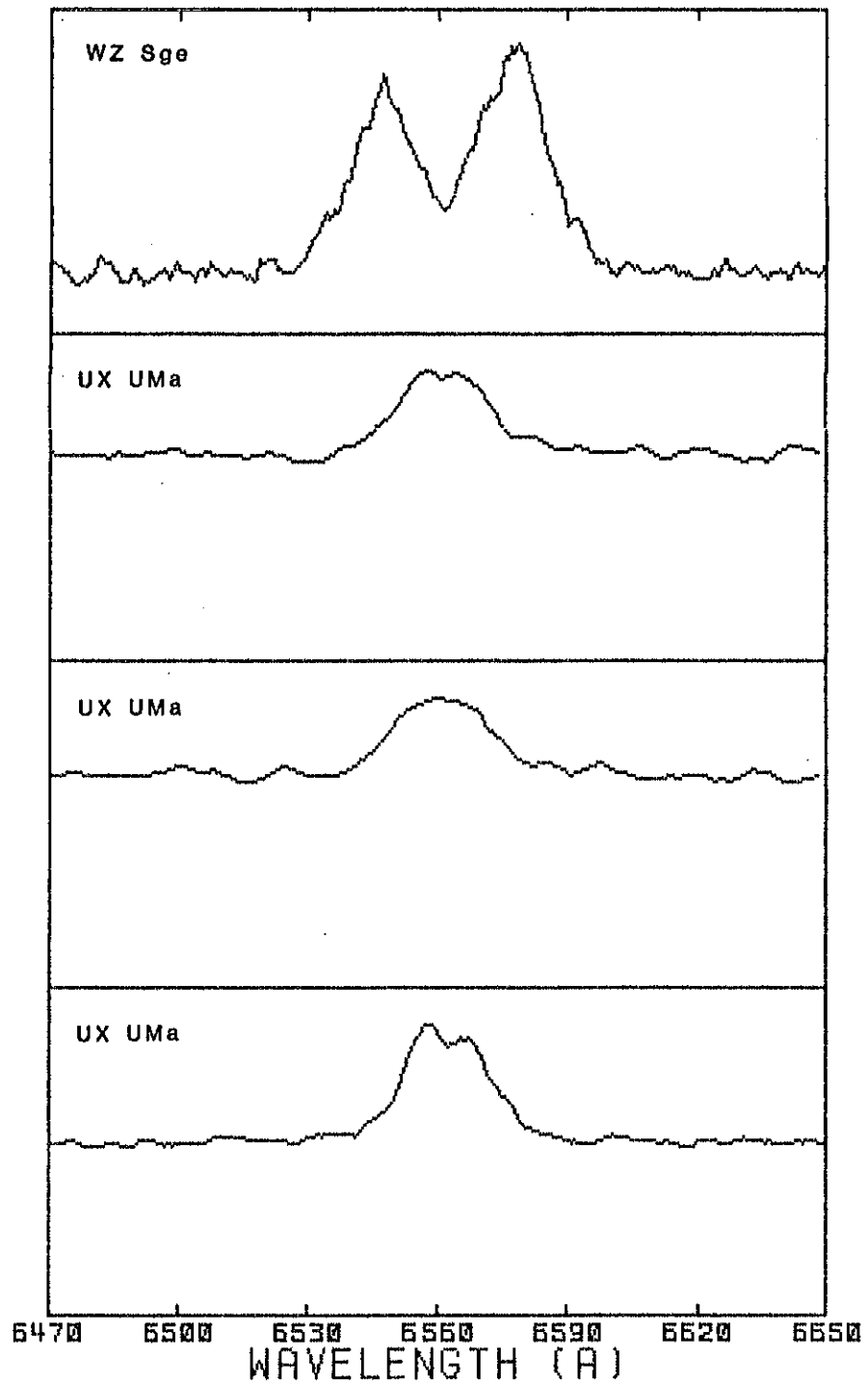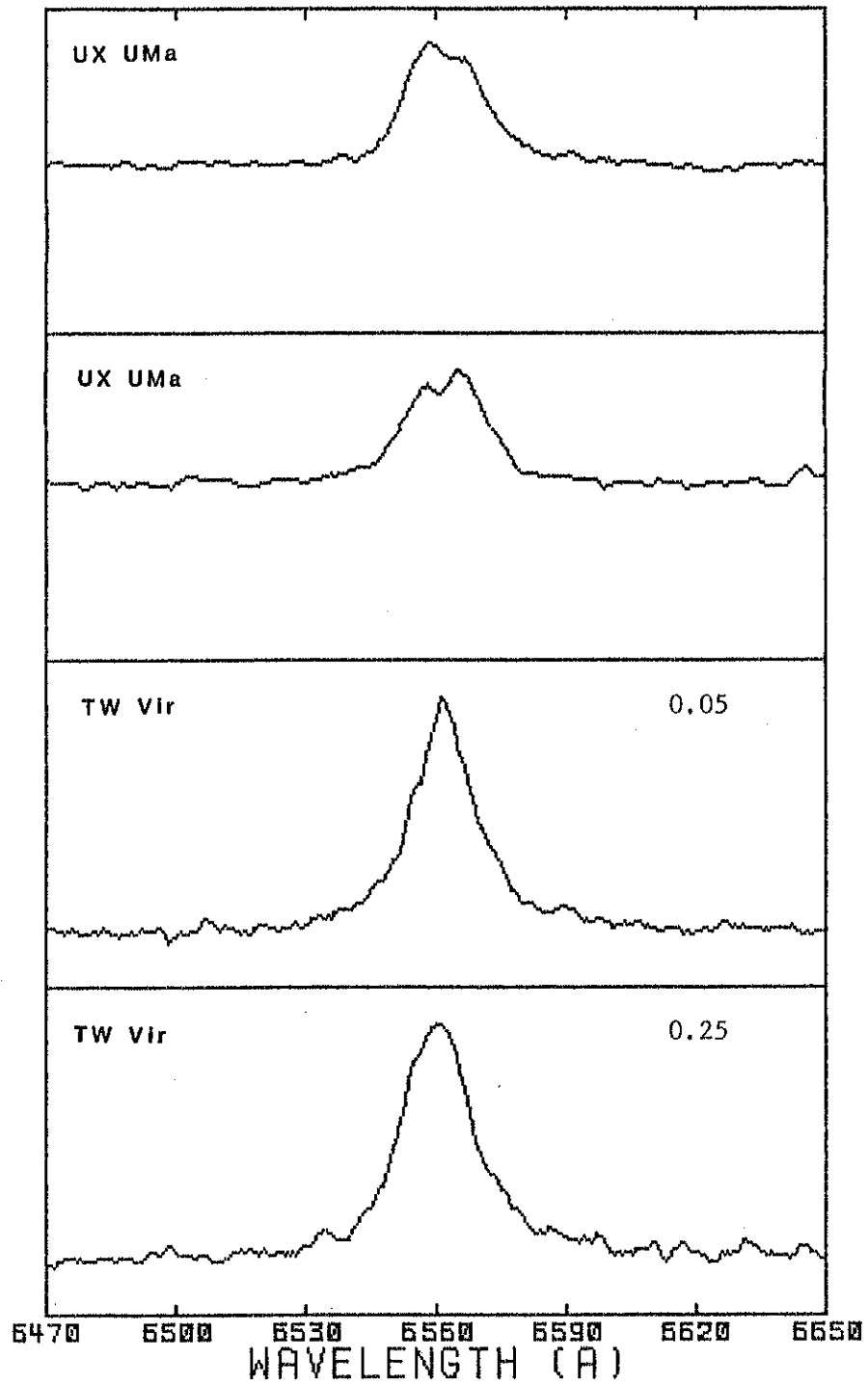
Figure 9h

Figure 9i

191
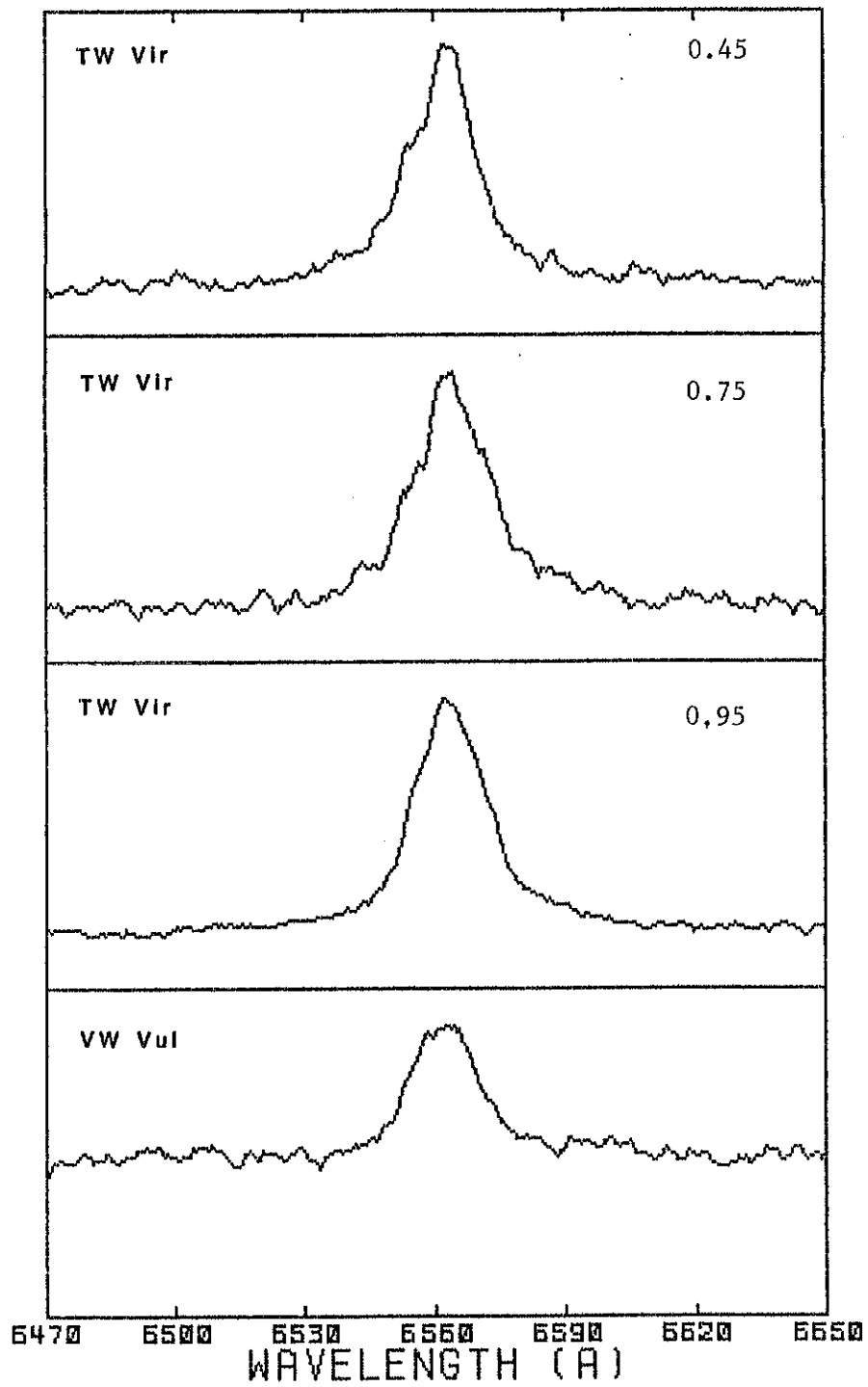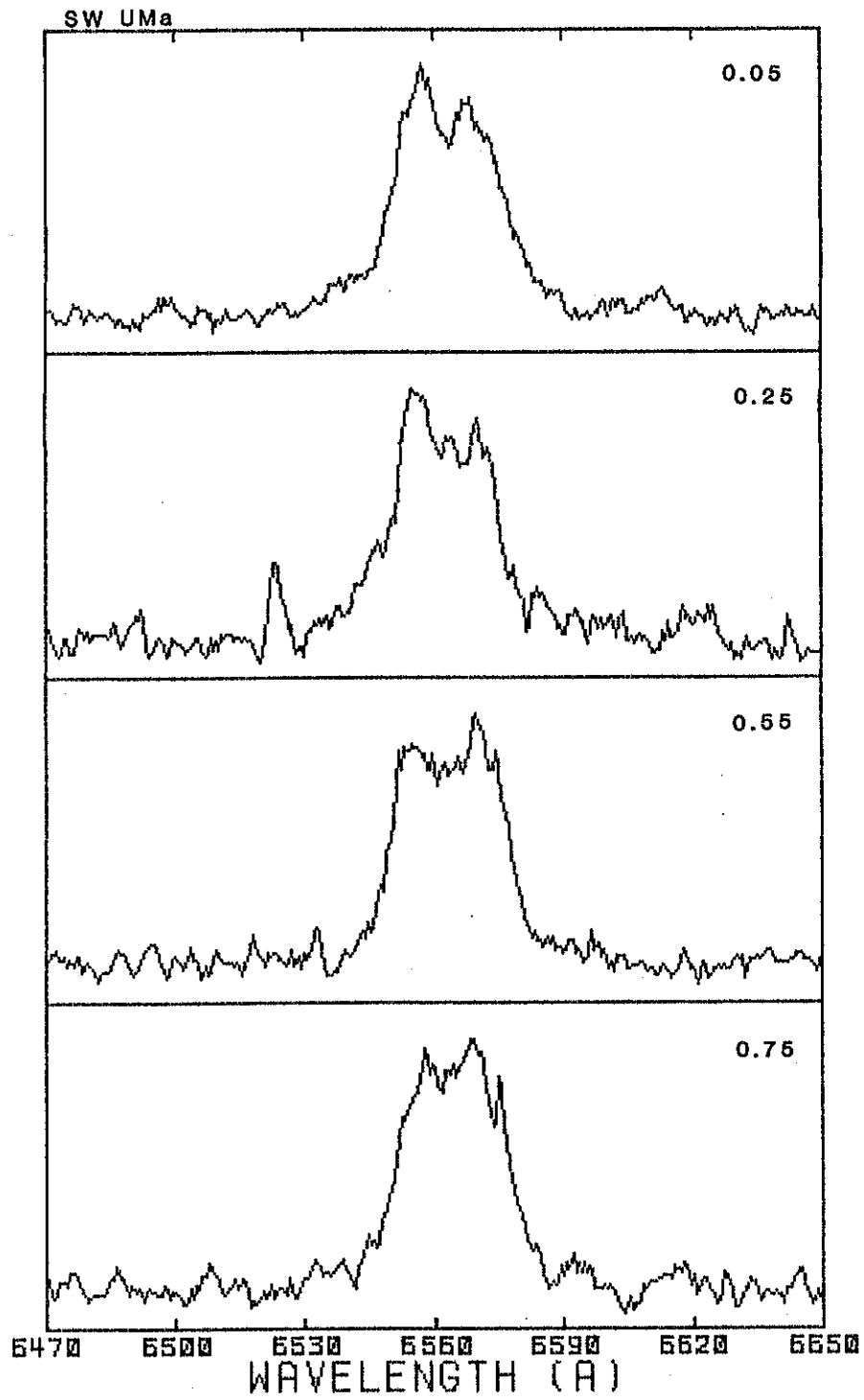
Figure 9j

Figure 9k
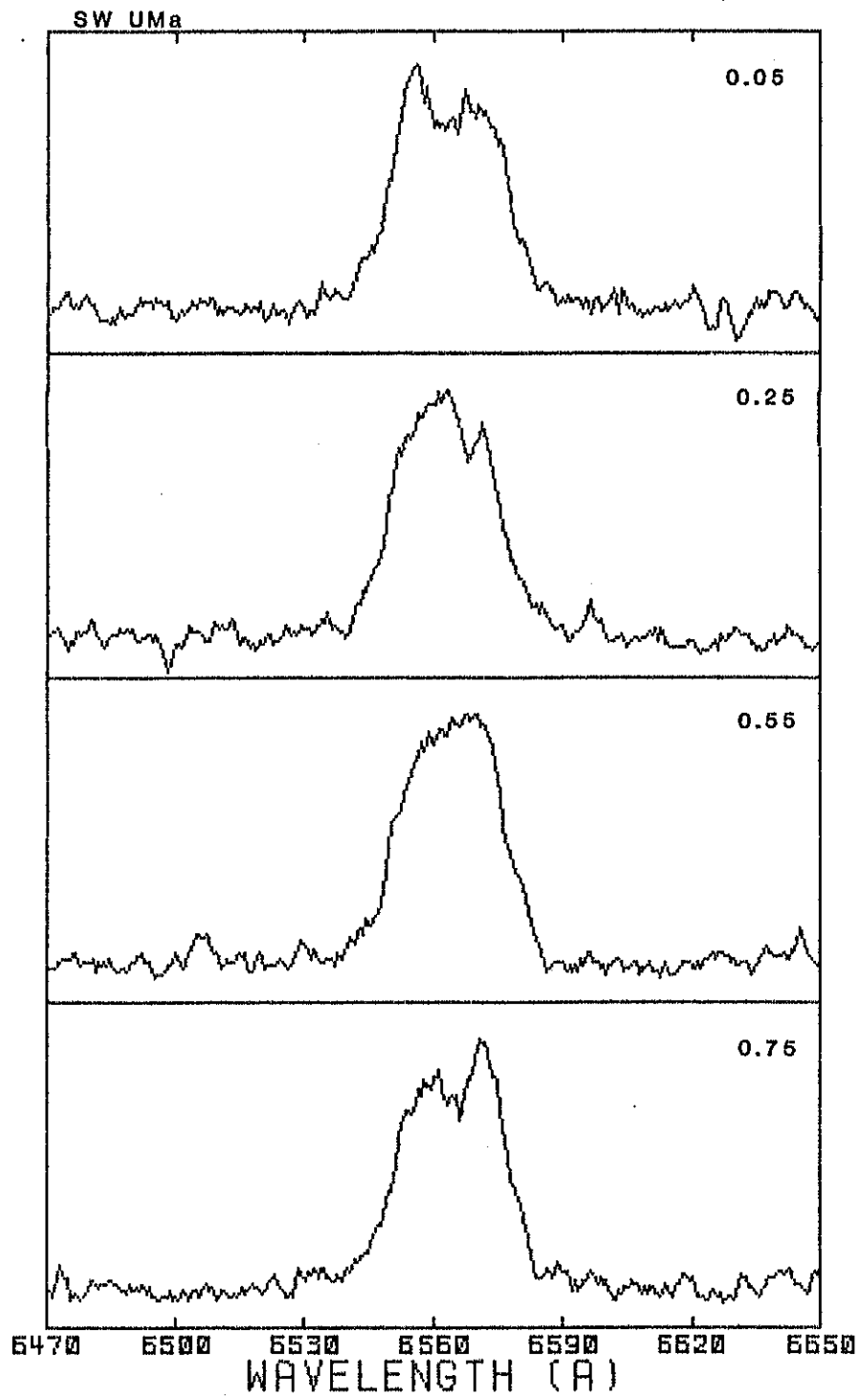
Figure 9 1
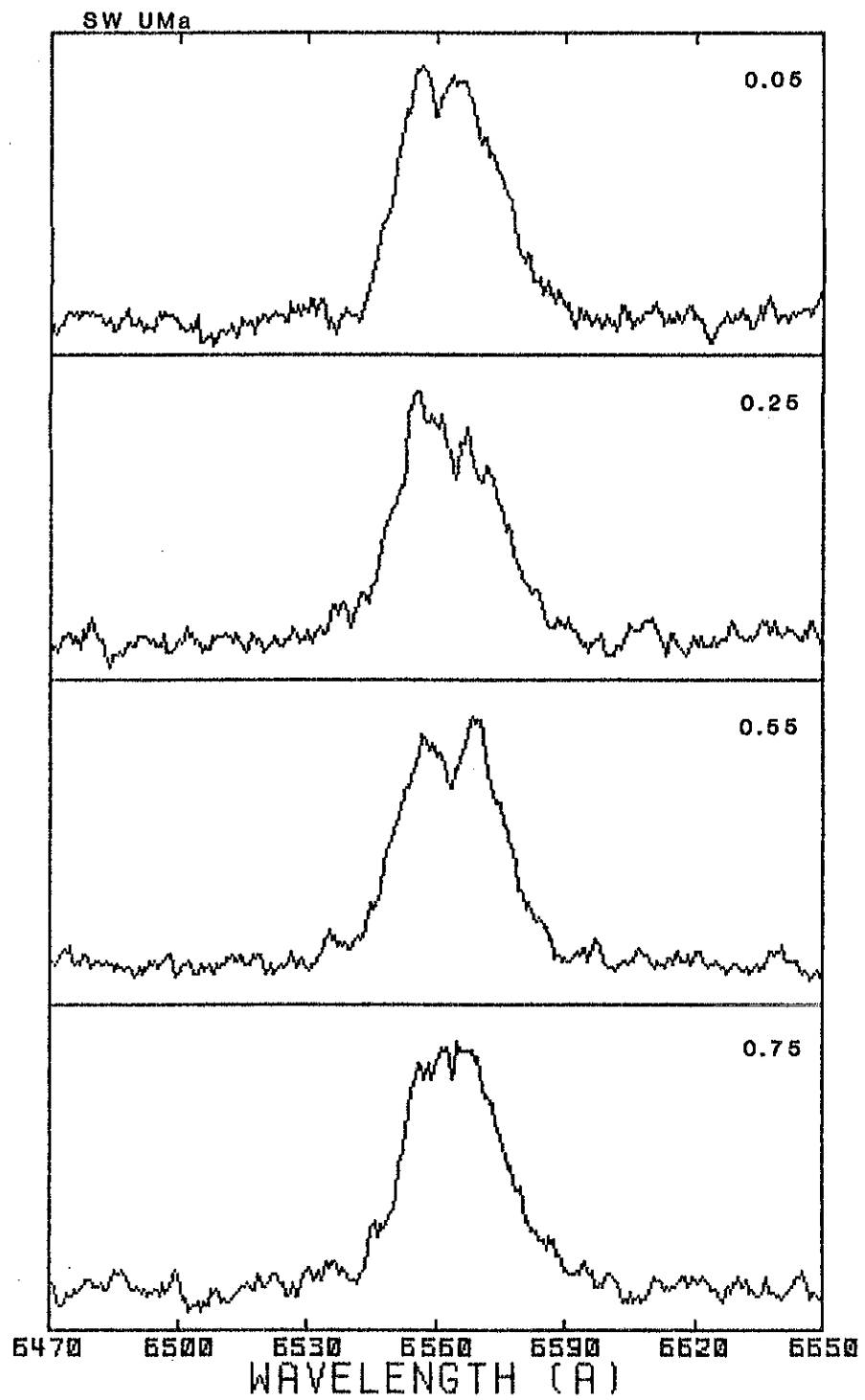
Figure 9m

Figure 10a-m. The absolute flux (ergs cm^{-2} s^{-1} $\mathring{A}^{-1}$) plotted as a function of wavelength for the 13 systems whose radial velocity curves are shown in Figure 8. Note the large equivalent widths of the emission lines for the ultrashort period systems T Leo, SW UMa, and VW Vul.
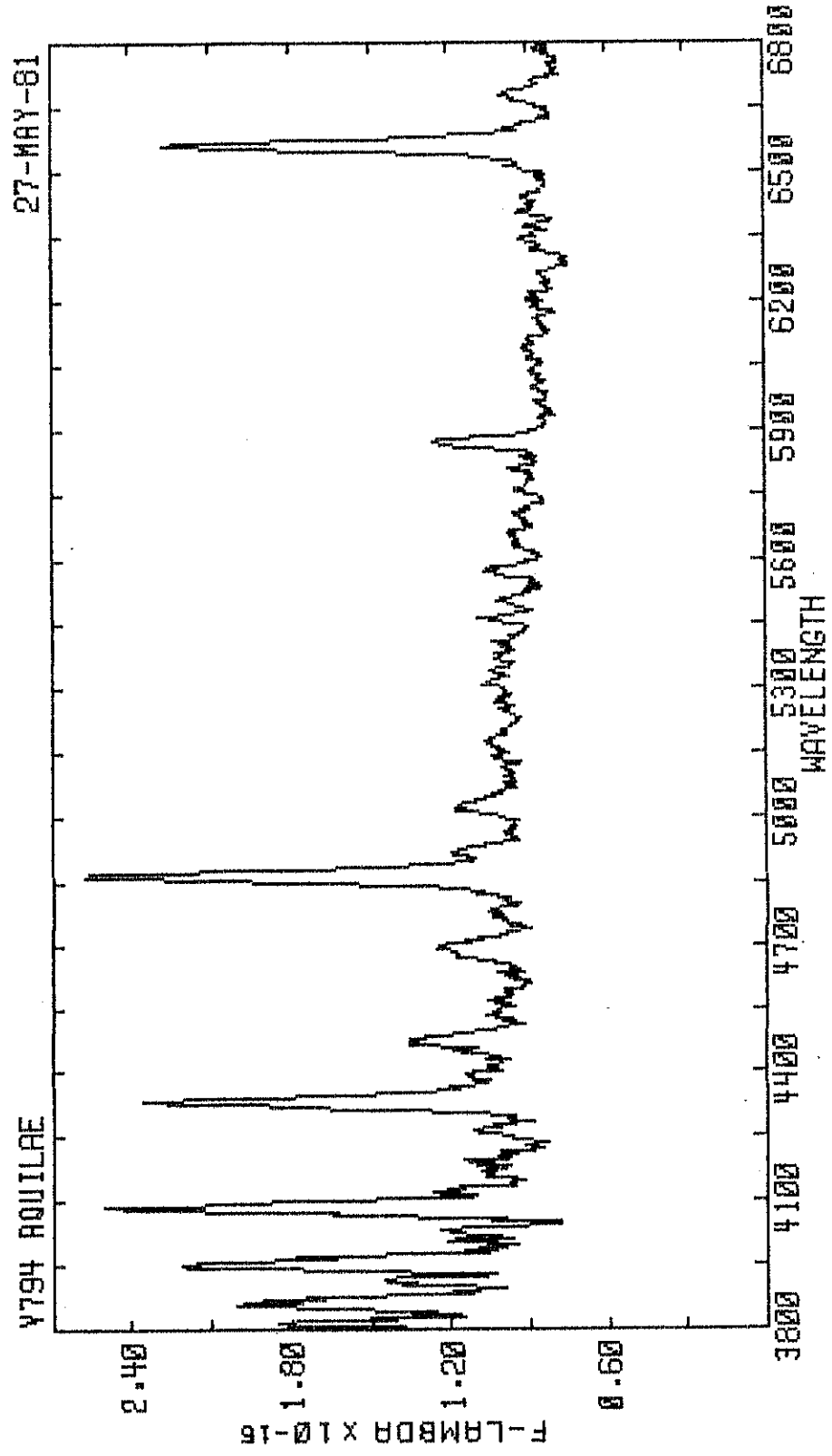
Figure 10a
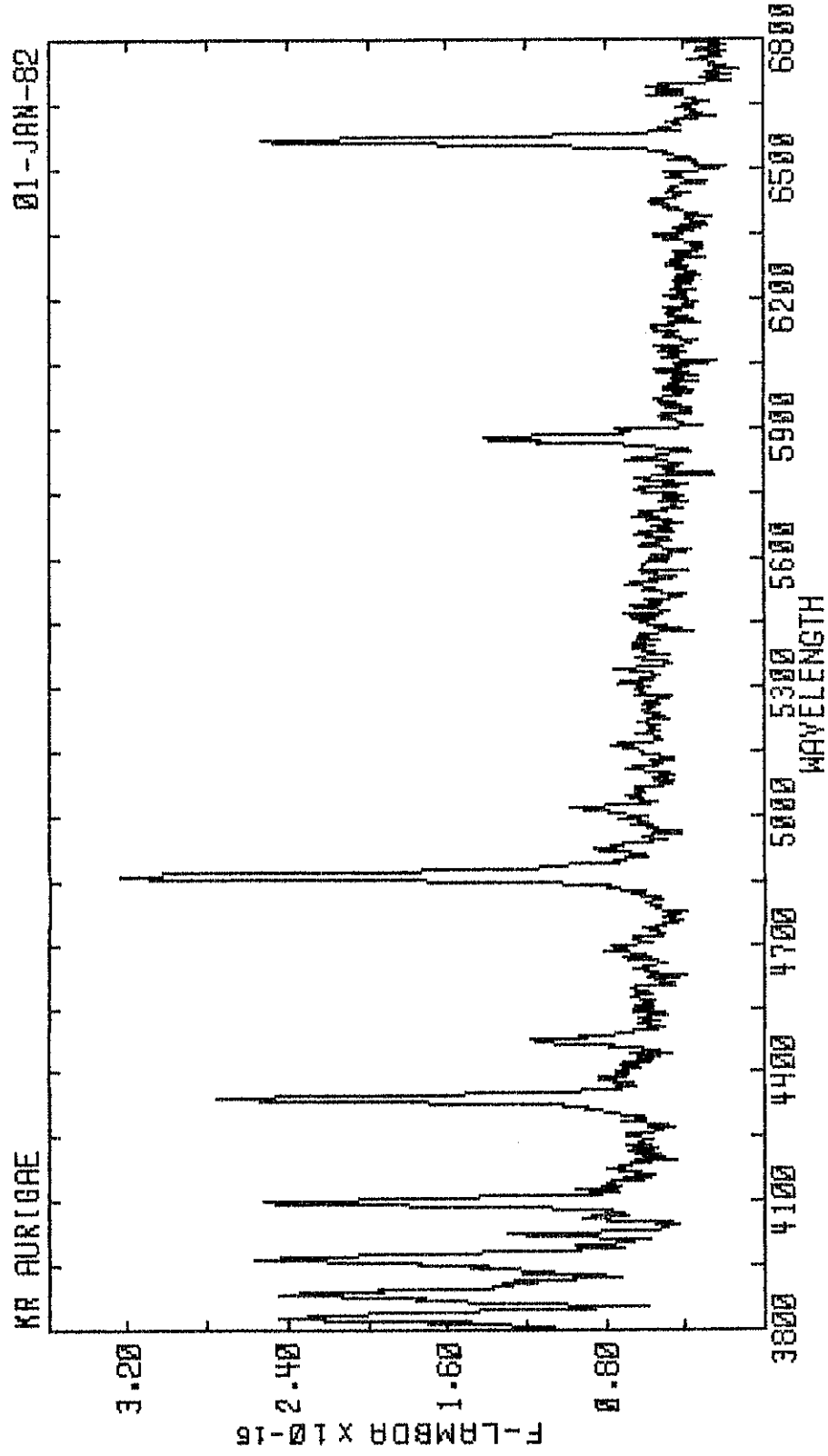
Figure 10b
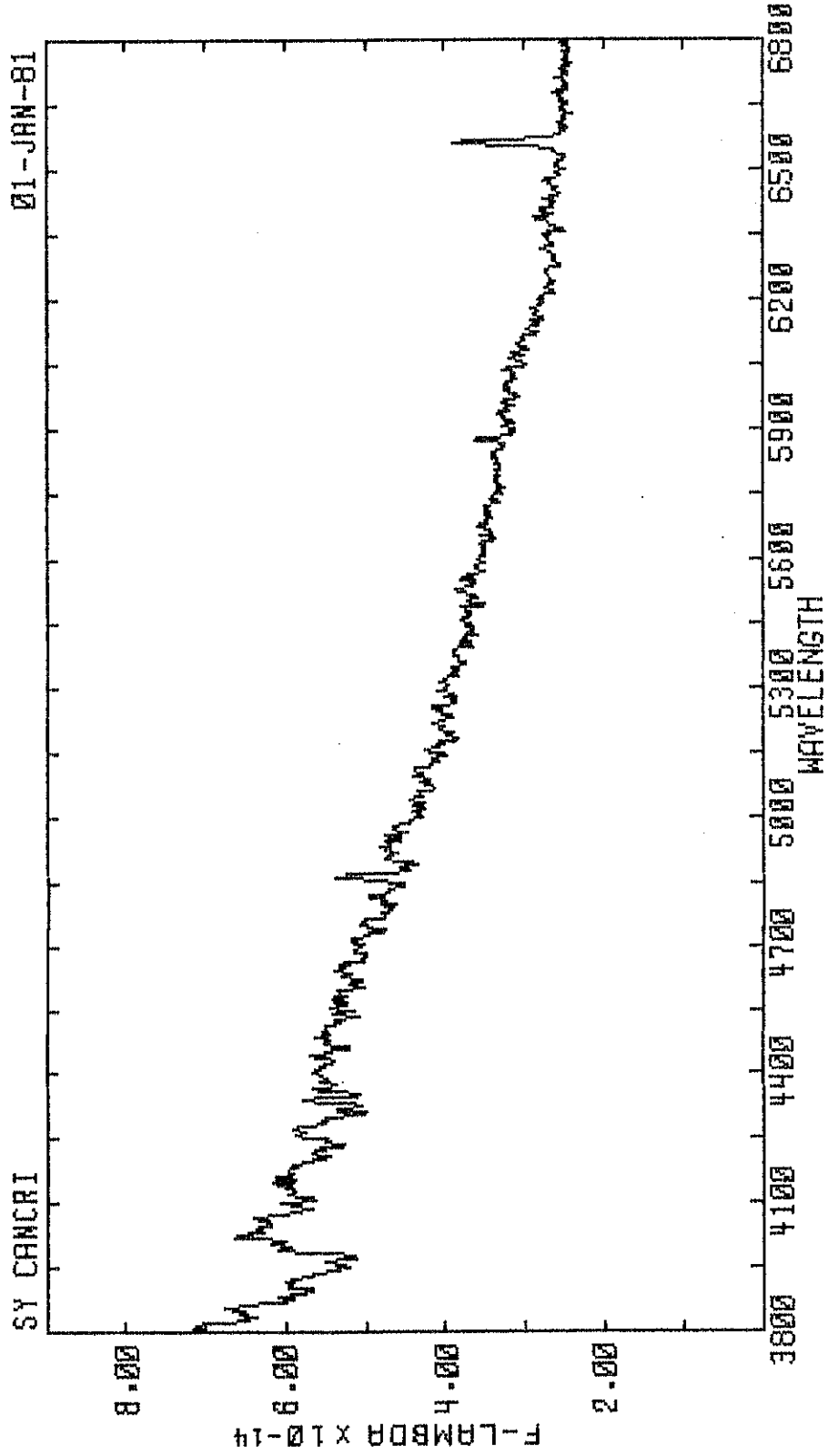
198

Figure 10c

Figure 10d

200

Figure 10e

201

Figure 10f

202

Figure 10g

203

Figure 10h

Figure 10i

205

SW URSAE MAJORIS   11-MAY-83

F-LAMBDA X10-16
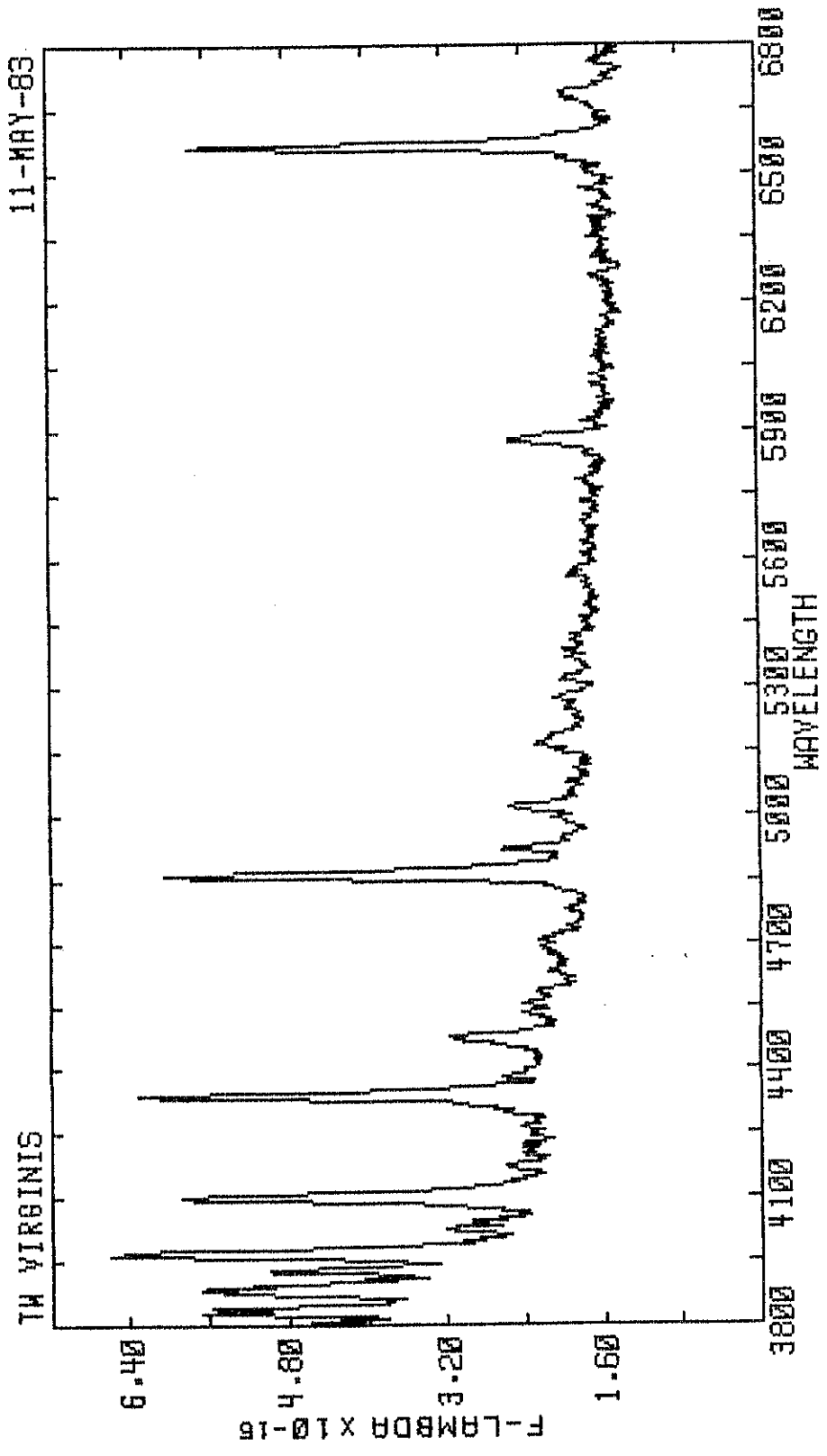
WAVELENGTH
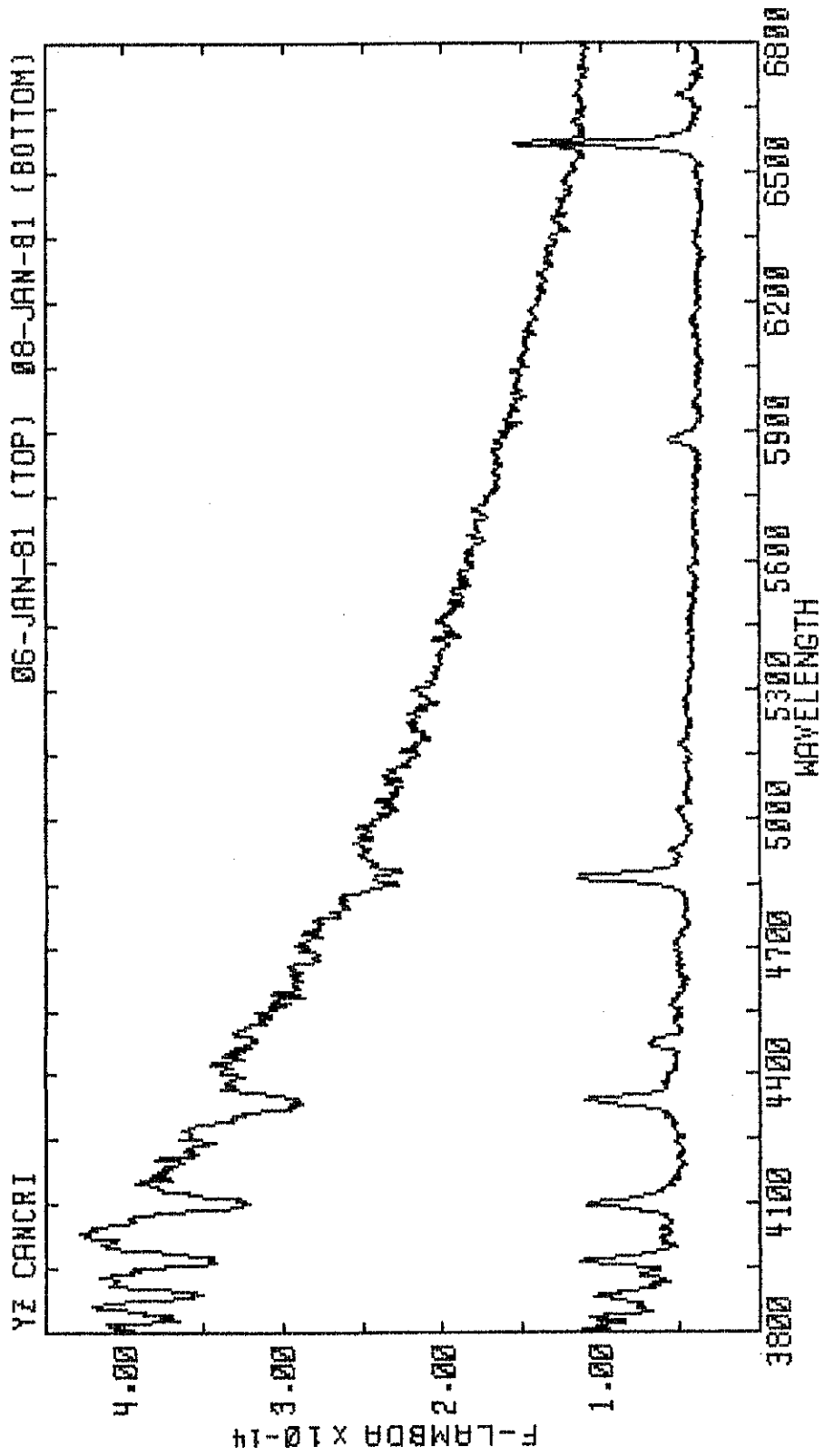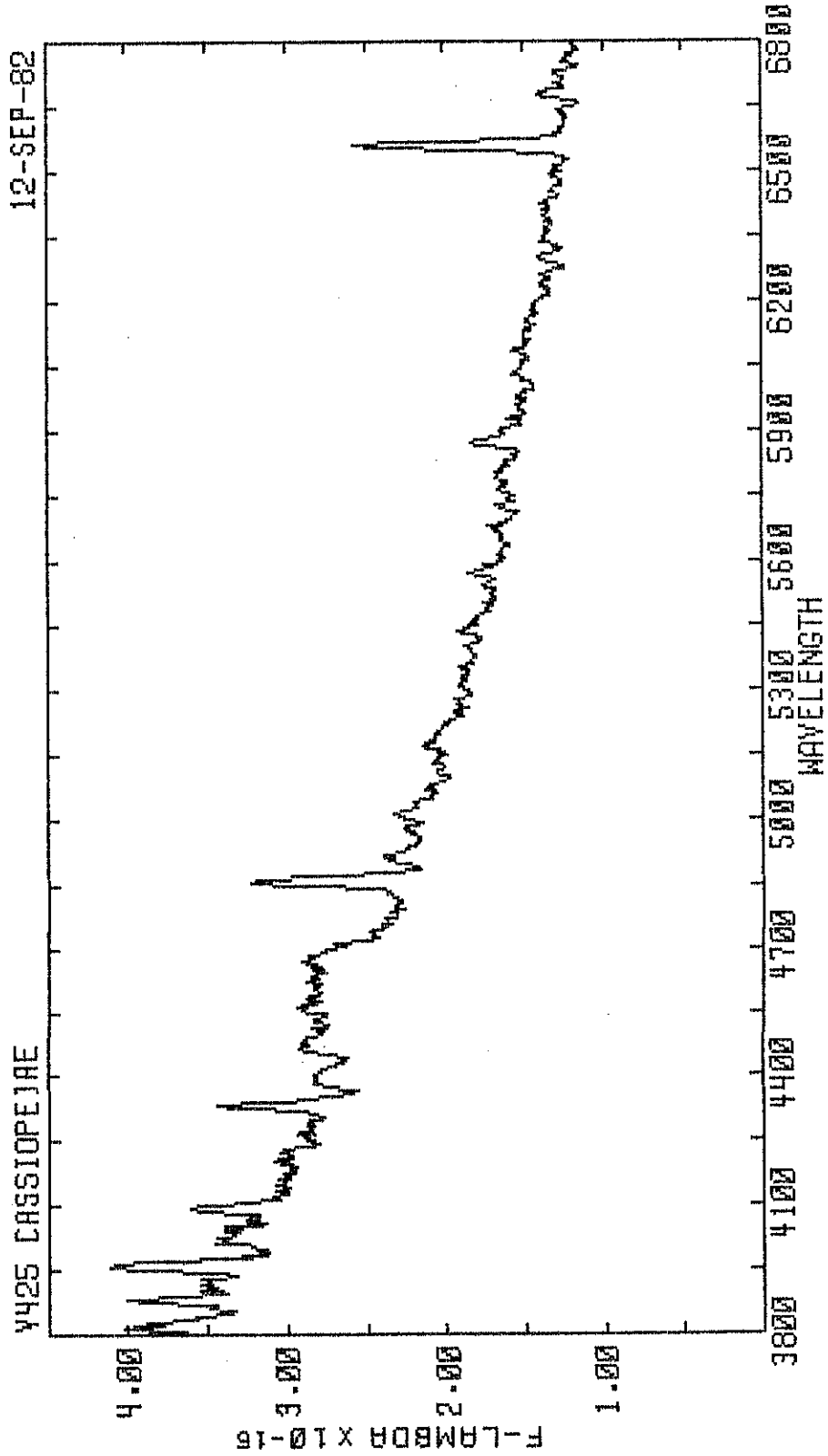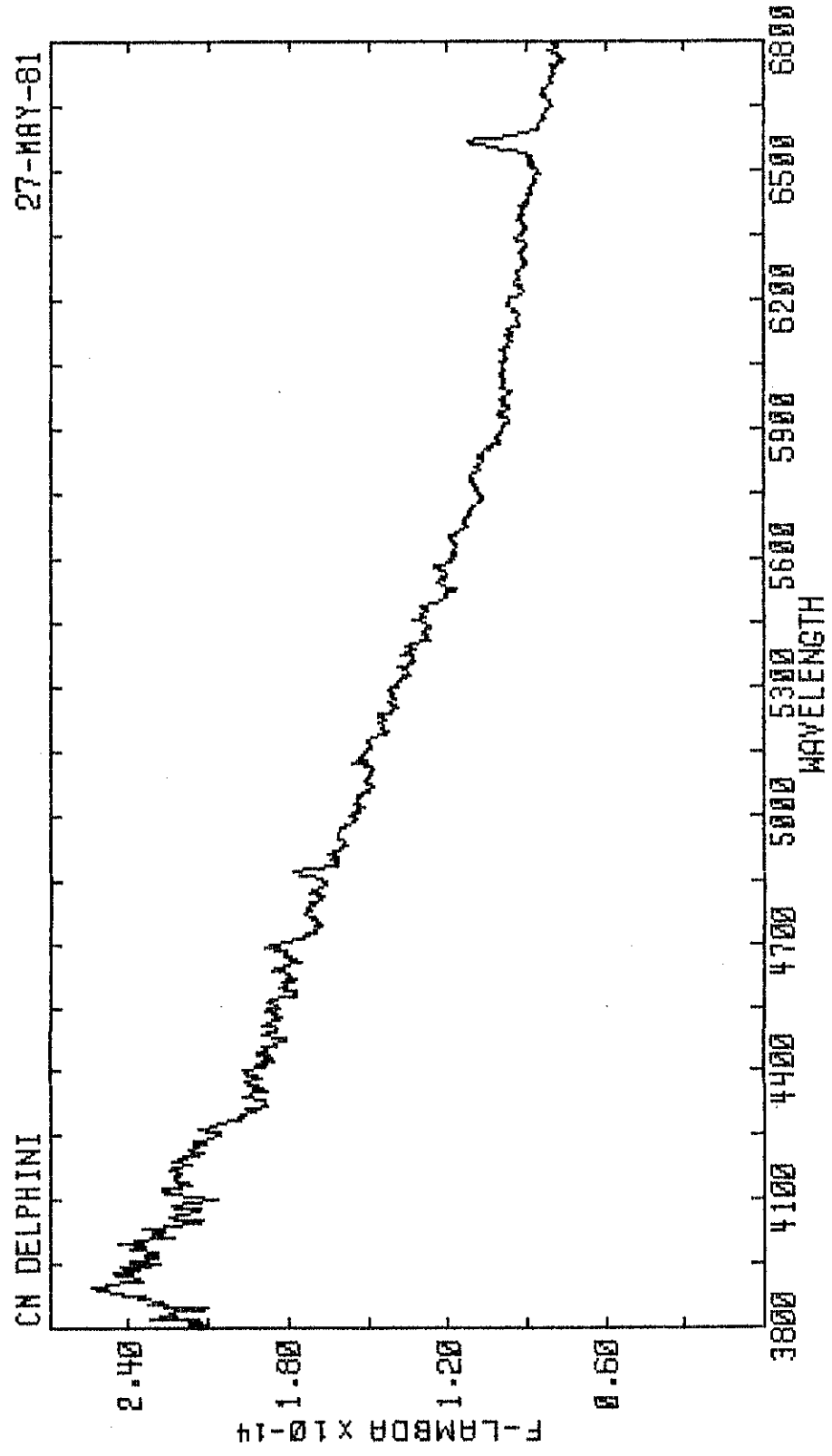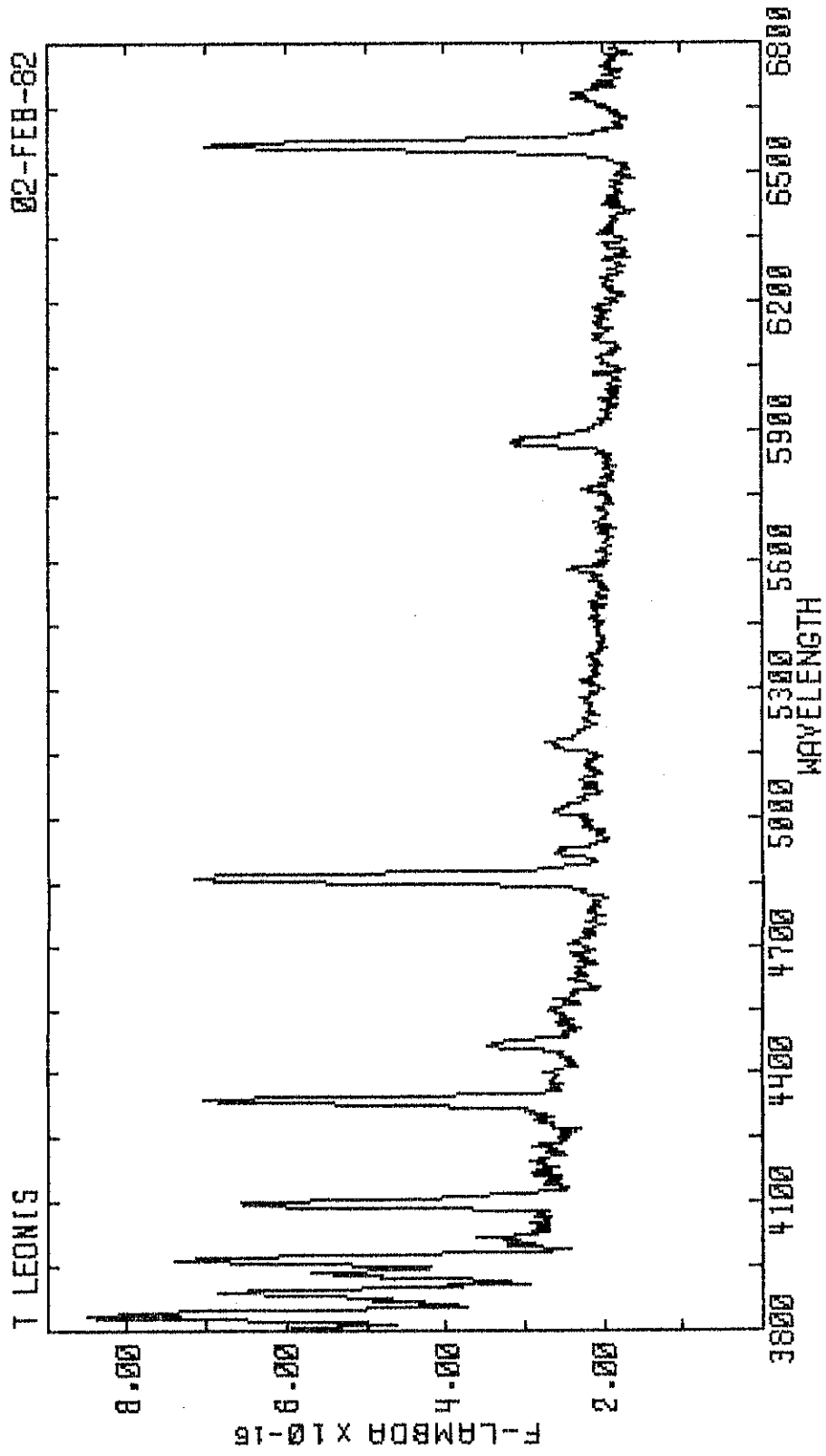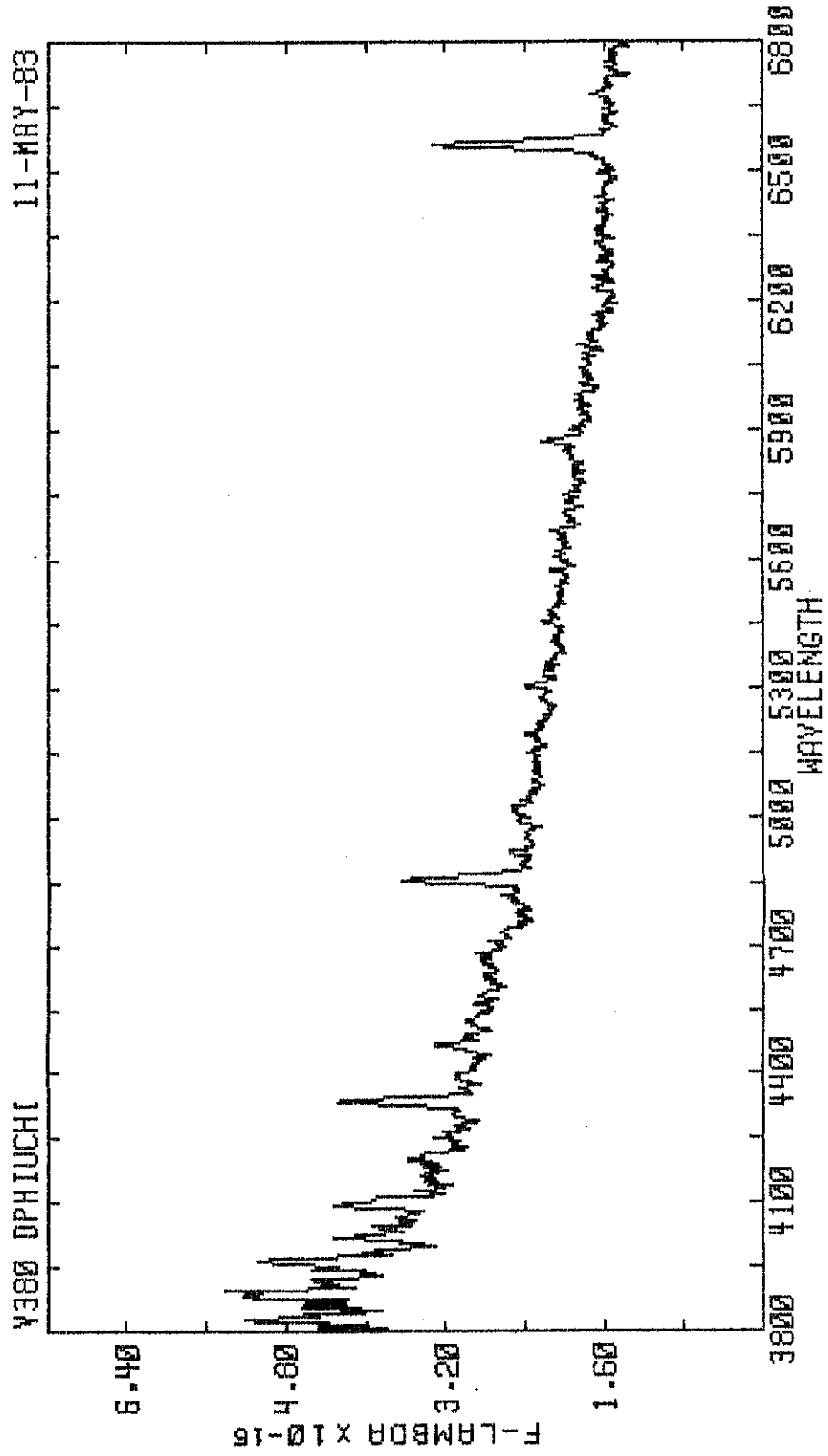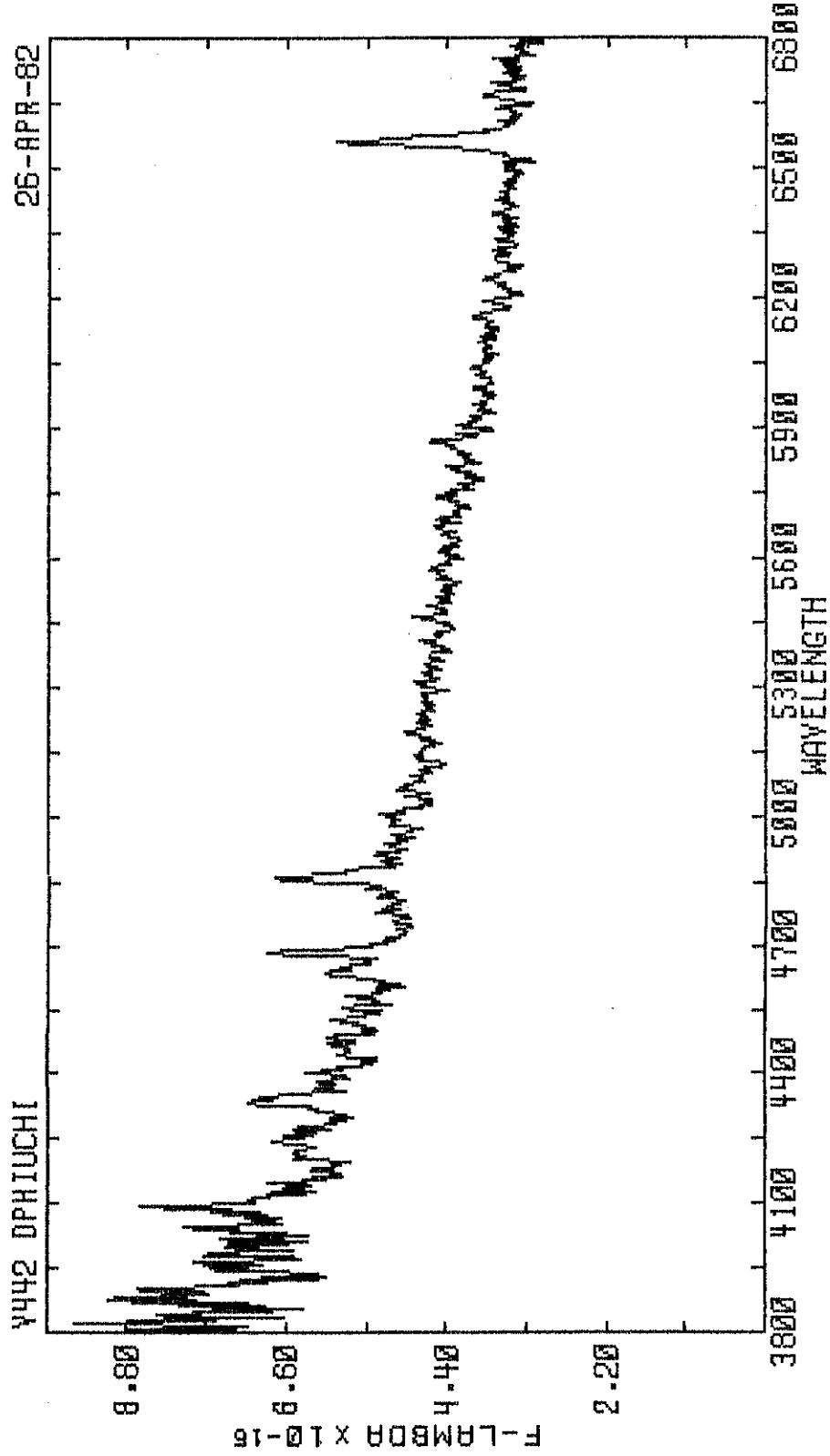
Figure 10j

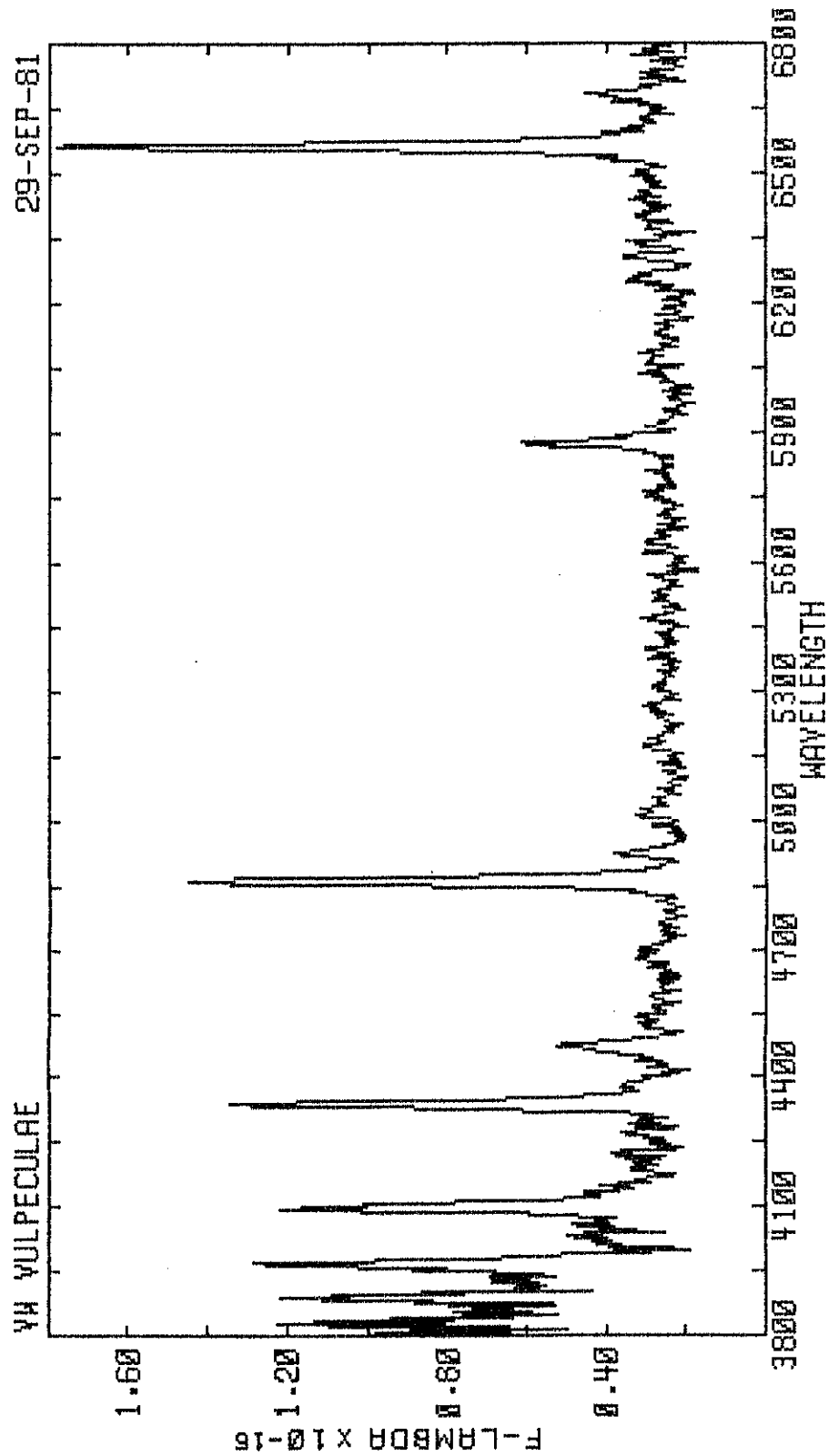Figure 10k

207

Figure 10 1

208

Figure 10m

209
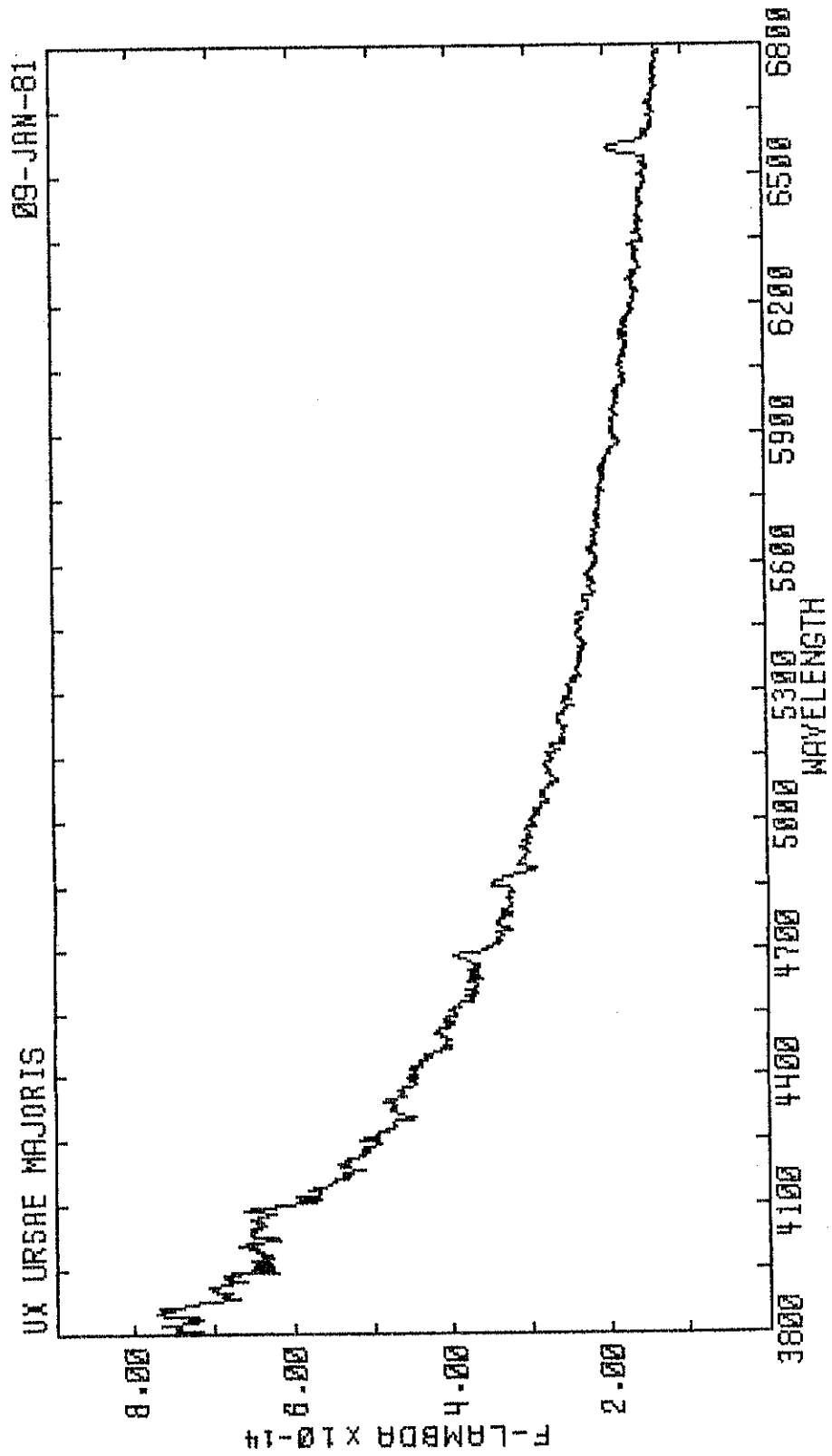
Figure 11. The mass ratio, $q(= M_2/M_1)$, for all systems is plotted as a

function of orbital period. The line represents a linear

least squares fit of the data. The scatter of the data

points about this line is rather large and does not imply an

explicit functional relationship between q and P. The line

has been included in order to compare my results with those

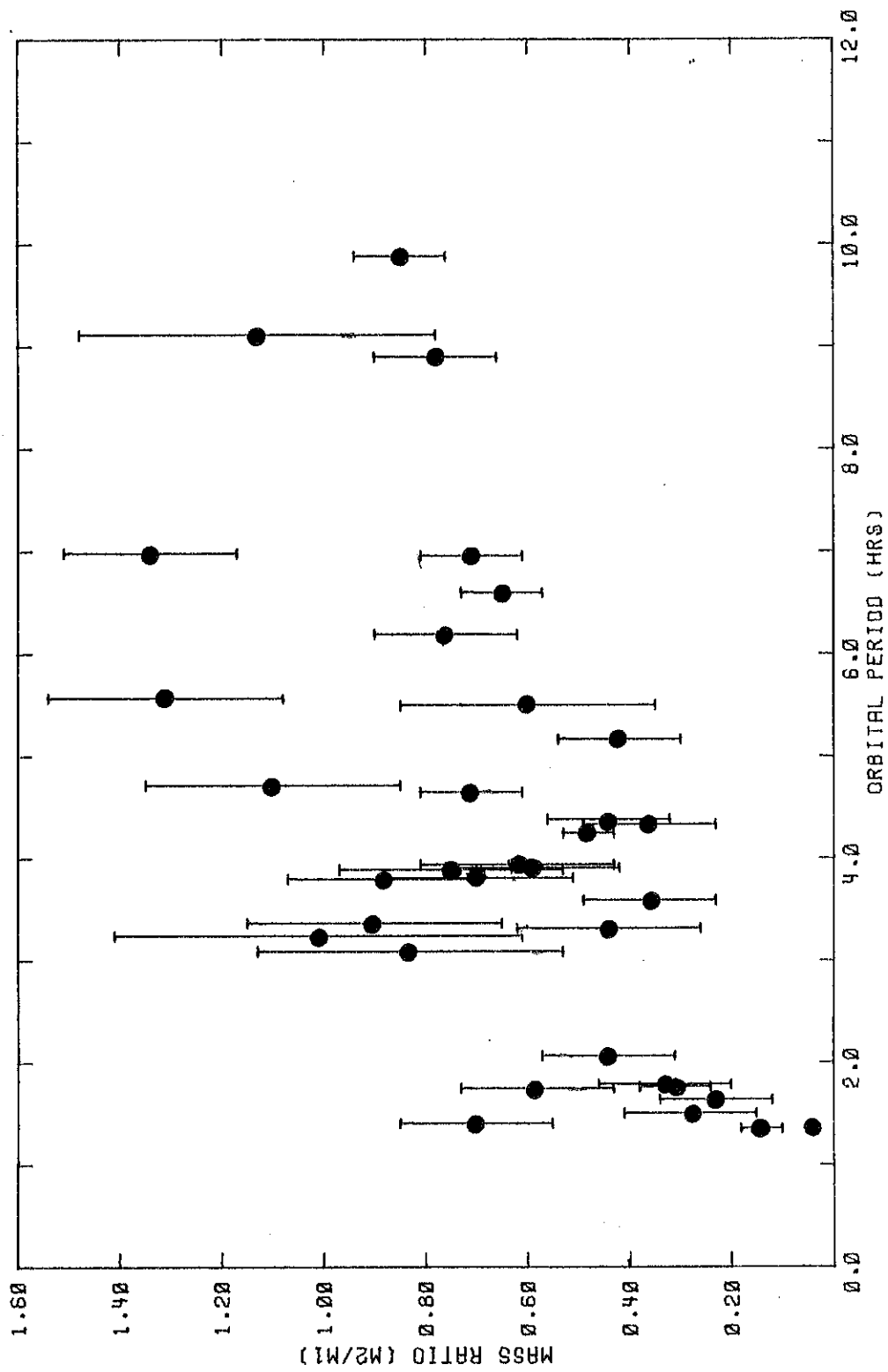of other workers. We can conclude that q is roughly

independent of P.

Figure 11

211

Figure 12. The mass of the white dwarf for all systems is plotted as a function of orbital period. The curve represents the locus defined by equation IV.2. Note the general tendency for M_1 to increase with increasing orbital period.

Figure 12

213

Figure 3. The average white dwarf mass for three period ranges.

(A) The ultrashort period regime: $1 < P(hr) < 3$; (B) The short period regime: $3 < P(hr) < 6$; (C) The long period regime: $6 < P(hr) < 10$. The average masses are 0.49 $M_\odot$, 0.65 $M_\odot$, and 0.91 $M_\odot$ for the three regimes (A), (B), and (C), respectively.

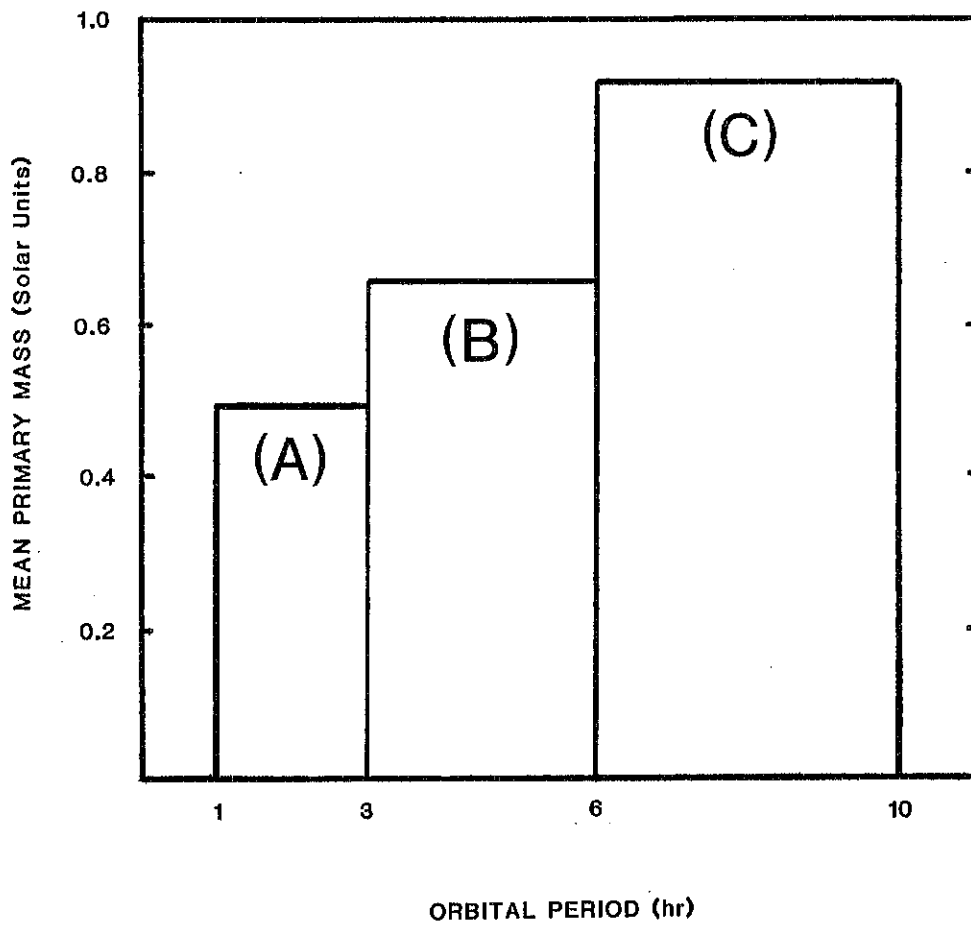Figure 13